Modelling Sources of Stratification within the Labrador Sea

by

Clark William Pennelly

A thesis submitted in partial fulfillment of the requirements for the degree of

Doctor of Philosophy

Department of Earth and Atmospheric Sciences
University of Alberta

Abstract

The Labrador Sea experiences deep convection, a process where the oceans' surface cools to the point where it may become more dense than the water at depth, promoting sinking and vertical mixing. This mixing can exceed 2000m in depth, producing a large volume of deep water, a crucial component in the meridional overturning circulation of heat and gases. Deep convection and subsequent water mass formation is heavily influenced by stratification. Sources that remove/supply buoyancy act to erode/strengthen the stratification of the Labrador Sea. This thesis investigates sources that modify the stratification of the Labrador Sea by using an ocean circulation model, NEMO. I first identify regions around the Labrador Sea where relatively buoyant freshwater leaves the boundary currents and enters the interior basin (Chapter 4). I find that while turbulent flow (eddies and meanders) drives freshwater offshore around the whole Labrador Sea, only the west coast of Greenland and the southern Labrador Coast have a net offshore flux of freshwater. I show differences between atmospheric datasets (up to 12 W m^{-2}) when used to force the NEMO model can drive Labrador Sea Water to vary in both its volume production as well as density (Chapter 5). I produced a complex numerical configuration capable of resolving sub-mesoscale processes (Chapter 3) and used the output to investigate eddies which spawn along the west coast of Greenland. I explore the evolution of these long lived eddies, noting how their stratification changes over their lifetime. While originally strongly stratified, they may encounter such conditions that promote Labrador Sea Water to be formed within their eddy core before their decay (Chapter 6).

Preface

Chapter 3 of this thesis has been published as:

Pennelly, C. and Myers, P.G. (2020): Introducing LAB60, a 1/60° NEMO 3.6 numerical simulation of the Labrador Sea, *Geoscientific Model Development,* Vol. 13, Issue 10, 4959-4975.

 P.G. Myers was my supervisor and was responsible for designing the model configuration and edits to the manuscript. C. Pennelly was responsible for producing the model configuration, carrying out the simulation, data analysis and manuscript writing.

Chapter 4 of this thesis has been published as:

Pennelly, C., Hu, X. and Myers, P.G. (2019): Cross-Isobath freshwater exchange within the North Atlantic subpolar gyre, *Journal of Geophysical Research: Oceans*, Vol 124, Issue 10, 6831-6853.

X. Hu was a post-doctoral fellow and produced two of the three simulations used and provided edits to the manuscript. P.G. Myers was my supervisor and was responsible for manuscript edits. C. Pennelly was responsible for data analysis and manuscript writing.

Chapter 5 of this thesis has been published as:

Pennelly, C. and Myers, P.G. (2021): Impact of different atmospheric forcing sets on modeling Labrador Sea Water production, *Journal of Geophysical Research: Oceans*, Vol 126, Issue 2.

P.G. Myers was my supervisor and was responsible for manuscript edits. C. Pennelly was responsible for performing the simulations, carrying out data analysis, and manuscript writing.

Acknowledgements

I first want to thank my supervisor, Paul Myers. Paul has been the support foundation that kept everything functioning. I've learned so much from Paul, from his deep understanding of the field, to understanding when things go wrong and how to correct them, to finding time to enjoying time outside of research. I appreciate the numerous opportunities Paul has afforded me: from multiple conference trips, a research expedition across the North Atlantic, meeting many experts in our field, to abandoning the Edmonton winter for a trip back to sunny (and warm) California. I couldn't have asked for a better supervisor.

To my parents, both of you inspired me along the way. Who would have thought that all that time in front of a computer, as well as a yearning for math and science, would turn out to be useful and cause me to play around with complex physics models? Dad, thanks for annoying me throughout the years about 'getting a real job' while being jealous of all the cool things and interesting locations I get involved with. Mom, thanks for always having coffee cake and an inviting place waiting for me when I came to visit to do some writing. And thanks to both of you for encouraging me to seek advanced degrees that I found exciting and intellectually stimulating.

To my own little family: Amanda, and our cats: Romeo and Marbles. You are all great role models: Amanda for her constant, unyielding cheerful attitude about everything; Romeo reminding us that we need plenty of relaxation time; and the kitten Marbles to remind us that we all need to experience some of the 'zoomies' from time to time. Without you, I'd likely become a mess. Amanda made sure that we went out and did exciting things, even when crunched for time. Romeo made sure that I sat still and kept him warm; a great environment for analysis and writing. Marbles made for endless entertainment- always romping around and making dinosaur noises. You are the perfect balance to my time working on this thesis, and life in general.

Labmates past and present: Xianmin, the original NEMO expert in our lab and #1 resource. Nathan, for endless time talking (and complaining) about little tiny technical issues that didn't really matter. Yarisbel, for an excellent discussion resource regarding

deepwater and forcing me to grow a beard while crossing the Atlantic. Natasha, for always being able to cheer you up and willing to chat about anything. Laura Kastro, for reminding (and encouraging) us all to enjoy physical exercise even when it was -30° C outside. Laura Gillard, for always being upbeat, even when life as a graduate student wasn't. Charlene Feucher, for reminding us to take time and enjoy the company of everyone here- we share a small piece of time together. Juliana Marson, for exciting discussions ranging from icebergs within the Labrador Sea, to video games while relaxing at home. Vasco Müller, for always being up for a beer and a chat about eddy fluxes following a conference. From travelling together to conferences, chatting about our projects, complaining about NEMO, inner-tube water polo, indoor rock climbing, Pandemic zoom calls, weekly run/bike challenges, to holiday parties- I want to thanks the many labmates I've had over the years.

Table of Contents

List of tables

List of figures

List of defined acronyms

AMOC – Atlantic Meridional Overturning Circulation

ANHA4 – 1/4° Arctic and Northern Hemisphere Atlantic NEMO configuration

ANHA12 – 1/12° Arctic and Northern Hemisphere Atlantic NEMO configuration

AW – Arctic Water

DWBC- Deep Western Boundary Current

EGC – East Greenland Current

EKE – Eddy Kinetic Energy

IW – Irminger Water

LAB60 – 1/60° Labrador Sea NEMO configuration

LC – Labrador Current

LSW – Labrador Sea Water

MLD – Mixed Layer Depth

NAC – North Atlantic Current

NEMO – Nucleus for European Modelling of the Ocean

SPG12 – 1/12° Sub-Polar Gyre NEMO configuration

WGC – West Greenland Current

Chapter 1: Introduction

The Labrador Sea (Figure 1.1), situated within the North Atlantic between Greenland and eastern Canada, is a very dynamic region. During winter, the overriding atmosphere cools the surface of the Labrador Sea to the point that it becomes as dense as the water at depth. Further cooling forces the water column to be vertically unstable, causing vertical mixing and homogenization of the upper water column. This is known as deep convection and it continues as long as the surface is cooling, producing a progressively deeper mixed layer throughout the winter, sometimes exceeding 2000m (Yashayaev, 2007). When the surface of the ocean finally starts warming up in spring, the bottom of the mixed layer returns to the surface, leaving behind a newly ventilated water mass we call Labrador Sea Water (LSW). Large lateral density gradients as a result of convection promote a rapid restratification of the basin (Lilly et al., 1999; Frajka-Williams et al., 2014), while the boundary currents continuously provide buoyant freshwater and heat (Straneo, 2006). This increases the interior Labrador Sea's stratification until winter approaches and the cycle repeats.

Deep convection and LSW formation depends on the delicate balance of buoyancy fluxes that set the overall stratification. Offshore exchange from boundary currents around the Labrador Sea tend to supply buoyancy (Schmidt and Send, 2007; Myers et al., 2009; Kawasaki and Hasumi, 2014; Lin et al., 2018; Schulze-Chretien and Frajka-Williams, 2018) while the atmosphere above the Labrador Sea tends to remove it during winter (Renfrew et al., 2002; Sathiyamoorthy and Moore, 2002; Moore et al., 2011; Duvivier et al., 2016; Schulze-Chretien et al., 2016). Along the eastern side of the basin is the West Greenland Current (WGC). The WGC has cold and fresh Arctic Water at the surface with warmer and saltier Irminger Water underneath (Cuny et al., 2002; Lazier et al., 2002; Chanut et al., 2008; Myers et al., 2009; Rykova et al., 2015; de Jong et al., 2016). This current system flows northwards along the western coast of Greenland. Some of this current splits before reaching Davis Strait and flows westwards, while the rest continues north out of the Labrador Sea into Baffin Bay. The westward branch combines with cold and fresh outflow from both Baffin Bay (Cuny et al., 2005; Curry et al., 2014) and Hudson Strait (Drinkwater 1988; Straneo and Saucier, 2008).

This current system, called the Labrador Current once close to Hudson Strait, flows southwards along the eastern continental slope of Canada. The WGC and Labrador Current contribute a significant amount of heat and freshwater towards the interior Labrador Sea (Schmidt and Send, 2007; Myers et al., 2009; McGeehan and Maslowski, 2011; Schulze-Chretien and Frajka-Williams, 2018), playing a role in the seasonal restratification that takes place. This modifies the stratification which must be eroded before deep convection can begin.
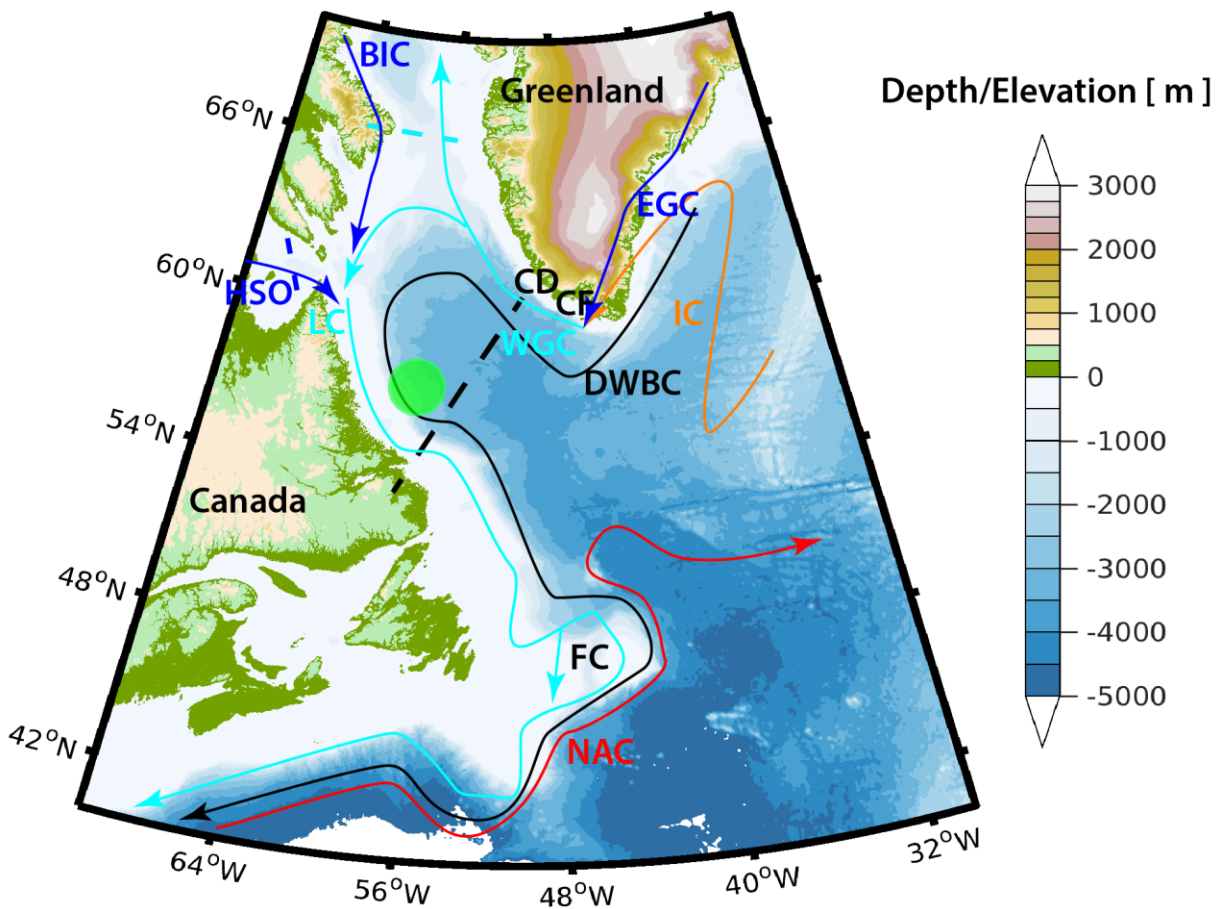
Figure 1. 1: The Labrador Sea includes multiple current systems (BIC= Baffin Island Current; DWBC= Deep Western Boundary Current; EGC= East Greenland Current; HSO= Hudson Strait Outflow; IC= Irminger Current; LC= Labrador Current; NAC= North Atlantic Current; WGC= West Greenland Current). Three sections are marked via dashed lines: AR7W in black, Davis Strait in light blue, and Hudson Strait in blue. A few landmarks are identified; CD for Cape Desolation, CF for Cape Farewell, and FC for Flemish Cap. The translucent green circle is the region where deep convection generally occurs.

1.1. Stratification

Stratification is a measure of the vertical density gradient. Regions with strong stratification resist vertical motion, while regions with weak stratification can overturn given sufficient conditions. The Labrador Sea is a weakly stratified region for multiple reasons. First, this region experiences cyclonic circulation which lifts isopycnals (Lab Sea Group, 1998). This lifting brings denser water closer to the surface (Fig. 1.2a). As this water exists closer to the surface, it is easier to penetrate into this layer. Second, the Arctic and Irminger Water masses above do not produce a very large vertical density gradient (Marshall and Schott, 1999). Third, the atmosphere over the Labrador Sea often drives a significant amount of heat from the region (Lab Sea Group, 1998; Marshall and Schott, 1999; Renfew et al., 2002), eroding the weakly stratified water such that deep convection occurs (Fig. 1.2b). While the atmosphere removes the stratification built up within the Labrador Sea, the boundary currents supply stratification.

1.1.1. Lateral sources of stratification

Arctic Water, being cold and fresh, is the most buoyant water mass within the Labrador Sea. While Arctic Water is colder and fresher than Labrador Sea Water, the nonlinear equation of state shows that Arctic Water's contribution to setting the density gradient is primarily due to the change in salinity; temperature changes are not nearly as important. Most of the focus on this water mass within the Labrador Sea is thus in regards to the volume and salinity of Arctic Water as opposed to the amount of heat contained within. Originating in the Arctic Ocean, Arctic Water has significant freshwater transport through flow through Fram (160 mSv; Dickson et al., 2007), Davis (100 mSv; Cuny et al., 2005; Curry et al., 2011; Curry et al., 2014), and Hudson Strait (40 mSv; Dickson et al., 2007; Straneo and Saucier, 2008). Continental runoff from Greenland (Yu et al., 2016) adds to the freshwater transport within the WGC. While freshwater that comes from Greenland melt is less than what crosses the above sections, Greenland's melt is significantly increasing (Bamber et al., 2012), and model

3
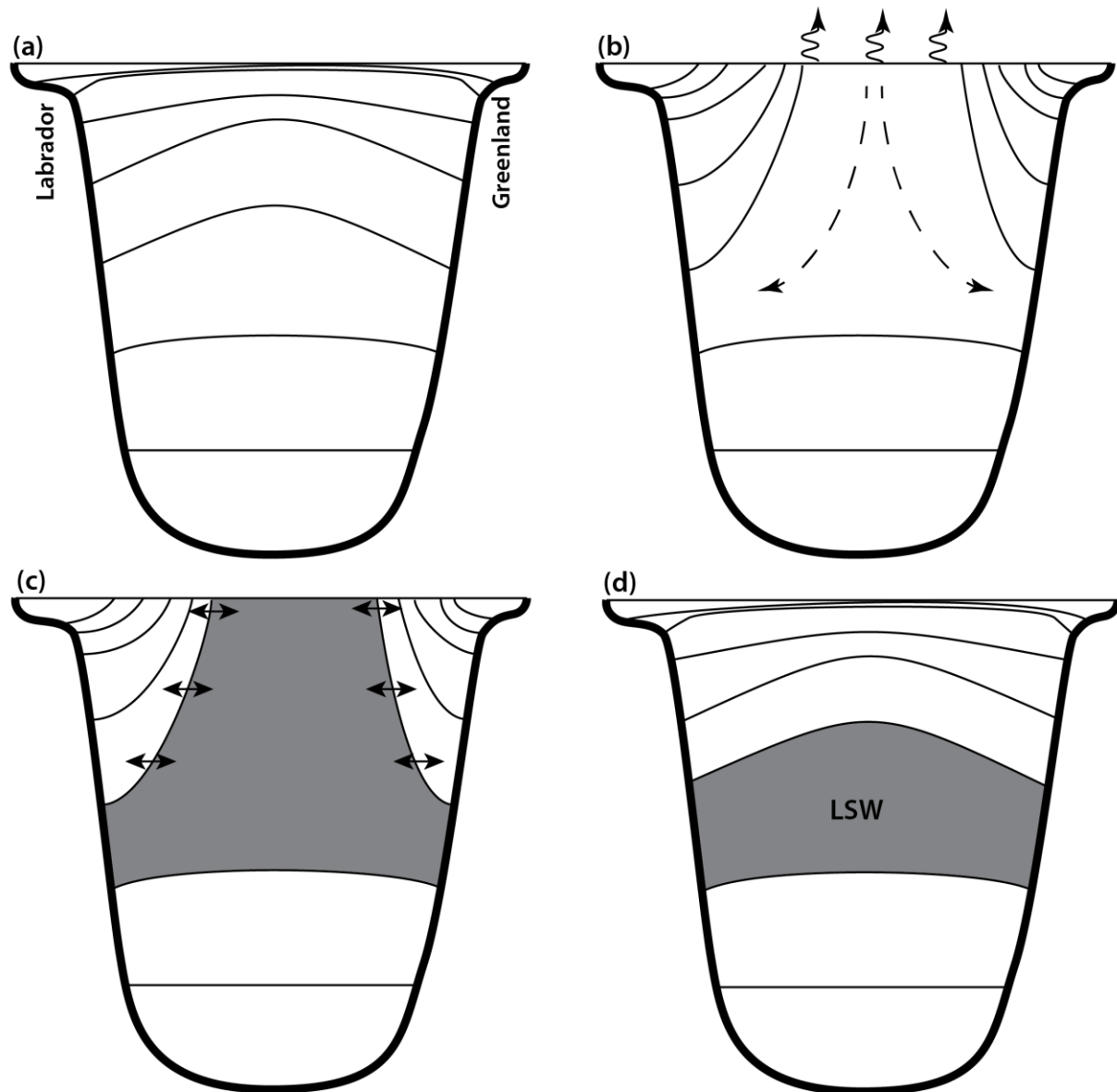
Figure 1. 2: Diagram showing the multiple phases within a region with deep convection: (a) the preconditioned phase with isopycnal doming, (b) active deep convection, (c) the cessation of deep convection, and (d) lateral exchange. Curvy arrows indicate a surface buoyancy loss while dashed curved arrows indicate vertical mixing and spreading. Horizontal arrows indicate lateral mixing across steep isopycnals. Areas highlighted in grey show the volume of Labrador Sea Water produced. Modified from Marshall and Schott, 1999.

simulations suggest that continued Greenland runoff will produce a basin which is too strongly stratified for deep convection to occur within the Labrador Sea (Böning et al., 2016).

There is much interest in where Arctic Water leaves the boundary currents and enters the interior of the Labrador Sea as freshwater strongly controls the convection which can occur (Avisc et al., 2006; Fischer et al., 2010; Böning et al., 2016). Schmidt and Send (2007) identified two seasonal freshening pulses within the interior Labrador Sea, though only one could be attributed to the boundary currents. They found that the WGC was the likely source of this seasonal freshening that takes place between July and September. Schulze-Chretien and Frajka-Williams (2018) explored wind-driven freshwater transport that enters the interior Labrador Sea and found that the majority of near-surface (top 30m) freshwater entered along western Greenland, though there was some transport in the vicinity of Hamilton Bank along the Labrador coast. They found that Ekman transport is responsible for the variability of near-surface Arctic Water which is exported to the inner Labrador Sea. Freshwater also leaves the boundary system at Cape Farwell due to a retroreflection, freshening the interior subpolar gyre (Holliday et al., 2007). Other studies are in agreement that freshwater leaves the western Greenland coast (Myers et al., 2007) and the Labrador coast (McGeehan and Maslowski, 2011). This buoyant water mass's thickness that resides in the surface of the Labrador Sea is subject to changes that occur in the Arctic Ocean.

Major changes within the Arctic Ocean heavily influence the storage/release of its freshwater (Proshutinsky et al., 2009). The Beaufort Gyre occasionally relaxes due to a shift in atmospheric forcing (Belkin et al., 1998; Gelderloos et al., 2012), releasing much more freshwater than otherwise. One such event occurred in the late 1960s, where a significant amount of freshwater exited the Arctic and a large portion entered the East Greenland Current (EGC), travelling around the Labrador Sea. Significant amounts of freshwater leaked offshore, producing a freshwater cap within the Labrador Sea, significantly increasing stratification that prevented deep convection from occurring between 1968 and 1971 (Gelderloos et al., 2012). Convection resumed in 1972 due to extreme atmospheric forcing that occurred during that winter along with advection of salty (fresh) water into (out of) the convection region (Gelderloos et al., 2012).

Irminger Water, much warmer and saltier than Arctic Water, also flows within the WGC and Labrador Current (Myers et al., 2007). Just as freshwater within these currents increases stratification, the heat within the Irminger Water mass does the same

(Straneo, 2006). The Irminger Water layer is much thicker than the Arctic Water layer within these current systems, thus holding a large amount of heat. The heat within the Irminger Water layer, if shed from the boundary current systems, can increase the stratification within the Labrador Sea. Irminger Water, being saltier than Labrador Sea Water, also helps keep the basin weakly stratified by offsetting the freshwater input via Arctic Water.

The West Greenland Current, already strongly baroclinic due to close proximity to the warm and saline water offshore, contains a region around 61° N which promotes the shedding of eddies due to a steepening of topography (Eden and Böning, 2002). These eddies contain both Arctic and Irminger Water. Known as Irminger Rings (Chanut et al., 2008, de Jong et al., 2016), some of these eddies drift westwards from their generation region. The regular release of Irminger Rings supplies sufficient buoyancy to the northern Labrador Sea, both from the surface freshwater as well as heat within, preventing convection in the north (Chanut et al., 2008). These eddies account for about 45% of the total heat which enters the Labrador Sea (Gelderloos et al., 2011; Saenko et al., 2014). While many Irminger Rings travel westward after being formed, some also travel southwestwards into the convection region. However, the amount of buoyancy delivered by these southwestwards Irminger Rings (Hátún et al., 2007; Gelderloos et al., 2011) does not outweigh that of the air-sea buoyancy loss, and convection in this region continues. Irminger Rings are relatively long lived eddies, with a lifespan up to 2 years (Chanut et al., 2008). While their initial significance to stratification in the Labrador Sea has been researched, the impact during the later period of their lifetime is relatively unknown.

1.1.2. Surface sources of stratification

The atmosphere above the Labrador Sea is often colder than the surface of the ocean, driving sensible heat from the ocean to the atmosphere. The air above the Labrador Sea is also drier than the ocean-air interface, driving evaporation and latent heat from the surface. Incident shortwave radiation always warms the ocean, though attenuated slightly from albedo. Outgoing longwave radiation is always negative and

higher in magnitude than incoming longwave radiation. These sensible, latent, and radiative heat fluxes combine to modify the surface temperature, providing a surface positive buoyancy flux (Sathiyamoorthy and Moore, 2002). Evaporation and precipitation, as well as sea ice melt/production modify the surface salinity, further modifying the surface buoyancy flux. While the salinity component of the net buoyancy flux has a lower magnitude than the thermal component, the former is positive while the latter is more often negative (Sathiyamoorthy and Moore, 2002). The combination of these buoyancy fluxes informs us of how the stratification changes in time: positive buoyancy flux will increase stratification strength while a negative buoyancy flux will reduce stratification.

The strongest buoyancy loss occurs during the winter months, February in particular (Schulze-Chretien et al., 2016), driven by the cold dry winds that come out of the northwest. However, the buoyancy loss strongly depends on the latent and sensible heat flux that occurs during winter and every winter is different. The North Atlantic Oscillation (NAO) index describes the pressure difference anomaly between the Azores High and the Icelandic Low. A positive value indicates a stronger pressure difference than normal, while a negative value indicates the opposite. During a positive NAO phase, the stronger pressure gradient generally produces stronger, and more frequent mid-latitude cyclones to pass over the Labrador Sea (Marshall et al., 2001). These storms enhance the latent and sensible heat flux from the ocean to the atmosphere, often removing a significant amount of buoyancy and result in an increase in deep convection (Yashayaev and Loder 2016; Curry et al., 1998). During a negative NAO phase, the storms within the Labrador Sea are often weaker, with winds coming from warmer regions, reducing the heat flux from the ocean (Yashayaev, 2007), likely resulting in weaker deep convection.

The latent and sensible heat fluxes are strongly controlled by the air-sea differences in humidity, temperature, and speed. Thus, strong mid-latitude cyclones which frequent the region during winter, bringing relatively dry, cold, and windy conditions, remove considerable heat from the ocean. Research carried out investigating the impact of these storms shows that the lack of their presence significantly reduces convection in the Labrador Sea (Holdsworth and Myers, 2015) as well as the production

rate and density of LSW (Garcia-Quiantana et al., 2019). Bramson (1997) showed that alterations in the atmospheric forcing (wind stress and precipitation) influenced the Labrador Sea's mixed layer. Storm frequency and wind speed appear to play a lesser role than the path which these cyclones take across the North Atlantic (Schulze-Chretien et al., 2016). Unrelated to mid-latitude cyclones, strong winds that occur over the southern tip of Greenland remove a large amount of heat from both the Labrador and Irminger Seas (Moore et al., 2011; Duvivier et al., 2016). The combination of buoyancy fluxes that arise from atmospheric forcing strongly control the stratification and degree of deep convection.

1.2. Deep convection and restratification seasons

Deep convection is a relatively rare occurrence known to occur across a handful of locations. These regions include the northern Atlantic where deep convection occurs within the Labrador Sea (Lazier et al., 2002; Yashayaev and Loder, 2009; Yashayaev and Loder, 2016; Yashayaev and Loder 2017), Irminger Sea (Bacon et al., 2003), and Nordic Seas (Hansen and Østerhus, 2000), though convection also forms deep water within the Mediterranean Sea (Marshall and Schott 1999; Brossier et al., 2017). Within the southern hemisphere, deep convection only occurs within the Weddell and Ross Seas near Antarctica (Whitworth and Orsi, 2006; Gordon et al., 2007). The above regions share similar characteristics that promote deep convection within the Labrador Sea: circulation which causes isopycnal doming as well as strong air-sea forcing that removes buoyancy.

The deep convection season is short, limited to part of the winter and spring seasons. These months have reduced solar input which keeps the buoyancy gain low. Furthermore, air-sea interactions are amplified during this time as winter storms often bring stronger, colder, and drier winds over these regions. These storms enhance the latent and sensible heat loss, further increasing the buoyancy loss from the ocean. Deep convection begins once the buoyancy loss erodes the surface stratification, allowing mixing to great depths. This vertical mixing is not only a pathway for salt and heat, but also for gases (Fröb et al., 2016) and turbulent energy supplied by wind stress (Yu and

Wei., 2018). Along the boundary of the convection path, baroclinic instability produces small convective eddies (Chanut et al., 2008; Gelderloos et al., 2011). These convective eddies exchange properties across the convective front in an attempt to restratify the region. Convection ceases when the ocean's surface starts to gain buoyancy (Fig. 1.2c), a combination of less frequent stormy weather as well as increased solar heating. The mixed layer then shallows to the surface, leaving behind a homogenous water mass with properties dependent on the region in which it was produced (Fig. 1.2d).

As the deep convection season removes stratification from the ocean, the remainder of the year is known as the restratification season. Large horizontal density gradients produced and maintained during the convection season quickly restratify the Labrador Sea after convection ends. This rapid restratification process lasts 2-3 months (Lilly et al., 1999; Frajka-Williams et al., 2014). The boundary currents around the Labrador Sea export their water mass properties towards the interior, slowly modifying the temperature and salinity of the interior basin (Straneo, 2006). This promotes the surface of the Labrador Sea to become fresher and colder while the underlying layer becomes warmer and saltier (Straneo, 2006). Unlike the rapid restratification process driven by large horizontal density gradients, this gradual restratification process occurs throughout the year.

The yearly supply and removal of buoyancy from the Labrador Sea determines a sort of convective inertia. Years with very strong buoyancy loss keep the Labrador Sea weakly stratified; convection the following year may start earlier and result in much deeper convection with minimal change in air-sea forcing (Lab Sea Group, 1998; Lazier et al., 2002; Yashayaev, 2007; Yashayaev and Loder, 2017). In contrast, a year with weak buoyancy loss can leave the Labrador Sea more strongly stratified such that the following year convection would be reduced. This sort of positive feedback often emerges when the NAO index remains in a prolonged positive (progressively deeper mixing) or negative (progressively weaker mixing) phase, as pointed out by Yashayaev (2007). The late 1980s through mid 1990s experienced a prolonged positive NAO phase and LSW produced up through 1994 was generally colder, denser, and thicker than the previous year (Yashayaev, 2007). While this convective inertia might predict the Labrador Sea to be more (less) preconditioned to deep convection, weaker (stronger)

atmospheric forcing can overcome the inertia (Pickart et al., 2002; Schulze-Chretien et al., 2016). Furthermore, changes in the lateral buoyancy flux can overpower the inertia and help initiate/prevent deep convection (Gelderloos et al., 2012).

1.3. Labrador Sea Water

The product of deep convection in the Labrador Sea produces a characteristic water mass, Labrador Sea Water. Labrador Sea Water is a mixture of the water masses above which were cooled sufficiently to allow vertical mixing. The result is water which is relatively cold and salty with intermediate density (1027.68 to 1027.80 kg m^{-3}), capable of being over 1000m thick (Yashayaev 2007; Yashayaev and Loder, 2009; Yashayaev and Loder, 2016; Yashayaev and Loder, 2017). After formation, Labrador Sea Water exits the Labrador Sea, either quickly via the Deep Western Boundary Current (Gary et al., 2012), or slowly spreading across the North Atlantic (Kieke et al., 2009; Holliday et al., 2009).

Labrador Sea Water is one part of the Atlantic Meridional Overturning Circulation (AMOC), the large-scale overturning system that brings warm equatorial surface water towards the poles while returning dense freshly-ventilated water at depth. The AMOC transports a very large amount of heat across the latitudes to deal with the unequal distribution of heating the Earth experiences. The AMOC has two limbs: the shallow limb which flows from equator toward the northern polar region, and the deep limb which flows in the opposite direction at depth. Labrador Sea Water is the lightest component of the deep AMOC limb (Dengler et al., 2006; Gary et al., 2012; Rhein et al., 2015), residing above other deep water formed in the north eastern Atlantic (Swift, 1984; Jonsson and Valdimarsson, 2004). Labrador Sea Water production has been linked to the northward AMOC, as changes within the deep limb impact the northward heat transport within the shallow limb (Chen and Tung, 2018). For example, a significant supply of freshwater into the interior of the Labrador Sea can limit convection, producing less LSW, eventually reducing the northward AMOC strength (Böning et al., 2016; Yang et al., 2016; Yu et al., 2016; Jackson and Wood, 2018). As the AMOC transports significant amounts of heat (Bryden et al., 2005) and dissolved

gasses, upstream changes in stratification are important to investigate. The Overturning in the Subpolar North Atlantic Program (OSNAP; Lozier et al., 2017), while still early in its monitoring, has investigated relative importance on the deepwater formed in the different basins within the subpolar gyre (Li et al., 2017). Recent OSNAP research suggests that the Labrador Sea may not be as strongly linked to the AMOC as previously determined (Li et al., 2019), although much more research remains.

1.4.   Thesis Objectives and Outline

This thesis focuses on stratification within the Labrador Sea. In particular, I examine lateral and vertical factors that modify the stratification. My first objective explores regions around the Labrador Sea where freshwater leaves the boundary current, exporting freshwater into the interior of the Labrador Sea, increasing stratification (O1). We know that freshwater leaves the WGC and LC, freshening the Labrador Sea, but relatively little apart from that. This objective explores the net offshore freshwater transport along the entire boundary current system around the Labrador Sea. Freshwater transport is separated into mean and turbulent transport, estimating the contribution from eddies and mesoscale features. As observations are relatively sparse and are not able to provide these transports, this is carried out in both an eddy-permitting (1/4°) and eddy-resolving (1/12°) numerical simulation. This objective will contribute to our knowledge on the regional importance of the boundary current system around the Labrador Sea. Some regions are expected to provide a significant exchange with the interior Labrador Sea, others are not. This is particularly important for future changes in our climate system that produce unequal regional freshening.

My second objective (O2) investigates vertical contributions to the stratification of the Labrador Sea. The atmosphere removes buoyancy from the Labrador Sea, weakening the stratification and priming the sea for deep convection. Others have explored how large changes in atmospheric forcing influences Labrador Sea Water production and density, but many of these studies examine unrealistic forcing. There are many atmospheric forcing products available to run ocean models, yet they all differ in

minor ways. These products generally use methods to reduce biases as much as possible, indicating that their forcing data is fairly accurate. This objective explores if small differences between relatively accurate atmospheric forcing products can produce significant differences in the production rate of Labrador Sea Water. This objective contains five simulations with identical settings other than the atmospheric product. The resulting heat, freshwater, and radiative fluxes produce changes in the surface buoyancy removal, the degree of stratification, deep convection, and eventually the volume and density of Labrador Sea Water. This objective shows that small changes in the surface forcing can significantly influence the Labrador Sea. This objective adds to our knowledge on the Labrador Sea by indicating that this basin is very sensitive to surface forcing. One does not need to dampen winter storms, reduce the NAO signal- simply using another realistic atmospheric forcing dataset is enough to alter the production of Labrador Sea Water.

My third and final objective (O3) investigates how Irminger Rings, relatively buoyant eddies produced from the WGC, evolve throughout their lifetime in the Labrador Sea. These eddies carry an imprint of their formation region as they flow downstream. As their rotation keeps them relatively protected from lateral mixing, Irminger Rings are modified primarily by the atmosphere above. This objective thus contains a feature within the Labrador Sea that is influenced by both vertical and lateral stratification. Irminger Rings are relatively small and observational efforts are not adequate to examine how such eddies evolve as they transit the Labrador Sea; very high resolution numerical modelling is needed. This objective uses a 1/60° numerical simulation to carry out 15+ years to understand how these eddies evolve as they carry very buoyant water through the Labrador Sea. Irminger Rings are often studied in regards to their initial properties, their trajectory, or perhaps what allows them to form. All studies identify that their inclusion in numerical models is vital to spatial extent and depth of deep convection. However, there is essentially no work carried out on how these eddies evolve from their initially very-buoyant state along the WGC. Our study is the first to identify how these eddies age. Furthermore, this objective also answer the question on the fate of eddies which experience 2 convective winter periods- they often reach a mixed layer and density that suggests the production of Labrador Sea Water

within an Irminger Ring. While rare, this reforms our previous definition of Irminger Rings, which were described as eddies that hinder convection due to their large initial heat and freshwater reserves. Ironically, they can also act as an oasis for the formation of Labrador Sea Water.

The organization of this thesis is the following: Chapter 1 contains the introduction material crucial to understanding the content of this thesis. Chapter 2 is comprised of the numerical model and associated components required for our simulations. Chapter 3 comprises of a description of the high-resolution configuration required for Chapter 6. Chapter 4 investigates the cross-shelf transport of freshwater from the boundary currents into the interior of the Labrador Sea (O1). Chapter 5 investigates the role that different atmospheric forcing products have on driving NEMO simulations within the Labrador Sea, focused on Labrador Sea Water production and density (O2). Chapter 6 investigates Irminger Rings that spawn from the West Greenland Current and documents how their properties change throughout their lifetime (O3). Chapter 7 summarizes the findings of this thesis and presents some future work that could follow.

Bibliography

Avisc, T., Karstensen, J., Send, U. and Fischer, J. (2006). Interannual variability of newly formed Labrador Sea Water from 1994 to 2005. Geophysical Research Letters, 33, 6p.

Bacon, S., Gould, W.J. and Jia, Y. (2003). Open-ocean convection in the Irminger Sea. Geophysical Research Letters, 30(5), 4p.

Bamber, J., van den Broeke, M., Ettema, J., Lenaerts, J. and Rignot, E. (2012). Recent large increases in freshwater fluxes from Greenland into the North Atlantic. Geophysical Research Letters, 39, 1-4p.

Belkin, I.M., Levitus, S., Antonov, J. and Malmberg, S.A. (1998). "Great salinity anomalies" in the North Atlantic. Progress in Oceanography, 41(1), 1-68.

Böning, C.W., Behrens, E., Biastoch, A., Getzlaff, K. and Bamber, J.L. (2016). Emerging impact of Greenland meltwater on deepwater formation in the North Atlantic Ocean. Nature Geoscience, 97(7), 523.

Bramson, L.S. (1997). Air-sea interactions and deep convection in the Labrador Sea. M.S. thesis, Dept. of Oceanography. Naval Postgraduate School, 115 pp.

Bryden, H.L., Longworth, H.R. and Cunningham, S.A. (2005). Slowing of the Atlantic meridional overturning circulation at 25°N. Nature, 438(7068), 655.

Chanut, J., Barnier, B., Large, W., Debreu, L., Penduff, T., Molines, J.M. and Mathiot, P. (2008). Mesoscale eddies in the Labrador Sea and their contribution to convection and restratification. Journal of Physical Oceanography, 28(8), 1617-1643.

Chen, X., and Tung, K.K. (2018). Global surface warming enhanced by weak Atlantic overturning circulation. Nature, 559(7714), 387.

Cuny, J., Rhines, P.B., Niiler, P.P. and Bacon, S. (2002). Labrador Sea boundary currents and the fate of the Irminger Sea Water. Journal of Physical Oceanography, 32(2), 627-647.

Cuny, J., Rhines, P.B., and Kwok, R. (2005). Davis Strait volume, freshwater and heat fluxes. Deep Sea Research Part I: Oceanographic Research Papers, 52.3, 519-542.

Curry, B., Lee, C.M., Petrie, B., Moritz, R.E. and Kwok, R. (2014). Multiyear volume, liquid freshwater, and sea ice transports through Davis Strait, 2004-10. Journal of Physical Oceanography, 44(4), 1244-1266.

Curry, B., Lee, C.M., and Petrie, B. (2011). Volume, freshwater, and heat fluxes through Davis Strait, 2004-05. Journal of Physical Oceanography, 41(3), 429-436.

Curry, R.G., McCartney, M.S. and Joyce, T.M. (1998). Oceanic transport of subpolar climate signals mid-depth subtropical waters. Nature, 391(6667), 575.

Dengler, M., Fischer, J., Schott, F.A., and Zantopp, R. (2006). Deep Labrador Current and its variability in 1996-2005. Geophysical Research Letters, 13, 1-5p.

Dickson, R., Rudels, B., Dye, S., Karcher, M., Meincke, J. and Yashayaev, I. (2007). Current estimates of freshwater flux through Arctic and subarctic seas. Progress in Oceanography, 73(3-4), 210-230.

Duvivier, A.K., Cassano, J.J., Craig, A., Hamman, J., Maslowski, W., Nijssen, B., Osinski, R. and Roberts, A. (2016). Winter atmospheric buoyancy forcing and oceanic response during String Wind Events around Southeastern Greenland in the Regional Arctic System Model (RASM) for 1990-2010. Journal of Climate, 29(3), 975-994.

Eden, C., and Böning, C. (2002). Sources of eddy kinetic energy in the Labrador Sea. Journal of Physical Oceanography, 32(12), 3346-3363.

Fischer, J., Visbek, M., Zantopp, R. and Nunes, N. (2010). Interannual to decadal variability of outflow from the Labrador Sea. Geophysical Research Letters, 37(24), 5p.

Frajka-Williams, E., Rhines, P.B. and Eriksen, C.C. (2014). Horizontal stratification during deep convection in the Labrador Sea. Journal of Physical Oceanography, 44(1), 220-228.

Fröb, F., Olsen, A., Våge, K., Moore, G.W.K., Yashayaev, I., Jeansson, E. and Rajasakaren, B. (2016). Irminger Sea deep convection injects oxygen and anthropogenic carbon to the ocean interior. Nature communications, 7, 13244.

Garcia-Quintana, Y., Courtois, P., Hu, X., Pennelly, C., Kieke, D. and Myers, P.G. (2019). Sensitivity of Labrador Sea Water formation to changes in model resolution, atmospheric forcing, and freshwater input. Journal of Geophysical Research: Oceans, 124(3), 2126-2152.

Gary, S.F., Lozier, M.S., Biastoch, A. and Böning, C.W. (2012). Reconciling tracer and gloat observations of the export pathways of Labrador Sea Water. Geophysical Research Letters, 39(24).

Gelderloos, R., Katsman, C.A. and Drijfhout, S.S. (2011). Assessing the roles of three eddy types in restratifying the Labrador Sea after deep convection. Journal of Physical Oceanography, 41(11), 2102-2119.

Gelderloos, R., Straneo, F. and Katsman, C.A. (2012). Mechanisms behind the temporary shutdown of deep convection in the Labrador Sea: Lessons from the great salinity anomaly years 1968-71. Journal of Climate, 25(19), 6743-6755.

Gordon, A.L., Visbeck, M. and Comiso, J.C. (2007). A possible link between the Weddell Polynya and the Southern Annular Mode. Journal of Climate, 20(11), 2558-2571.

Hansen, B., and Østerhus, S. (2000). North Atlantic-Nordic Seas exchanges. Progress in Oceanography, 45(2), 109-208.

Hátún, H., Eriksen, C.C. and Rhines, P.B. (2007). Buoyant eddies entering the Labrador Sea observed with gliders and altimetry. Journal of Physical Oceanography, 37(12), 2838-2854.

Holdsworth, A.M. and Myers, P.G. (2015). The influence of high-frequency atmospheric forcing on the circulation and deep convection of the Labrador Sea. Journal of Climate, 28(12), 4980-4996.

Holliday, N.P., Meyer, A., Bacon, S., Alderson, S.G., and de Cuevas, B. (2007). Retroreflection of part of the east Greenland current at Cape Farewell. Geophysical Research Letters, 34(7).

Holliday, N.P., Bacon, S., Allen, J. and McDonagh, E.L. (2009). Circulation and transport in the western boundary currents are Cape Farewell, Greenland. Journal of Physical Oceanography, 39(8), 1854-1870.

Jackson, L.C. and Wood, R.A. (2018). Hysteresis and Resilience of the AMOC in an Eddy-Permitting GCM. Geophysical Research Letters, 45(16), 8547-8556.

de Jong, M.F., Bower, A.S. and Furey, H.H. (2016). Seasonal and interannual variations of Irminger ring formation and boundary-interior heat exchange in FLAME. Journal of Physical Oceanography, 46(6), 1717-1734.

Jonsson, S. and Valdimarsson, H. (2004). A new path for the Denmark Strait overflow water from the Iceland Sea to Denmark Strait. Geophysical Research Letters, 31(3).

Kawasaki, T. and Hasumi, H. (2014). Effect of freshwater from the West Greenland Current on the winter deep convection in the Labrador Sea. Ocean Modelling, 75, 51-64.

Kieke, D., Klein, B., Stramma, L., Rhein, M. and Koltermann, K.P. (2009). Variability and propagation of Labrador Sea Water in the southern subpolar North Atlantic. Deep Sea Research Part I: Oceanographic Research Papers, 56(10), 1656-1674.

Lab Sea Group (1998). The Labrador Sea deep convection experiment. Bulletin of the American Meteorological Society, 79(10), 2033-2058.

Lazier, J., Hendry, R., Clarke, A. Yashayaev, I. and Rhines, P. (2002). Convection and restratification in the Labrador Sea, 1990-2000. Deep Sea Research Part I: Oceanographic Research Papers, 49(10), 1819-1835.

Li, F., Lozier, M.S. and Johns, W.E. (2017). Calculating the meridional volume, heat, and freshwater transports from an observing system in the subpolar North Atlantic: Observing system simulation experiment. Journal of Atmospheric and Oceanic Technology, 34(7), 1483-1500.

Li, F., Lozier, M.S., Danabasoglu, G., Holliday, N.P., Kwon, Y.O., Romanou, A., Yeager, S.G. and Zhang, R. (2019). Local and downstream relationships between Labrador Sea Water volume and North Atlantic Meridional Overturning Circulation variability. Journal of Climate, 32(13), 3883-3898.

Lilly, J.M., Rhines, P.B., Visbeck, M., Davis, R., Lazier, J.R.N., Schott, F. and Farmer, D. (1999). Observing deep convection in the Labrador Sea during winter 1994/95. Journal of Physical Oceanography, 29, 2065-2098.

Lin, P., Pickart, R.S., Torres, D.J. and Pacini, A. (2018). Evolution of the freshwater coastal current at the southern tip of Greenland. Journal of Physical Oceanography, 48(9), 2127-2140.

Lozier, M.S., Bacon, S., Bower, A.S., Cunningham, S.A., de Jong, M.F., de Steur, L., deYoung, B., and coauthors (2017). Overturning in the Subpolar North Atlantic Program: A new international ocean observing system. Bulletin of the American Meteorological Society, 98(4), 737-752.

Marshal, J., Jognson, H. and Goodman, J. (2001). A study of the interaction of the North Atlantic Oscillation with ocean circulation. Journal of Climate, 14(7), 1399-1421.

Marshall, J. and Schott, F. (1999). Open-ocean convection: Observations, theory, and models. Reviews of Geophysics, 37(1), 1-64.

McGeehan, I. and Maslowski, W. (2011). Impact of shelf-basin freshwater transport on deep convection in the western Labrador Sea. Journal of Physical Oceanography, 41(11), 2187-2210.

Moore, G.W.K., Pickart, P.S. and Renfrew, I.A. (2011). Complexities in the climate of the subpolar North Atlantic: a case study from the winter of 2007. Quarterly Journal of the Royal Meteorological Society, 137(656), 757-767.

Myers, P.G., Donnelly, C. and Ribergaard, M.H. (2009). Structure and variability of the West Greenland Current in Summer derived from 6 repeat standard sections. Progress in Oceanography, 80(1-2), 93-112.

Myers, P.G., Kulan, N. and Ribergaard, M.H. (2007). Irminger water variability in the West Greenland Current. Geophysical Research Letters, 34(17).

Pickart, R.S., Torres, D.J. and Clarke, R.A. (2002). Hydrography of the Labrador Sea during active convection. Journal of Physical Oceanography, 32(2), 428-457.

Proshutinsky, A., Krishfield, R., Timmermans, M-L., Toole, J., Carmack, E., McLaughlin, F., Williams, W.J., Zimmermann, S., Itoh, M. and Shimada, K. (2009). Beaufort Gyre freshwater reservoir: State and variability from observations. Journal of Geophysical Research, Vol 114, 1-25pp.

Renfrew, I.A., Moore, G.W.K., Guest, P.S. and Bumke, K. (2002). Comparison of Surface Layer and Surface Turbulent Flux Observations over the Labrador Sea with ECMWF Analysis and NCEP Reanalysis. Journal of Physical Oceanography, 32, 383-400.

Rhein, M., Kieke, D. and Steinfeldt, R. (2015). Advection of North Atlantic Deep Water from the Labrador Sea to the southern hemisphere. Journal of Geophysical Research: Oceans, 120(4), 2471-2487.

Rykova, T. Straneo, F. and Bower, A.S. (2015). Seasonal and interannual variability of the West Greenland Current System in the Labrador Sea in 1993-2008. Journal of Geophysical Research: Oceans, 120(2), 1318-1332.

Saenko, O.A., Dupont, F., Yang, D., Myers, P.G., Yashayaev, I. and Smith, G.C. (2014). Role of resolved and parameterized eddies in the Labrador Sea balance of heat and buoyancy. Journal of Physical Oceanography, 44(12), 3008-3032.

Sathiyamoorthy, S. and Moore G.K. (2002). Buoyancy flux at ocean weather station Bravo. Journal of Physical Oceanography, 31(2), 458-474.

Schmidt, S. and Send, U. (2007). Origin and composition of seasonal Labrador Sea freshwater. Journal of Physical Oceanography, 37(6), 1445-1454.

Schulze-Chretien, L.M. and Frajka-Williams, E. (2018). Wind-driven transport of fresh shelf water into the upper 30m of the Labrador Sea. Ocean Science, 14(5), 1247-1264.

Schulze-Chretien, L.M., Pickart, R.S. and Moore, G.W.K. (2016). Atmospheric forcing during active convection in the Labrador Sea and its impact on mixed-layer-depths. Journal of Geophysical Research: Oceans, 121(9), 6978-6992.

Straneo, F. (2006). Heat and freshwater transport through the central Labrador Sea. Journal of Physical Oceanography, 36(4), 606-628.

Straneo, F. and Saucier, F. (2008). The outflow from Hudson Strait and its contribution to the Labrador Current. Deep Sea Research Part I: Oceanographic Research Papers, 55(8), 926-946.

Yashayaev, I. (2007). Hydrographic changes in the Labrador Sea, 1960-2005. Progress in Oceanography, 73(3-4), 242-276.

Yashayaev, I. and Loder, J.W. (2009). Enhanced production of Labrador Sea water in 2008. Geophysical Research Letters, 36(1).

Yashayaev, I. and Loder, J.W. (2016). Recurrent replenishment of Labrador Sea Water and associated decadal-scale variability. Journal of Geophysical Research: Oceans, 121(11), 8095-8814.

Yashayaev, I. and Loder, J.W. (2017). Further intensification of deep convection in the Labrador Sea in 2016. Geophysical Research Letters, 44(3), 1429-1438.

Yang, Q., Dixon, T.H., Myers, P.G., Bonin, J., Chambers, D., van den Broeke, M.R., Ribergaard, M.H. and Mortensen, J. (2016). Recent increases in Arctic freshwater flux affects Labrador Sea convection and Atlantic overturning circulation. Nature Communications, 7.1, 8p.

Yu, J., Gao, Y. and Otterå, O.H. (2016). The sensitivity of the Atlantic Meridional Overturning Circulation to enhanced freshwater discharge along the entire, eastern and western coast of Greenland. Climate Dynamics, 46(5-6), 1351-1369.

Yu. Z., and Wei, W. (2018). Convection: a neglected pathway for downward transfer of wind energy in the oceanic mixed layer. Journal of Oceanology and Limnology. 36.4, 1189-1197.

Chapter 2: Modelling framework

2.1. Nucleus for European Modelling of the Ocean (NEMO)

The Nucleus for European Modelling of the Ocean (NEMO) modelling framework is used across all chapters of this thesis. NEMO contains multiple components which can be coupled together. These include the ocean (OPA; Madec, et al., 1998), sea-ice (LIM2; Fichefet and Maqueda, 1997; Bouillon et al., 2009), passive tracers (TOP), and biogeochemistry (PISCES) components. A few other components exist that can be coupled to NEMO, including an assimilation component (TAM), a coupler which allows for other models (i.e. weather) to pass information back and forth (OASIS; Valcke et al., 2006), an iceberg model (ICB), as well as an adaptive mesh refinement tool (AGRIF; Debreu et al., 2008). This thesis uses the ocean, sea-ice, and mesh refinement components, which will be discussed in order below. The passive tracer component is also used, though no analysis takes place on these tracers and is not discussed here.

2.1.1. Model Approximations

NEMO simulations always contain a state of the art numerical ocean model, OPA. While the equations which govern the flow of fluids are well represented, some approximations are carried out in the interest of simplicity, computing cost, and programming difficulty. The NEMO model has six such approximations. They are as follows:

1) Spherical Earth approximation: The Earth is treated as a sphere and the resulting gravity vector is parallel to the radius of the Earth.
2) Thin-Shell approximation: The ocean's depth is very shallow (0-10km) compared to the radius of the Earth (6400 km). The effect of the ocean's depth on the force of gravity is thus neglected.
3) Turbulent closure approximation: Turbulent fluxes, which may be sub-grid in nature, are expressed within large scale features.

4) Boussinesq approximation: variations in density are only used to determine the buoyancy force.

5) Hydrostatic approximation: The vertical momentum equation is balanced between the vertical pressure gradient and the buoyancy force. This prevents the explicit representation of convection which must be parameterized.

6) Incompressibility approximation: The divergence of the velocity vector is zero.

2.1.2. Primitive Equations

The NEMO model has 6 primitive equations which govern the state of the ocean. They are the momentum equation (2.1), hydrostatic equilibrium (2.2), incompressibility equation (2.3), conservation equation for heat (2.4), conservation equation for salt (2.5), and the equation of state (2.6). They are as follows:

$$\frac{\partial U_h}{\partial t} = - \left[(\nabla \times U) \times U + \frac{1}{2}\nabla U^2 \right]_h - fk \times U_h - \frac{1}{\rho}\nabla_h p + D^U + F^U \tag{2.1}$$

$$\frac{\partial p}{\partial z} = -\rho g \tag{2.2}$$

$$\nabla \cdot U = 0 \tag{2.3}$$

$$\frac{\partial T}{\partial t} = -\nabla \cdot (TU) + D^T + F^T \tag{2.4}$$

$$\frac{\partial S}{\partial t} = -\nabla \cdot (SU) + D^S + F^S \tag{2.5}$$

$$\rho = \rho(T, S, p) \tag{2.6}$$

The terms are defined as: U is the 3 dimensional velocity vector, h is a subscript denoting the horizontal component, f is the Coriolis parameter, k denotes the vertical component, ρ is the in-situ density, p is the pressure, g is the gravitational acceleration, T is the potential temperature, S is the salinity, while D denotes parameterization of small scale features, and F is the surface forcing terms.

2.1.3. Boundary Conditions

The ocean is constrained by numerous boundaries. Below, and laterally, solid earth exists. Above the ocean is the atmosphere, sea-ice, or a combination of both. Along

the coastline, significant amounts of river runoff enter the ocean. These boundary conditions must be prescribed to accurately simulate the ocean:

Land-ocean boundary: The freshwater within river runoff can promote regions of the ocean to have a dramatically reduced salinity than the open ocean nearby. All simulations use runoff data to supply freshwater and glacial melt along the coastline.

Solid Earth-ocean boundary: Our simulations do not allow a flux of heat and salt through the sea floor. Momentum also has zero flow across a solid boundary, and must have a velocity parallel to the ocean bottom. This is expressed by

$$w = -U_h \cdot \nabla_h(H) \tag{2.7}$$

where H is the depth of the sea floor and w is the vertical velocity. While no momentum is transferred across a solid boundary, the solid boundary provides friction across a small boundary layer. The friction is parameterized for bottom and lateral boundary conditions as the vertical and horizontal grid spacing are not fine enough (~1m) to resolve such a boundary. Across our simulations we use a non-linear quadratic bottom friction and a free-slip lateral boundary condition.

Atmosphere-ocean boundary: changes in the sea surface height (η) as well as a flux of freshwater via precipitation (P) and evaporation (E) promote a change in the vertical velocity:

$$w = \frac{\partial \eta}{\partial t} + U_h|_{z=\eta} \cdot \nabla_h(\eta) + P - E \tag{2.8}$$

Multiple air-sea heat fluxes exist, including from both solar and longwave radiation, precipitation and evaporation. The atmosphere and ocean exchange momentum and heat via turbulent processes. These heat and freshwater fluxes are calculated from CORE bulk formulae (Large and Yeager, 2008). The following are equations which govern the supply of heat and momentum between the atmosphere and ocean where ice is not present:

$$Q_S = Q_I(1 - \alpha) \tag{2.9}$$

$$Q_L = Q_D - \sigma(SST)^4 \tag{2.10}$$

$$Q_P = P * \Delta T * c_{pw} + Snow * \Delta T * c_{pi} - Snow * L_f \tag{2.11}$$

$$Q_E = -E * SST * c_{pw} \tag{2.12}$$

$$\tau = \rho C_D |\Delta U| \Delta U \tag{2.13}$$

$$Q_{TL} = \rho L_v C_E (q_a - q_o) |\Delta U| \tag{2.14}$$

$$Q_{TS} = \rho c_{pa} C_H (T_a - SST) |\Delta U| \tag{2.15}$$

where Q_S is the net solar flux, Q_I is the solar insolation at the surface, α is the surface albedo, Q_L is the net longwave radiation flux, Q_D is the incident downwelling longwave radiation on the surface, σ is the Stefan-Boltxmann constant (5.67 x 10^{-8} W m^{-2} K^{-4}), Q_P is the heat flux due to precipitation, ΔT is the temperature difference between air and the sea surface, c_{pw} is the specific heat capacity of water (3991 J kg^{-1} °C^{-1}), c_{pi} is the specific heat capacity of ice (2067 J kg^{-1} °C^{-1}), L_f is the latent heat of fusion 0.334 x 10^6 J kg^{-1}), Q_E is the evaporation heat flux, E is the evaporation rate, τ is the wind stress, Q_{TL} is the heat flux via latent processes, Q_{TS} is the heat flux via sensible processes, ΔU is the scalar difference between the air velocity and ocean velocity, L_v is the latent heat of vaporization (2.5 x 10^6 J kg^{-1}), c_{pa} is the specific heat of air (1000.5 J kg^{-1} °C^{-1}), q is the specific humidity, T_a is the air temperature, and C_D, C_E, and C_H are transfer coefficents.

Sea-Ice-Ocean boundary: An exchange of heat, salt, and momentum occurs at the interface between the ocean and sea-ice. The sea surface temperature is set to that of the sea-ice where present. As the freezing and melting of sea ice produces a flux of salt, heat, and freshwater, sea ice is crucial in numerical ocean simulations. The sea-ice model will be described later.

2.1.4. Grid Structure

Our NEMO simulations use a curvilinear z-coordinate system and we use the option which keeps the vertical levels invariant in time. The vertical coordinate system is at specified depths, though we also enforce partial steps (Barnier et al., 2006) to better resolve the local topography and the flow near the seafloor. Vertical spacing is not

linear, as grid spacing is higher resolution close to the ocean's surface (~1 m thick) than it is at depth (hundreds of meters; see Fig. 2.1). This is carried out to keep the high spatial features with the upper ocean and mixed layer relatively well resolved. Deep water tends to have far less spatial variability and does not require such high resolution as at the surface.
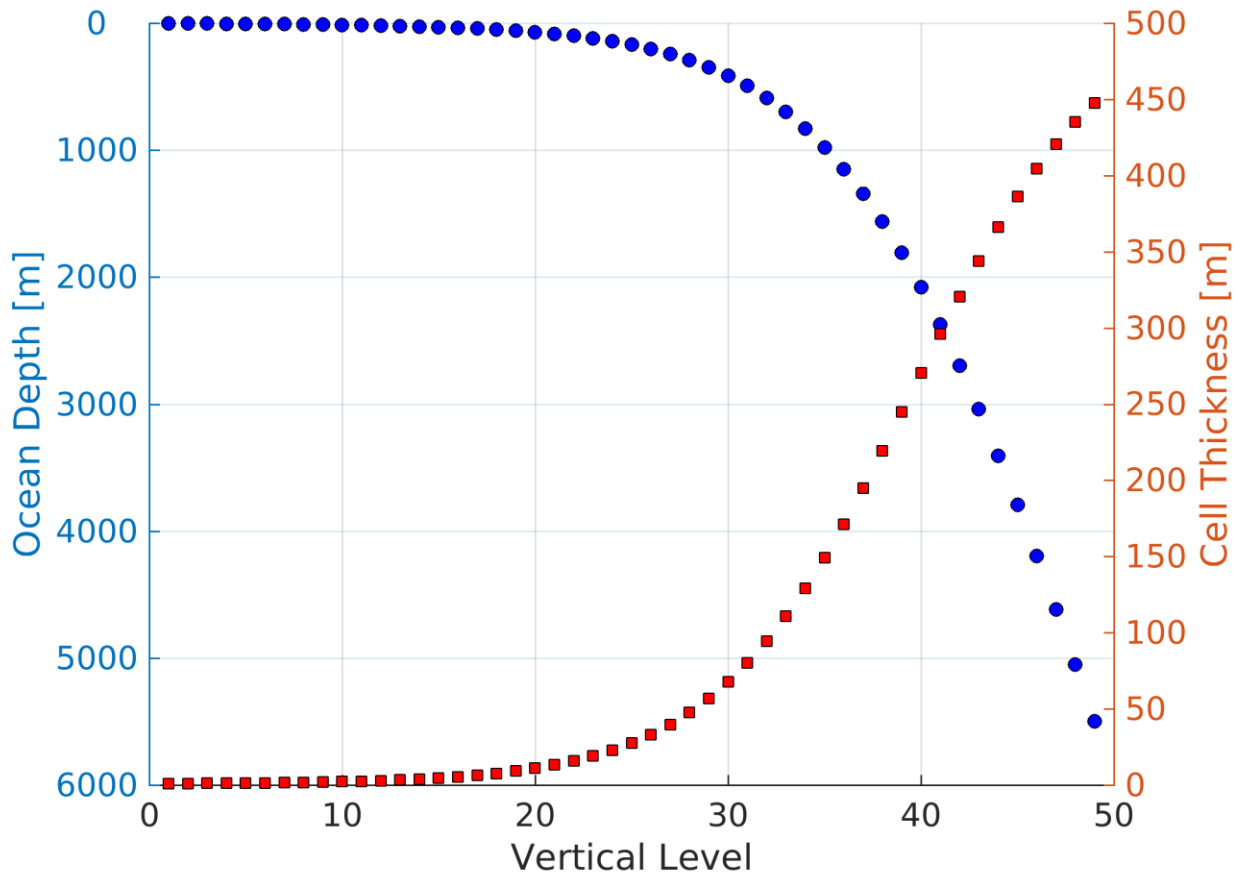
Figure 2. 1: Vertical grid structure of the NEMO simulations which use 50 levels.

The horizontal grid is a staggered Arakawa C grid (Mesinger and Arakawa, 1976) which has tracers including salinity, temperature, pressure, density, and passive tracers within the middle of each cell (T, Fig. 2.2). Velocity vectors are along the outside of each grid (U, V), while the vertical velocity vector, W, is at the top of each cell. Vorticity and Coriolis terms are calculated at the centre of the grid edge (F) which U and V share in common. The horizontal grid is shifted to move the poles onto land to avoid a singularity within the ocean.
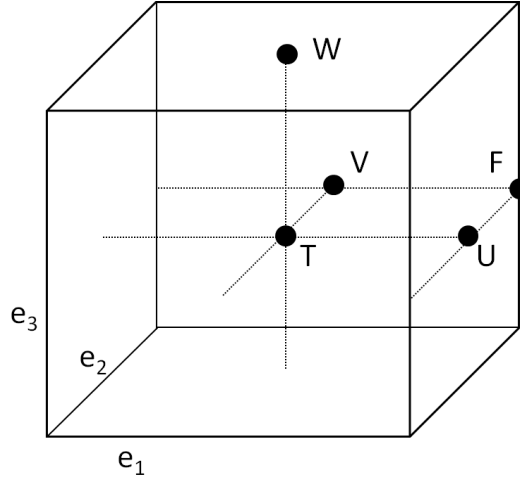
Figure 2. 2: Staggered Arakawa C grid, identifying the tracer point (T), horizontal velocity points (U,V), vertical velocity point (W), and vorticity/Coriolis point (F) for a single grid box.

2.1.5. Subgrid scale physics

Regardless of the horizontal and vertical spacing, there is always motion which takes place at a smaller spatial and temporal scale. These small scale motions are very important and they must be parameterized in order to capture their influence. The momentum equation (2.1) and conservation of heat and salt (2.4 and 2.5) include these effects which are represented by D^U, D^T, and D^S. With very different degrees of lateral and vertical motion, each of these are divided into a horizontal and vertical component for their respective subgrid scale parameterization.

Parameterization of the vertical subgrid scale physics (D^{v*}) relies on treating the non-resolvable turbulent fluxes in a diffusive manner which depends on the gradient of the tracer or momentum. The following second order equations are used:

$$D^{vU} = \frac{\partial}{\partial z}\left(A^{vU}\frac{\partial U_h}{\partial z}\right) \tag{2.16}$$

$$D^{vT} = \frac{\partial}{\partial z}\left(A^{vT}\frac{\partial T}{\partial z}\right) \tag{2.17}$$

$$D^{vS} = \frac{\partial}{\partial z}\left(A^{vT}\frac{\partial S}{\partial z}\right) \tag{2.18}$$

26

where A^{vU} and A^{vT} are vertical eddy viscosity and diffusivity coefficients which are described using the Turbulent Kinetic Energy (TKE) scheme describe below.

$$\bar{\epsilon} = \frac{1}{2}\left(\overline{u'^2} + \overline{v'^2} + \overline{w'^2}\right) \tag{2.19}$$

$$\frac{\partial \bar{\epsilon}}{\partial t} = \frac{A^{vU}}{e_3}\left[\left(\frac{\partial u}{\partial k}\right)^2 + \left(\frac{\partial v}{\partial k}\right)^2\right] - A^{vT}N^2 + \frac{1}{e_3}\frac{\partial}{\partial k}\left(\frac{A^{vU}}{e_3}\frac{\partial \bar{\epsilon}}{\partial k}\right) - c_\epsilon \frac{\epsilon^{\frac{3}{2}}}{l_\epsilon} \tag{2.20}$$

$$A^{vU} = c_k l_k \sqrt{\bar{\epsilon}} \tag{2.21}$$

$$A^{vT} = \frac{A^{vU}}{P_{rt}} \tag{2.22}$$

$$l_k = l_\epsilon = \frac{\sqrt{2\bar{\epsilon}}}{N} \tag{2.23}$$

$$N = \sqrt{-\frac{g}{\rho_o}\frac{\partial \rho}{\partial z}} \tag{2.24}$$

where u', v', and w' are the eddy velocity components, P_{rt} is the Prandtl number, N is the Brunt-Väisälä frequency, c_ϵ is $\frac{\sqrt{2}}{2}$, c_k is 0.1, l_k and l_ϵ are dissipation and mixing turbulent length scales.

For the lateral motion which is below the subgrid scale, a similar approach is carried out. A Laplacian operator ($\nabla \cdot \nabla$) is carried out for tracer diffusion, which reduces to the following formula:

$$D^{lT} = \frac{1}{e_1 e_2}\left[\frac{\partial}{\partial i}\left(\frac{e_2}{e_1}A^{lT}\frac{\partial T}{\partial i}\right)\right] + \frac{\partial}{\partial j}\left(\frac{e_1}{e_2}A^{lT}\frac{\partial T}{\partial j}\right) \tag{2.25}$$

where A^{lT} is the lateral eddy diffusivity coefficient. Momentum diffusion is carried out using a bilaplacian operator, meaning the Laplacian operator is carried out twice, giving the following:

$$D^{lU} = \Delta_h^2(A^{lU}U) \tag{2.26}$$

where U contains the rotational (ξ) and divergent components (χ) of the flow.

$$D^{lU} = \nabla_h\{\nabla_h \cdot [A^{lU}\nabla_h(\chi)]\} + \nabla_h \times \{k \cdot \nabla \times [A^{lU}\nabla_h \times (\xi k)]\} \tag{2.27}$$

2.1.6. Discretization

The NEMO model uses a three level time-stepping scheme:

$$x^{t+\Delta t} = x^{t-\Delta t} + 2\Delta t RHS_x^{(t-\Delta t, t, t+\Delta t)} \tag{2.28}$$

for which x stands for a horizontal velocity (u or v), or tracer (T or S), RHS is the right hand side of the time evolution equation, and Δt is the timestep. Non-diffusive processes including the pressure gradient, Coriolis, momentum, and advection use a leapfrog scheme (Mesinger and Arakawa, 1976). To prevent divergence between even and odd timesteps, a Robert-Asselin time filter (Asselin, 1972) is implemented within the leapfrog scheme:

$$x_F^t = x^t + \gamma\left[x_F^{t-\Delta t} - 2x^t + x^{t+\Delta t}\right] \tag{2.29}$$

where F denotes the filtered value and γ is the Asselin coefficient. Our experiments use a Asselin coefficient of 0.1. While non-diffusive terms use the leapfrog scheme, diffusive processes are unstable using a leapfrog scheme. A forward scheme is used instead:

$$x^{t+\Delta t} = x^{t-\Delta t} + 2\Delta t D_x^{t-\Delta t} \tag{2.30}$$

where D_x is a diffusion term. Our simulations use a Laplacian diffusion operator for tracers, and a biplacian operator for momentum. To preserve model stability, the diffusion coefficients are bounded by

$$D^{lT} < \frac{e^2}{8\Delta t} \text{ Laplacian diffusion for tracers} \tag{2.31}$$

$$D^{lU} < \frac{e^4}{64\Delta t} \text{ Laplacian diffusion for momentum} \tag{2.32}$$

where e is the smallest horizontal grid scale. These values clearly depend on the model setup, and having a diffusion coefficient higher than (2.31) or (2.32) will quickly lead to numerical instability. Values for our simulations are shown in Table 2.1.

2.1.7. Convective parameterization

With both insufficient grid spacing to explicitly resolve convection, and the hydrostatic assumption, convection must be parameterized. While a few options are available within NEMO, we use the enhanced vertical diffusion approach. In regions of instability, with negative Brunt-Väisälä frequency, the vertical eddy mixing rate is assigned a very large value for both tracers and momentum. Background values of vertical eddy diffusivity may be 10^{-4} m² s⁻¹ or so, but increase to between 1 and 100 m² s⁻¹ when unstable. Furthermore, a turbulent closure scheme is also implemented. Due to static instabilities rendering the Brunt-Väisälä frequency negative (see eqn. 2.20), the turbulent closure scheme increases the turbulent diffusivity coefficients. This mimics a similar effect as the enhanced vertical diffusion mentioned above, except the turbulent closure scheme does not mix the near-surface water as vigorously. It is recommended to use the enhanced vertical diffusion scheme when using the turbulent closure scheme (Madec, 2008)

2.2.   Sea Ice Model

2.2.1. Sea-ice dynamics

The LIM2 model (Fichefet and Maqueda, 1997; Bouillon et al., 2009) is coupled with the ocean model of NEMO. LIM2 is a 3-layer model where the first layer is snow on top of ice. The remaining 2 levels are ice of equal thicknesses. Simulated sea-ice acts as a levitating layer above the water, not physically within it. However, heat and momentum are transferred between the ocean and sea-ice, and between the sea-ice and atmosphere. The following momentum equation for sea-ice is

$$m\frac{\partial u}{\partial t} = -mfk \times u + \tau_{ai} + \tau_{oi} - mg\nabla\xi + F \qquad (2.33)$$

where m is the mass per unit area of ice and snow, u is the horizontal ice velocity, f is the Coriolis parameter, τ is the surface stress, the subscripts *ai* and *oi* indicate atmosphere-

ice and ocean-ice, g is gravity, ξ is the sea surface height, and F is internal ice stress. These surface stresses are defined as

$$\tau_{ai} = \rho_a C_a |u_a| u_a \tag{2.34}$$

$$\tau_{oi} = \rho_o C_o |u_o - u_i|(u_a - u_i) \tag{2.35}$$

where ρ is the density of air or the ocean, C is the drag coefficient determined by CORE bulk formula (Large and Yeager, 2008), and u is the horizontal velocity of the atmosphere (a) typically at 10m, ocean (o) or sea-ice (i). The internal ice stress, F, is the divergence of the stress tensor. LIM2 uses an Elastic-Viscous-Plastic approach, where sea-ice acts elastically on short time scales, but as a viscous plastic on long time scales.

2.2.2. Sea-ice thermodynamics

Multiple processes allow sea-ice to either grow or melt based on the transport of heat. The internal temperature within the snow and sea-ice layers is a 1 dimension heat diffusion equation

$$\rho c_p \frac{\partial T}{\partial t} = Gk \frac{\partial^2 T}{\partial z^2} \tag{2.36}$$

where, ρ, c_p, and k are the density, specific heat capacity and thermal conductivity of the material within the layer. G is a correction factor as heat conduction through ice varies with thickness.

The surface, either snow or ice, experiences the following heat flux:

$$B = Q_s + Q_L + Q_h + Q_l + Q_{cs} \tag{2.37}$$

$$Q_S = Q_I(1 - \alpha)(1 - i_o) \tag{2.38}$$

$$Q_L = \varepsilon(Q_D - \sigma(SST)^4) \tag{2.39}$$

$$Q_h = \rho_a c_{pa} C_H (T_a - SST)|\Delta U| \tag{2.40}$$

$$Q_l = \rho_a L_v C_E (q_a - q_s)|\Delta U| \tag{2.41}$$

These equations are very similar to the heat flux between the atmosphere and ocean (equations 2.9, 2.10, 2.14, and 2.15) with some modifications: (1) a portion of the incident solar radiation, Q_i, passes through each layer, represented by $1-i_o$; (2) an emissivity, ε, is included here with a value of 0.97 for snow or ice where it would have a value of 1 for ocean; (3) the specific humidity at the ice/snow surface is q_s; and (4) a term for the conductive heat flux from below (Q_{cs}) is included. Melting will occur if the surface temperature exceeds the melting point, for which the amount of melting is calculated by

$$\frac{\partial h}{\partial t} = \frac{B}{L} \tag{2.42}$$

where h denotes the thickness of ice or snow

At the interface between ocean and sea-ice, sea-ice can be generated or removed depending on the heat flux. This growth is written as:

$$\frac{\partial h}{\partial t} = \frac{Q_{cb} - Q_{oi}}{L_i} \tag{2.43}$$

where Q_{cb} is the conductive heat flux at the bottom of the ice and Q_{oi} is the heat flux between the ocean and sea-ice. Sea-ice growth at the ocean's surface is positive where there is more heat transferred from the sea-ice to the ocean than the reverse.

Sea-ice can also grow laterally. The sea-ice concentration (A) within a grid cell can change in time as given by:

$$\frac{\partial A}{\partial t} = (1 - A^2)^{1/2} \frac{(1-A)B_o}{Lh} \tag{2.44}$$

where B_o is the open water heat flux. Should this heat flux be positive, all the heat gained will be used to melt sea-ice from below.

2.2.3. Ice-Ocean coupling

Sea-ice provides a flux of heat, salt, and momentum towards the ocean, and these two models must be coupled together for this to be carried out. For areas of the ocean with overlying sea-ice, the shortwave radiation flux, Q_{swoi}, is

$$Q_{swoi} = AQ_{pen} + (1 - A)(1 - \alpha_o)Q_I \tag{2.45}$$

$$Q_{pen} = i_o(1 - \alpha_i)Q_I exp^{(-1.5(h_i - 0.1))} \tag{2.46}$$

where Q_{pen} is the amount of shortwave radiation which penetrates the ice layers, α_o is the ocean's albedo, α_i is the sea-ice/snow albedo. This amount of heat penetrates the snow/sea-ice into the upper ocean within the mixed layer. Any additional heat supplied to the ocean within this layer acts to reduce the sea-ice, while heat loss promotes the growth of sea-ice. Sea-ice processes result in a salt flux to the underlying ocean's surface:

$$F_{salt} = S_m \frac{\partial m_s}{\partial t} + (S_m - S_i)\frac{\partial m_i}{\partial t} + (S_m - S_i)\left(\frac{\partial m_s}{\partial t} + \frac{\partial m_i}{\partial t}\right) + S_i \frac{\partial m_s}{\partial t} + S_m(AE - P) \tag{2.47}$$

where m refers to mass per unit area, S is the salinity, E is the evaporation rate, and P is the precipitation rate. Subscripts m and i denote the mixed layer and ice, respectively. These 5 terms are, in order, the flux of salt due to snow melt, ice melt, brine rejection, meteoric ice, and evaporation-precipitation.

2.3. Adaptive Grid Refinement In FORTRAN (AGRIF)

The Adaptive Grid Refinement in Fortran (AGRIF) software package has been implemented into the NEMO modelling framework. This software allows the placement of "nests"- sub-domains within the original model grid which have increased horizontal resolution. A NEMO simulation with one or more nests will require much more computational resources. The additional cost is directly related to the horizontal mesh dimension and grid spacing. However, such a simulation requires fewer resources than running a simulation with the same resolution as within the AGRIF nest across the

entire domain (Table 2.1). It is possible to implement multiple nests within your parent domain, even nesting within a nest. These nests function very similarly to that as a simulation without any nests. In essence, each nest runs its own NEMO simulation, though special code allows for communication between domains.

Table 2. 1: NEMO configuration table including 2 Arctic Northern Hemisphere Atlantic (ANHA) domains and 2 ANHA4 domains which feature AGRIF nests (SPG12 and LAB60). The configurations using AGRIF (**bolded**) only include values for the AGRIF nest.

Configuration	ANHA4	ANHA12	ANHA4-**SPG12**	ANHA4-SPG12-**LAB60**
Time step	1080s	180s	180s	48s
Horizontal Resolution	1/4°	1/12°	1/12°	1/60°
Horizontal Grids	544x 800y	1632x 2400y	710x 616y	1180x 2660y
Vertical Levels	50	50	50	75
CPUs used	64	256	64	3000
Cost in core years	0.3 yr^{-1}	25 yr^{-1}	1.7 yr^{-1}	65 yr^{-1}
Output Frequency	5 day	5 day	5 day	1 day
Storage	15 Gb yr^{-1}	130 Gb yr^{-1}	18.4 Gb yr^{-1}	1.2 Tb yr^{-1}

This sub-chapter will cover how AGRIF works within NEMO, a useful primer for a later chapter which describes our high resolution (1/60°) configuration within the Labrador Sea. All ocean, atmosphere, and sea-ice physics within a nest is identical as written in the above sections and will not be discussed further.

2.3.1. Spatial and temporal aspects of AGRIF

The primary reason a nest is used is to increase the horizontal resolution by decreasing the grid spacing. Currently, AGRIF does not allow for any vertical refinement with NEMO. To decrease the horizontal grid spacing, each nest increases the horizontal resolution by some integer value. This integer value is often referred to as the refinement factor. Typically, the refinement factor is an odd number (3x or 5x are common) to preserve the identical spatial placement of the T-point, such as in Fig. 2.3.

This figure illustrates a refinement factor of 3, and will be used to further describe multiple aspects of how a nest is implemented within NEMO.
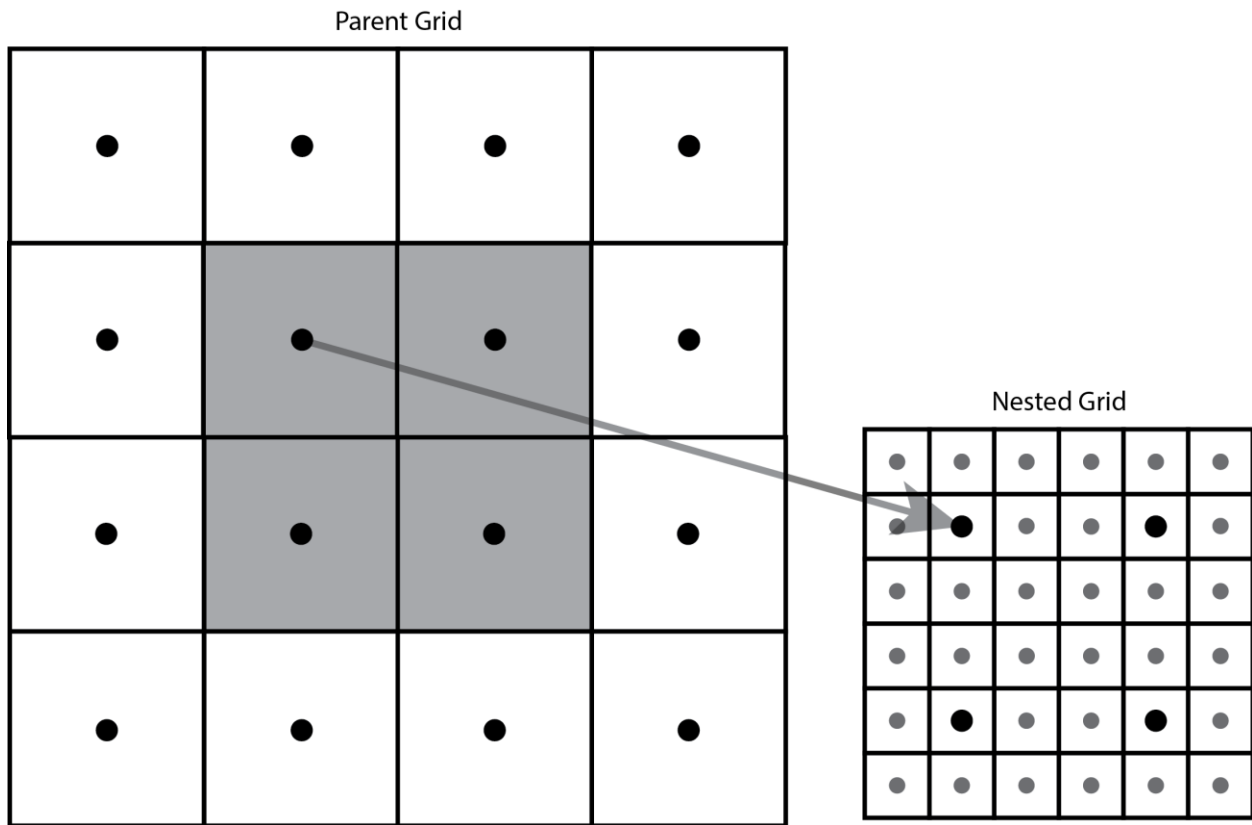
Figure 2. 3: Refinement (3x) of a parent grid to a nested grid. The grey squares indicate the region being refined. Large black dots indicate the T-points that correspond to the center of parent grid cells. Grey circles indicate the T-points that correspond to the center of the nested grid points.

The illustrated parent grid contains a domain with 4 points in each horizontal direction. A nest (3x grid refinement) is implemented within the center 4 points. Each of the parent grid points has some standard horizontal resolution set by the original configuration; for our purposes here we will state this resolution is 1°. As the AGRIF refinement factor is set to 3x in this example, the nested grid has a spatial resolution of 1/3°. The T-points of the parent grid (black circles) overlap with their associated nested T-points as the refinement factor is odd. Grey circles identify the remaining nested T-points that do not overlap with the parent grid. The refinement factor of 3x caused this second domain to have 9x more grid points than the associated region within the parent grid. Without any further changes, this means that such a simulation which has this nest

will require 9x as much computing expense to carry out. However, a reduction in grid spacing requires other modifications.

Our sample domain requires a reduction in the timestep to keep the simulation stable. This comes about from the Courant-Friedrichs-Lewy stability criteria (Courant et al., 1928): reducing the grid spacing by 3 also requires that we reduce the timestep by 3, otherwise the simulation will likely become unstable. If our fictitious 1° parent grid had a timestep which was 60 minutes, the 1/3° nest would be forced to have a timestep of 20 minutes. A simulation at time t^n will require a single parent timestep (Δt_p) to progress to the next hour, while the nest requires three nested timesteps (Δt_n); see Figure. 2.4.
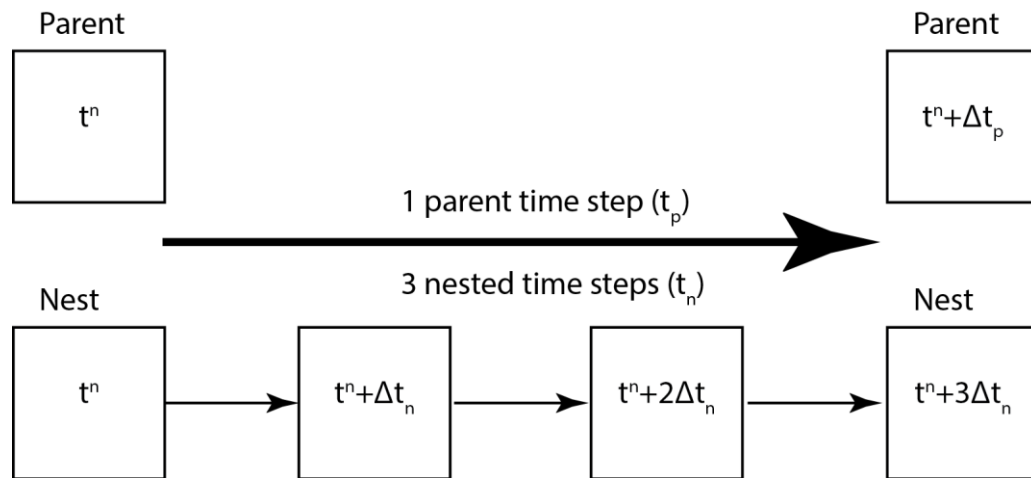
Figure 2. 4: Time stepping structure of an AGRIF simulation with one nest which uses a grid refinement of 3.

2.3.2. AGRIF domain communication

A disconnect in time occurs between the parent and nested domain, aligning on every parent timestep. NEMO is only able to carry out calculations on one domain at a time, as communication between domains is required. This communication can be either 'two-way' or 'one-way'. 'Two-way' communication means that the parent domain sends information to the nested domain and the nested domain communicates back to the parent. 'One-way' communication does not have the nested domain communicating back to the parent. 'Two-way' communication is more often selected as it allows the

transfer of information from the nested grid back to the parent grid, likely improving aspects of the parent grid away from the nested region. 'Two-way' nesting is described below as the simulations using nest(s) within this thesis use it.

The time stepping procedure for a configuration with a nest requires that the parent grid has information to send to the nest. Once the parent grid finishes its timestep, information along the nested boundary within the parent grid is sent to the nested domain (Fig. 2.5). These conditions are interpolated to the nested grid, replacing the values close to the nested boundary. The nested domain now carries out 3 timesteps so it aligns in time with the parent domain. An update of the information across the entire nested domain is interpolated onto the parent domain. At this point the cycle continues until the simulation is complete.
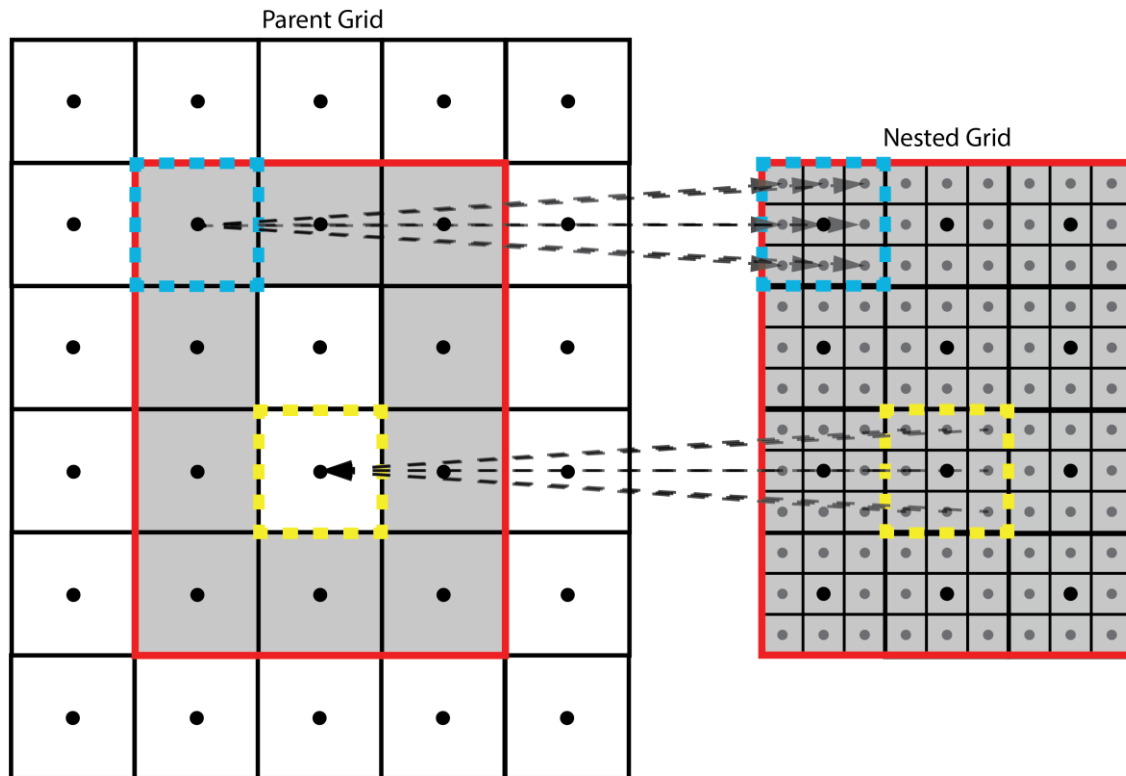
Figure 2. 5: One and two-way communication between the parent domain and AGRIF nest (red outline) using 3x refinement. The parent domain sends the boundary data (grey squares) to the nest (one-way) while the nest sends all data (grey squares) back to the parent (two-way). A single one-way communication is shown where a parent grid point (blue) along the nested boundary is interpolated onto a few nested boundary points. Two-way communication is shown where the 9 nested grid points (yellow) are interpolated onto the associated parent grid.

2.3.3. AGRIF files needed

As each nest functionally runs its own NEMO simulation that is coupled to the parent domain, a complete set of forcing files is required for each nest. This includes the bathymetry file, a coordinate file, all initial conditions (salt, temperature, U, V, SSH, ice. runoff, etc.), as well as the atmospheric weight file allowing on-the-fly interpolation between the atmospheric dataset and the ocean grid. FORTRAN code has been produced to easily make most of the above files, and is included within NEMO. Unlike the parent domain, no boundary condition files are required for nests as they update their boundary conditions as detailed above. Furthermore, any additional model

components (such as passive tracers) likely would require additional files if the parent domain required them.

2.3.4. Benefits and consequences of nesting software

The primary purpose of implementing a nest within a numerical simulation is to increase resolution in regions of interest while keeping numerical expenses low. AGRIF achieves this rather well; implementing one quarter of your parent domain with a 3x grid refinement is much less expensive than having the same spatial domain configuration at 1/3 the horizontal resolution. Not only does this cut down on the amount of required RAM, but also the number of hours used by each simulation. Nesting allows researchers to carry out numerous high-resolution simulations for the same computing expense as a single domain-wide simulation of the same resolution (See Table 2.1).

However, nesting software isn't perfect. The interpolation of data between parent and nested domain can produce spurious effects. NEMO uses a sponge layer within the AGRIF nest to reduce noise generated from interpolation effects. This is achieved by increasing the diffusivity such that the sponge layer has increased lateral mixing, dampening discontinuities from the interpolation process. This approach not only reduces unwanted noise, but it also can impact physical features such as boundary currents. Unfortunately, there appears no better solution that reduces boundary effects while preserving physical fields. Many nested domains will place their boundaries far from the region of interest to minimize these effects on the research questions being investigated. While nested boundary issues are an aspect that numerical modelers need to be aware of, many find that nesting is a useful tool that should be considered.

Bibliography

Asselin, R. (1972). Frequency filter for time integrations. *Monthly Weather Review, 100*(6), 487-490.

Barnier, B., Madec, G., Penduff, T., Molines, J-M., Treguier, A-M., Le Sommer, J., Beckmann, A., Biastoch, A., Böning, C., Dengg, J., Derval, C., Durand, E., Gulev, S., Remy, R., Talandier, C., Theetten, S., Maltrud, M., Mcclean, J., and De Cuevas, B.: Impact of partial steps and momentum advection schemes in a global ocean circulation model at eddy permitting resolution. Ocean Dynamics, 56 (5-6), 543-567, 2006.

Bouillon, S., Maqueda, M.A.M., Legat, V. and Fichefet, T. (2009). An elastic-viscous-plastic sea ice model formulated on Arakawa B and C grids. *Ocean Modelling*, 26(3-4), 174-184.

Courant, R., Friedrichs, K. and Lewy, H. (1928). Über die partiellen Differenzengleichugen der mathematischen Physik. *Mathematische Annalen*, 100, 32-74.

Debreu, L., Vouland, C. and Blayo, E. (2008). Agrif: Adaptive grid refinement in fortran. *Computers and Geosciences*, 34, 8-13.

Fichefet, T. and Maqueda, M.A.M. (1997). Sensitivity of a global sea ice model to the treatment of ice thermodynamics and dynamics. Journal of Geophysical Research: Oceans, 102(C6), 12609-12646.

Large, W.G. and Yeager, S.G. (2008). The global climatology of an interannually varying air-sea flux data set. *Climate Dynamics*, 33(2-3), 341-364.

Madec, G. (2008). Note du Pôle de modélisation, Institut Pierre-Simon Laplace (IPSL), France, No 27, ISSN No 1288-1619.

Madec, G., Delecluse, P., Imbard, M. and Lévy, C. (1998). OPA 8.1 ocean general circulation model reference manual. Note du Pôle de modélisation, Institut Pierre-Simon Laplace (IPSL), France, No 1, 91p.

Mesinger, F., and Arakawa, A. (1976). Numerical methods used in atmospheric models. *GARP Publ. Ser., 17(1), WMO, Geneva, 64.*

Valcke, S. (2006). OASIS3 user guide (prism_2-5). *PRISM support initiative report*, 3, 64.

Chapter 3: Introducing LAB60: A 1/60° NEMO 3.6 numerical simulation of the Labrador Sea

Clark Pennelly[1*] and Paul G. Myers[1]

[1]1-26 Earth Sciences Building, University of Alberta, Edmonton, Alberta, Canada, T6G 2E3

[*]*Correspondence to*: Clark Pennelly (pennelly@ualberta.ca)

3.1. Abstract

A high-resolution coupled ocean sea-ice model is set up within the Labrador Sea. With a horizontal resolution of 1/60°, this simulation is capable of resolving the multitude of eddies which transport heat and freshwater into the interior of the Labrador Sea. These fluxes strongly govern the overall stratification, deep convection, restratification, and production of Labrador Sea Water. Our regional configuration spans the full North Atlantic and Arctic, while the high resolution is only applied in smaller nested domains within the North Atlantic and Labrador Sea. Using nesting reduces computational costs and allows for a long simulation from 2002 to the near-present time. Three passive tracers are also included: Greenland runoff, Labrador Sea Water produced during convection, and Irminger Water which enters the Labrador Sea along Greenland. We describe the configuration setup and compare against similarly forced lower-resolution simulations to better describe how horizontal resolution impacts the representation of the Labrador Sea in the model.

3.2. Introduction

The Labrador Sea, between Canada and Greenland, plays a crucial role in the climate system. Situated between the Canadian Arctic and the North Atlantic, multiple current systems influence this deep basin. Cold and fresh Arctic water flows south through Fram Strait along Greenland (de Steur et al., 2009), producing the East Greenland Current (EGC). The EGC flows to the southern tip of Greenland, merging

with warm and salty Irminger Water to become the West Greenland Current (WGC) before flowing northwards along the western coast (Fratantoni and Pickart, 2007). The WGC flows cyclonically around the Labrador Sea as well as into Baffin Bay. Significant amounts of freshwater are supplied to this current system from both Davis (Cuny et al., 2005; Curry et al., 2011; Curry et al., 2014) and Hudson Strait (Straneo and Saucier, 2008) as it travels around the Labrador Sea. The current system is called the Labrador Current where it merges with the outflow from Hudson Strait (Lazier and Wright, 1993). The Labrador Current travels southwards along the eastern coast of North America eventually leaving the Labrador Sea.

Numerous eddies are generated throughout the Labrador Sea, both from high lateral density gradients which exist during the convection season (Frajka-Williams et al., 2014) as well as from baroclinic and barotropic instabilities that occur within the boundary currents (Chanut et al., 2008; Gelderloos et al., 2011). The continental slope along the west coast of Greenland has a pronounced change in topography that induces instability of the current system, generating eddies (de Jong et al., 2016). These eddies, known as Irminger Rings, contain a significant amount of freshwater at the surface as well as subsurface heat. Irminger Rings (15-30km radius) typically travel southwestwards into the interior of the Labrador Sea and have a lifespan of up to two years (Lilly et al., 2003). Eddies generated along the Labrador Coast also contain a significant amount of freshwater (Schmidt and Send, 2007; McGeehan and Maslowski, 2011; Pennelly et al., 2019). Regardless of where they are produced, these boundary current eddies often export their properties towards the centre of the basin (Pennelly et al., 2019), influencing the deep convection which occurs. Convective eddies are generated from baroclinic instability which arises from large horizontal density gradients during the convective season (Marshall and Schott, 1999). Convective eddies are much smaller with a radius between 5 and 18 km (Lilly et al., 2003). These eddies are less studied than the other eddy types, partly due to a lack of observations (Lilly et al., 2003) as well as their small size which requires high-resolution models to adequately resolve. Research into the role of each of the above eddies and their role in restratifying the Labrador Sea is still ongoing; there is no consensus on which eddy may

be more important, though many have narrowed it down to Irminger Rings and convective eddies (Chanut et al., 2008; Gelderloos et al., 2011; Rieck et al., 2019).

Deep convection is a rather rare occurrence, only known to occur at a few places in the ocean. The reason so few places exist is the stringent criteria to produce deep convection: weak stratification that can be enhanced via isopycnal doming as a result of cyclonic circulation, and intense air-sea buoyancy loss (Lab Sea Group, 1998; Marshall and Schott, 1999). Cyclonic circulation and the lateral input of salty Irminger Water helps keep the Labrador Sea weakly stratified. Furthermore, the Labrador Sea experiences strong heat loss during the winter period due to the very cold mid-latitude cyclones which frequent the region (Schulze-Chretien et al., 2016). The overlying cold and dry air forces a significant flux of heat from the ocean to the atmosphere. This loss of heat promotes the surface layer to increase in density, overturning the weakly stratified water column such that the mixed layer can exceed 2000m in depth (Yashayaev, 2007), producing a thick uniform water mass known as Labrador Sea Water (LSW).

Once the convective winter ends, the Labrador Sea quickly restratifies itself within 2-3 months (Lilly et al., 1999), primarily due to large horizontal density gradients that form convective eddies (Lilly et al., 2003; Rieck et al., 2019) as a result of the deep convection period (Frajka-Williams et al., 2014). The boundary currents continuously shed eddies with relatively buoyant water towards the interior Labrador Sea (Straneo, 2006), increasing stratification. This occurs along the west Greenland and Labrador coasts, though research suggests that the former supplies more freshwater (Myers, 2005; Schmidt and Send, 2007; McGeehan and Maslowski, 2011; Pennelly et al., 2019).

LSW is exported out of the Labrador Sea primarily by the Deep Western Boundary Current (Kieke et al., 2009), though it also spreads eastwards at a slower rate. While LSW is the lightest component within the Deep Western Boundary Current, it is one of the water masses which make up the lower limb of the Atlantic Meridional Overturning Circulation (AMOC). As the overturning circulation transports a significant amount of heat and dissolved gasses between the equator and polar regions, changes in the production of deepwater can influence the overturning circulation and ultimately

the climate (Bryden et al., 2005). With polar amplification driven by the positive ice-albedo feedback loop, additional freshwater from melted ice enters the EGC and WGC (Bamber et al., 2012). The Labrador Sea is experiencing an increase in freshwater that can be capable of capping convection and preventing LSW from being formed, ultimately reducing the AMOC strength (Böning et al., 2016). However, a non-local increase in the surface freshwater flux may promote AMOC strengthening (Cael and Jansen, 2020) or compensate the local effects of additional freshwater (Latif et al., 2000). Long climate simulations allow investigation into any AMOC regime shifts that shorter, higher-resolution simulations may miss. With such different conclusions, freshwater's influence on the AMOC is not fully known and may vary at different convection regions.

While satellite altimetry provides a wealth of information including sea surface height anomalies, geostrophic currents, and waves, hydrographic cruises within the Labrador Sea are often limited to the restratification period when the Labrador Sea is more hospitable for scientific operations. Argo floats, autonomous drifting profilers which can sample down to 2000m, have become a popular instrument to acquire in-situ data. However, they still lack coverage within the Labrador Sea which can experience deep convection below their sampling depth (Yashayaev, 2007). Numerical modelling is a useful tool to explore this data-sparse region, though it has its limits. Simulations within the Labrador Sea often experience a drift in model data, producing a Labrador Sea which slowly increases in salinity, and thus density (Treguier et al., 2005; Rattan et al., 2010). Coarse-resolution simulations suffer even further, often overproducing the spatial area of deep convection (Courtois et al., 2017), primarily as a result of not resolving important small-scale features including eddies. These eddies supply the Labrador Sea with significant heat (Gelderloos et al., 2011) and freshwater fluxes (Hátún et al., 2007), both strongly impact the stratification, convection, and production of deep water. Increased horizontal resolution helps produce these eddies and their important fluxes into the interior of the Labrador Sea but numerical drift still is present within high-resolution simulations, albeit reduced in severity (Marzocchi et al., 2015).

Numerous high-resolution simulations have been carried out within the North Atlantic. VIKING20X (Rieck et al., 2019), and its predecessor VIKING20, are global

1/4° simulations which have a high-resolution 1/20° nest. VIKING20X is a multi-decade simulation which is capable of resolving eddies within the Labrador Sea. However, simulations with 1/20° horizontal resolution may not resolve sub-mesoscale processes (Su et al., 2018) that can impact stratification by carrying heat and freshwater; higher-resolution is needed. The 1/50° HYCOM (Chassignet and Xu, 2017), 1/60° NATL60 (Fresnay et al., 2018) and eNATL60 (Le Sommer et al., in prep) provide great insights on the importance of resolving eddies. However, computational expense with such high-resolution simulations is very high, both in computer time and operational costs. This often forces higher-resolution simulations to have a reduced length, perhaps only a few years. The Labrador Sea experiences significant interannual variability (Fischer et al., 2010) and such short simulations may completely miss any connection between LSW production and changes in the AMOC. As such, any high-resolution simulation which is capable of resolving the fine scale features within the Labrador Sea should be carried out for many years to further understand the climate system. Resolving the full North Atlantic at high resolution (1/60°) and carrying out a simulation for longer than 10 years would currently be extremely expensive; the above 1/60° simulations are 5 or so years in length. However, one can incorporate nested domains to increase horizontal resolution with a relatively minor increase in computing cost.

To simulate the Labrador Sea as accurately as possible, we set up a complex numerical configuration which achieves very high resolution within the Labrador Sea while keeping computing costs low such that we will produce over 15 years of simulated data. This simulation will be kept up to near-present time, lagged a few months depending on the availability of forcing data. The high resolution allows for explicit representation of eddies which are crucial to controlling the stratification within the region. We will first describe the model configuration in detail and then compare against similarly-forced lower-resolution simulations to understand how changes in horizontal resolution impacts model results in the Labrador Sea.

3.3. Methods

The numerical model used for our high-resolution simulation is the Nucleus for European Modelling of the Ocean (NEMO; Madec, 2008), version 3.6, which is coupled to a sea-ice model, LIM2 (Fichefet and Maqueda, 1997). The 1/4° Arctic Northern Hemisphere Atlantic configuration (ANHA4; Fig. 3.1a) is used and includes a double nest via the Adaptive Grid Refinement in FORTRAN package (AGRIF; Debreu et al., 2008). The AGRIF software allows for high-resolution nests to communicate along their boundaries, passing information back and forth between domains. The parent ANHA4 domain extends from Bering Strait, though the Arctic and North Atlantic, to 20°S in the South Atlantic. The parent domain's nest uses a spatial and temporal refinement factor of three, bringing resolution to 1/12° and the time step to 240s (Table 3.1) in the North Atlantic Sub Polar Gyre domain (SPG12; Fig. 3.1b). An ANHA4 configuration with a SPG12 nest has been evaluated before by investigating how model resolution influences Labrador Sea Water formation (Garcia-Quintana et al., 2019) as well as eddy formation and eddy fluxes in the North Atlantic Current (Müller et al., 2017; Müller et al., 2019). Another nest is implemented within the SPG12 domain, using a spatial and temporal refinement of five, increasing the horizontal resolution from 1/12° to 1/60° and reducing the time step to 48s within the Labrador Sea (LAB60; Fig. 3.1c). All nests allow two-way communication such that the parent domain supplies boundary conditions while the daughter domain returns interpolated values to all associated parent grid points. All domains have different horizontal grid spacing but they share the same vertical grid which is set to 75 geopotential levels (Fig. 3.1d) using partial steps (Barnier et al., 2006). This simulation involves three domains (ANHA4, SPG12, and LAB60) although we primarily discuss what occurs within the 1/60° nest.
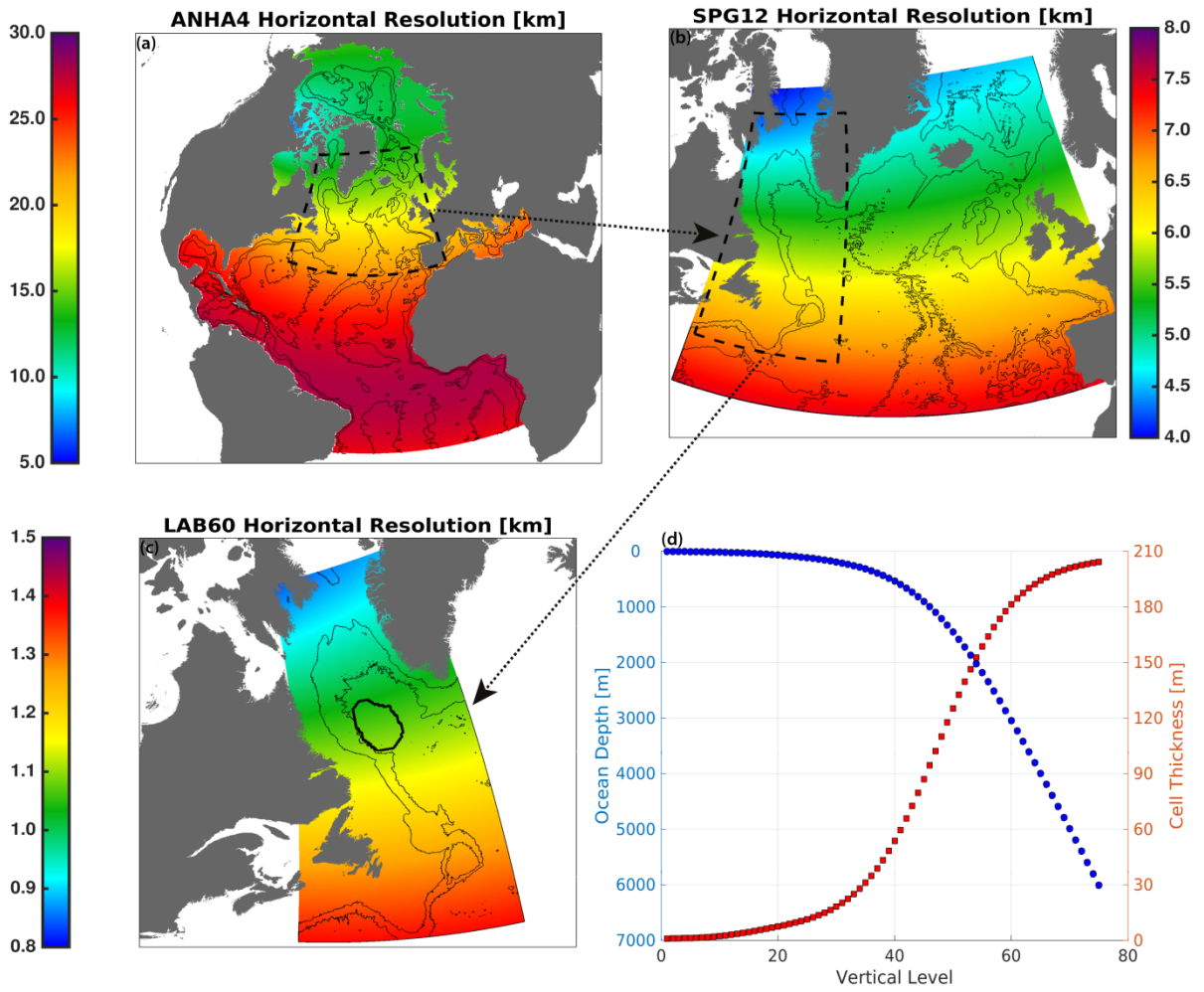
Figure 3. 1: Domain setup for the (a) ANHA4 parent domain, (b) the SPG12 nest, and (c) the LAB60 nest. Horizontal grid resolution, in km, is identified by color. All domains share identical vertical grid structure (d). The thick black contour in (c) identifies a region of interest where calculations of LSW's density, thickness, and mixed layer depth are determined. The 1000m, 3000m, and 5000m isobaths are shown via the thin black contours.

Table 3. 1: Domain settings for the ANHA4 parent domain, SPG12 and LAB60 nested domains. Other settings which are invariant to the domain are shown in Table 3.2.

Setting	ANHA4	SPG12	LAB60
Horz. Resolution	1/4°	1/12°	1/60°
X points	544	724	1179
Y points	800	694	2659
Timestep [s]	720	240	48
Horiz. Eddy Viscosity [$m^4\,s^{-1}$]	1.5x10^11	1.5x10^10	3.5x10^8
Horiz. Eddy Diffusivity [$m^2\,s^{-1}$]	300	50	20
Lateral Slip Conditions	Free slip	Free slip	No slip

A total variance dissipation scheme (Zalesak, 1979) was used in all domains to calculate horizontal advection. A Laplacian operator was used to compute lateral diffusion in all domains, while a bi-laplacian operator was used for lateral momentum mixing. As some model parameters are grid-scale dependent, Table 3.1 displays these settings. As lateral boundary conditions have been shown to be very important at producing Irminger Rings in high-resolution simulations (Rieck et al. 2019), we used no-slip lateral boundary conditions within the LAB60 domain while the other domains had free-slip conditions. Model mixed layer depths were calculated via the vertical gradient in temperature and salinity (Holte and Talley, 2009) as opposed to a 0.01 kg m^{-3} change in potential density between the surface and the bottom of the mixed layer; the latter method can produce deeper mixed layers than observations suggest (Courtois et al., 2017). Settings not listed in Table 3.1 indicate that all domains have an identical value or option; some of these important settings are shown in Table 3.2.

Model bathymetry was interpolated from the 1/60° ETOPO GEBCO dataset (Amante and Eakins, 2009) to each domain's grid and bathymetric smoothing along nest boundaries was carried out in order to conserve volume where the parent domain supplies boundary conditions to the daughter domain. All domains were initialized from GLORYS1v1 (Ferry et al., 2009), a global reanalysis ocean simulation, at the beginning of 2002. Monthly open boundary conditions (3D T, S, U, V, and 2D SSH and ice values) across Bering Strait and 20° S were supplied to the ANHA4 domain. These boundary conditions were linearly interpolated from monthly values, overriding the values within the boundary without the use of a sponge layer. Runoff was supplied via Dai et al.

Table 3. 2: Model configuration settings which are identical between all three domains. Bold values indicate values which were changed when we migrated LAB60 from the Graham cluster to Niagara.

Configuration Setting	Value
Vertical grid	75 geopotential levels
Sea-ice model	LIM 2 (Fichefet and Maqueda, 1997)
Bulk formula	CORE (Large and Yeager, 2008)
Liquid discharge	Dia et al. (2009) + Bamber (2012: Greenland)
Solid discharge	Input as liquid
Surface Restoring	None
Initial conditions	Glorys1v1 (T,S,U,V,SSH,ice)
Open boundary conditions	Glorys1v1 (T,S,U,V,ice)
Atmospheric forcing:	
2002-2006	CGRF (Smith et al, 2014)
2007-2017	Drakkar Forcing Set 5.2 (Dussin et al. 2016)
Lateral momentum	Bilaplacian operator
Lateral diffusion	Laplacian operator
Vertical eddy viscosity	1×10^{-4} m^2 s^{-1}
Vertical eddy diffusivity	1×10^{-5} m^2 s^{-1}
Mixed layer scheme	Holte and Talley (2009)
Bottom friction	Nonlinear
Hydrostatic approximation	Yes
Passive tracers	Three (see Figure 2)
CPU requested	672 (**3000**), Broadwell 2.1 GHz (Skylake 2.4 GHz)
Time to complete 1 year	Approximately 700 (**200**) hours
Initialization date	January 1st, 2002

(2009) while we also included Greenland runoff as estimated from a surface mass-balance model (Bamber et al., 2012). Without an iceberg model functioning with the AGRIF software, we treated all solid runoff as a liquid, thus capturing the full freshwater mass at the cost of accuracy in the spatial and temporal placement of freshwater emitted from icebergs.

Precipitation, shortwave radiation, downward longwave radiation, 2 meter specific humidity, 2 meter temperature, 10 meter meridional and 10 meter zonal winds originally were supplied from the Canadian Meteorological Centre's Global Deterministic Prediction System's Reforecast product (CGRF; Smith et al., 2014). While high in temporal (hourly) and spatial resolution (33 km in the Labrador Sea), we found

the air-sea fluxes were slightly too weak to sustain deep convection after 2010. Rather than start completely over, we switched the atmospheric forcing in 2007 (Fig. 3.2) when LAB60's mixed layer was still similar to observations. Starting on 1 Jan 2007, we used the DRAKKAR Forcing Set 5.2 (DFS; Dussin et al., 2016). DFS supplies data at 3 hour increments for wind, temperature, and humidity, while precipitation and radiation are daily. DFS has a spatial resolution which is approximately 45 km within the Labrador Sea. Our own analysis of the CGRF data showed a 2002-2015 average yearly heat loss of 47 W m^{-2} from the interior Labrador Sea while DFS removed 53 W m^{-2} (Pennelly and Myers, 2021). Increasing the horizontal resolution likely increased the horizontal buoyancy fluxes and rendered the CGRF's air-sea heat loss, which was appropriate in our ANHA4 and ANHA12 configurations, inadequate. The decision to swap to DFS was based on its greater heat loss, promoting a better mixed layer depth throughout the Labrador Sea, though a different forcing product will eventually be needed as DFS does not currently extend past 2017. Supplemental Fig. 3.1 depicts the difference in mixed layer depth between the LAB60 simulation forced by CGRF, when forced with CGRF through 2007 and then forced by DFS, as well as what ARGO observations suggest. The weaker air-sea heat loss as forced by the CGRF product leaves the mixed layer with little interannual variability that doesn't compare well with observations.

Early testing showed that adding passive tracers increases the computing resources required by about 20% per passive tracer. To keep the simulation from requiring too many resources, we limited LAB60 to three passive tracers:

- Liquid runoff from Greenland (Fig. 3.3a)
- Irminger Water (T> 3.5°C, S>34.88) which flows westward past Cape Farewell (Fig. 3.3b)
- Labrador Sea Water (σ_θ>27.68 kg m^{-3}) formed within the mixed layer of the Labrador Sea (Fig. 3.3c)

Runoff from Greenland was included due to the importance of Greenland's freshwater contribution to changes within the Labrador Sea. Water mass definitions for Irminger Water and Labrador Sea Water were selected based on previous studies (i.e. Kieke et al., 2006; Myers et al., 2007). Note that there is no maximum density criteria given to our
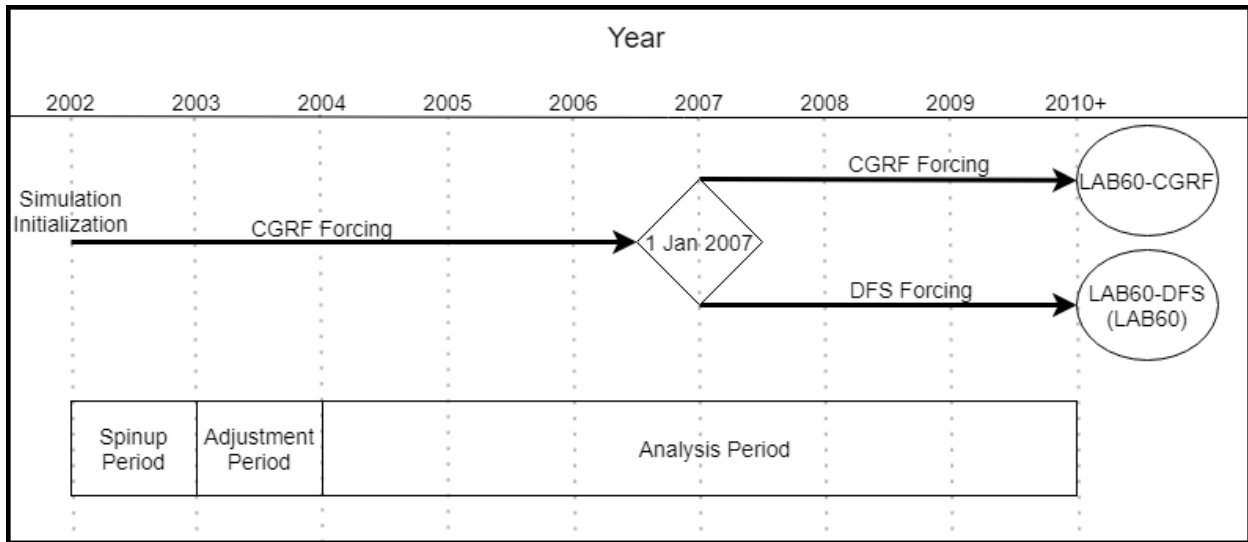
Figure 3. 2: Diagram showing the multiple periods of the LAB60 simulation. The original simulation was initialized with CGRF atmospheric forcing in 2002, although a branch swapping to DFS occurred at the start of 2007. This DFS branch is what is primarily presented in this study.

Labrador Sea Water tracer- the tracer is formed throughout the water column until it reaches the bottom of the mixed layer. Figure 3.3 illustrates both the source regions as well as the tracer extent as of 1 Jan 2010. While these water masses have been studied before (Kieke et al., 2006; Myers et al., 2007; Böning et al., 2016), there has been no attempt to use them as passive tracers at a resolution higher than 1/20° (Böning et al., 2016).

The LAB60 simulation originally started on the Graham cluster of Compute Canada. Other high-resolution simulations often use thousands of computer processors but our simulation could not run on more than 672 CPUs on this cluster as it would stall during domain construction. The years 2002-2007 were carried out on Graham, after which a new allocation on a different high performance Compute Canada cluster, Niagara, became available to us. The LAB60 simulation on Niagara did not suffer from the same issue as it did on Graham and we were able to use many more processors. Initial testing found a substantial increase in the number of days simulated per job submission when the number of CPUs was increased from 672 to 3000; tests using 4000 CPUs showed no further improvement. Thus, we carried out the remainder of the LAB60 simulation with 3000 CPUs. Each job submission required around 22 hours to
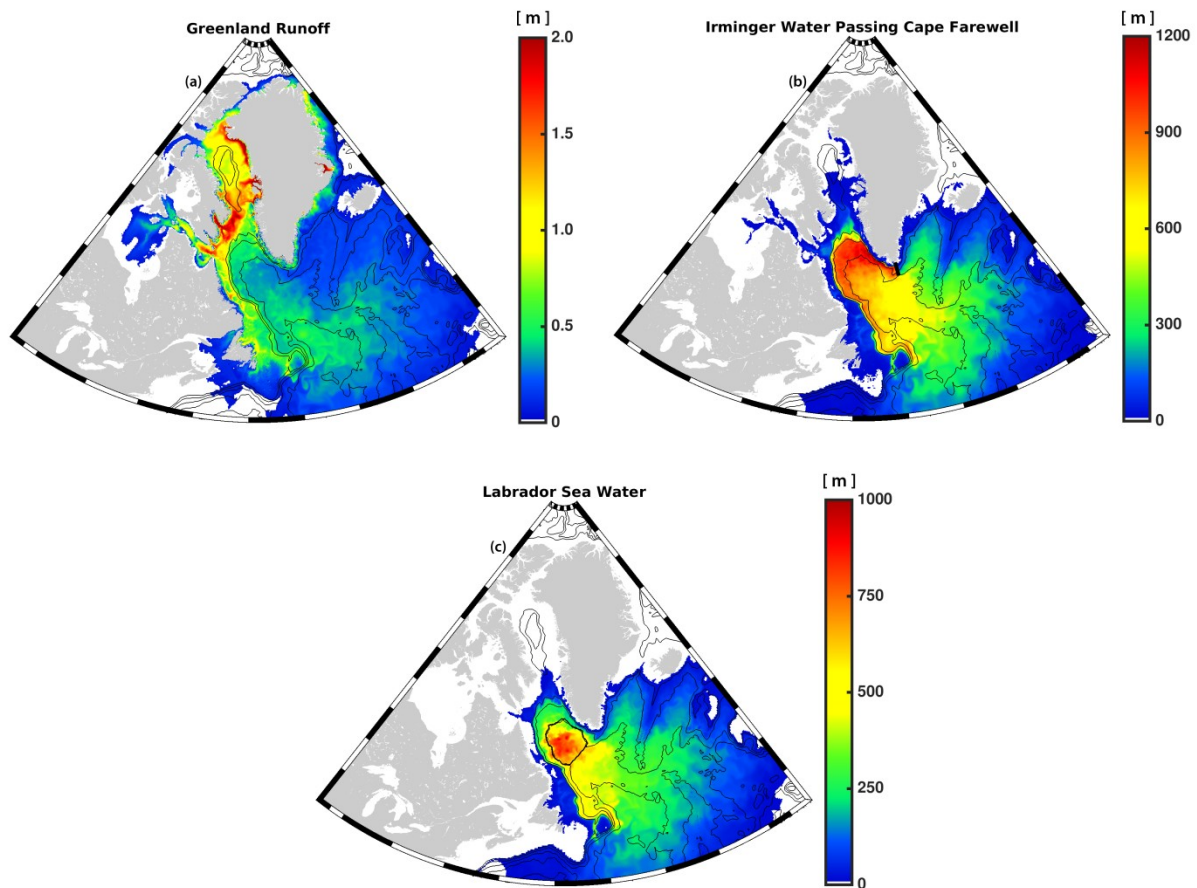
Figure 3. 3: The three passive tracers used within our LAB60 simulation with source regions indicated by thick black lines: (a) Greenland runoff, (b) Irminger Water (T > 3.5°C, S > 34.88) which flows west past Cape Farewell, and (c) Labrador Sea Water (σ_θ>27.68 kg m^{-3}) produced each convective season. Images are from the simulation date 1 Jan 2010. Bathymetric contours are every 1000m. Units are the thickness, in meters, of the tracer. Note: as all three domains are included in this figure, spatial resolution changes within each subfigure.

carry out, providing 40 days of model output. The real time to finish each 40 day submission naturally varied across the year, increasing during winter which we attribute to the sea-ice model.

A spin-up period (Fig. 3.2) was required as the model quickly went unstable and crashed. We attribute this to the interpolation of the 1/12° GLORYS1v1 data onto the LAB60 grid; the resulting data were not smooth enough and numerical noise was generated, leading to model failure. To reduce this noise, a gradual spin-up procedure

took place. First, we kept the numerical timestep very low (2s in LAB60) when the model was initialized. We also set the 1/60° nests' eddy viscosity and diffusivity values to be equal to those within the SPG12 nest. We gradually increased the timestep and reduced the viscosity and diffusivity values over the first year (2002) to what is within Table 3.1. Other than also increasing the timestep in LAB60, no other values were changed across the coarser ANHA4 and SPG12 domains. To allow LAB60 to adjust to the final settings, we consider the 2003 year to be an adjustment year (Fig. 3.2).

To assess the validity of LAB60, model results were compared against AVISO satellite data (https://www.aviso.altimetry.fr/), specifically U/V geostrophic velocities which are derived from the sea surface height. Argo profiler data (http://www.argo.net/) was also used to assess the mixed layer. Bottle data from cruise 18HUD20080520, accessed from CCHDO (https://cchdo.ucsd.edu/cruise/18HU20080520) on 10 April 2018 was used to compare observations across the AR7W section.

3.4.   Model Simulation Results

To understand what is gained by resolving the Labrador Sea at 1/60°, we compare the output of our LAB60 simulation with similarly forced ANHA simulations at both 1/4° (ANHA4) and 1/12° (ANHA12). The large-scale circulation (top 50m) is shown for our 3 simulations (Fig. 3.4) as well as AVISO geostrophic velocities. All simulations have greater speed within the West Greenland Current (ANHA4: up to 0.8; ANHA12: 0.8; LAB60: 0.6; AVISO: 0.4 m s^{-1}) and Labrador Current (ANHA4: up to 0.6; ANHA12: 0.6; LAB60: 0.4; AVISO: 0.4 m s^{-1}) as altimetry observations suggest slower speeds here. However, Lin et al., (2018) found maximum speed up to 0.74 m s^{-1} along the west coast of Greenland. Both the ANHA4 and ANHA12 configuration have larger values further up the western coast of Greenland, as well as connecting the West Greenland Current and the Labrador Current; features that do not occur in both LAB60 and observations. As LAB60 and observations have less average speed occurring within these boundary currents, we suspect that all configurations have some large differences in eddy activity, particularly where these boundary currents are.
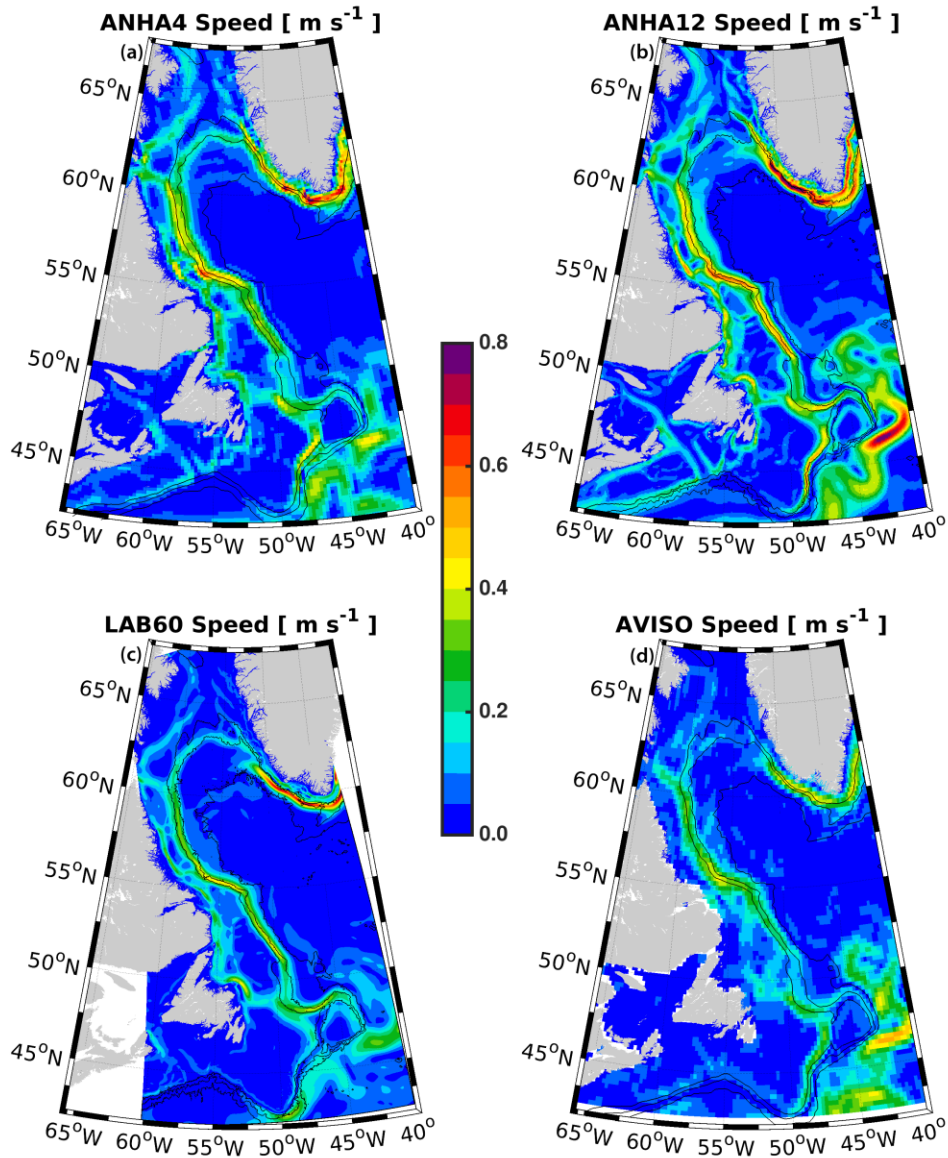
Figure 3. 4: Top 50m average speed (2004-2013) for the (a) ANHA4, (b) ANHA12, (c) and LAB60 simulations, as well as (d) from AVISO observations. The 1000, 2000, and 3000m isobaths are shown by the black contour lines.

Eddy kinetic energy (EKE: $0.5(\overline{U_g'^2} + \overline{V_g'^2})$, Fig. 3.5) was calculated from geostrophic velocity anomalies based on the sea level anomaly (SLA) from the 2004-2013 mean state:

$$U_g' = -\frac{g}{f}\frac{SLA}{\Delta y}$$

$$V_g' = \frac{g}{f}\frac{SLA}{\Delta x}$$

where g is the gravitational constant, f is the Coriolis parameter, and Δy and Δx are model grid length. Overbars indicate the 2004-2013 mean value while primed variables indicate a deviation from the mean state. AVISO observations were already supplied as geostrophic velocities.

High levels of EKE can be found along the west coast of Greenland (Fig. 3.5), extending into the interior of the basin around 62° N, as well as along the Labrador coast's shelf break. The path extending from the west coast of Greenland is mostly due to Irminger Rings which leave this coast and travel westward (Chanut et al., 2008). While the EKE extending from west Greenland enters the interior of the Labrador Sea, that which stems from the Labrador coast does not penetrate far into the interior. The ANHA4 simulation has low EKE along the west coast of Greenland (around 100 cm² s⁻²) and along the Labrador Coast's shelf break (10-30 cm² s⁻²). The ANHA12 simulation shows improvement, having much higher EKE extending from west Greenland (100-300 cm² s⁻²) however the EKE does not quite extend into the interior of the Labrador Sea but instead remains in the northern Labrador Sea. Furthermore, there is additional EKE along the Labrador shelf break (30-50 cm² s⁻²) compared against ANHA4. The LAB60 simulation shows further improvement as the EKE signature from the west Greenland coast is greater (100-1000 cm² s⁻²) and now enters into the interior of the Labrador Sea. A notable increase in EKE also occurs along the Labrador shelf break (100-200 cm² s⁻²) and within the interior Labrador Sea (10-100 cm² s⁻²). LAB60 matches well against observations along the west coast of Greenland and the Labrador shelf break (both above 1000 cm² s⁻²) as well as the interior Labrador Sea (10-100 cm² s⁻²). LAB60's higher interior EKE may be partially from convective eddies that are formed during the wintertime. However, LAB60 has lower EKE within the Northwest Corner where ANHA4, ANHA12, and the observations exceed 1000 cm² s⁻² over a wide area. LAB60 matches the spatial distribution albeit with reduced EKE.
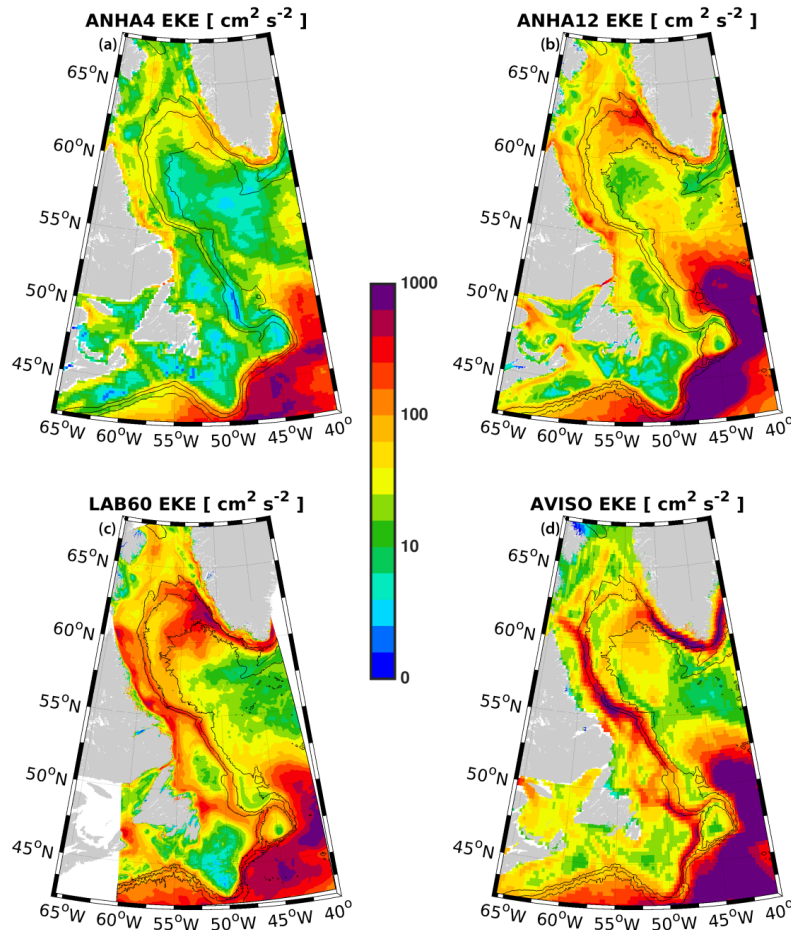
Figure 3. 5: Eddy kinetic energy (EKE), as calculated from geostrophic velocities resulting from the sea level height anomaly, are shown for (a) ANHA4, (b) ANHA12, and (c) our LAB60 simulation, from 2004 to 2013. Observations via AVISO are identified in (d). The 1000m, 2000m, and 3000m isobaths are shown by the black contour lines. A log scale was used for clarity.

The differences in the EKE field between these configurations identify that each simulation is resolving features of varying spatial scales. The ANHA4 simulation, with low EKE within the Labrador Sea, does not adequately resolve eddies in this region, as illustrated with a snapshot of normalized model relative vorticity (Fig. 3.6). However, the larger scale meanders within the North Atlantic Current are visible. ANHA12 shows a greater degree of mesoscale features (50 to 500 km), though distinct eddies within the Labrador Sea are also not resolved. LAB60 resolves eddies along both the west coast of Greenland as well as the Labrador Coast. A video showing LAB60's normalized relative vorticity is shown in Supplementary Video 3.1.
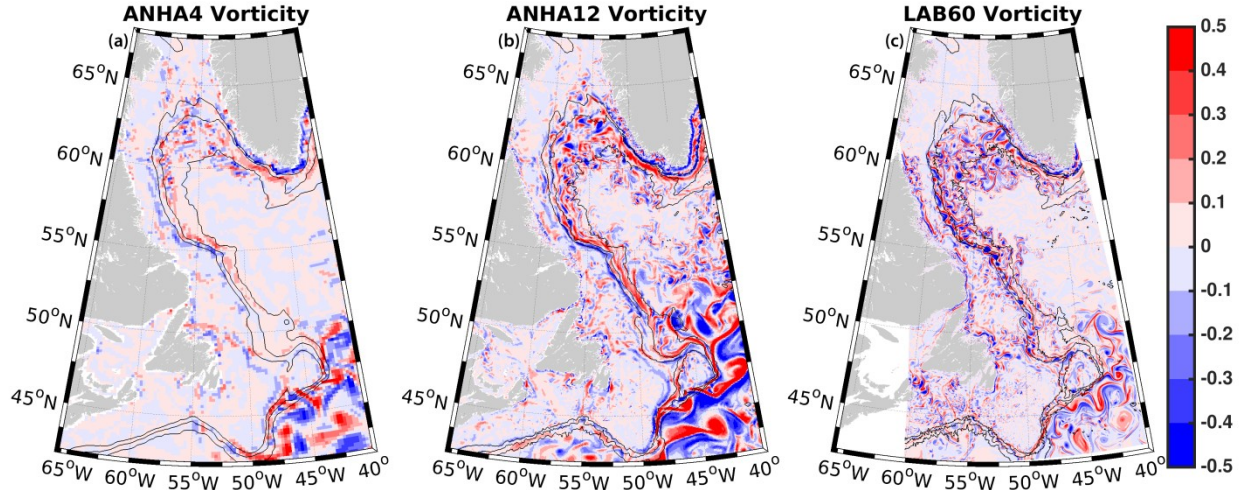
Figure 3. 6: Top 50m relative vorticity, normalized by the planetary vorticity, as simulated by (a) ANHA4, (b) ANHA12, and (c) LAB60 on 16 March 2008. The 1000m, 2000m, and 3000m isobaths are shown by the black contour lines.

A few Irminger Rings are shown in Fig. 3.7, a snapshot in time from 26 July 2007. A newly spawned ring (Fig. 3.7c) shows very strong surface speeds (up 0.6 m s^{-1} for Ring A; Fig. 3.7a) while older eddies to the south have reduced speeds (up to 0.3 m s^{-1} for Ring B; Fig. 3.7a). To investigate the stratification strength, we calculate the amount of energy needed to produce a neutrally stratified column extending down to some reference depth, h. This proxy, called convective energy, is given by:

$$Convective\ energy(h) = \frac{g}{Area} \int \int \left[h\,\rho_\theta(h) - \int_0^h \rho_\theta(z)\,dz \right] dA$$

where g is the gravitational constant, Area is the total surface area over our region of interest (Fig. 3.1c), h is the reference depth (2000m used in this study), $\rho_\theta(z)$ and $\rho_\theta(h)$ are the potential density at each grid cell and the potential density of the grid cell at the reference depth, and A is the surface area of each grid cell. A strongly stratified column of water corresponds to a high convective energy value. A snapshot of convective energy (Fig. 3.7b) shows that most of these eddies have substantially higher amounts compared

56
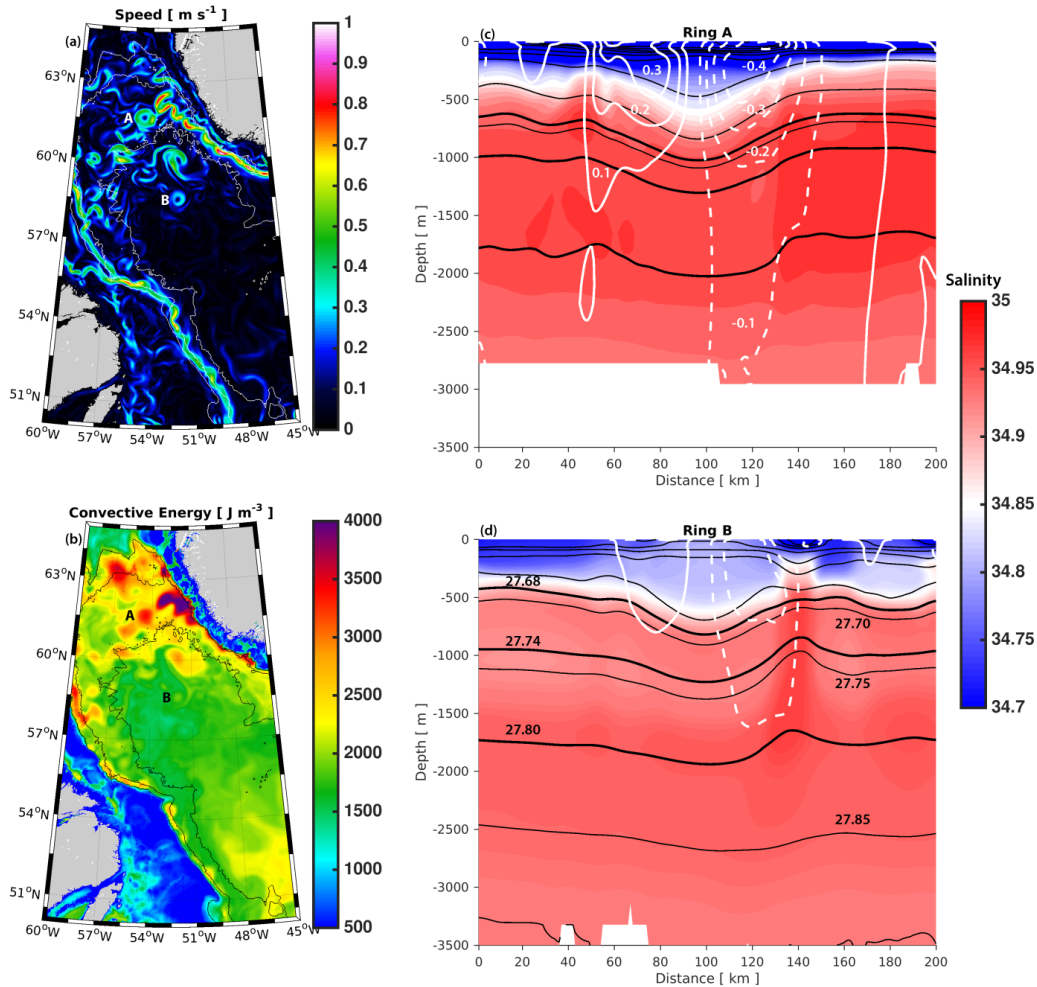
Figure 3. 7: LAB60 snapshot (26 July 2007) of the surface speed (a) and convective energy (b) within the Labrador Sea. Two Irminger Rings are identified by their age with letters: Ring A is a young Irminger Ring, while Ring B is comparatively older. An east-west cross section through each of these Irminger Rings is shown in (c) and (d) where colors indicate salinity, black contours indicate potential density using a contour interval of 0.05 kg m⁻³, and white contours indicate meridional velocity where southern flow is dashed and northern flow is solid, using a contour interval of 0.1 m s⁻¹. Thick black contours indicate the potential density classification of Upper Labrador Sea Water (σ_θ=27.68 to 27.74 kg m⁻³) and Classical Labrador Sea Water (σ_θ= 27.74 to 27.80 kg m⁻³).

to the background Labrador Sea, suggesting that the cool and fresh WGC water, as well as warm and salty Irminger Water keep these eddies strongly stratified. However, these eddies age within the Labrador Sea, and while a new eddy has strong stratification (>3000 J m⁻³), an eddy which has evolved over many months (Fig. 3.7d) has weaker stratification (about 2000 J m⁻³). Older eddies may have very weak stratification as they may have experienced two convective winter periods of buoyancy removal. This has

57

been noted before, as Lilly et al. (2003) found aged Irminger Rings with a mixed layer that surpassed 1000m.

These differences in resolving the mesoscale (50 to 500 km) and sub-mesoscale (<50 km) processes within each simulation produced significant changes within the Labrador Sea as seen from modeled convective energy values as averaged from 2004-2013 (Fig. 3.8). Resolving few eddies, the ANHA4 simulation's interior Labrador Sea lacks the buoyancy flux and remains very weakly stratified across a wide region. The ANHA12 simulation partially resolves some mesoscale features and eddy fluxes from the Greenland coast which supplies buoyancy to the Northern Labrador Sea and has higher convective energy. Furthermore, the spatial extent of the weakly stratified region has shrunk and resides primarily within the Labrador Sea, as opposed to ANHA4 which spills out of the basin. LAB60, fully capable of resolving buoyant eddies from the Greenland and Labrador coast, as well as convective eddies, has a much stronger degree of stratification in the interior region. A visible path of strong stratification appears around 60°N along this coastline, eventually extending away from the coastline around 62°N. This path is consistent with the general path that simulated Irminger Rings take (Chanut et al., 2008). Supplemental Video 3.2 shows the convective energy of the LAB60 simulation from 2004 through the end of 2013.

The ANHA4 simulation experiences weaker stratification in the Labrador Sea than ANHA12 and LAB60, driving a deeper maximum mixed layer that also covers a larger spatial extent (Fig. 3.9). However, the maximum mixed layer depth as simulated by ANHA4 and ANHA12 greatly exceed what Argo observations suggest (Fig. 3.9d). ANHA12 has higher EKE within the WGC, supplying more buoyancy to the northern portion of the Labrador Sea, reducing both the vertical extent of the mixed layer as well as the spatial extent where the mixed layer is deeper than 1000m. LAB60 has higher EKE than ANHA12, and the vertical and spatial extent of deep mixing is reduced even further. LAB60's mixed layer is far more similar to what ARGO observations suggest, suggesting the additional eddy fluxes to be fairly accurate. The evolution of LAB60's mixed layer depth is shown in Supplemental Video 3.3 from 2004 through the end of 2013.
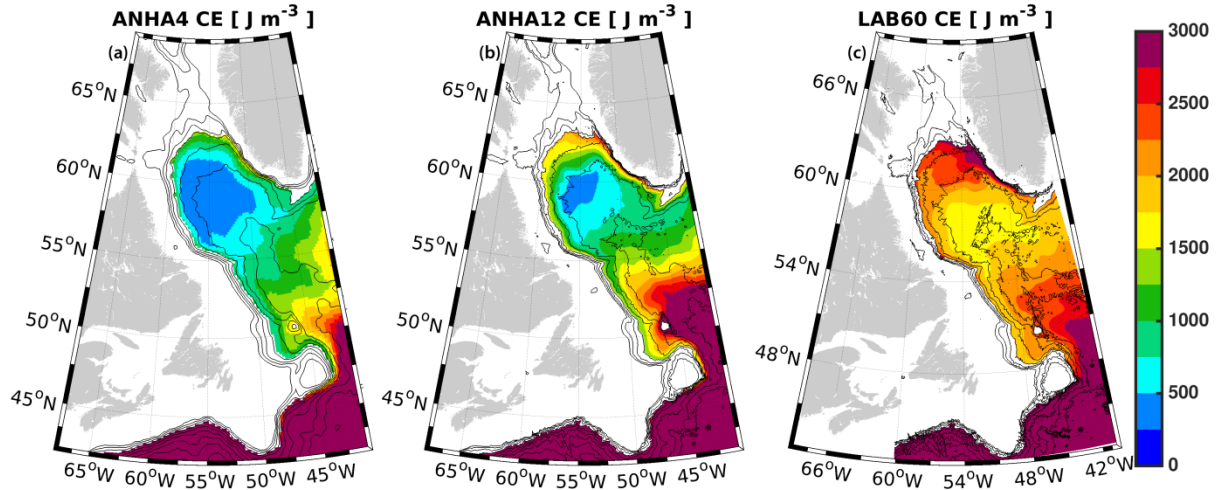
Figure 3. 8: Convective energy (CE), the strength of stratification down to a reference depth of 2000m, is shown for (a) ANHA4, (b) ANHA12, and (c) LAB60. Convective energy was averaged from 2004 through 2013. Values where the depth of the seafloor was less than 2000m were removed to preserve clarity. Bathymetric contours (black lines) are shown every 500m.

After the bottom of the mixed layer returns to the near-surface, a newly formed LSW mass is left behind. To account for density drift, we allow the LSW classification to evolve in time, unlike our LSW passive tracer. We calculated LSW density and thickness by binning by potential density, referenced to 1000 dbar, with bin lengths of 0.001 kg m^{-3}. This was carried out within the black outlined polygon in Fig 3.1c for each daily output file per year. The density bin which had the thickest layer across the year was set as the maximum density of LSW for that year. The minimum density was defined to be 0.02 kg m^{-3} less than the maximum density. Linear interpolation occurred between years to allow for a gradual shift in density to prevent staircase patterns from emerging. Large differences in both the density as well as the thickness are present between the simulations shown in Fig. 3.10. The ANHA4 and ANHA12 simulations have similar density values of LSW while the LAB60 simulation is less dense. While the interannual variability matches fairly well across all configurations, the density values suggested by LAB60 are closer to ARGO observations (32.34 to 32.36 kg m^{-3}; Yashayaev and Loder, 2016) during the same time period. We suspect the denser LSW formed by ANHA4 and ANHA12 is primarily attributed to the lack of buoyancy coming from Greenland. As similar air-sea heat losses should occur in all three configurations, the weaker stratification of ANHA4 and ANHA12 indicates that deep mixing is more likely
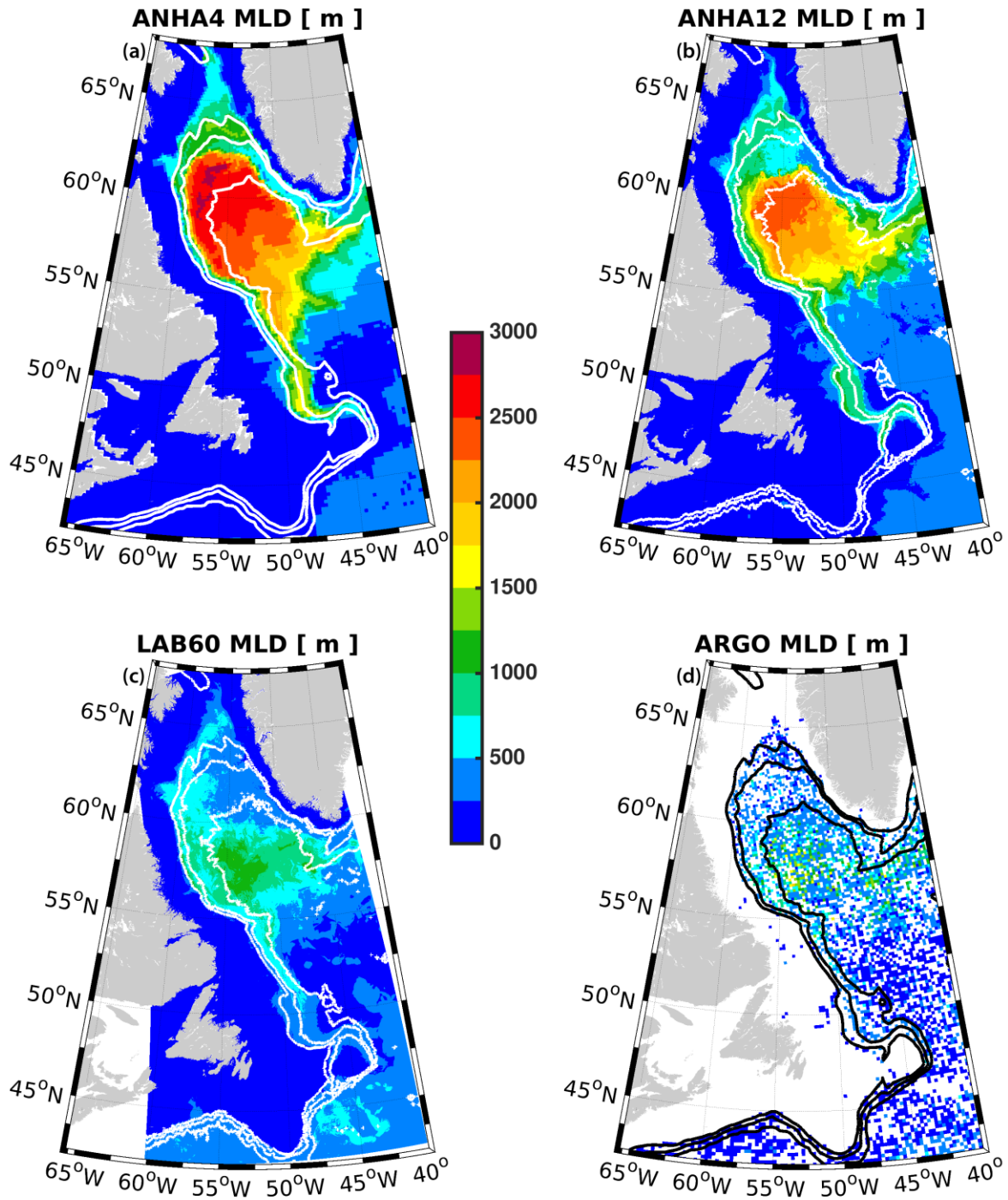
Figure 3. 9: Maximum mixed layer depth for (a) ANHA4, (b) ANHA12, (c) LAB60, as well as (d) ARGO observations, where available, from 2004 through the end of 2013. For clarity, the ARGO data were placed on the same grid as ANHA4. The 1000m, 2000m, and 3000m isobaths are shown via the white and black contours

producing not only a denser LSW layer, but also a thicker one. Yashayaev and Loder (2016) also investigated the thickness of LSW (their Fig. 8), and while our simulations

do not quite capture the same interannual variability and amplitude suggested by their analysis using ARGO profilers, LAB60 is far more accurate than the lower-resolution configurations.

All simulations encounter some degree of numerical drift within the Labrador Sea (Fig. 3.11), judging from the salt and heat content change as calculated between the surface and seafloor within the polygon in Figure 3.1 since 2004. ANHA4 experiences the largest drift in both salt and heat, helping us understand why LSW is so dense in this simulation. ANHA12 also experiences drift, though slightly less severe. LAB60 has a small but gradual increase in both salt and heat content although it is difficult to state if this is drift or simply interannual to decadal variability. Regardless of the cause, LAB60's change in both heat and salt content is very minimal compared against the lower-resolution simulations.

When compared against bottle data collected during a single hydrographic cruise across Atlantic Repeat Hydrography Line 7 West (AR7W; Fig 3.12), LAB60 is slightly warmer (about 0.25 °C) and saltier (about 0.05 kg m^{-3}) throughout the interior. This causes LAB60 to be slightly denser with isopycnals residing higher than observations during this cruise suggest. Observations were not carried out above Greenland's continental slope, although they show some presence of the warm core of the WGC which the model captures. Salinity values close to the Labrador coast compare well while LAB60 is slightly warmer (about 0.5 °C) above the continental shelf.

The three passive tracers implemented within the full LAB60 configuration (Fig. 3.3) show where Greenland runoff, Irminger Water, and Labrador Sea Water travel to. These tracers were selected because they either contain a significant amount of buoyant water compared to the Labrador Sea, or are produced via convection in the Labrador Sea. From this image on 1 Jan 2010, we see a large portion of Greenland's runoff (Fig. 3.3a) resides within Baffin Bay as well as along the Labrador Coast. Some of this tracer is present where the ocean depth is greater than 2000m. A few Irminger Rings are identifiable, due to their thicker freshwater cap, which are in water deeper than 3000m. Little exchange with the interior basin appears to occur along the Labrador Current until the vicinity of Flemish Cap, after which a significant portion of the tracer propagates
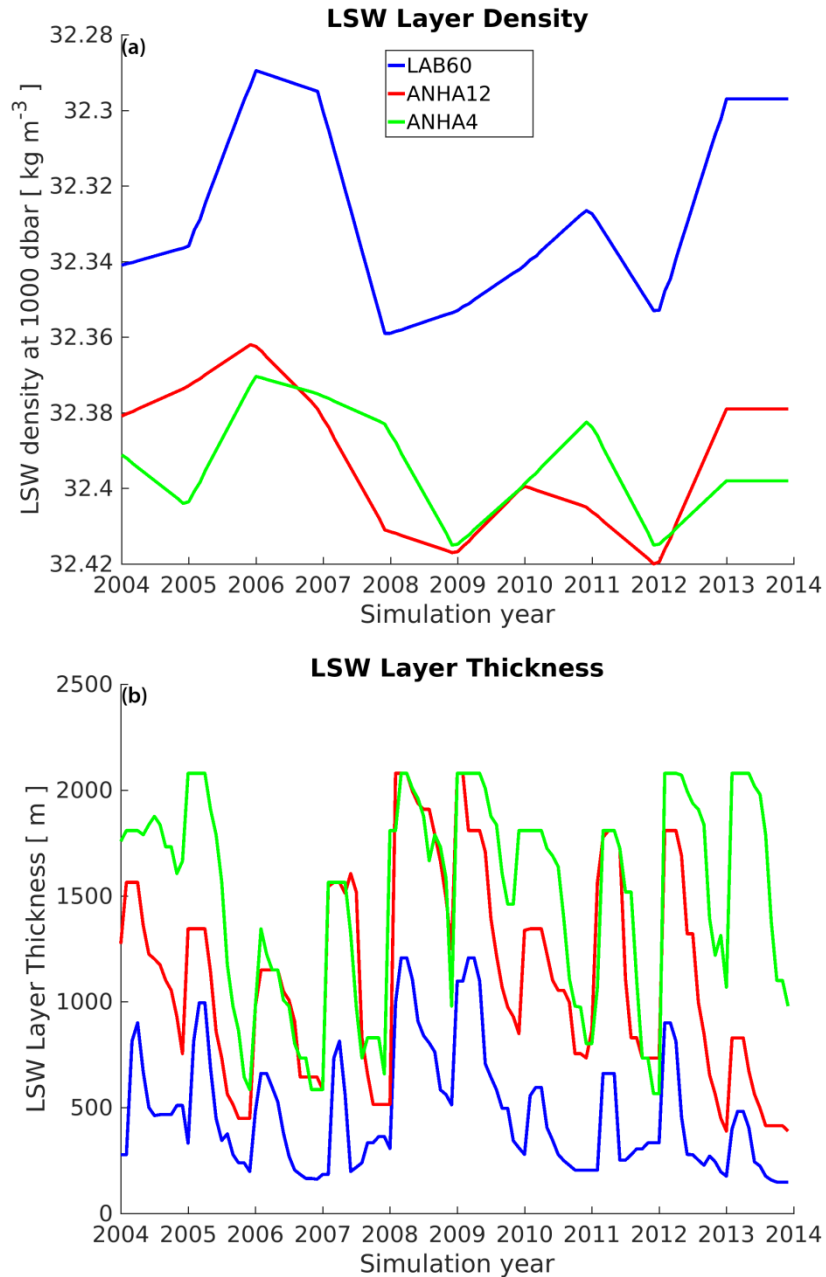
Figure 3. 10: Labrador Sea Water (LSW) density (a) and thickness (b) for the LAB60, ANHA12, and ANHA4 configurations. LSW density was determined from the thickest layer where a 0.001 kg m-3 change in potential density (ref: 1000 dbar) occurred within the black polygon outlines in Fig 1c. The LSW layer was then calculated between this density and one which was 0.02 kg m-3 less dense.
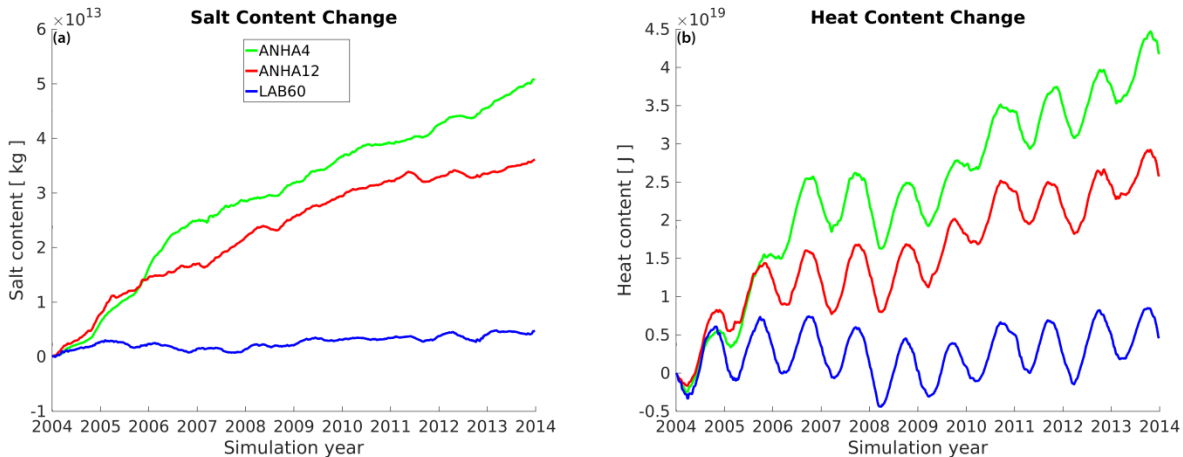
Figure 3. 11: Numerical salt (a) and heat (b) drift in our three simulations as they evolve since 1 Jan 2004. Salt and heat content is calculated over the full ocean column within the polygon in Fig. 1c.

eastward. Supplemental Video 3.4 shows this the evolution of this tracer from 2004 through the end of 2013.

Irminger Water (T>3.5°C, S> 34.88; Fig. 3.3b) which flows west past Cape Farewell, enters the interior Labrador Sea with the greatest amounts where the seafloor is at a depth between 2000 and 3000m. Similar as above, individual Irminger Rings are visible, containing a larger amount of Irminger Water than the surrounding water. This water mass also flows along the Labrador Coast until it is in the vicinity of Flemish Cap. Supplemental Video 3.5 shows this the evolution of this tracer from 2004 through the end of 2013.

Our Labrador Sea Water tracer (Fig. 3.3c) is traced where the mixed layer produces water with a potential density above 1027.68 kg m-3 within the black contour identified in the figure. This definition differs compared to our method of classifying LSW as we did not implement any FORTRAN code to detect and compensate for density drift of our simulation, instead sticking to a strict density classification for this tracer. As this image was made at the start of the convection season, the current deep patch is a freshly produced layer that reaches up to 800m deep. After forming, LSW spreads southwards along the Labrador shelf break as well as to the southeast. Supplemental Video 3.6 shows this the evolution of this tracer from 2004 through the end of 2013.
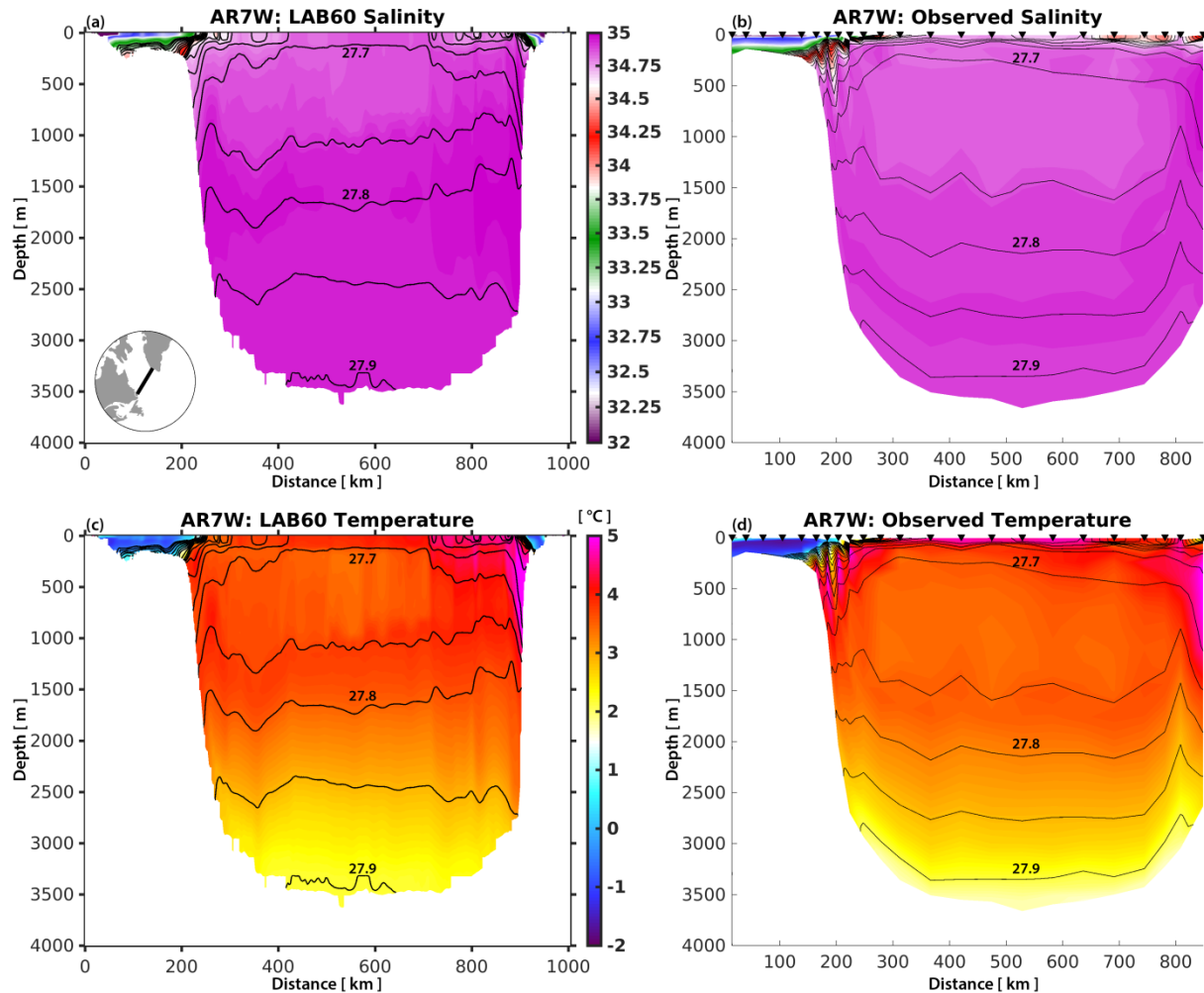
Figure 3. 12: Salinity (top) and temperature (bottom) section across AR7W as determined by the LAB60 simulation (left) and observations (right) from May 2008. Downward triangles identify collection sites across the AR7W transit carried out by the CCGS Hudson. Potential density (black contours) isopycnal interval is 0.05 kg m⁻³.

3.5. Discussion

We describe a 10+ year long, high-resolution simulation which achieves 1/60° horizontal resolution in the Labrador Sea via two nests inside a regional configuration, resolving mesoscale and sub-mesoscale processes which strongly impact the deep convection which occurs here. We show that lower-resolution simulations fail to resolve these key processes that strongly control the production of Labrador Sea Water, an important water mass within the Atlantic Meridional Overturning Circulation. While the NATL60 and eNATL60 simulations were designed with the SWOT altimetry satellite

mission in mind (NATL60 website: https://meom-group.github.io/swot-natl60/virtual-ocean.html), their integration period, like many other high-resolution simulations, is a handful of years. LAB60, although covering a much smaller region, could be a valuable asset to many users who require a lengthy period of high-resolution model output. We also have included three passive tracers which are often excluded in simulations at this resolution. Our three passive tracers highlight regions where each water mass enters the interior region of the Labrador Sea, demonstrating the pathways of buoyant Greenland melt and Irminger water. Furthermore, we trace Labrador Sea Water which is formed during the convective winter period.

We show that LAB60 has greater EKE than our lower-resolution simulation, resolving eddy fluxes including Irminger Rings, boundary current eddies, and likely convective eddies as indicated by greater EKE within the interior. Boundary current eddies still appear relatively disconnected from the interior basin, adding further support that these eddies have limited influence on convection and restratification (Rieck et al., 2019). We offer no additional support regarding the relative importance of Irminger Rings and convective eddies on controlling deep convection; this is currently being investigated for a later manuscript. Model drift appears very low, a large improvement over the ANHA4 and ANHA12 configurations. The drift might produce slightly denser LSW than observations suggest, however LAB60s density is much more accurate than ANHA4 and ANHA12. The boundaries of LAB60, supplied by the inner SPG12 nest, may influence the high-resolution nest. We note that the North Atlantic Current, which is close to the boundary, has less EKE and vorticity than the ANHA4 and ANHA12 simulations. Conversely, the WGC close to the eastern nested boundary has multiple jets which have been noted in hydrographic data (Pickart, personal communication). Boundary communication is always a concern in nested simulations and LAB60 is no different. More investigation will reveal any potential boundary issues but our results so far indicate no further areas of potential concern.

Others have investigated the Labrador Sea using numerical simulations with different resolution. Böning et al. (2016) traced Greenland meltwater with the 1/20° VIKING20 and 1/4° ORCA025 simulations, noting more meltwater entered the interior Labrador Sea at higher resolution partially as a result of greater WGC eddy fluxes but

not from the Labrador coast. The minor amount of eddy fluxes from the Labrador coast has been noted earlier even at lower resolution (1/3°; Myers, 2005). Steadily increasing horizontal resolution has so far not changed this for the Labrador coast, though this is opposite for the WGC. LAB60 has a clear increase in EKE and likely greater eddy fluxes from the WGC into the interior of the Labrador Sea.

We have many ambitious research topics which we plan to use LAB60 to investigate. This includes, but is not limited to, the variability and structure of the West Greenland Coastal Current, Labrador Sea Water production, and the role of both Irminger Rings and convective eddies in controlling stratification in the Labrador Sea. This lengthy high-resolution simulation with three passive tracers will provide valuable information for many numerical studies within the Labrador Sea for years to come.

Code and/or data availability

The FORTRAN code used to carry out the LAB60 simulation can be accessed from the NEMO version 3.6 repository (https://forge.ipsl.jussieu.fr/nemo/browser/NEMO/releases/release-3.6). A few FORTRAN files were modified to handle our passive tracers. The complete FORTRAN files as well as the CPP.keys, namelists, and associated files can be found on Zenodo (Pennelly, 2020). Initial and boundary conditions, atmospheric forcing, and numerical output were too large to host on a repository and instead are hosted on our lab's servers as well as the Compute Canada Niagara server. These data can be requested by emailing the corresponding author.

Author Contribution

PM designed the layout of the LAB60 configuration which included the region of interest, numerical length, and which forcing and initial conditions to supply, as well as supervised CP. CP produced the configuration, modified the FORTRAN code, set up the configuration on the high-performance computing systems, carried out the simulation, and performed the analysis. The manuscript was prepared by CP with contributions by PM.

Bibliography

Amante, C. and Eakins, B.W.: ETOPO1 1 Arc-minute global relief model: procedures data sources and analysis. NOAA Technical Memorandum NESDIS, NGDC-24 19, 2009.

Bacon, S., Gould, W.J., and Jia, Y.: Open-ocean convection in the Irminger Sea. Geophysical Research Letters, 30(5), 2003.

Bamber, J., van den Broeke, M., Ettema, J., Lenaerts, J., and Rignot, E.: Recent large increases in freshwater fluxes from Greenland into the North Atlantic. Geophysical Research Letters, 39(19), 2012.

Barnier, B., Madec, G., Penduff, T., Molines, J-M., Treguier, A-M., Le Sommer, J., Beckmann, A., Biastoch, A., Böning, C., Dengg, J., Derval, C., Durand, E., Gulev, S., Remy, R., Talandier, C., Theetten, S., Maltrud, M., Mcclean, J., and De Cuevas, B.: Impact of partial steps and momentum advection schemes in a global ocean circulation model at eddy permitting resolution. Ocean Dynamics, 56 (5-6), 543-567, 2006.

Böning, C.W., Behrens, E., Biastoch, A., Getzlaff, K., and Bamber, J.L.: Emerging impact of Greenland meltwater on deepwater formation in the North Atlantic Ocean. Nature Geoscience, 97(7), 523, 2016.

Brossier, C.L., Léger, L., Giordani, H.,Beuvier, J., Bouin, M.N., Ducrocq, W., and Fourrié, N.: Dense water formation in the north-western Mediterranean area during HyMeX-SOP2 in 1/36° ocean simulations: Ocean-atmosphere coupling impact. Journal of Geophysical Research: Oceans, 122(7), 5749-5773, 2017.

Bryden, H.L., Longworth, H.R., and Cunningham, S.A.: Slowing of the Atlantic meridional overturning circulation at 25°N. Nature, 438(7068), 655, 2005.

Cael, B.B. and Jansen, M.F.: On freshwater fluxes and the Atlantic meridional overturning circulation. Limnology and Oceanography, 5(2), 185-192, 2020.

Chanut, J., Barnier, B., Large, W., Debreu, L., Penduff, T., Molines, J.M., and Mathiot, P.: Mesoscale eddies in the Labrador Sea and their contribution to convection and restratification. Journal of Physical Oceanography, 28(8), 1617-1643, 2008.

Chassignet, E.P. and Xu, X.: Impact of horizontal resolution (1/12 to 1/50) on Gulf Stream separation, penetration, and variability. Journal of Physical Oceanography, 47(8), 1999-2021, 2017.

Courtois, P., Hu, X., Pennelly, C., Spence, P., and Myers, P.G.: Mixed layer depth calculation in deep convection regions in ocean numerical models. Ocean Modelling, 120, 60-78, 2017.

Cuny, J., Rhines, P.B., and Kwok, R.,: Davis Strait volume, freshwater and heat fluxes. Deep Sea Research Part I: Oceanographic Research Papers, 52.3, 519-542, 2005.

Curry, B., Lee, C.M., and Petrie, B.: Volume, freshwater, and heat fluxes through Davis Strait, 2004-05. Journal of Physical Oceanography, 41(3), 429-436, 2011.

Curry, B., Lee, C.M., Petrie, B., Moritz, R.E. and Kwok, R.: Multiyear volume, liquid freshwater, and sea ice transports through Davis Strait, 2004-10. Journal of Physical Oceanography, 44(4), 1244-1266, 2014.

Dai, A., Qian, T., Trenberth, K.E., and Milliman, J.D.: Changes in continental freshwater discharge from 1948 to 2004. Journal of Climate, 22(10), 2773-2792, 2009.

de Steur, L., Hansen, E., Gerdes, R., Karcher, M., Fahrbach, E., Holfort, J.: Freshwater fluxes in the East Greenland Current: A decade of observations. Geophysical Research Letters, 36(23), 2009.

Debreu, L., Vouland, C., and Blayo, E.: AGRIF: Adaptive grid refinement in Fortran. Computers and Geosciences, 34(1), 8-13, 2008.

Dussin, R., Barnier, B., and Brodeau, L.: The making of Drakkar forcing set DFS5, Grenoble, France: LGGE, 2016.

Ferry, N., Parent, L., Garric, G., Barnier, B., and Jourdain, N.C.: Mercator global eddy permitting ocean reanalysis GLORYS1V1: Description and results. Mercator-Ocean Quarterly Newsletter, 36, 15-27, 2010.

Fichefet, T., and Maqueda, M.A.M.: Sensitivity of a global sea ice model to the treatment of ice thermodynamics and dynamics. Journal of Geophysical Research: Oceans, 102(C6), 12609-12646, 1997.

Fischer, J., Visbek, M., Zantopp, R., Nunes, N.: Interannual to decadal variability of outflow from the Labrador Sea. Geophysical Research Letters, 37(24), 2010.

Frajka-Williams, E., Rhines, P.B., and Eriksen, C.C.: Horizontal stratification during deep convection in the Labrador Sea. Journal of Physical Oceanography, 44(1), 220-228, 2014.

Fratantoni, P.S. and Pickart, R.S.: The Western North Atlantic Shelfbreak Current System in Summer. Journal of Physical Oceanography, 37(10), 2509-2533, 2007.

Fresnay, S., Ponte, A.L., Le Gentil, S., Le Sommer, J.: Reconstruction of the 3-D dynamics from surface variable in a high-resolution simulation of the North Atlantic. Journal of Geophysical Research: Oceans, 123(3), 1612-1630, 2018.

Garcia-Quintana, Y., Courtois, P., Hu, X., Pennelly, C., Kieke, D., and Myers, P.G.: Sensitivity of Labrador Sea Water formation to changes in model resolution, atmospheric forcing, and freshwater input. Journal of Geophysical Research: Oceans, 124(3), 2126-2152, 2019.

Gelderloos, R., Katsman, C.A. and Drijfhout, S.S.: Assessing the roles of three eddy types in restratifying the Labrador Sea after deep convection. Journal of Physical Oceanography, 41(11), 2102-2119, 2011.

Gordon, A.L., Visbeck, M., and Comiso, J.C.: A possible link between the Weddell Polynya and the Southern Annular Mode. Journal of Climate, 20(11), 2558-2571, 2007.

Hansen, B., and Østerhus, S.: North Atlantic-Nordic Seas exchanges. Progress in Oceanography, 45(2), 109-208, 2000.

Hátún, H., Eriksen, C.C., and Rhines, P.B.: Buoyant eddies entering the Labrador Sea observed with gliders and altimetry. Journal of Physical Oceanography, 37(12), 2838-2854, 2007.

Holte, J., and Talley, L.: A new algorithm for finding mixed layer depths with applications to Argo data and Subantarctic Mode Water formation. Journal of Atmospheric and Oceanic Technology, 26(9), 1920-1939, 2009.

Kieke, D., Klein, B., Stramma, L., Rhein, M., and Koltermann, K.P.: Variability and propagation of Labrador Sea Water in the southern subpolar North Atlantic. Deep Sea Research Part I: Oceanographic Research Papers, 56(10), 1656-1674, 2009.

Lab Sea Group: The Labrador Sea deep convection experiment. Bulletin of the American Meteorological Society, 79(10), 2033-2058, 1998.

Large, W.G., and Yeager, S.G.: The global climatology of an interannually varying air-sea flux data set. Climate Dynamics, 33(2-3), 341-364, 2008

Latif, M., Roechner, E., Mikolajewicz, U., and Voss, R.: Tropical stabilization of the thermohaline circulation in a greenhouse warming simulation. Journal of Climate, 13(11), 1809-1813, 2000.

Lazier, J., Hendry, R., Clarke, A., Yashayaev, I., and Rhines, P.: Convection and restratification in the Labrador Sea, 1990-2000. Deep Sea Research Part I: Oceanographic Research Papers, 49(10), 1819-1835, 2002.

Lazier, J.R.N., and Wright, D.G.: Annual velocity variations in the Labrador Current, Journal of Physical Oceanography, 23(4), 659-678, 1993.

Lilly, J.M., Rhines, P.B., Visbeck, M., Davis, R., Lazier, J.R.N., Schott, F., and Farmer, D.: Observing deep convection in the Labrador Sea during winter 1994/95. Journal of Physical Oceanography, 29, 2065-2098, 1999.

Lilly, J.M., Rhines, P.B., Schott, F., Lavender, K., Lazier, J., Send, U., and D'Asaro, E.: Observations of the Labrador Sea eddy field. Progress in Oceanography, 59(1), 75-176, 2003.

Lin, P., Pickart, R.S., Torres, D.J., and Pacini, A.: Evolution of the freshwater coastal current at the southern tip of Greenland. Journal of Physical Oceanography, 48(9), 2127-2140. 2018

Madec, G.: Note du Pôle de modélisation. Institut Pierre-Simon Laplace (IPSL), France, No 27, ISSN No 1288-1619, 2008.

Marshall, J. and Schott, F.: Open-ocean convection: Observations, theory, and models. Reviews of Geophysics, 37(1), 1-64, 1999.

Marzocchi, A., Hurshi, J.J.M., Holiday, N.P., Cunningham, S.A., Blaker, A.T., and Coward, A.C.: The North Atlantic subpolar circulation in an eddy-resolving global ocean model. Journal of Marine Systems, 142, 126-143, 2015.

McGeehan, I. and Maslowski, W.: Impact of shelf-basin freshwater transport on deep convection in the western Labrador Sea. Journal of Physical Oceanography, 41(11), 2187-2210, 2011.

Müller, V., Kieke, D., Myers, P.G., Pennelly, C., and Mertens, C.: Temperature flux carried by individual eddies across 47° in the Atlantic Ocean. Journal of Geophysical Research: Oceans, 122(3), 2441-2464, 2017.

Müller, V., Kieke, D., Myers, P.G., Pennelly, C., Steinfeldt, R., and Stendardo, I.: Heat and freshwater transport by mesoscale eddies in the southern subpolar North Atlantic. Journal of Geophysical Research: Oceans, 124(8), 5565-5585, 2019.

Myers, P.: Impact of freshwater from the Canadian Arctic Archipelago on Labrador Sea water formation. Geophysical Research Letters, 32(6), 2005.

Pennelly, C.: A 1/60 degree NEMO configuration within the Labrador Sea: LAB60, Zenodo, http://doi.org/10.5281/zenodo.3762748, 2020.

Pennelly, C. Hu, X., and Myers, P.G.: Cross-isobath freshwater exchange within the North Atlantic Subpolar Gyre. Journal of Geophysical Research: Oceans, 124(10), 6831-6853, 2019.

Pennelly, C. and Myers, P.G.: Impact of different atmospheric forcing sets on modelling Labrador Sea Water production. Journal of Geophysical Research: Oceans, 126(2), 2021.

Rattan, S., Myers, P.G., Treguier, A.M., Theetten, S., Biastoch, A., and Böning, C. Towards an understanding of Labrador Sea salinity drift in eddy-permitting simulations. Ocean Modelling, 35(102), 77-88, 2010.

Rieck, J.K., Böning, C.W., and Getzlaff, K.: The nature of eddy kinetic energy in the Labrador Sea: Different types of mesoscale eddies, their temporal variability, and impact on deep convection. Journal of Physical Oceanography, 49(8), 2075-2094, 2019.

Schmidt, S. and Send, U.: Origin and composition of seasonal Labrador Sea freshwater. Journal of Physical Oceanography, 37(6), 1445-1454, 2007.

Schulze-Chretien, L.M., Pickart, R.S., and Moore, G.W.K.: Atmospheric forcing during active convection in the Labrador Sea and its impact on mixed-layer-depths. Journal of Geophysical Research: Oceans, 121(9), 6978-6992, 2016.

Smith, G.C., Roy, F., Mann, P., Dupont, F., Brasnett, B., Lemieux, J.F., Laroche, S., and Bélair, S.: A new atmospheric dataset for forcing ice-ocean models: Evaluation of reforecasts using the Canadian global deterministic prediction system. Quarterly Journal of the Royal Meteorological Society, 140(680), 881-894, 2014.

Straneo, F.: Heat and freshwater transport through the central Labrador Sea. Journal of Physical Oceanography, 36(4), 606-628, 2006.

Straneo, F. and Saucier, F.: The arctic-subarctic exchange through Hudson Strait. Arctic-Subarctic Ocean Fluxes, Springer, Dordrecht, 249-261, 2008.

Su, Z., Wang, J., Klein, P., Thompson, A.F., and Menemenlis, D.: Ocean submesoscales as a key component of the global heat budget. Nature communications, 9(1), 1-8, 2018.

Tréquier, A.M., Theetten, S., Chassignet, E.P., Penduff, T., Smith, R., Talley, L., Beismann, J.O., and Böning, C.: The North Atlantic subpolar gyre in four high-resolution models. Journal of Physical Oceanography, 35(5), 757-774, 2005.

Yashayaev, I. and Loder, J.W.: Recurrent replenishment of Labrador Sea Water and associated decadal-scale variability. Journal of Geophysical Research: Oceans, 121(11), 8095-8814, 2016.

Yashayaev, I.: Hydrographic changes in the Labrador Sea, 1960-2005. Progress in Oceanography, 73(3-4), 242-276, 2007.

Whiteworth, T. and Orsi, A.H.: Antarctic Bottom Water production and export by tides in the Ross Sea. Geophysical Research Letters 33(12), 2006.

Zalesak, S.T.: Fully multidimensional flux-corrected transport algorithms for fluids. Journal of computational physics, 31(3), 335-362, 1979.

Supplemental Material:

Supplemental Video 3.1: A video showing LAB60's relativey vorticity normalized by the planetary vorticity from 2004 through the end of 2013: https://doi.org/10.7939/r3-2yts-nw62

Supplemental Video 3.2: A video showing LAB60's stratification strength from 2004 through the end of 2013: https://doi.org/10.7939/r3-nen0-g831

Supplemental Video 3.3: A video showing LAB60's mixed layer depth (colored contours) and where the 10% sea ice concentration (red contour) occurs, from 2004 through the end of 2013: https://doi.org/10.7939/r3-m6rk-h867

Supplemental Video 3.4: A video showing LAB60's passive Greenland meltwater tracer from 2004 through the end of 2013: https://doi.org/10.7939/r3-43mg-db88

Supplemental Video 3.5: A video showing LAB60's passive Irminger Water tracer which flows past Cape Farewell from 2004 through the end of 2013: https://doi.org/10.7939/r3-zwkr-0w35

Supplemental Video 3.6: A video showing LAB60's passive Labrador Sea Water created from 2004 through the end of 2013: https://doi.org/10.7939/r3-7295-ks15

Chapter 4: Cross-Isobath Freshwater Exchange within the North Atlantic Sub-Polar Gyre

Clark Pennelly[1*], Xianmin Hu[1,2], Paul G. Myers[1]

[1] Department of Earth and Atmospheric Sciences, University of Alberta

[2] Bedford Institute of Oceanography, Fisheries and Oceans Canada, Dartmouth, Nova Scotia, Canada

*Corresponding author: Pennelly@ualberta.ca

Key points:

1. An increase of the freshwater transport within the West Greenland Current will result in an increase in offshore freshwater transport.

2. The transport of turbulent freshwater from all regions around the Labrador Sea acts to freshen the interior basin.

3. Salty Irminger and Labrador Sea Water typically flow onshore, removing salt from the interior basin.

4.1. Abstract

The amount of cross-isobath freshwater exchange within the North Atlantic sub-polar gyre is estimated from numerical modelling simulations. A regional configuration of the Nucleus for European Modelling of the Ocean model is used to carry out three simulations with horizontal resolutions of 1/4°, 1/12°, and 1/4° with a 1/12° nested domain. Freshwater transport is calculated across five isobaths in six regions for three distinct water masses. Fresh Polar Water is only transported offshore from the western coast of Greenland and the southern coast of Labrador; other regions have onshore transport of freshwater or little offshore transport. The salty water masses of Irminger and Labrador Sea Water typically have onshore transport, acting to promote subsurface freshening of the Labrador Sea. The freshwater transport via the Polar Water mass experiences a large degree of seasonal variability while the Irminger and Labrador Sea

Water masses do not. Decomposing the freshwater transport into the mean and turbulent components indicates that most regions and water masses have stronger freshwater transport associated with the mean flow while the turbulent flow in often the opposite direction. The only water mass and region where the mean and turbulent freshwater transport act in the same direction is Polar Water along the western margin of Greenland. Model resolution plays an important role in determining cross-isobath exchange as our results from an identically forced simulation at 1/4° has reduced seasonal cycles, reduced transport, and sometimes transport in the opposite direction when compared against the 1/12° resolution simulations.

4.2. Plain Language Summary

The Labrador Sea, between Greenland and Canada, is a region where deepwater is formed, a crucial component in the oceanic transport of heat between the equator and the poles. An input of freshwater can interrupt this process by making deepwater more difficult to produce. While we know the Labrador Sea receives freshwater from the surrounding currents, we are not confident where, and how much, freshwater leaves the boundary of the Labrador Sea to enter the interior region. We explore this using numerical simulations in a region where real data collection is difficult due to extreme ocean conditions. Our simulations suggest that the west coast of Greenland is the region where most of the freshwater leaves the boundary current and enters the deeper basin. The other regions either have freshwater travelling the opposite direction or very little transport to begin with. We also investigated the short-lived turbulent transport of freshwater which was generally flowing from the coastal region to the deep basin, often acting opposite the long-term flow.

Keywords: Labrador Sea, Freshwater, Numerical Modelling, Stratification, Boundary currents

4.3. Introduction

The Labrador Sea, located between Greenland and the northeastern coast of Canada, is surrounded by boundary currents carrying significant volumes of freshwater. However, the regions where freshwater leaves the boundary current and enters the interior of the Labrador Sea, impacting deep convection within, is not well understood. Fram Strait, between Svalbard and Greenland, serves as a gateway for a significant amount of fresh Arctic water which travels southwards (de Steur et al., 2018). This East Greenland Current carries around 2 Sv (1 Sv = 10^6 m^3 s^{-1}) of cold and fresh Arctic water (Sutherland and Pickart, 2008; Tsubouchi et al., 2012) along the southern tip of Greenland (Fig. 4.1d), and between 59 and 96 mSv of freshwater relative to a salinity of 34.8 (Sutherland and Pickart, 2008; de Steur et al., 2009). As the East Greenland Current flows westwards past Cape Farewell it merges with a warm and salty current carrying Irminger Water (de Jong et al., 2016; Lazier et al., 2002; Myers et al., 2009; Cuny et al., 2002), with a freshwater transport of between -8 and -10 mSv (referenced to 35.0, Myers et al., 2007). This current system becomes the West Greenland Current with cold and fresh water of Arctic origin at the surface as well as warm and salty Irminger Water beneath (Fratantoni and Pickart, 2007). Meltwater from Greenland supplies additional freshwater to the current system (Myers et al., 2009; Luo et al., 2016), further increasing the East and West Greenland Current's freshwater transport. After flowing north along the western coast of Greenland, the West Greenland Current splits with one path through Davis Strait into Baffin Bay (Curry et al., 2014), and the remaining path westwards along the northern extent of the Labrador Sea. Outflow from Baffin Bay carries cold and fresh Arctic and Canadian Arctic water through Davis Strait with a freshwater transport between 92 and 116 mSv relative to 34.8 (Cuny et al., 2005; Curry et al., 2014; Curry et al., 2011). Hudson Strait also releases a significant amount of freshwater to the Labrador Sea, with a net freshwater transport around 38 mSv relative to 34.8 (Straneo and Saucier, 2008b). Both outflows join with the West Greenland Current, merging to become the Labrador Current (Lazier and Wright, 1993), and promote freshening of the northern Labrador Shelf (Straneo and Saucier, 2008a). The

Labrador Current flows southwards along the Labrador coast, past Flemish Cap, leaving the Labrador Sea.
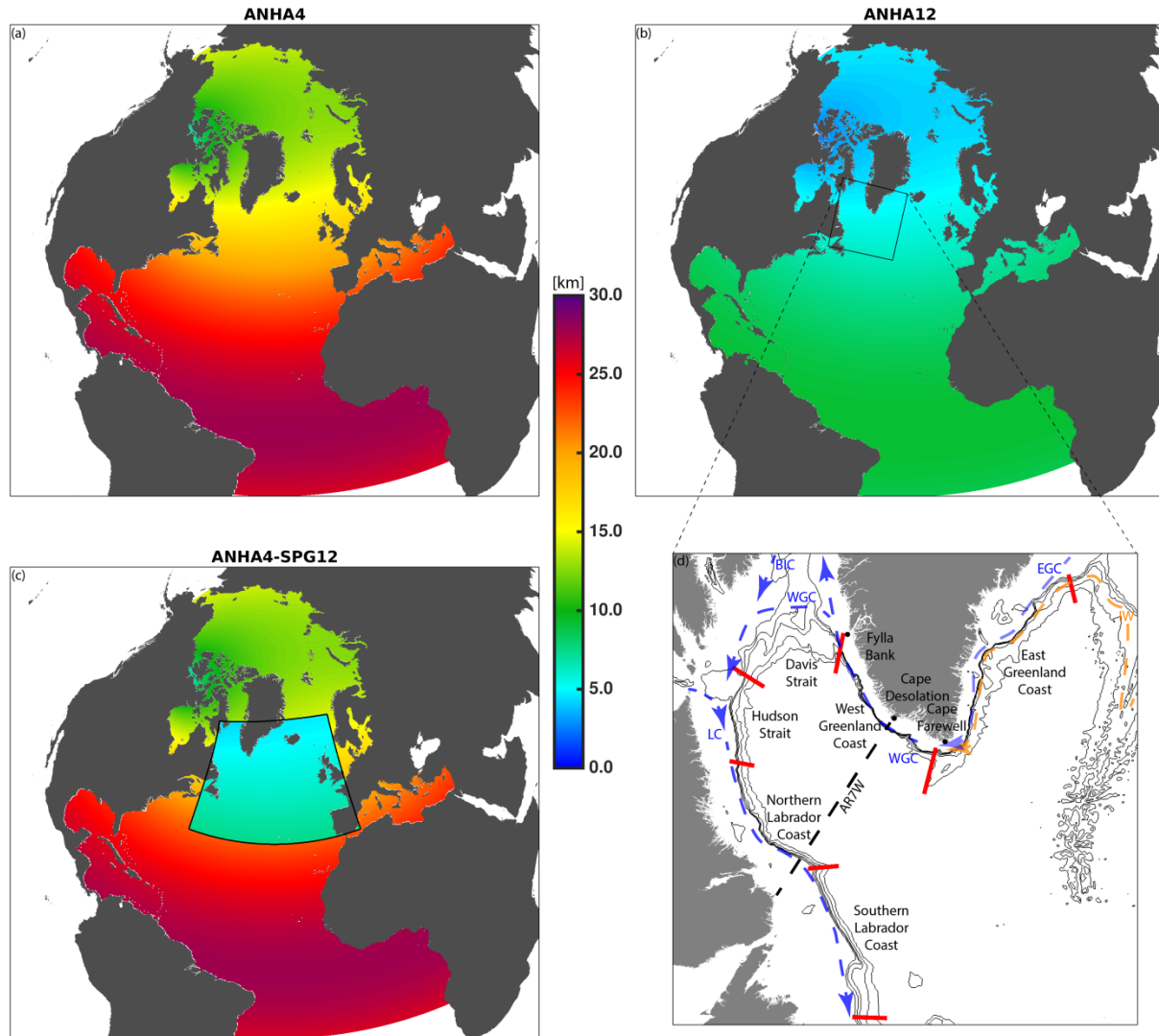
Figure 4. 1: Domain setup for simulation ANHA4 (a), ANHA12 (b), and ANHA4 with a 1/12° nest within the sub-polar gyre (SPG12) (c), with colored contours representing horizontal grid resolution. The box in (b) contains the North Atlantic sub-polar gyre region (d), showing bathymetry contours for 500, 750, 1000, 1500, and 2000 meters of depth. Red lines indicated the start and end section of the regions analyzed in this manuscript. Surface and subsurface currents are show in (d), where abbreviations in are as follows: EGC - East Greenland Current; WGC - West Greenland Current; BIC - Baffin Island Current; LC - Labrador Current; IW - Irminger Water.

While the above currents flow cyclonically around the Labrador Sea, regions around the Labrador Sea experience freshwater exchange between the boundary current

and the interior. The western coast of Greenland has been well documented, though this is not the case for other regions around the Labrador Sea. At the southwestern tip of Greenland, offshore freshwater transport begins downstream of Cape Farewell (Lin et al., 2018). As the West Greenland Current continues northwards towards Davis Strait, a significant amount of offshore freshwater exchange occurs, upwards of 60-80 mSv (Myers et al., 2009; Schmidt and Send, 2007). Ekman transport along this coast is strengthened during the winter and spring, due to northwesterly winds, amplifying offshore freshwater transport (Schulze-Chretien and Frajka-Williams, 2018). Unique eddies, known as Irminger Rings, spawn within this region where topographic changes promote instability within the current system (Chanut et al., 2008; de Jong et al., 2016). These eddies are steered offshore from the current system, impacting the interior of the Labrador Sea by transporting both freshwater and heat (Kawasaki and Hasumi, 2014).

Regions downstream of the western coast of Greenland also play an important role in the freshwater exchange between the boundary currents and the Labrador Sea. From a 1/3° numerical simulation, Myers (2005) found that Arctic water flowing within the East and West Greenland Current enters the interior of the Labrador Sea with much larger quantities than Arctic water which flows southwards through Davis Strait. When Myers (2005) increased freshwater transport through Davis Strait, relatively little additional freshwater entered the interior of the Labrador Sea, suggesting that freshwater along the western rim of the Labrador Sea does not penetrate into the interior easily. Schmidt and Send (2007) suggest that the Labrador Current could supply a significant amount of freshwater towards the interior Labrador Sea. While McGeehan and Maslowski (2011) used a higher resolution 1/12° numerical model to suggest that the Labrador Current transports freshwater offshore, they found the transport was small but non-insignificant. Lagrangian particle analysis from the output of a 1/12° model simulation further support both notions; that freshwater does exchange from the Labrador Current into the Labrador Sea although in relatively low amounts (Schulze-Chretien and Frajka-Williams, 2018). Many other regions around the Labrador Sea remain relatively unexplored in terms of any cross-shelf freshwater exchange.

Freshwater acts to stabilize the water column by increasing stratification which then limits vertical movement. However, some regions around the world have favorable conditions which promote deep convection, a process which is strongly dependent of the

stratification of the water column. These regions are the Weddell and Ross Sea off Antarctica (Gordon et al., 2007; Whitworth and Orsi, 2006), the Mediterranean Sea (Marshall and Schott 1999; Brossier et al., 2017), the Nordic Seas (Hansen and Østerhus, 2000), the Irminger Sea (Bacon et al., 2003), and the Labrador Sea (e.g. Yashayaev and Loder, 2017; Yashayaev and Loder, 2009; Yashayaev, 2007; Straneo, 2006; Lazier et al., 2002; Lab Sea Group, 1998). Deep convection in these regions arises from certain characteristics: they have weak stratification, cyclonic circulation, and strong surface buoyancy loss (Marshall and Schott, 1999). Weak stratification is promoted by both the doming of the isopycnals governed by cyclonic gyre circulation (Yashayaev, 2007) and local properties of water masses present (Gelderloos et al., 2012). Stratification strength also depends on the history of convection, as consecutive winters with strong convection promote weak stratification while the opposite occurs during prolonged periods with weak or no deep convection (Yashayaev and Loder, 2017; Lab Sea Group, 1998; Yashayaev, 2007; Lazier et al., 2002). While both gyre circulation (Häkkinen and Rhines, 2004) and atmospheric forcing (Yashayaev, 2007) can vary from year to year, the primary result of convection is the homogenization of the water column, creating a deep mixed layer exceeding 1000 meters of depth in some regions. The result of this deep vertical mixing brings deepwater towards the surface and modifies temperature and salinity properties throughout the mixed water column (Lazier et al., 2002; Kieke et al., 2006; Yashayaev and Loder, 2009; Straneo, 2006). Once convection ceases, the mixed layer returns close to the surface and a water mass with nearly uniform properties is minted.

The Labrador Sea convective season ends during spring, giving way to the restratification period. Rapid post-convection restratification occurs the first few months (Lilly et al., 1999) due to high lateral density gradients induced by convection (Frajka-Williams et al., 2014). A slower restratification process occurs afterwards, though this gradual shifting of the interior to similar properties as the nearby boundary currents is thought to be always present (Lilly et al., 1999; Straneo, 2006). This was evident during a period when convection was shutdown in the Labrador Sea (Gelderloos et al., 2011) as interior subsurface water mass properties were warming and becoming more saline matching the lateral input of Irminger Water while the surface properties were cooling and freshening matching Arctic water input (Straneo, 2006). The

baroclinic boundary currents occasionally shed eddies, particularly Irminger Rings, which help restratify the region, supplying upwards of 45% of the heat lost during the convective winter (Gelderloos et al., 2011; Saenko et al., 2014). While this is the current understanding of the lateral input during the restratification period, questions remain regarding the relative regional importance of the slow restratification process.

The addition of freshwater into the interior of the Labrador Sea has a strong impact on deep convection. As stratification controls how much buoyancy must be removed to promote convection, an input of freshwater which increases stratification can reduce convection and subsequent water mass transformation (Avisc et al., 2006; Fischer et al., 2010). While the boundary currents carry freshwater in the liquid phase, sea ice can play an important role as well. The interior of the Labrador Sea remains relatively ice free, though ice is produced in the northern portion as well as advected along the Labrador Coast (Close et al., 2017). Sea ice can be advected or blown towards the warmer interior region, supplying freshwater via melting (McGeehan and Maslowski, 2011; Close et al., 2017), influencing the stratification within the convective region. The input of a sufficient amount of freshwater may strengthen the stratification such that the buoyancy loss via atmospheric cooling cannot result in convection (Schmidt and Send, 2007). During the 1960s, a large amount of Arctic water reached the Labrador Sea, an event later called a Great Salinity Anomaly (Gelderloos et al., 2012; Dickson et al., 1988; Belkin et al., 1998). The combination of additional freshwater from the Great Salinity Anomaly and weak atmospheric forcing produced multiple years with a shutdown in deep convection (Gelderloos et al., 2012). While a massive input of freshwater over a short period has been shown to limit Labrador Sea convection, numerical simulations suggest that a gradual increase in the freshwater input to the Labrador Sea could alone shut down convection (Böning et al., 2016) and stop the production of Labrador Sea Water.

A reduction in Labrador Sea Water formation has implications on the Atlantic Meridional Overturning Circulation (AMOC). While measurements made back in the 1990s (Pickart and Spall, 2007) suggest that the northward transport within the AMOC is not strongly affected by deep convection within the Labrador Sea, Böning et al. (2016) investigated how runoff from Greenland affected convection within the Labrador Sea and the strength of the AMOC. Using numerical simulations, they found that, under

current Greenland melting rates estimated for the near-future, enough freshwater could reach the convection region within the Labrador Sea, build sufficient stratification to prevent deep convection and Labrador Sea Water formation, and significantly reduce the northward AMOC transport. However, the impact of Labrador Sea Water production and the AMOC is still being investigated, as recent research suggests that deepwater formation within the eastern North Atlantic plays a much stronger role than that within the Labrador Sea (Lozier et al., 2019; Chafik and Rossby, 2019).

This study seeks to further understand the net freshwater transport between the boundary currents and the interior of the Labrador Sea. We put emphasis on regions around the western portion of the North Atlantic sub polar gyre (Fig. 4.1d) which have cross-shelf freshwater transport, either onshore or offshore, across multiple isobaths ranging in depth from 500m to 2000m. Considering stratification is not only dependent on the surface freshwater, three water masses are selected for freshwater transport quantification: fresh water from polar origins, salty and warm water of Atlantic origins, and salty and cold Labrador Sea Water. This allows for increased understanding and quantification regarding regions which act to supply or sequester freshwater/saltwater from the interior of the Labrador Sea. The influence of mesoscale features, including eddies, on freshwater transport is also investigated by decomposing the total freshwater transport into the mean and turbulent components.

4.4.   Methods

To examine the amount of fresh and saline water which enters the interior of the Labrador Sea, we perform three simulations using the Nucleus for European Modelling of the Ocean (NEMO), version 3.4 (Madec, 2008), coupled with the Louvain-La-Neuve sea ice model (LIM 2, Fichefet and Maqueda, 1997). We use a regional ORCA configuration (Barnier et al., 2007), called ANHA, (Arctic Northern Hemisphere Atlantic; Hu et al., 2018; Grivault et al., 2018; Holdsworth and Myers 2015; Müller et al., 2017; Courtois et al., 2017) at both 1/4° in horizontal resolution (ANHA4; Fig. 4.1a), as well as at 1/12° resolution (ANHA12; Fig. 4.1b). A third simulation uses the ANHA4 configuration with a 1/12° nest (Fig. 4.1c) over the North Atlantic Sub-Polar Gyre (SPG12; Müller et al., 2017), using the Adaptive Grid Refinement In FORTRAN (AGRIF;

Debreu et al., 2008) package. The SPG12 nest uses a 3-1 horizontal ratio between the number of nested grid points and the parent grid points over the same region. Two-way feedback was used to allow communication from the parent domain to the nest along the boundary, as well as from the nest back to the parent for all nested points. All simulations use a geopotential vertical coordinate with 50 levels where 9 model levels fit within the top 10m and our last level is 458m thick. Even at 1/12° of horizontal resolution, regions exist around the Labrador Sea which would not be considered eddy-resolving due to a small baroclinic Rossby radius in these waters (see Müller et al., in press, Fig. 4.2c), so one should consider the 1/12° simulations to be eddy-permitting, bordering on eddy-resolving. All three simulations share identical forcing and parameters, except for the time step, horizontal resolution, and time-step dependant values (Table 4.1). Horizontal advection was carried out using a total variance dissipation scheme (Zalesak, 1979), while lateral diffusion used a Laplacian operator. A biLaplacian operator was used for lateral momentum mixing. Model mixed layer depths were calculated using a 0.01 kg m^{-3} change in potential density from the surface. This method can produce mixed layer depths which are deeper than water properties suggest in this region as Courtois et al. (2017) found. Furthermore, Courtois et al. (2017) identify that their NEMO simulations of varying resolution share some distinct spatial and vertical scales of the mixed layer (their Fig. 8). Part of this may be due to biases linked to the freshwater within the boundary currents (Rattan et al., 2010; Trequier et al., 2005) which then is exported towards the convection region, influencing the mixed layer depth. However, others find that resolving Irminger Rings dramatically improve the representation of convection due to the significant buoyancy provided by these eddies (Gelderloos et al., 2011), though this requires high spatial resolution and coarser resolution simulations may suffer.

   Our simulations were forced with the Canadian Meteorological Centre's Global Deterministic Prediction System (Smith et al., 2014), using hourly 2-metre temperature, precipitation, downwelling longwave and shortwave radiation, 2-metre specific humidity, and 10-metre zonal and meridional wind velocity. Interannual monthly runoff was remapped from 1° gridded data (Dai et al., 2009) to the configuration grid. Liquid runoff from Greenland was further improved by remapping the surface mass balance from a regional climate simulation (Bamber et al., 2012) onto the ocean model grid with
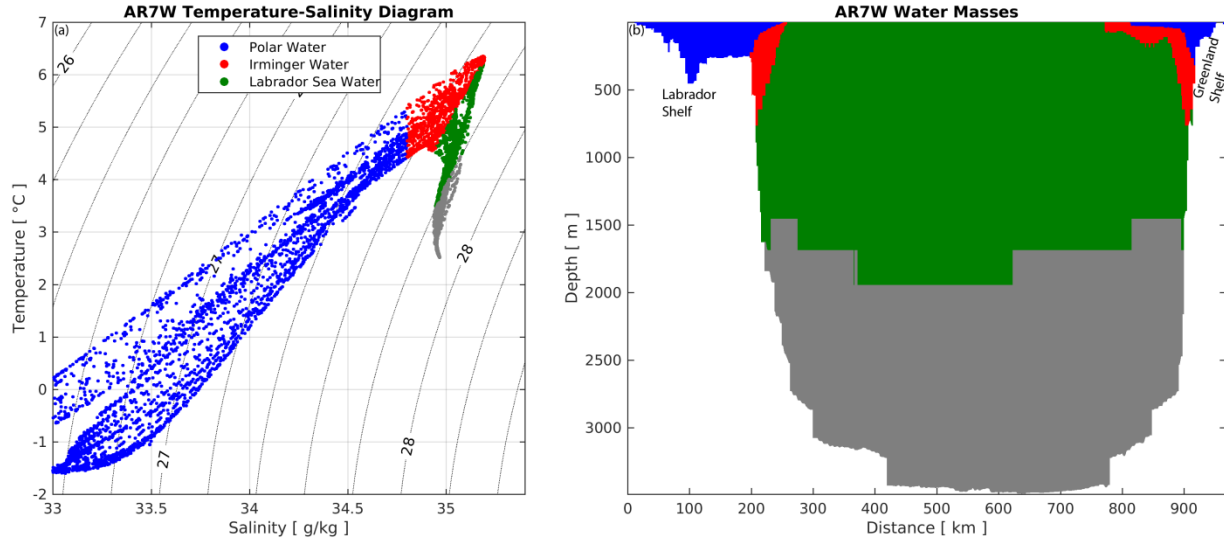
Figure 4. 2: Model snapshot for 5 May 2009, across AR7W depicting the temperature-salinity graph (a) and cross-section profile (b). Three water masses are shown: Polar Water (blue) with any value for potential temperature, salinity less than 34.8, and potential density less than 27.68 kg m^{-3}; Irminger Water (red) with potential temperature above 3.5 °C, salinity above 34.8, and potential density less than 27.68 kg m^{-3}; Labrador Sea Water (green) with any value for potential temperature or salinity, but with potential density between 27.68 and 27.8 kg m^{-3}.

Table 4. 1: Configuration settings for each given simulation. One core year is the amount of computation that would occupy a single core for 365 days

	Resolution [°]	Time Step [s]	Eddy Viscosity [$m^4 s^{-1}$]	Eddy Diffusivity [$m^2 s^{-1}$]	Computing Cost [Core Years]
ANHA4	1/4	1080	1.5×10^{11}	300	0.75
ANHA12	1/12	180	1.0×10^{10}	50	13
SPG12	1/12	180	1.0×10^{10}	50	2

a volume conservation approach. Without an iceberg module coupled with NEMO at the starting time of our simulations, solid discharge was ignored. Initial conditions of sea surface height, temperature, salinity, and horizontal velocities were obtained from the year 2002 from GLORYS2v3 (Ferry et al., 2010), a global ocean configuration with horizontal resolution of 1/4° and the same horizontal grid (ORCA) as our regional NEMO simulations were constructed from. Boundary conditions of temperature, salinity, and velocity at Bering Strait and 20° S latitude were also obtained from GLORYS2V3. Bathymetry was interpolated from ETOPO GEBCO (Amante and Eakins, 2009) for the ANHA4 simulation, while ANHA12 used bathymetry from Smith and

Sandwell (1997) except over the Arctic Ocean where ETOPO GEBCO was used. Little difference (not shown) was noted between these two bathymetry datasets. All simulations were integrated from 2002 until the end of 2016, with model output as an average over 5 days, producing 73 output periods per model year. As 3D initial velocities were prescribed from GLORYS2v3, each simulation was considered already spun-up. However, we allowed each simulation four years of adjustment from the initial conditions; all analysis took place between 2006 and 2016.

To calculate cross-isobath freshwater transport values, a reference salinity, S_{ref} (eq. 4.1), of 34.8 was used, consistent with the literature focused on the Labrador Sea (e.g. Aagaard and Carmack, 1989; Cuny et al., 2005; Curry et al., 2014). Multiple regions around the sub-polar gyre are constructed (Fig. 4.1d) to determine regional freshwater transport. We decompose the total velocity into both the mean and turbulent components (eq. 4.2 and eq. 4.3) to quantify how the turbulent freshwater transport differs from the mean freshwater transport. To determine the average velocity (u_{ave}, v_{ave}), a 25-day moving average was performed on both the meridional (v) and zonal (u) velocities. To determine the turbulent velocity, the meridional and zonal velocities were subtracted from the 25-day moving average. Other moving average windows were examined (not shown) though the 25-day moving average gave the highest turbulent transport values indicating that the mean velocity is changing significantly at timescales of nearly 1 month. While calculation of freshwater via individual eddies could be carried out, we chose to calculate the flow which deviated from the 25-day moving average as this would contain any contribution from short time scale features: the turbulent transport. As the simulations are not fully eddy-resolving, the subgrid scale physics should produce the effect of eddies and turbulence to some degree while not explicitly resolving these eddies and their associated transport.

We calculate the freshwater flux by integrating horizontally and vertically along each region's isobath using the grid cell's salinity and velocity normal to the horizontal path of integration (eq. 4.4). Five isobaths were used: 500m, 750m, 1000m, 1500m, and 2000m (see Fig. 4.1d). Freshwater calculations include both water fresher than the reference salinity, as well as water which was saltier. The direction of freshwater transport is defined to be positive if there was fresher water transported into the interior of the sup-polar gyre, or if saltier water was transported towards the shore. The

direction of freshwater transport will henceforth be called an *import* if there was freshwater (saline water) transported onshore (offshore), and an *export* for freshwater (saline water) transported offshore (onshore).

$$FW = (Sref - Salinity)/Sref \qquad \text{eq. 4.1}$$

$$Mean\ Velocity = \sqrt{(u_{ave}^2 + v_{ave}^2)} \qquad \text{eq. 4.2}$$

$$Turbulent\ Velocity = \sqrt{[(u_{ave} - u)^2 + (v_{ave} - v)^2]} \qquad \text{eq. 4.3}$$

$$Cross\ Isobath\ Freshwater\ flux = \int_0^L \int_0^z FW * velocity\ dz\ dl \qquad \text{eq. 4.4}$$

To determine if the freshwater transport is due to the flow of water which is fresher, or more saline than our reference salinity, we partition the transport into three water masses: the cold and fresh Polar Water, warm and salty Irminger Water, and cold and salty Labrador Sea Water. By selecting multiple water masses we can better understand where freshwater exchanges between the shelf and the interior, further addressing open questions regarding lateral exchange and restratification in the Labrador Sea. We separate Labrador Sea Water by potential density, from 27.68 to 27.80 kg m^{-3} as used by Kieke et al. (2006), with no additional temperature or salinity criteria. The Irminger Water mass was chosen to be warm (>3.5 °C) and salty (>34.8), but with density less than Labrador Sea Water. We selected a lower salinity criteria for Irminger Water than traditionally used (see Myers et al., 2007) so there would be no gap in freshwater transport between Polar Water and Irminger Water. While we could have called this water mass Atlantic Water or some variant of, we felt it was important to keep the name closely attached to the water within the boundary current which has a strong impact on restratification. Polar Water was selected to be less dense than 27.68 kg m^{-3}, with salinity below 34.8, consistent with previous studies (de Steur et al., 2017; Sutherland and Pickart, 2008), and for any temperature range. These three water masses do not encompass all water within the Labrador Sea, such as the overflow waters of Iceland-Scotland (Swift, 1984) and Denmark Strait (Jonsson and Valdimarsson, 2004), though they encompass the water masses which influence the stratification that must be eroded before deep convection begins. Figure 4.2 illustrates the various water masses within Atlantic Repeat Hydrography Line 7 West (AR7W) at a snapshot during the simulation. Due to the vertical grid and the AR7W section which is not orthogonal to the model grid, a stair-step pattern emerges in the horizontal and vertical dimensions.

The large vertical changes between the boundary of Labrador Sea Water and that which is underneath is simply a consequence of our selection criteria and how they deviate over one model grid, which is around 250 m thick at 1500 m of depth.

One caveat of the above water mass selection criteria is that we are unable to state the specific origin of each water parcel as they cross the shelf break. For example, transport along the western slope of Greenland may include fresh glacial melt, East and West Greenland Current water, Irminger Water, East Greenland Coastal Current water, and more. While interesting, it is beyond the scope of this manuscript which seeks to quantify the regional fresh and salt water transport between the shelf and interior basin, impacting the stratification within the Labrador Sea.

To determine regional differences in the freshwater transport to the interior of the Labrador Sea, six different geographic regions were selected: the east coast of Greenland, the west coast of Greenland, the Davis Strait region, the Hudson Strait region, the northern coast of Labrador, and the southern coast of Labrador (Fig. 4.1d). As ANHA4 and ANHA12 used slightly different bathymetry data, and are different in horizontal grid resolution, the isobaths depicted in Fig. 4.1d would appear slightly different for the ANHA4 simulation. The bathymetry for ANHA12 and SPG12 are identical other than within the sponge layer of SPG12 as that is a combination of the ANHA12 bathymetry and the corresponding parent (ANHA4) grid cell's bathymetry.

4.5.   Model Evaluation

The ANHA12 simulation has been used in several previous studies, including examining sea ice thickness in the Canadian Arctic Archipelago (Hu et al., 2018) and the importance of surface stresses due to ice motion in the Canadian Arctic Archipelago (Grivault et al., 2018). A previous ANHA12 simulation with slightly different settings was used to examine the mixed layer depth within the Labrador Sea (Courtois et al., 2017), mixing in the Canadian Arctic Archipelago (Hughes et al., 2017), and meltwater pathways from Greenland's glaciers (Gillard et al., 2016). However, further comparison against observations is necessary to quantify the model's fidelity within the Labrador Sea.

To evaluate our simulation, we first compare some model processes against observations within the Labrador Sea. To determine if the temperature and salinity field is comparable to observations, bottle data from four different AR7W (see Fig. 4.1d) occupations (CCGS Hudson: 2002, 2006, 2010, and 2013) are plotted against model data (Fig. 4.3a). At first glance, the model appears in close alignment with observations, though some model drift appears present. Model drift of the salinity field is a known issue in regards to numerical simulations within the North Atlantic sub-polar gyre (e.g. Rattan et al., 2010; Treguier et al., 2005). This long-term issue is still present, as Marzocchi et al. (2015) recently discussed salinity drift within the Labrador Sea with a high resolution 1/12° NEMO simulation. While our three model simulations exhibit drift (not shown but discussed below), the comparison against observations is reasonable, and the temperature, salinity, and thus density field of the Labrador Sea is reliable.

Geostrophic current speed derived from AVISO data (http://www.aviso.altimetry.fr/duacs/) are subtracted from ANHA12 (Fig. 4.3b) for the period from 2006 through 2015. Due to different resolution and grid spacing, and interpolating the ANHA12 data onto the same grid as AVISO, some spatial differences are anticipated. Swift boundary currents around the Labrador Sea contain much higher discrepancies than that of the quiescent interior. A likely culprit arises from issues with altimetry products close to the coast or near ice, impacting the AVISO derived speed. However, some spatial discrepancies occur along the shelf-break, perhaps due to differences in the spatial placement of the boundary current between the observation product and the ANHA12 simulation. Regardless of the cause, the ANHA12 simulation produces slightly faster boundary currents than observations derived via satellite, though the satellite product has higher variability in these regions, as we show below.

Eddy kinetic energy (EKE: $0.5(\overline{U_g'^2} + \overline{V_g'^2})$), where U_g' and V_g' are the geostrophic velocities computed from the sea surface height anomaly (see Jia et al., 2011), is calculated from the AVISO dataset (Fig. 4.3c) and ANHA12 simulation (Fig. 4.3d). As shown in this image, the Northwest Corner has the highest EKE, upwards of 1000 cm^2 s^{-2}. Other noticeable regions with strong EKE are along the western side of Greenland, a location where Irminger Rings are shed, as well as along the Labrador Shelf. Similarities emerge between the ANHA12 simulation and AVISO. First, the Northwest Corner has a
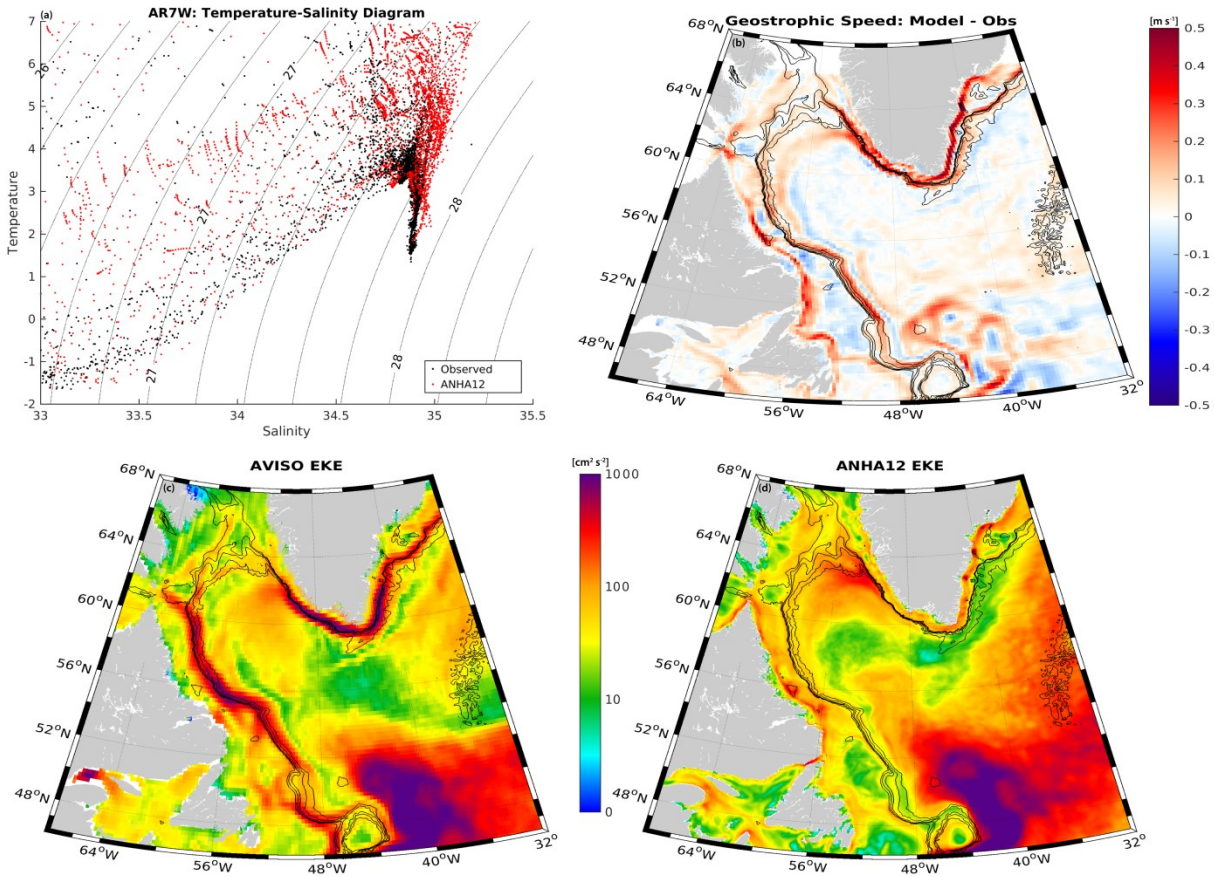
Figure 4. 3: (a) Temperature-Salinity graph across AR7W (dotted line in (c)) comparing bottle data from four CCGS Hudson cruises (2002, 2006, 2010, 2013: black) against ANHA12 (red). Mean geostrophic velocities difference between ANHA12 and AVISO from 2006-2015 are shown in (b). AVISO derived eddy kinetic energy (cm^2 s^{-2}) from 2006-2015 is shown in (c) and the same for ANHA12 (d).

similar spatial extent where the maximum in observed EKE exists, though the ANHA12 simulation has an extension of high EKE to the northwest. The high observed EKE values off the west coast of Greenland are shifted northwards in ANHA12 and do not penetrate south into the interior of the Labrador Sea but instead follow the isobaths around the Labrador Sea. While the EKE signatures off this coast are comparably different than observations, the modelled EKE values suggest high levels of eddy activity which are observed nearby. The strong boundary currents along Greenland and the Labrador coast show high levels of observed EKE while the model does not quite capture it, often having higher EKE closer to shore. This is likely a result from multiple features. First, altimetry products tend to have inaccuracies at coastal regions and near sea ice

89

(see Volkov et al., 2007), leading to inaccuracies in EKE along the coast and in regions where sea ice is present, including the Labrador Shelf. Second, while coarser in spatial resolution, the observation product includes higher variability of the geostrophic flow and produces higher EKE where the simulation does not. This is not surprising as many numerical simulations have lower EKE than observations (e.g. Luo et al., 2011). However, we note that regions which experience high EKE are also simulated with elevated levels of EKE. Third, numerical simulations within the Labrador Sea may produce the western boundary current to be too barotropic (Handmann et al., 2018) and likely reduces the baroclinic instability that influences the eddy field in this region (Rieck et al., in press). Our 1/12° simulations are not fully eddy resolving and some small scale features will instead be resolved as part of the mean flow, reducing the EKE in some regions. Fortunately, our 1/12° simulations are able to resolve Irminger Rings (not shown), eddies which divert substantial heat flux to the interior of the Labrador Sea (Gelderloos et al., 2011), a critical component of the restratification season. As the EKE mismatch between observations and model is elevated along the shelf-break, we anticipate some reduction in the eddy fluxes across these regions. However, this reduction should increase the mean freshwater transport while the net freshwater transport, the primary objective of this study, should remain unchanged. Thus we have some degree of confidence in the ability for the ANHA12 simulation to represent eddy fluxes within the Labrador Sea, though we anticipate the observed eddy fluxes would be stronger than our simulations suggest.

Some limitations based on the evaluation above should be expressed. First, our 1/12° simulations are not fully eddy-resolving, and may have different freshwater transport via eddy processes as observations may suggest, based on EKE differences. The differences between modeled and observed EKE may be due to our choice of lateral boundary conditions, set as free-slip, as simulations which feature partial-slip or no-slip are more likely to produce eddies and propagate offshore (Quartly et al., 2013). However, part of this manuscript identifies the differences between our high resolution simulations and low resolution simulation, quantifying each, and understanding if horizontal resolution matters when it comes to cross-shelf freshwater transport in the Labrador Sea. And second, model drift can play an important role when differentiating between water masses, since salinity and temperature drift will also impact the density.

A slight change in either the salinity or density via our classifications can push water into a different classification. We investigated salinity drift within our ANHA4 simulation by quantifying the salt content within a section from Cape Farewell extending south to the 2500m isobath. Salt content of our three water masses identify (not shown) that while the entire section gradually gains in salt, the interannual variability (20-50%) greatly exceeds that of the slow increase in total salt (<0.5%) during the 2006-2015 analysis period. Furthermore, even with some model drift present, the ANHA12 simulation generally produces Labrador Sea Water within the observed density range (see Fig 13 by Courtois et al, 2020; see Fig.5 by Feucher et al., 2019) indicating the drift over our simulation length still results in accurate Labrador Sea Water properties. Under such circumstances, the authors decided to keep our water mass classifications constant in time rather than allow for water mass evolution taking model drift into account.

4.6. Results

4.6.1. Regional Freshwater Transport

The net mean and turbulent freshwater transport from the ANHA12 simulation is shown in a spatial-temporal manner (Fig. 4.4), showing each region's annual freshwater transport across the 2000m isobath. The deepest isobath was selected as some of the freshwater crossing this isobath may penetrate further into the interior of the Labrador Sea, impacting deep convection. The west coast of Greenland and the Davis Strait region are particularly active in terms of freshwater transport for all three water masses, while the southern coast of Labrador and Hudson Strait are fairly quiescent. While the direction of mean freshwater transport varies across the regions, turbulent freshwater transport is generally offshore (Fig. 4.4b). Other than a few regions where transport is very low, neither the transport associated with the mean velocity nor the turbulent velocity shifts direction during the course of the simulation. Furthermore, we can identify regions which have little or no transport by select water masses. For example, the east coast of Greenland has essentially no Polar Water exchange across the 2000m isobath. The turbulent freshwater transport is relatively low across most of the regions

and isobaths around the sub-polar gyre. As such, most of the remaining figures will illustrate the total freshwater transport while both the mean and turbulent freshwater transport, as well as their standard deviations, are shown in Table 4.2. Almost all regions experienced fresh/saltwater transport which was significantly different from 0, as determined by a Student's t-test at the 0.05 alpha level (bold values in Table 4.2). Henceforth, discussion of results will be carried out for regions where the freshwater transport, either via mean or turbulent transport, is strong or seasonally variable. While Figure 4.4 identifies spatial regions with varying freshwater transport across a single isobath, no seasonal variation is shown. A description of the ANHA12 simulation's cross-isobath freshwater transport for multiple regions of the North Atlantic sub-polar gyre follows below.

4.6.2. Polar Water Mass

The net liquid freshwater transport associated with Polar Water crossing various isobaths along the east coast of Greenland is shown in Figure 4.5 (black bars). Little freshwater exchanges along this coast regardless of the isobath examined, with a maximum around 5 mSv. This appears a result of the mean and turbulent flow (Table 4.2) acting in opposite directions with a similar magnitude of freshwater transport. The total freshwater transport by liquid and sea ice is indicated by the black dots in Figure 4.5. Sea ice almost always supplies freshwater towards the interior basin. While only a few regions experience freshwater transport via sea ice across the 2000m isobath (Fig. 4.5e), it is possible that sea ice melt makes its way into the deeper basin as Close et al. (2017) suggest.

While little freshwater was exchanged along the eastern coast of Greenland via both liquid and solid transport, the western coast of Greenland (Fig. 4.5; red bars) has significant offshore liquid freshwater transport (5-70 mSv), though only a small amount of freshwater is exchanged via sea ice (<5 mSv). The freshwater transport changes significantly month to month, with a minimum in freshwater export during the summer and a maximum during the winter. Similar to the east coast of Greenland, the magnitude of freshwater transport generally decreases across deeper isobaths. Seasonality is strong here such that winter months have upwards of three times as much
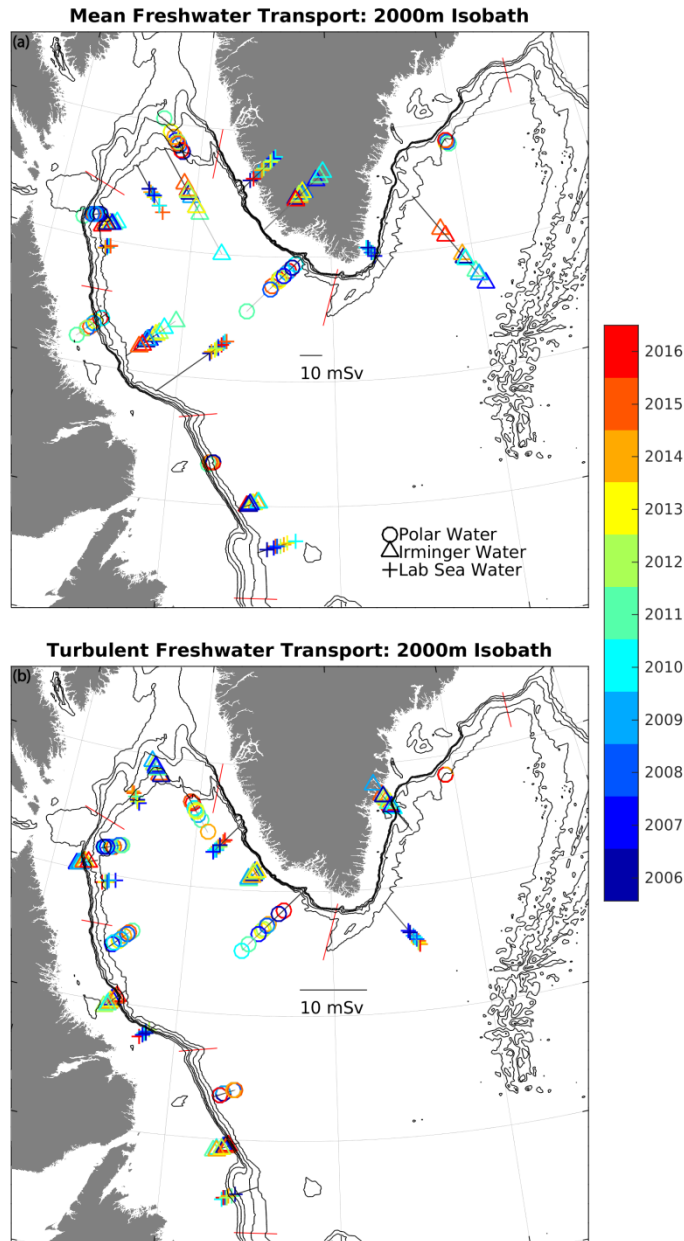
Figure 4. 4: Yearly mean (a) and turbulent (b) freshwater transport crossing the 2000-meter isobath of the North Atlantic sub-polar gyre. Three water masses are used: Polar Water (O), Irminger Water (Δ), and Labrador Sea Water (+). The distance from the isobath determines freshwater strength, with a 10 mSv sample line illustrated. Values which are directed off-shore indicate a freshening of the Labrador Sea via the given water mass.

freshwater export as summer months. From observations, Schmidt and Send (2007) estimated freshwater transport between the West Greenland Current and the interior of the Labrador Sea to be around 24 mSv which coincided with a pulse of freshwater within

Table 4. 2: Freshwater transport (mSv) for each of the three water masses, for all six regions, across all five isobaths. Both the net mean and net turbulent freshwater transport are identified, and the standard deviation is shown in brackets. Bold values indicate a transport which is statistically significant from 0 at the 0.05 alpha level. An import refers to net freshwater transport onshore while an export is offshore. Values are from the ANHA12 simulation averaged from 2006 to 2016.

Section	Water Mass	FW component	500m Export	500m Import	750m Export	750m Import	1000m Export	1000m Import	1500m Export	1500m Import	2000m Export	2000m Import
East Greenland Coast	Polar	Mean [sd]		**7.8 [4.1]**		**3.6 [2.4]**		1.1 [1.7]	0.6 [0.8]		0.6 [0.6]	
		Turbulent [sd]	**6.0 [2.2]**		**3.4 [1.3]**		**2.5 [0.9]**		**1.3 [0.6]**		0.0 [0.1]	
	Irminger	Mean [sd]	1.7 [3.5]		**16.8 [2.6]**		0.3 [2.0]			1.2 [2.8]	**37.4 [9.4]**	
		Turbulent [sd]		**1.3 [1.2]**		**5.3 [0.7]**		**2.3 [0.5]**	**1.8 [1.2]**			**6.1 [1.3]**
	LSW	Mean [sd]	9.5 [12.0]		2.7 [3.9]			**32.4 [10.7]**		**34.9 [3.9]**		**9.1 [1.9]**
		Turbulent [sd]		**1.6 [0.8]**		0.3 [0.8]	**4.7 [1.7]**		**8.9 [0.9]**		**7.2 [0.9]**	
West Greenland Coast	Polar	Mean [sd]	**44.0 [12.0]**		**27.2 [11.5]**		**32.1 [10.7]**		**30.1 [12.8]**		**13.3 [8.4]**	
		Turbulent [sd]	**1.7 [0.5]**		**10.3 [2.7]**		**7.7 [2.2]**		**6.7 [2.3]**		**7.6 [2.5]**	
	Irminger	Mean [sd]		**6.7 [0.9]**		**28.1 [2.4]**		**39.9 [3.7]**		**51.9 [7.8]**		**26.6 [6.0]**
		Turbulent [sd]	**3.4 [0.5]**		**11.4 [1.2]**		**12.8 [1.6]**		**11.1 [1.9]**		**1.7 [0.6]**	
	LSW	Mean [sd]	0.0 [0.0]		0.0 [0.4]			8.8 [9.1]		**19.3 [5.1]**		**17.1 [5.1]**
		Turbulent [sd]	0.0 [0.0]		0.0 [0.1]		**19.3 [7.0]**		**6.4 [1.2]**		**4.2 [0.8]**	
Davis Strait	Polar	Mean [sd]	**13.0 [3.9]**		**9.4 [3.3]**			**18.8 [5.0]**		**10.6 [4.8]**		**11.0 [4.8]**
		Turbulent [sd]		**2.8 [1.6]**		**3.1 [1.2]**	0.6 [1.1]		**1.3 [1.3]**		**2.6 [1.5]**	
	Irminger	Mean [sd]		**0.3 [0.2]**		**2.4 [0.6]**	**17.6 [6.1]**		**21.5 [6.5]**		**27.7 [10.0]**	
		Turbulent [sd]	0.5 [1.2]		**1.6 [0.3]**			**0.9 [0.3]**		**2.8 [0.9]**		**2.5 [0.8]**
	LSW	Mean [sd]	0.0 [0.0]			0.1 [0.1]		4.6 [6.1]	**12.2 [2.4]**		**16.8 [3.7]**	
		Turbulent [sd]	0.0 [0.0]		**0.0 [0.0]**		3.5 [4.1]			**3.9 [1.2]**		0.2 [0.7]
Hudson Strait	Polar	Mean [sd]		**30.9 [7.2]**		**17.5 [6.0]**		**9.4 [4.3]**		1.5 [1.8]		3.0 [2.1]
		Turbulent [sd]	**8.1 [1.3]**		**6.7 [1.4]**		**5.5 [1.3]**		**2.4 [0.9]**		1.7 [1.0]	
	Irminger	Mean [sd]	**1.6 [0.5]**		**2.2 [0.6]**		1.1 [0.8]			**5.6 [1.9]**	**5.3 [2.0]**	
		Turbulent [sd]		**0.2 [0.1]**		**0.6 [0.2]**		**0.4 [0.1]**	**1.2 [0.5]**			**2.4 [0.5]**
	LSW	Mean [sd]	0.0 [0.0]			0.2 [0.2]		**7.6 [3.0]**		**9.0 [1.3]**		**2.2 [0.7]**
		Turbulent [sd]	0.0 [0.0]		0.0 [0.0]		**3.2 [1.5]**		**3.8 [0.4]**		0.6 [0.5]	
North Labrador Coast	Polar	Mean [sd]		**25.4 [6.5]**		**27.0 [7.8]**		**21.1 [7.2]**		**13.0 [5.9]**		**7.0 [4.5]**
		Turbulent [sd]	**15.0 [2.6]**		**13.2 [2.7]**		**10.7 [2.5]**		**5.0 [1.5]**		**2.8 [1.3]**	
	Irminger	Mean [sd]		**0.8 [0.2]**	4.8 [2.1]		6.2 [2.6]		**15.8 [5.2]**		**15.3 [5.7]**	
		Turbulent [sd]	**0.6 [0.1]**		0.1 [0.2]			0.2 [0.3]		**1.9 [0.4]**		**2.8 [0.8]**
	LSW	Mean [sd]	0.0 [0.0]		0.9 [0.7]			0.5 [7.9]	**20.0 [3.1]**		**34.3 [2.9]**	
		Turbulent [sd]	0.0 [0.0]		0.0 [0.0]			0.9 [7.1]		**0.7 [0.3]**		**1.9 [0.5]**
South Labrador Coast	Polar	Mean [sd]		**5.5 [2.8]**		1.1 [1.4]	0.9 [1.1]		1.8 [1.1]			0.7 [0.6]
		Turbulent [sd]	**6.8 [1.7]**		**5.0 [1.5]**		**4.1 [1.4]**		**3.0 [1.2]**		**2.2 [1.1]**	
	Irminger	Mean [sd]	0.2 [0.7]		0.1 [2.7]		1.6 [3.1]		2.8 [2.0]		**6.5 [1.9]**	
		Turbulent [sd]	**0.3 [0.2]**			0.2 [0.4]		**1.2 [0.4]**		**2.5 [0.6]**		**2.5 [0.8]**
	LSW	Mean [sd]	0.1 [0.1]		0.7 [0.4]			5.7 [4.2]		**7.3 [1.9]**	**10.1 [3.5]**	
		Turbulent [sd]	0.0 [0.0]			0.1 [0.1]		1.7 [4.4]		1.1 [0.6]		**4.8 [0.6]**

the West Greenland Current between April and September. Rykova et al. (2015) used observations to state that the April-September period held a thicker and fresher amount of Polar Water within the West Greenland Current, which thinned during the typically un-observed winter period. Our results suggest that the total freshwater transported across the 2000m isobath during April was about 30 mSv, while September was about 10 mSv. Observations suggest this 6-month offshore transport can vary between 11 (Khatiwala et al., 2002) and 30 mSv (Lazier, 1980) making our ANHA12 simulation appearing in good agreement. Schulze-Chretien and Frajka-Williams (2018) used
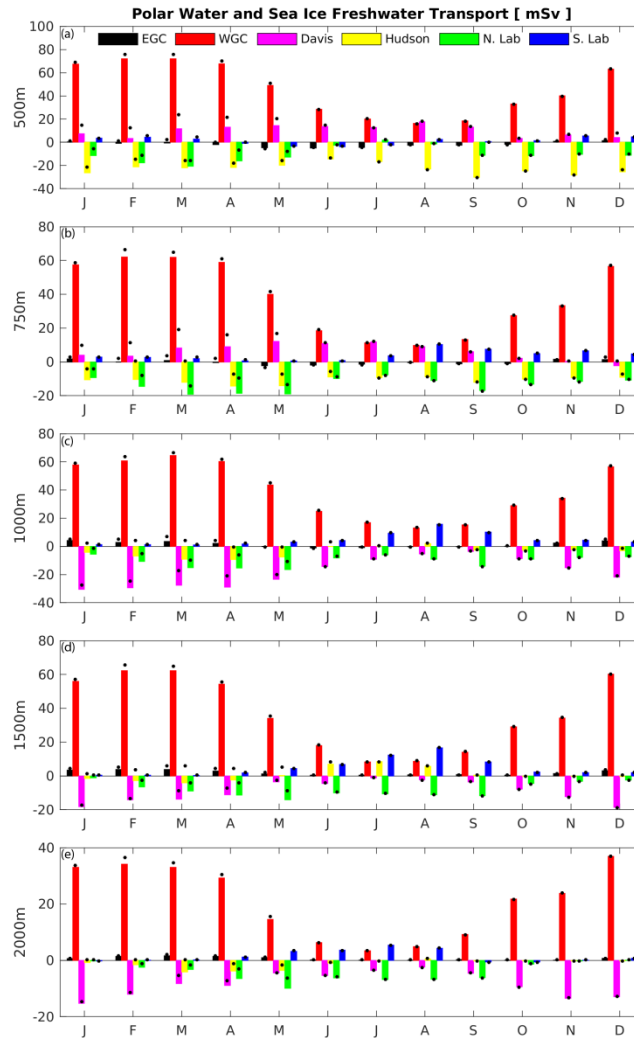
Figure 4. 5: Monthly transport of liquid freshwater (bars) across five isobaths around the North Atlantic sub-polar gyre, as simulated by ANHA12 from 2006 through 2016. Bar colors correspond to the region of interest: black for the eastern coast of Greenland, red for the western coast of Greenland, magenta for Davis Strait, yellow for Hudson Strait, green for the northern coast of Labrador, and blue for the southern coast of Labrador. The total freshwater (liquid and solid) freshwater transport at each region is indicated by the black points.

Lagrangian particle tracking software and found that while March had the highest number of particles crossing from the western coast of Greenland into the interior of the Labrador Sea, the winter months also had high transport, further agreeing with our findings. This region also experiences significant freshwater transport due to turbulent features (Fig. 4.6a), as most isobaths export freshwater towards the interior basin (Luo et al., 2016; Schulze-Chretien and Frajka-Williams, 2018). Turbulent freshwater export appears heightened during the winter period, from December through April, likely

Ekman driven from enhanced wind stress (Schulze-Chretien and Frajka-Williams, 2018). A significant amount of the freshwater transport within this watermass as it flows past Cape Desolation is exported from the western coast of Greenland into the deep basin (Fig. 4.7). The alongshore freshwater transport corresponds rather well against the offshore freshwater transport across the 500m (r^2=0.71) and 2000m (r^2= 0.49) isobaths of the western coast of Greenland, suggesting that an increase in alongshore transport will result with an increase in offshore transport within this region.
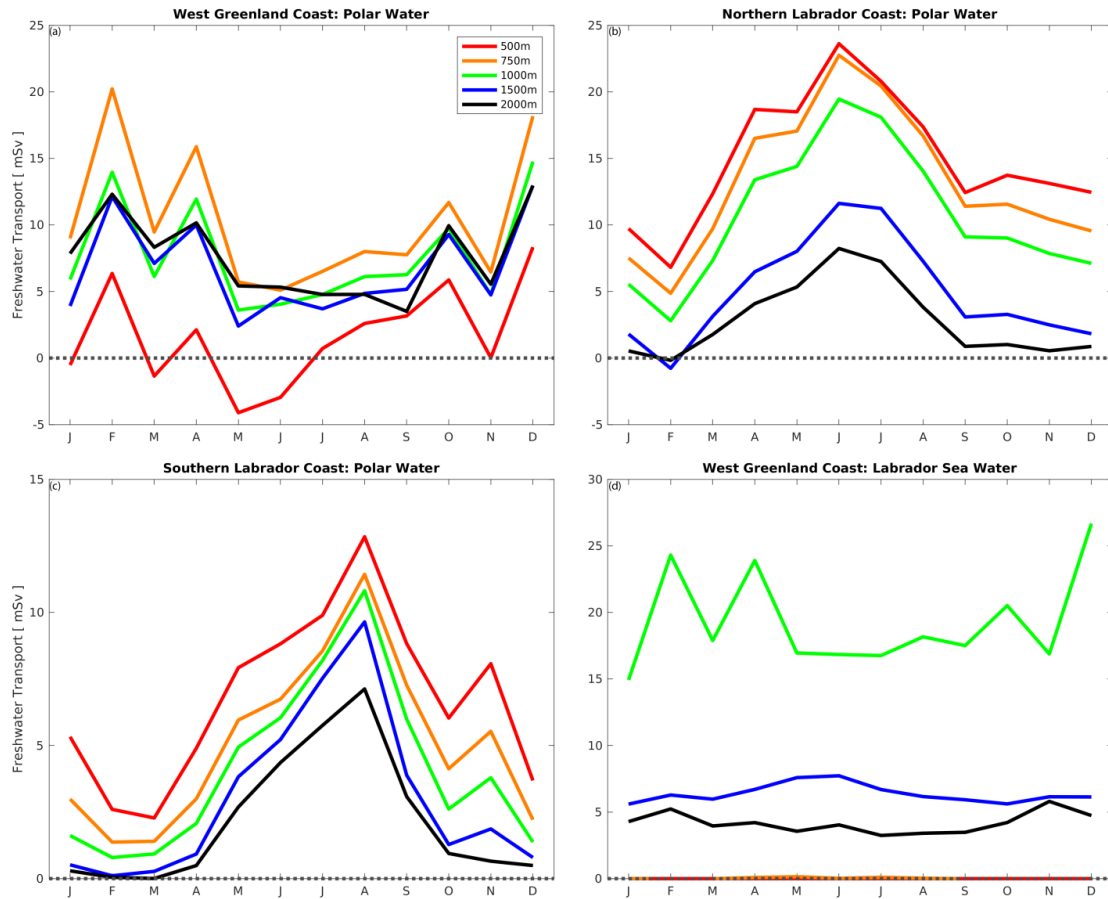
Figure 4. 6: Turbulent freshwater transport for each month as simulated by ANHA12 from 2006 through 2016. Color indicates the isobath in question: red for the 500m isobath, yellow for 750m, green for 1000m, blue for 1500m, and black for 2000m. Two water masses are selected: Polar Water at the western coast of Greenland (a), the northern (b) and southern (c) coast of Labrador, as well as Labrador Sea Water at the west coast of Greenland (d).

The Davis Strait region (Fig. 4.5; magenta bars) exports freshwater across the shallow 500m and 750m isobath, while importing freshwater from across the remaining
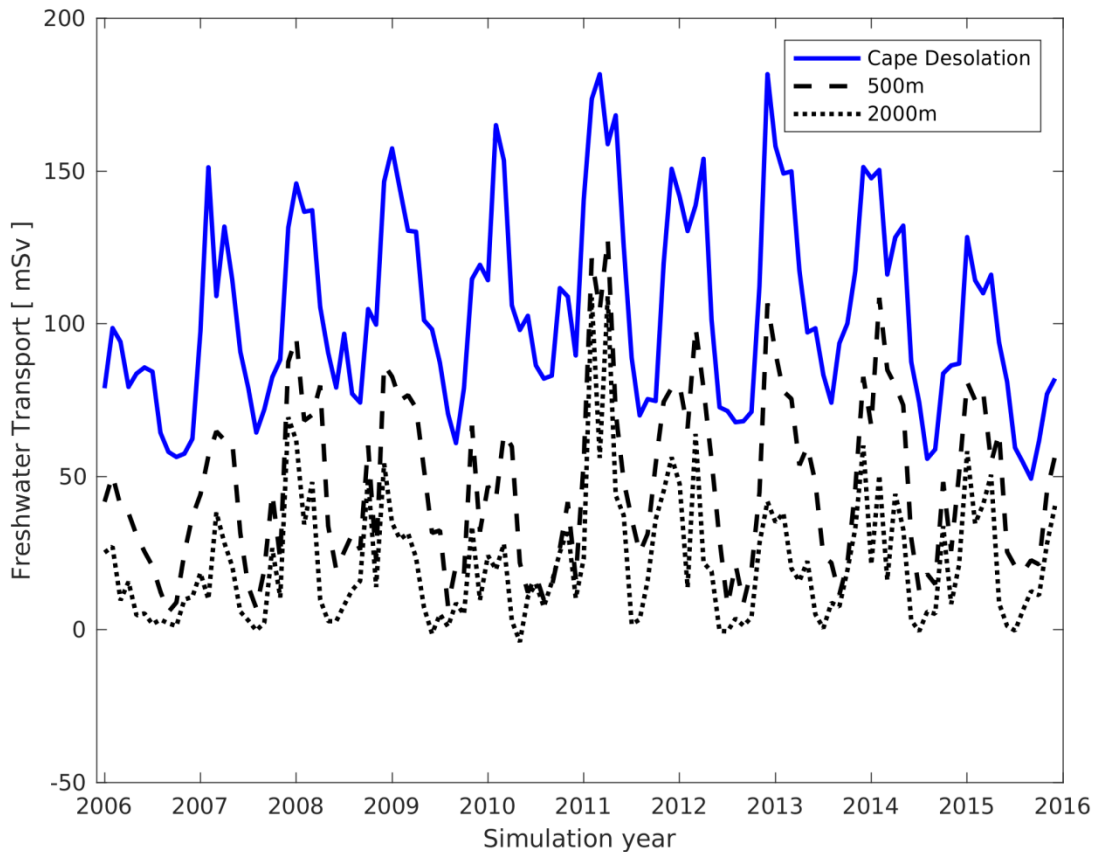
Figure 4. 7: Monthly values for alongshore freshwater transport across Cape Desolation with Polar Water classification (blue), as well as the freshwater transport across the 500 meter isobath of western Greenland (dash) and the 2000m isobath (dotted).

isobaths. The largest import of freshwater (5 to 30 mSv) occurs across the 1000m isobath. The nearby 750m isobath has considerably different freshwater transport, exporting between -2 and 10 mSv. The deeper isobaths have higher seasonality than the shallow isobaths, with a minimum in freshwater import during the summer season and a maximum during winter. Considering how the shallow isobaths show a similar pattern associated with the export of freshwater, we suspect this is due to additional offshore transport across all isobaths, though not nearly enough to counter the import occurring between 1000m and 2000m. While the liquid component shows a split of import and export across the five isobaths, sea ice only exports freshwater, consistent with the above regions as well as those to be later described. Sea ice carries up to 10 mSv of freshwater transport, far more than upstream Greenland coast regions. While Davis

Strait has a history of observations (Cuny et al., 2005; Curry et al., 2011), the isobaths selected here exist too far south of the mooring array to be comparable.

The Hudson Strait region is characterized by freshwater import (Fig. 4.5; yellow bars) across all but the 1500m isobath, with monthly import rates between 30 and -10 mSv. The strongest import occurs at the shallowest isobath, while the deep isobaths have weak transport. Hudson Strait experiences monthly variability with a minimum import rate during the late spring and early summer, though a maximum is reached at different times depending on the isobath. Relatively few similarities emerge between the Davis Strait and Hudson Strait regions, suggesting the seasonal variability is likely caused from within Hudson Bay and not upstream. Sea ice export is stronger here than any other region, with up to 15 mSv of freshwater transport. Sea ice freshwater transport is always positive while the liquid component is generally negative; suggesting that while this region has a general onshore transport of liquid freshwater, the offshore motion of sea ice acts to reduce the net freshwater import. Our Hudson Strait Region exists in a region where observations and study is rather sparse, and, similar to the Davis Strait region above, there exists little comparison between our results and other studies.

The Polar Water mass is characterized by a net import of freshwater (-20 mSv to 2 mSv) across all isobaths of the northern portion of the Labrador coast (Fig. 4.5; green bars). Import rates were higher across the 750m isobath than 500m, while deeper isobaths experience decreased import. This region experiences two periods of import maximum and minimum across most isobaths; an import maximum occurs in May and September across the 750m, 1000m, and 1500m isobath, while a minimum occurs during the late fall and again in the summer. While the 500m and 2000m isobath do not experience two minima and maxima, the monthly variability across the 500m is similar to the other isobaths while the 2000m isobath does not encounter any freshwater change during the springtime. Schmidt and Send (2007) identified two freshwater pulses within the Labrador Current, one from April to May, and the other July to August. Our results identify two distinct changes in the freshwater transport that are lagged 1-2 months compared to Schmidt and Send (2007), but both of these pulses still result in a net onshore transport of freshwater. The northern Labrador Coast experiences significant turbulent transport of freshwater (Fig. 4.6b). As the

restratification period begins, the density gradient between the boundary current and the interior of the Labrador Sea peaks, likely promoting exchange with the interior (Straneo, 2006), increasing the offshore turbulent freshwater transport. A clear seasonal cycle is present across all isobaths, with a maximum up to 24 mSv. This matches with McGeehan and Maslowski (2011) who modeled and observed offshore freshwater transport due to eddies in this region. However, with a net freshwater import across the 2000m isobath in this region, our simulations match numerical studies including Myers (2005) and McGeehan and Maslowski (2011) in finding that this region supports a net onshore transport of freshwater.

Compared to the northern coast of Labrador, while lower in magnitude, the southern coast (Fig. 4.5; blue bars) is generally characterized by an export of freshwater, also found by both Myers (2005) and McGeehan and Maslowski (2011). The 1000m and 1500m isobaths share similar monthly variability, with freshwater export rates at a minimum during the winter and a maximum during the summer. Freshwater transport generally increases with deeper isobaths, though the 2000m isobath has much lower transport compared to 1500m. This region of the Labrador Coast shows evidence of a single freshwater pulse identified by Schmidt and Send (2007), taking place between July and August, and unlike the northern coast, this pulse results with a net offshore transport of freshwater, crossing the 2000m isobath, resulting in some freshening of the interior of the Labrador Sea. Similar to the northern coast, the southern coast also experiences significant offshore transport of freshwater via turbulent flow (Fig. 4.6c), upwards of 12 mSv. The seasonal cycle of turbulent freshwater transport is similar to the northern region, with low export during the fall and winter, though the summer maximum is lagged by 2 months. Turbulent transport of freshwater across the southern coast's 1000m isobath (4.1 mSv) is very close in magnitude as well as seasonality when compared to glider observations by Howatt et al. (2018), further strengthening the ability of our simulation to represent reality. While the net offshore freshwater transport that occurs along this coast acts to freshen the Labrador Sea, it does not outweigh the import that occurs along the northern region, implying that the whole Labrador Coast does not provide a net transport of freshwater towards the interior of the Labrador Sea.

4.6.3. Irminger Water

Heat supplied by Irminger Water acts to restratify the Labrador Sea after the convection period has ceased (Cuny et al., 2002, Lazier et al., 2002; Straneo, 2006), though the salt input helps keep the Labrador Sea weakly stratified and preconditioned for another year of convection. Irminger Water, as defined earlier, is always saltier than our reference salinity and is not a real freshwater source. However, onshore transport of Irminger Water results in an offshore freshwater transport. In this way, Irminger Water can act as a freshwater source, as is the case along the east coast of Greenland (Table 4.2). However, the east coast of Greenland, along with Hudson Strait and the southern coast of Labrador have, in general, low amounts of freshwater transport and are not illustrated in figures but are presented in Table 4.2. Furthermore, little seasonal variability exists for this water mass, noted by the low standard deviations within Table 4.2.

Along the west coast of Greenland (Fig. 4.8; opaque red bars), freshwater is imported along all isobaths via offshore saltwater transport, consistent with an observational study by Myers et al., (2007). The largest amount of Irminger Water is transported across the 1500m isobath (34-50 mSv), while similar amounts traverse both the 2000m and 1000m isobaths. Freshwater import tends to increase as the isobath depth increases from 500m to 1500m (Table 4.2). The shallow isobaths between 500m and 1000m show limited seasonal variability, though the deeper isobaths experience a maximum during the fall and a minimum during the late winter and spring. This matches well with observations, as Rykova et al. (2015) identified that the Irminger Water thickens and becomes saltier between October and February. Significant amounts of freshwater are exported via turbulent processes in this region between the 750m and 1500m isobath (Table 4.2), though with limited seasonality as indicated by low standard deviations.
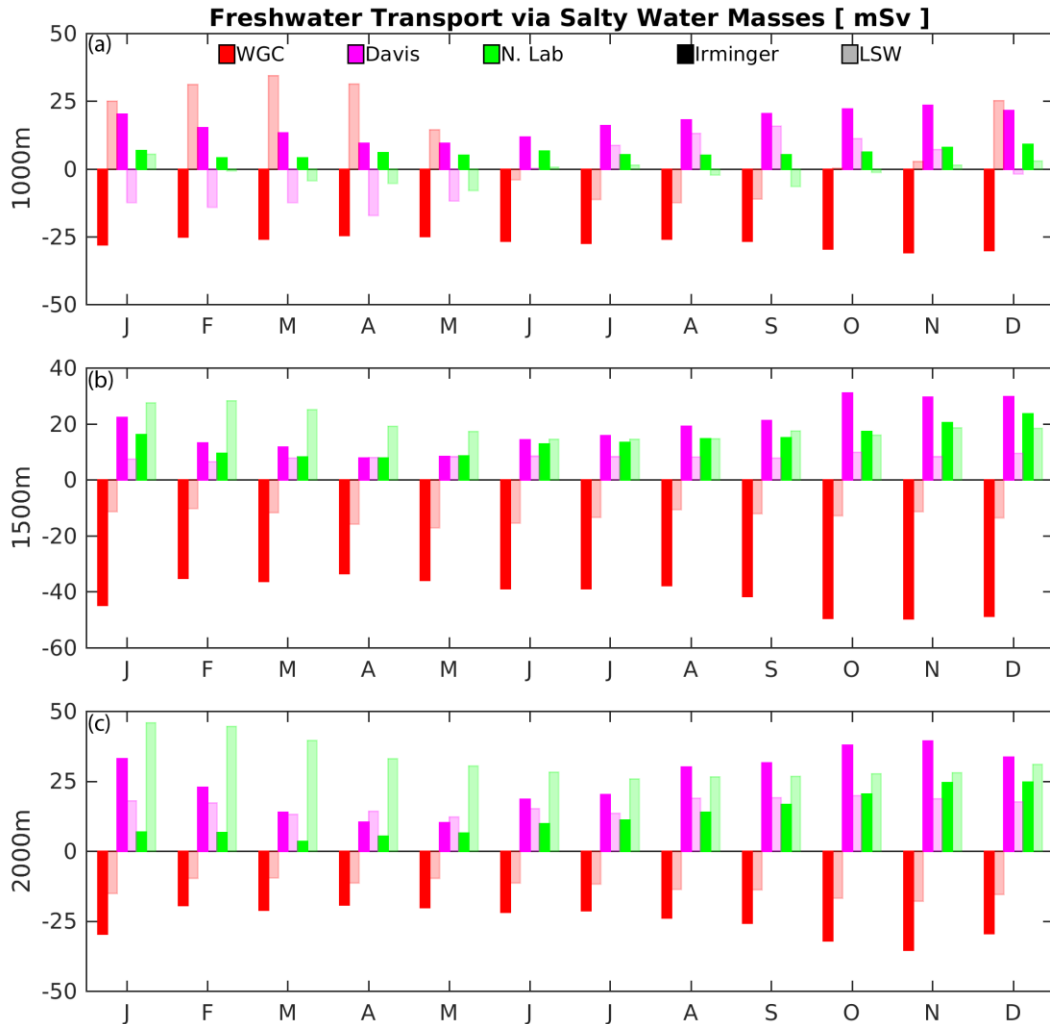
Figure 4. 8: Monthly freshwater transport associated with Irminger Water (opaque bars) and Labrador Sea Water (translucent) crossing three isobaths of the North Atlantic sub-polar gyre. Three regions with significant transport are shown: red bars are for the western coast of Greenland, magenta bars for Davis Strait region, and green bars for the northern coast of Labrador.

A significant amount of freshwater export occurs along the Davis Strait region via onshore transport of this saline water mass (Fig. 4.8; opaque magenta bars). Upwards of 40 mSv crosses the 2000m isobath during the fall, while a minimum occurs during spring. The 1000m and 1500m isobaths show similar magnitude of transport as well as seasonality. Unlike the western coast of Greenland, there is essentially no net freshwater transport across the 500m and 750m isobath (Table 4.2).

Similar to the Davis Strait region, Irminger water provides an export of freshwater via onshore transport along the northern coast of Labrador (Fig. 4.8; opaque

green bars). While the 1000m isobath has low seasonal variability and weak transport (about 5 mSv), the 1500m and 2000m isobath exhibit seasonality with a minimum in freshwater export during the late winter and early spring, and a maximum in the fall. The 2000m isobath also experiences a rapid decline in freshwater export between December and January which warrants further investigation.

4.6.4. Labrador Sea Water

Our Labrador Sea Water mass, defined strictly by density, shows limited seasonality across the eastern coast of Greenland, Hudson Strait, and the northern coast of Labrador (see Table 4.2). However, significant freshwater export occurred along the Davis Strait region (16.6 mSv) and northern Labrador coast (34.4 mSv) via onshore transport from the deep basin where LSW is produced. Illustrations and further results are provided below for regions which experienced seasonal variability or significant turbulent transport.

While the western coast of Greenland (Fig. 4.8; translucent red bars) experienced limited seasonality across the 1500m and 2000m isobath with 10 to 18 mSv via offshore transport of saline water, transport across the 1000m isobath shows strong seasonality. A maximum freshwater export occurred during March (34 mSv) while a minimum occurred during the summer (-11 mSv). As there is no onshore transport across 2000m and 1500m, the changes seen across the 1000m isobath are not from the interior of the Labrador Sea. Rather, the seasonality across 1000m comes from Labrador Sea Water present between the 1500m and 750m isobaths, and flows onshore as a response to circulation changes during the year. The turbulent transport of freshwater is generally very low for Labrador Sea Water (Table 4.2), however about 20 mSv of export occurs across the 1000m isobath (Fig. 4.7d). This is not only double the mean freshwater transport of the deeper isobaths, but also opposite in direction. This suggests that the transport of LSW in this region is strongly driven by events with relatively short timescales, and given the water mass in question, likely tied to deep convection. However, with no evidence of turbulent transport across isobaths deeper than 1000m, this signal could be related to upstream convection within the Irminger Sea which may be entrained within the East Greenland Current. A large part of this variability occurs

near Fyllas Bank (see Fig. 4.1d), where the 27.68 kg m^{-3} isopycnal resides higher in the water column during the convective winter and spring (not shown), and recedes during the summer. The seasonal cycle across the 1000m isobath averages to a freshwater export of 10 mSv. If we consider the minimum during summer (10 mSv import) as the base transport, the seasonal cycle can be viewed as a 20 mSv onshore pulse of Labrador Sea Water.

The Labrador Sea Water mass generally has onshore transport of saline water across the Davis Strait region which manifests as a freshwater export (Fig. 4.8; transluscent magenta bars). Similar as the above west Greenland current region, the two deepest isobaths have little seasonality while the 1000m isobath shows significant changes throughout the year. While this region is close in proximately to an area which experiences cascading (Marson et al., 2017), no signal propagates across the 500m and 750m isobath (not shown), suggesting this seasonality is not attributed to cascading, and likely a continuation of the pulse describe above. This pulse of Labrador Sea Water appears to return across this region, lagged one month from the signal present along the western coast of Greenland, with a freshwater transport which is nearly 0 mSv. Using the same process as above, the summer minimum transport is about 15 mSv. This means that about 15 mSv of the earlier pulse is returning across our Davis Strait region; most of the 20 mSv exported upstream along the western Greenland coast. The remainder of the pulse appears to cross at Hudson Strait (not shown), with little evidence of the pulse along the Labrador coast.

Significant amounts of Labrador Sea Water are transported onshore the northern coast of Labrador's 1500m (15-30 mSv) and 2000m isobath (26-46 mSv; translucent green bars in Fig. 4.8). Both the 1500m and 2000m isobath show similar levels of seasonality, with a maximum in freshwater export during the winter, and a minimum in summer. As this region is very close in proximity to the convection site within the Labrador Sea (Lab Sea Group, 1998), the maximum in transport across both these isobaths is indicative of recently formed Labrador Sea Water which has migrated towards the coast and likely entered into the Deep Western Boundary Current. This closely matches with the results of a 1/12° numerical simulation carried out by Brandt et al., (2006) who found the export of Labrador Sea Water to the Labrador Current was elevated from January through May. While the Labrador Sea Water within the Deep

Western Boundary current will travel southwards (Rhein et al., 2015), pathways of Labrador Sea Water are also east through the Charlie Gibbs Fracture Zone as well as a recirculation northwards towards the interior basin (Fischer and Schott 2002; Zantopp et al., 2017).

4.6.5. Impact of resolution

The above results were derived from the ANHA12 simulation, though questions regarding the impact of horizontal resolution and the exchange of freshwater across shelf-breaks remain. Using our ANHA4 simulation, as well as an identical ANHA4 simulation with a 1/12° nest within the sub polar gyre (SPG12), we address how horizontal domain structure influences our earlier results. While each simulation is different, our sensitivity study did not allow for an understanding if the changes in freshwater transport were due to any particular setting, such as the bathymetry product used or the eddy diffusivity value. Instead, we are forced to state that differences in the simulated cross-isobath freshwater transport arise due to a variety of factors. We suspect the primary factor is higher resolution which can resolve finer scale mesoscale processes, and we will make the assumption that all freshwater transport changes are due to horizontal resolution. However, we will indicate other sources which could promote differences between these simulations. We highlight each water mass at a single region where the ANHA12 simulation reported large freshwater transport values (Section 4.2-4.4) and compare against the ANHA4 and SPG12 simulations.

Examination of the Polar Water across the west coast of Greenland (Fig. 4.9a-b) shows that the low resolution simulation, ANHA4, exported much less freshwater across the 500m isobath than the two 1/12° simulations, which were fairly similar. As the ANHA4 simulation resolved the boundary current here with a similar salinity as ANHA12 and SPG12 (not shown), we attribute the differences in freshwater transport to a weaker velocity field. Seasonal variability showed some disagreement across these isobaths, namely that ANHA4 presented little variability while ANHA12 and SPG12 had similar degrees of seasonality. The use of a nest within SPG12 resulted in a minor reduction in freshwater transport across the 500m isobath compared against ANHA12, though the 2000m isobath transport was relatively similar across all three simulations.

As the low resolution simulation showed poorer performance in this region compared to both high resolution simulations, this illustrates the importance of resolution in this region of high baroclinicity which promotes the development of eddies and other mesoscale features.
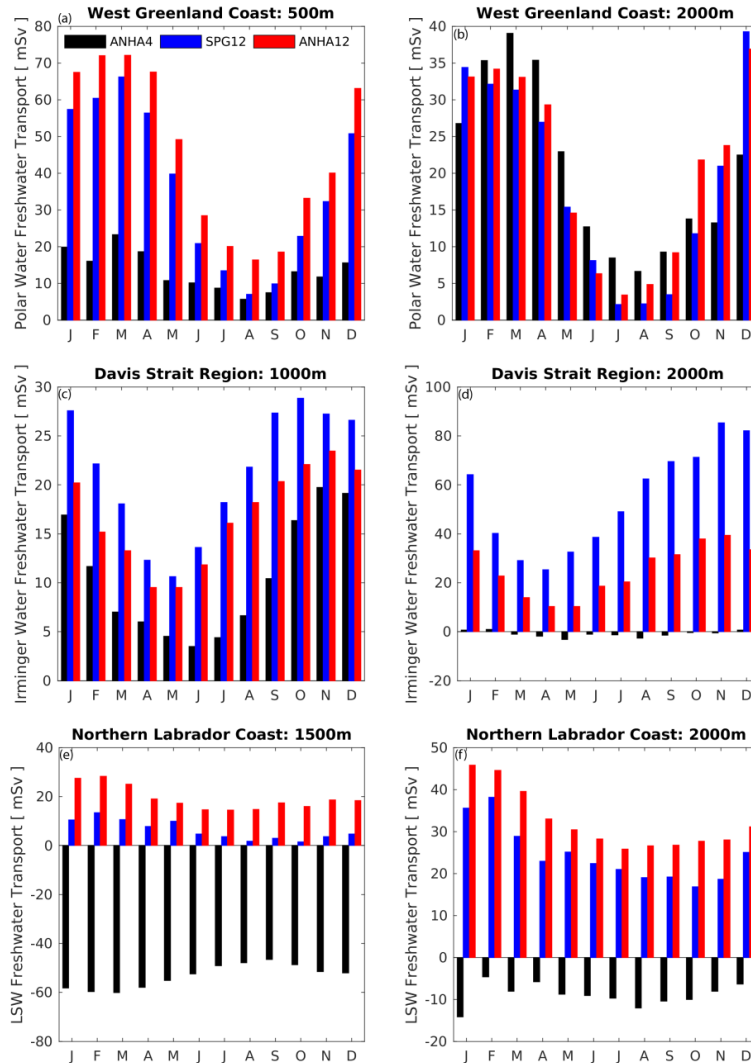
Figure 4. 9: Monthly average freshwater transport for three different simulations: ANHA4 (black bars), SPG12 (blue) and ANHA12 (red). Three water masses are shown: Polar water crossing the 500m (a) isobath and 2000m (b) isobath of the western coast of Greenland, Irminger Water crossing the 1000m (c) and 2000m (d) isobath of the Davis Strait Region, and Labrador Sea Water crossing the 1500m (e) and 2000m isobath (f) of the Northern coast of Labrador.

Irminger Water, having strong export rates across the Davis Strait region described earlier (Fig. 4.8), showed similar seasonal variability between all simulations across the 1000m isobath (Fig. 4.9c), though the magnitude of transport was different.

The transport across the 2000m isobath shows an interesting case where SPG12 simulated much more transport than ANHA12 while ANHA4 simulated nearly zero freshwater transport. Similar as across the western coast of Greenland described above, ANHA4 simulated less freshwater transport than the higher resolution simulations and showed noticeably reduced seasonality. While not shown, ANHA4 had a distinct lack of interannual variability while the higher resolution simulations were similar.

Large differences exist between the three simulations when examining Labrador Sea Water crossing the shelf break along the northern coast of Labrador (Fig. 4.9e-f).The ANHA4 simulation not only had excessive freshwater transported across the 1500m isobath, but was also opposite in direction compared against the higher resolution simulations. SPG12 was also significantly reduced compared to ANHA12, though the seasonal variability between these two simulations share similarities. ANHA4 also had low amounts of freshwater imported across the 2000m isobath while the high resolution simulations had larger amounts that were an export. In essence, ANHA4 had the opposite direction of Labrador Sea Water compared to the high resolution simulations, though this may have been due to a larger convective patch than the 1/12° simulations (not shown).

4.7. Discussion

Three numerical model simulations were carried out to further understand the relative freshwater and saltwater transport which occurs between the regions of the continental shelf around the western North Atlantic sub-polar gyre and that of the interior basin. From the ANHA12 simulation, we note that cross-shelf freshwater transport varies across these regions. The west coast of Greenland transports a long-term (2006-2016) annual mean 21 +/- 11 mSv of freshwater across the 2000m isobath to the interior of the Labrador Sea (Fig. 4.5e), the only region with significant amounts of net offshore transport of freshwater with Polar Water classification. Other regions either transported freshwater onshore or transported relatively low amounts of freshwater offshore. Of this 21 mSv (Table 4.2), roughly 2/3 was transported via the mean flow (13.3 mSv) while the remainder was from turbulent processes (7.6 mSv). While significant amounts of freshwater is exported from the western coast of

Greenland, a net transport of 9 mSv is exported across the continuous 2000m isobath, of which -8 mSv is from mean processes and 17 mSv from turbulent processes (Table 4.2), suggesting the offshore emission of freshwater is dominated by short-lived features such as eddies. With minimal net offshore freshwater transport, much of the freshwater remains within the boundary current and reaches the Grand Banks, bypassing the Labrador Sea as Fratantoni and McCartney (2010) and Loder et al. (1988) also suggest.

While lateral advection of Irminger Water typically acts to restratify the Labrador Sea after convection has ceased (Cuny et al., 2002; de Jong et al., 2016), the onshore transport of this saline water also acts to freshen the Labrador Sea. About 50 mSv of saline water is transported onshore of the 2000m isobath across our six regions, 65 mSv of mean transport and -15 mSv from turbulent transport (Table 4.2). Other than the west coast of Greenland, all regions had net onshore transport of this saline water mass. While our analysis does not fully enclose the Labrador Sea, we suggest that any influence of near-coastal Irminger Water actively restratifying the Labrador Sea occurs off the western coast of Greenland; the remaining regions act to hinder restratification. This provides further elucidation of the restratification period, normally considered to include both surface freshening and subsurface heating (Straneo, 2006). However, while the net transport of salt water was onshore, the same may not occur for the net heat transport for this water mass as it is modified during its circulation around the Labrador Sea.

The cold and salty Labrador Sea Water acts in a similar fashion as the Irminger Water discussed above. About 42 mSv of saline water is transported onshore the continuous 2000m isobath of all six regions (Table 4.2). With very weak turbulent processes (5 mSv onshore) associated with this water mass, the mean flow (37 mSv onshore) is the primary contributor. The northern coast of Labrador, in close proximity to the Labrador Sea convection site, has the largest seasonal changes for this water mass; the 1500m and 2000m isobaths have elevated onshore transport of saline water during the convective period. The west coast of Greenland, far from the convective site, also experiences an interesting seasonal pattern across the 1000m isobath, where a saltwater pulse of 20 mSv is onshore due to lifting of the 27.68 kg m^{-3} isopycnal. This pulse passes around the northern Labrador Sea slowly leaking offshore between Davis and Hudson Strait.

Across most regions and isobaths, the transport of freshwater via turbulent flow has relatively low variability and weak transport. Some notable exceptions are Polar Water across the north and south coast of Labrador (Fig. 4.6), both of which contain both strong transport and seasonality. Upstream along the west coast of Greenland, Polar Water always exported freshwater via both the mean and turbulent flow, the only region and water mass with significant transport to do so. Both the Irminger and Labrador Sea Water masses have limited seasonality to their turbulent processes within this region, supplying fairly constant transports across the year. These salt water masses almost always had a different direction between their mean and turbulent freshwater transport, regardless of region. While the mean and turbulent transport act opposite in directions, the magnitude of mean freshwater transport was greater than the turbulent transport (Table 4.2) and determines the direction of net freshwater transport per water mass. While our analysis was performed using the turbulent transport as a deviation based on a 25 day moving mean, we found that changing the averaging period to be between 10 and 35 days did not produce much difference in our results while the 25 day moving mean maximized the turbulent transport.

An increase in resolution from 1/4° to 1/12° appears to have made significant changes in the cross-shelf freshwater transport within the Labrador Sea (Fig. 4.9). At 1/4° resolution, both bathymetry and turbulent processes can be expected to be poorly resolved compared to a similar simulation with 1/12° resolution. As such, the differences in freshwater transport across certain isobaths between the ANHA4 simulation and the two 1/12° simulations were anticipated to some degree. The ANHA4 simulation not only simulated less freshwater exchange at shallow regions (<1000m), but also had lower seasonal variability when compared against ANHA12. We suspect the poor performance in shallow regions was in part due to poorly resolved coastal current systems. ANHA4 also suffered when simulating freshwater exchange across deeper isobaths, in some cases having nearly no net transport of Irminger Water and rather low amounts of Labrador Sea Water while both 1/12° simulations showed significant transport. Perhaps most interesting was a completely directional shift between ANHA4 and the 1/12° simulations in terms of Labrador Sea Water; at 1500m depth, ANHA4 had freshwater import rates greater than the export rates of the 1/12° simulations (Fig. 4.9e). This may be attributed to a far larger spatial extent of convection in 1/4° simulations than at 1/12°

(not shown), perhaps forming Labrador Sea Water further onshore which is later transported offshore. This follows well with Marzocchi et al. (2015) who found a significant improvement in circulation present within the North Atlantic sub-polar gyre when horizontal resolution was increased from 1/4° to 1/12°. The increase in resolution allows for an improved representation of eddies within the Labrador Sea, particularly Irminger Rings which are essential in providing heat to the interior of the Labrador Sea (Gelderloos et al., 2011), reducing the spatial extent of the convective region. Our results suggest that lower resolution not only impacts freshwater transport along the west coast of Greenland, but also all water masses within the basin. These freshwater transport differences imply that low resolution simulations will produce a Labrador Sea with a different degree of stratification than higher resolution simulations.

Fewer differences were noticed between the 1/12° simulations, though SPG12 often had additional freshwater transport compared to ANHA12. This was somewhat a surprise, due to the SPG12 domain setup, since SPG12 used nesting software to interpolate from the 1/4° parent simulation onto the 1/12° nest. We would have expected SPG12's freshwater transport values to be between that of ANHA4 and ANHA12. We attribute these differences to the nested domain's boundary conditions, which, after interpolation from the coarse parent domain, may fail to resolve the same current systems as resolved by ANHA12. As the SPG12 domain's border is rather close to Davis Strait and Hudson Strait, these are areas where boundary issues may creep into the nested domain, influencing regions downstream. While the use of nesting software allows for high resolution at a reduced computational expense, the drawbacks of nesting are not negligible.

4.8. Conclusions

Further clarification on the exchange of fresh and saltwater between the boundary and interior of the Labrador Sea is carried out using three numerical simulations. Liquid freshwater leaves the boundary current system and enter the deeper basin off the western coast of Greenland as well as along the southern coast of Labrador. Other regions either exchange relatively little freshwater, or sequester freshwater from the interior of the Labrador Sea. However, freshwater locked within sea ice passes into

deeper water across all regions, though at relatively low amounts. Salty water masses exhibit onshore transport at many regions, resulting in a freshening of the Labrador Sea at subsurface depths. Numerical resolution appears important in resolving the cross-shelf freshwater transport, with significant differences between the 1/4° and 1/12° simulations. The 1/12° simulations had relatively similar cross-shelf freshwater transport despite differences in their domain construction. These results help to paint a more complete picture of the lateral exchange of fresh and saltwater between the boundary currents and the interior of the Labrador Sea by isolating particular regions where, and how much, freshwater exchange occurs. While previous studies have focused on freshwater exchange along the western Greenland coast (e.g. Myers et al., 2009; Schmidt and Send, 2007) and the Labrador coast (e.g. Myers, 2005; McGeehan and Maslowski (2011), Schulze-Chretien and Frajka-Williams, 2018), we provide estimates on the freshwater that is exchanged at other regions around the North Atlantic sub-polar gyre. Furthermore, we estimate the freshwater transport via two saltwater masses and update the current knowledge on subsurface restratification within the Labrador Sea.

Climate implications of this study suggest that changes to freshwater pathways can modify the degree of stratification in the Labrador Sea. For example, Grivault et al. (2017) suggest that under a future climate scenario, the addition of freshwater and heat to Baffin Bay reduces the freshwater transport between Baffin Bay and the Labrador Sea, increasing freshwater transport around Greenland. This could cause the East and West Greenland Current systems to become fresher. With additional freshwater now passing the west coast of Greenland, a larger amount of freshwater should enter the interior of the Labrador Sea and strengthen the stratification. Furthermore, as a significant portion of meltwater from Greenland's Ice Sheet enters the Labrador Sea (Luo et al., 2016; Gillard et al., 2016), a warming climate could result with a shutdown in deep convection within the next few decades if the melting of Greenland continues at its current rate (Böning et al., 2016). On the other hand, an increase in freshwater transport to the Labrador Sea from Hudson or Baffin Bay would likely not impact the convection within the Labrador Sea as little exchange occurs downstream of these regions, as Schulze-Chretien and Frajka-Williams (2018) also concluded. Koenigk et al. (2007) investigated that climate change simulations promoted a significant increase in

freshwater export through the Canadian Archipelago, though with minimal net freshwater change through Fram Strait, somewhat at odds with Grivault et al. (2017). Our analysis suggests that the regions around the Labrador Sea export freshwater into the deep basin very differently than one another and the impact on convection depends on which region experiences any changes in freshwater.

Bibliography

Aagaard, K., & Carmack, E.C. (1989). The role of sea ice and other fresh water in the Arctic circulation. *Journal of Geophysical Research: Oceans*, 94(C10),14485-14498.

Amante, C., & Eakins, B.W. (2009). ETOPO1 1 Arc-minute global relief model: procedures data sources and analysis. *NOAA Technical Memorandum NESDIS*, NGDC-24 19.

Avisc, T., Karstensen, J., Send, U., Fischer, J. (2006). Interannual variability of newly formed Labrador Sea Water from 1994 to 2005. *Geophysical Research Letters*, 33,

Bacon, S., Gould, W.J., & Jia, Y. (2003). Open-ocean convection in the Irminger Sea. *Geophysical Research Letters*, 30(5).

Bamber, J., Broeke, van den M., Ettema, J., Lenaerts, J., & Rignot, E. (2012). Recent large increase in freshwater fluxes from Greenland into the North Atlantic. *Geophysical Research Letters*, 39(19).

Barnier, B., Brodeau, L., Le Sommer, J-M., Molines, T., Penduff, S., Theetten, A-M., et al. (2007). Eddy-permitting ocean circulation hindcasts of past decades. *Clivar Exchanges*, 42(12 (3)), 8-10.

Belkin, I.M., Levitus, S., Antonov, J., & Malmberg, S.A. (1998). "Great salinity anomalies" in the North Atlantic. *Progress in Oceanography*, 41(1), 1-68.

Böning, C.W., Behrens, E., Biastoch, A., Getzlaff, K., & Bamber, J.L. (2016). Emerging impact of Greenland meltwater on deepwater formation in the North Atlantic Ocean. *Nature Geoscience*, 9(7), 523.

Brandt, P., Funk, A., Czeschel, L., Eden, C., Böning, C.W. (2007). Ventilation and transformation of Labrador Sea Water and its rapid export in the deep Labrador Current. *Journal of Physical Oceanography*, 37(4), 946-961.

Brossier, C.L., Léger, L., Giordani, H., Beuvier, J., Bouin, M.N., Ducrocq, V., & Fourrié, N. (2017). Dense water formation in the northern-western Mediterranean area during HyMeX-SOP2 in 1/36° ocean simulations: Ocean-atmosphere coupling impact. *Journal of Geophysical Research: Oceans*, 122(7), 5749-5773.

Chafik, L., & Rossby, T. (2019). Volume, Heat, and Freshwater Divergences in the Subpolar North Atlantic Suggest the Nordic Seas as Key to the State of the Meridional Overturning Circulation. *Geophysical Research Letters*, 46, 4799-4808.

Chanut, J., Barnier, B., Large, W., Debreu, L., Penduff, T., Molines, J.M., & Mathiot, P. (2008). Mesoscale eddies in the Labrador Sea and their contribution to convection and restratification. *Journal of Physical Oceanography*, 28(8), 1617-1643.

Close, S., Herbaut, C., Houssais, M.N., & Blaizot, A.C. (2018). Mechanisms of interannual-to decadal-scale winter Labrador Sea ice variability. *Climate Dynamics*, 51(7-8), 2485-2508.

Courtois, P., Gardia-Quintana, G., Hu, X., Myers, P.G. (2020). Kinematic subduction rate of Labrador Sea Water from an eddy-permitting numerical model. *Journal of Geophysical Research: Oceans*

Courtois, P., Hu, X., Pennelly, C., Spence, P., & Myers, P.G. (2017). Mixed layer depth calculation in deep convection regions in ocean numerical models. *Ocean Modelling,* 120,60-78.

Cuny, J., Rhines, P.B., & Kwok, R. (2005). Davis Strait volume, freshwater and heat fluxes. *Deep Sea Research Part I: Oceanographic Research Papers*, 52(3), 519-542.

Cuny, J., Rhines, P.B., Niiler, P.P., & Bacon, S. (2002). Labrador Sea boundary currents and the fate of the Irminger Sea Water. Journal of Physical Oceanography*, 32(2), 627-647.*

Curry, B.C., Lee, C.M., & Petrie, B. (2011). Volume, freshwater, and heat fluxes through Davis Strait, 2004-2005. *Journal of Physical Oceanography*, 41(3), 429-436.

Curry, B., Lee, C.M., Petrie, B., Moritz, R.E., & Kwok, R. (2014). Multiyear volume, liquid freshwater, and sea ice transports through Davis Strait, 2004-10. *Journal of Physical Oceanography,* 44(4), 1244-1266.

Dai, A., Qian, T., Trenberth, K.E., & Milliman, J.D. (2009). Changes in continental freshwater discharge from 1948 to 2004. *Journal of Climate*, 22(10), 2773-2792.

de Jong, M.F., Bower, A.S., & Furey, H.H. (2016). Seasonal and interannual variations of Irminger ring formation and boundary-interior heat exchange in FLAME. *Journal of Physical Oceanography,* 46(6), 1717-1734.

de Steur, L., Hansen, E., Gerdes, R., Karcher, M., Fahrbach, E., & Holfort, J. (2009). Freshwater fluxes in the East Greenland Current: A decade of observations. *Geophysical Research Letters*, 36(23).

de Steur, L., Peralta-Ferriz, C., & Pavlova, O. (2018). Freshwater export in the East Greenland Current freshens the Northern Atlantic. *Geophysical Research Letters*, 45, 13359-13366.

de Steur, L., Pickart, R.S., Macrander, A., Våge, K., Harden, B., Jónsson, S., et al. (2017). Liquid freshwater transport estimates from the East Greenland Current based on continuous measurements north of Denmark Strait. *Journal of Geophysical Research: Oceans*, 122(1), 93-109.

Debreu, L., Vouland, C., & Blayo, E. (2008). AGRIF: Adaptive grid refinement in Fortran. *Computers and Geosciences*, 34(1), 8-13.

Dickson, R.R., Meincke, J., Malmberg, S.A., & Lee, A.J. (1988). The "great salinity anomaly: in the northern North Atlantic 1968-1982. *Progress in Oceanography*, 20(2), 103-151.

Ferry, N., Parent, L., Garric, G., Barnier, B., & Jourdain, N.C. (2010). Mercator global Eddy permitting ocean reanalysis GLORYS1V1: Description and results. *Mercator-Ocean Quarterly Newsletter*, 36, 15-27.

Feucher, C., Garcia-Quintana, Y., Yashayaev, I., Hu, X., Myers, P.G. (2019). Labrador Sea Water formation and its impact on the local Meridional Overturning Circulation. *Journal of Geophysical Research: Oceans*

Fichefet, T., & Maqueda, M.A.M. (1997). Sensitivity of a global sea ice model to the treatment of ice thermodynamics and dynamics. *Journal of Geophysical Research: Oceans*, 102(C6), 12609-12646.

Fischer, J., & Schott F.A. (2002). Labrador Sea Water tracked by profiling floats- From the boundary current into the open North Atlantic. *Journal of Physical Oceanography,* 32(2), 573-584.

Fischer, J., Visbek, M., Zantopp, R., Nunes, N. (2010). Interannual to decadal variability of outflow from the Labrador Sea. *Geophysical Research Letters*, 37(24).

Frajka-Williams, E., Rhines, P.B., & Eriksen, C.C. (2014). Horizontal stratification during deep convection in the Labrador Sea. *Journal of Physical Oceanography*, 44(1), 220-228.

Fratantoni, P.S., & McCartney M.S. (2010). Freshwater export from the Labrador Current to the North Atlantic Current and the Tail of the Grand Banks of Newfoundland. *Deep Sea Research Part I: Oceanographic Research Papers,* 57(2), 258-283.

Fratantoni, P.S, & Pickart, R.S. (2007). The Western North Atlantic Shelfbreak Current System in Summer. *Journal of Physical Oceanography,* 37(10), 2509-2533.

Gelderloos, R., Katsman, C.A., & Drijfhout, S.S. (2011). Assessing the roles of three eddy types in restratifying the Labrador Sea after deep convection. *Journal of Physical Oceanography*, 4(11), 2102-2119.

Gelderloos, R., Straneo, F., & Katsman, C.A. (2012). Mechanisms behind the temporary shutdown of deep convection in the Labrador Sea: Lessons from the great salinity anomaly years 1968-71. *Journal of Climate*, 25(19), 6743-6755.

Gillard, L., Hu, X., Myers, P.G., & Bamber, J.L. (2016). Meltwater pathways from marine terminating glaciers of the Greenland ice sheet. *Geophysical Research Letters*, 43(20).

Grivault, N., Hu, X., & Myers, P.G. (2017). Evolution of Baffin Bay water masses and transports in a numerical sensitivity experiment under enhanced Greenland Melt. *Atmosphere-Ocean*, 55(3), 169-194.

Grivault, N., Hu, X., & Myers, P.G. (2018). Impact of the surface stress on the volume and freshwater transport through the Canadian Arctic Archipelago from high resolution numerical modelling. *Journal of Geophysical Research: Oceans,* 123, 9038-9060.

Gordon, A.L., Visbeck, M., & Comiso, J.C. (2007). A possible link between the Weddell Polynya and the Southern Annular Mode. *Journal of Climate*, 20(11), 2558-2571.

Häkkinen, S., & Rhines, P.B. (2004). Decline of subpolar North Atlantic circulation during the 1990s. *Science*, 304(5670), 555-559.

Handmann, P., Fischer, J., Visbeck, M., Karstensen, J., Biastoch, A., Böning, C., & Patara, L. (2018). The Deep Western Boundary Current in the Labrador Sea From Observations and a High-Resolution Model. *Journal of Geophysical Reaearch: Oceans*, 123, 2828-2850.

Hansen, B., & Østerhus, S. (2000). North Atlantic-Nordic Seas exchanges. *Progress in Oceanography*, 45(2), 109-208.

Holdsworth, A.M., & Myers, P.G. (2015). The influence of high-frequency atmospheric forcing on the circulation and deep convection of the Labrador Sea. *Journal of Climate*, 28(12), 4980-4996.

Howatt, T., Palter, J.B., Matthews, R., deYoung, B., Bachmayer, R., & Claus, R. (2018). Ekman and Eddy Exchange of Freshwater and Oxygen across the Labrador Shelf Break. *Journal of Physical Oceanography*, 48(5), 1015-1031.

Hu, X., Sun, J., Chan, T.O., & Myers, P.G. (2018). Thermodynamic and dynamic ice thickness contributions in the Canadian Arctic Archipelago in NEMO-LIM2 numerical simulations. *Cryosphere*, 12(4).

Hughes, K.G., Klymak, J.M., Hu, X., & Myers, P.G. (2017). Water mass modification and mixing rates in a 1/12° simulation of the Canadian Arctic Archipelago. *Journal of Geophysical Research: Oceans*, 122(2), 803-820.

Jonsson, S., & Valdimarsson, H. (2004). A new path for the Denmark Strait overflow water from the Iceland Sea to Denmark Strait. *Geophysical Research Letters,* 31(3).

Kawasaki, T., & Hasumi, H. (2014). Effect of freshwater from the West Greenland Current on the winter deep convection in the Labrador Sea. *Ocean Modelling*, 75, 51-64.

Khatiwala, S., Schlosser, P., & Visbeck, M. (2002). Rates and mechanisms of water mass transformation in the Labrador Sea as inferred from tracer observations. *Journal of Physical Oceanography*, 32(2), 666-686.

Kieke, D., Rhein, M., Stramma, L., Smethie, W.M., LeBel, D.A., & Zenk, W. (2006). Changes in the CFC inventories and formation rates of Upper Labrador Sea Water, 1997-2001. *Journal of Physical Oceanography,* 36(1), 64-86.

Koenigk, T., Mikolajewicz, U., Haak, U., & Jungclaus, J. (2007). Arctic freshwater export in the 20th and 21st centuries. *Journal of Geophysical Research: Biogeosciences*, 112(G4).

Lab Sea Group (1998). The Labrador Sea deep convection experiment. *Bulletin of the American Meteorological Society*, 79(10), 2033-2058.

Lazier, J.R. (1980). Oceanographic conditions at ocean weather ship Bravo, 1964-1974. *Atmosphere-Ocean*, 18(3), 227-238.

Lazier, J., Hendry, R., Clarke, A. Yashayaev, I., & Rhines, P. (2002). Convection and restratification in the Labrador Sea, 1990-2000. *Deep Sea Research Part I: Oceanographic Research Papers*, 49(10), 1819-1835.

Lazier, J.R.N., & Wright, D.G. (1993). Annual velocity variations in the Labrador Current. *Journal of Physical Oceanography*, 23(4), 659-678.

Lilly, J.M., Rhines, P.B., Visbeck, M., Davis, R., Lazier, J.R.N., Schott, F., & Farmer, D. (1999). Observing Deep Convection in the Labrador Sea during Winter 1994/95.*Journal of Physical Oceaongraphy*, 29, 2065-2098.

Lin, P., Pickart, R.S., Torres, D.J., & Pacini, A. (2018). Evolution of the freshwater coastal current at the southern tip of Greenland. *Journal of Physical Oceanography*, 48(9), 2127-2140.

Loder, J.W., Ross, C.K, & Smith, P.C. (1988). A space-and time-scale characterization of circulation and mixing over submarine banks, with application to the northwestern Atlantic continental shelf. *Canadian Journal of Fisheries and Aquatic Sciences,* 45(11), 1860-1885.

Lozier, M.S., Li, F., Bacon, S., Bahr, F., Bower, A.S., Cunningham, S.A., et al. (2019). A sea change in our view of overturning in the subpolar North Atlantic. *Science*, 363(6426), 516-521.

Luo, H., Bracco, A., & Di Lorenzo, E. (2011). The interannual variability of the surface eddy kinetic energy in the Labrador Sea. *Progress in Oceanography*, 91(3), 295-311.

Luo, H., Castelao, R.M., Rennermalm, A.K., Tedesco, M., Bracco, A., Yager, P.L., & Mote, T.L. (2016). Oceanic transport of surface meltwater from the southern Greenland ice sheet. *Nature Geoscience*, 9(7), 528.

Madec, G. (2008). Note du Pôle de modélisation, Institut Pierre-Simon Laplace (IPSL), France, No 27, ISSN No 1288-1619.

Marshall, J., & Schott, F. (1999). Open-ocean convection: Observations, theory, and models. *Reviews of Geophysics,* 37(1), 1-64.

Marson, J.M., Myers, P.G., Hu, X., Petrie, B., Azetsu-Scott, K., & Lee, C.M. (2017). Cascading off the West Greenland Shelf: A numerical perspective. *Journal of Geophysical Research: Oceans*, 122(7), 5316-5328.

Marzocchi, A., Hurschi, J.J.M., Holliday, N.P., Cunningham, S.A., Blaker, A.T., & Coward, A.C. (2015). The North Atlantic subpolar circulation in an eddy-resolving global ocean model. *Journal of Marine Systems,* 142, 126-143.

McGeehan, I., & Maslowski, W. (2011). Impact of shelf-basin freshwater transport on deep convection in the western Labrador Sea. *Journal of Physical Oceanography,* 41(11), 2187-2210.

Müller, V., Kieke, D., Myers, P.G., Pennelly, C., & Mertens, C. (2017). Temperature flux carried by individual eddies across 47° N in the Atlantic Ocean. *Journal of Geophysical Research: Oceans,* 122(3), 2441-2464.

Müller, V., Kieke, D., Myers, P.G., Pennelly, C., Steinfeldt, R., & Stendardo, I. (2019). Heat and freshwater transport by mesoscale eddies in the southern subpolar North Atlantic. *Journal of Geophysical Research: Ocean.*

Myers, P. (2005). Impact of freshwater from the Canadian Arctic Archipelago on the Labrador Sea water formation. *Geophysical Research Letters*, 32(6).

Myers, P.G., Donnelly, C., & Ribergaard, M.H. (2009). Structure and variability of the West Greenland Current in summer derived from 6 repeat standard sections. *Progress in Oceanography*, 80(1-2), 93-112.

Myers, P.G., Kulan, N., & Ribergaard, M.H. (2007). Irminger water variability in the West Greenland Current. *Geophysical Research Letters*, 34(17).

Pickart, R.S., & Spall, M.A. (2007). Impact of Labrador Sea convection on the North Atlantic meridional overturning circulation. *Journal of Physical Oceanography,* 37(9), 2207-2227.

Quartly, G.D., de Cuevas, B.A., Coward, A.C. (2013). Mozambique Channel eddies in GCMs: A question of resolution and slippage. *Ocean Modelling*, 63, 56-67.

Rattan, S., Myers, P.G., Treguier, A.M., Theetten, S., Biastoch, A., & Böning, C. (2010). Towards and understanding of Labrador Sea salinity drift in eddy-permitting simulations. *Ocean Modelling*, 35(1-2), 77-88.

Rhein, N., Kieke, D., Steinfeldt, R. (2015). Advection of North Atlantic Deep Water from the Labrador Sea to the southern hemisphere. *Journal of Geophysical Research: Oceans*, 120(4), 2471-2487.

Rieck, J.K., Böning, C.W., Getzlaff, K. (2019). The Nature of Eddy Kinetic Energy in the Labrador Sea: Different Types of Mesoscale Eddies, their Temporal Variability and Impact on Deep Convection. *Journal of Physical Oceanography*.

Rykova, T., Straneo, F., & Bower, A.S. (2015). Seasonal and interannual variability of the West Greenland Current System in the Labrador Sea in 1993-2008. *Journal of Geophysical Research: Oceans*, 120(2), 1318-1332.

Saenko, O.A., Dupont, F., Yang, D., Myers, P.G., Yashayaev, I., Smith, G.C. (2014). Role of resolved and parameterized eddies in the Labrador Sea balance of heat and buoyancy. *Journal of Physical Oceanography*, 44(12), 3008-3032.

Schmidt, S., & Send, U. (2007). Origin and composition of seasonal Labrador Sea freshwater. *Journal of Physical Oceanography*, 37(6), 1445-1454.

Schulze-Chretien, L.M. & Frajka-Williams, E. (2018). Wind-driven transport of fresh shelf water into the upper 30m of the Labrador Sea. *Ocean Science*, 14(5), 1247-1264.

Smith, G.C., Roy, F., Mann, P., Dupont, F., Brasnett, B., Lemieux, J.F., et al. (2014). A new atmospheric dataset for forcing ice-ocean models: Evaluation of reforcasts using the Canadian global deterministic prediction system. *Quarterly Journal of the Royal Meteorological Society*, 140(680), 881-894.

Smith, W.H.F, & Sandwell, D.T. (1997). Global seafloor topography from satellite altimetry and ship depth soundings. *Science*, 277, 1957-1962.

Straneo, F. (2006). Heat and freshwater transport through the central Labrador Sea. *Journal of Physical Oceanography*, 36(4), 606-628.

Straneo, F., & Saucier, F. (2008a). The arctic-subarctic exchange through Hudson Strait. *Arctic-Subarctic Ocean Fluxes*, Springer, Dordrecht, 249-261.

Straneo, F., & Saucier, F. (2008b). The outflow from Hudson Strait and its contribution to the Labrador Current. *Deep Sea Research Part I: Oceanographic Research Papers*, 55(8), 926-946.

Sutherland, D.A., & Pickart, R.S. (2008). The East Greenland coastal current: Structure, variability, and forcing. *Progress in Oceanography,* 78(1), 58-77.

Swift, J.H. (1984). The circulation of the Denmark Strait and Iceland-Scotland overflow waters in the North Atlantic. *Deep Sea Research Part A. Oceanographic Research Papers,* 31(11), 1339-1355.

Tréquier, A.M., Theetten, S., Chassignet, E.P., Penduff, T., Smith, R., Talley, L., et al. (2005). The North Atlantic subpolar gyre in four high-resolution models. *Journal of Physical Oceanography*, 35(5), 757-774.

Tsubouchi, T., Bacon, S. Naveira Garabato, A.C., Aksenov, Y., Laxon, S.W., Fahrbach, E., et al. (2012). The Arctic Ocean in summer: a quasi-synoptic inverse estimate of

boundary fluxes and water mass transformation. *Journal of Geophysical Research: Oceans*, 117(C1).

Volkov, D.L., Larnicol, G., & Dorandeu, J. (2007). Improving the quality of satellite altimetry data over continental shelves. *Journal of Geophysical Research: Oceans*, 112(C6).

Whiteworth, T. & Orsi, A.H. (2006). Antarctic Bottom Water production and export by tides in the Ross Sea. *Geophysical Research Letters* 33(12).

Yashayaev, I. (2007). Hydrographic changes in the Labrador Sea, 1960-2005. *Progress in Oceanography*, 73(3-4), 242-276.

Yashayaev, I., & Loder, J.W. (2009). Enhanced production of Labrador Sea water in 2008. *Geophysical Research Letters,* 36(1).

Yashayaev, I., & Loder, J.W. (2017). Further intensification of deep convection in the Labrador Sea in 2016. *Geophysical Research Letters*, 44(3), 1429-1438.

Zalesak, S.T. (1979). Fully multidimensional flux-corrected transport algorithms for fluids. *Journal of Computational Physics,* 31(3), 335-362.

Zantopp, R, Fischer, J., Visbek, M., Karstensen, J. (2017). From interannual to decadal: 17 years of boundary current transports at the exit of the Labrador Sea. *Journal of Geophys. Res. Oceans*, 122, 1724-1748

Chapter 5: Impact of Different Atmospheric Forcing Sets on Modelling Labrador Sea Water Production

Clark Pennelly[1*] and Paul G. Myers[1]

[1]Department of Earth and Atmospheric Sciences, University of Alberta, Edmonton, Alberta, Canada

[*]Pennelly@ualberta.ca

Key Points:

Five NEMO simulations with different atmospheric forcing had average annual air-sea heat fluxes vary up to 12 W m^{-2} over the Labrador Sea.

The combination of air-sea and lateral buoyancy fluxes produced variations in stratification that impacted the convection depth.

Greater buoyancy loss promoted denser, but not more voluminous, Labrador Sea Water.

5.1. Abstract

A numerical modelling sensitivity study is carried out within the Labrador Sea by varying the atmospheric conditions. From forcing NEMO simulations with five atmospheric products commonly used in ocean modelling (DFS5.2, ERA-Interim, CGRF, ERA5, and JRA55-do), we calculate the air-sea heat fluxes that occur over the Labrador Sea (2002 to 2015 annual-average net-heat flux: -53.4, -51.0, -46.6, -58.5, and -47.9 W m^{-2}). With differences up to 12 W m^{-2} in net surface heat flux averaged over a central region of the Labrador Sea, each product supplied different atmospheric conditions. While the salinity-dependent surface buoyancy flux were similar across all

simulations, differences between each simulation's solar and non-solar heat flux led to significant changes in the level of stratification (up to 400 J m^{-3}), depth of the mixed layer (up to 300 m), and thickness of Labrador Sea Water (up to 300 m). Greater buoyancy loss from the Labrador Sea produced LSW with greater density. However, the production rate of LSW was not clearly affected by small changes in the surface buoyancy flux.

5.2. Plain Language Summary:

The Labrador Sea, between Canada and Greenland, experiences deep convection, a process where the ocean's surface is cooled to such a point that it becomes denser than the water beneath it, causing the surface layer to mix downwards. The overlying atmospheric conditions, such as wind speed, temperature and humidity, strongly control this cooling. We carry out five ocean simulations to explore how small changes in atmospheric conditions influence the Labrador Sea. Our simulations show that atmospheric forcing which enhances the cooling of the Labrador Sea causes the deep water formed here to become denser. While a denser water mass is produced, we find that the volume of this water mass is not necessarily enhanced with the additional cooling.

5.3. Introduction

Situated within the North Atlantic sub-polar gyre between eastern Canada and Greenland, the Labrador Sea (Fig. 5.1a) routinely experiences intense air-sea forcing. Mid-latitude cyclones frequently pass over the Labrador Sea. These winter storms, which often come from Canada, are cold and relatively dry. The underlying ocean releases heat to the atmosphere, cools and becomes denser. This densification is crucial to the deep convection which occurs within the Labrador Sea (Lab Sea Group, 1998).

Two aspects are common across regions with deep convection: a weakly stratified basin and strong surface buoyancy loss (Marshall and Schott, 1999; Lab Sea Group, 1998). Cyclonic circulation, while not required for convection, helps keep the basin weakly stratified by doming isopycnals. Cold winter winds remove buoyancy, eroding the stratification and promoting deep convection which can surpass 2000m (Yashayaev, 2007). However, even with substantial surface buoyancy loss, a significant freshwater layer at the surface can prevent convection from occurring (Gelderloos et al., 2012; Böning et al., 2016) as more buoyancy removal would be required than the atmosphere could provide. Furthermore, even with weak stratification, winter periods with relatively calm atmospheric conditions can result in limited convection (Lazier et al., 2002). The North Atlantic Oscillation (NAO; Hurrell, 1995) index, calculated from the pressure difference between the Icelandic Low and the Azores High, can give insight into the degree which the atmosphere removes buoyancy from the sub-polar gyre (Yashayaev and Loder, 2016). A positive NAO phase is often associated with stronger winds than the usual climatology (Hurrell and Deser, 2010), enhancing the buoyancy loss from the ocean (Curry et al., 1998) and driving deep convection. A negative NAO phase is often
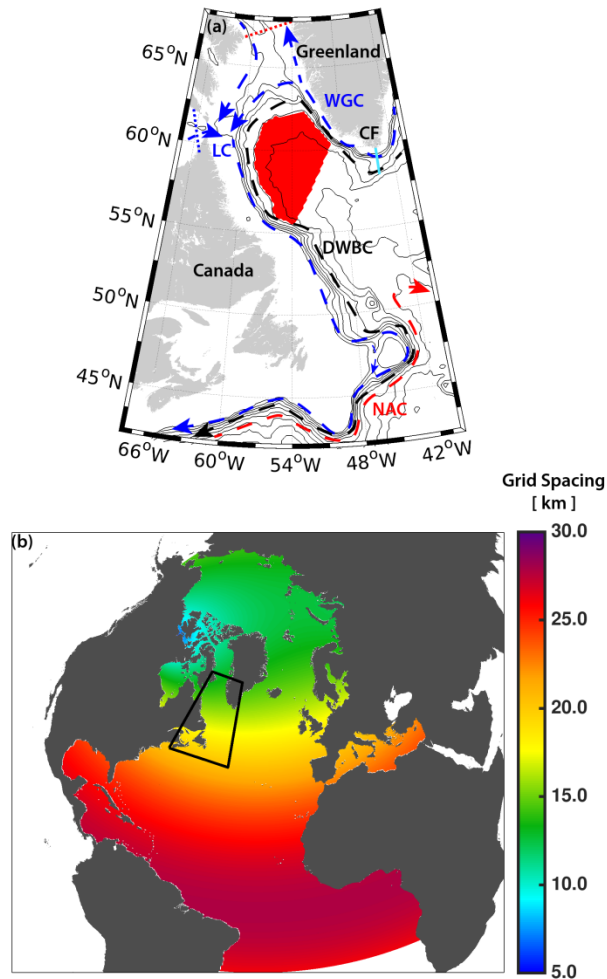
Figure 5. 1: The Labrador Sea (a) with Davis (Hudson) Strait identified as the dotted red (blue) line. Isobath contour interval is 500m. Dashed arrows are as follows: NAC is the North Atlantic Current, WGC is the West Greenland Current, LC is the Labrador Current, and DWBC is the Deep Western Boundary Current. The filled red polygon indicates our region of interest where analysis takes place. CF stands for our Cape Farewell section in teal. The ANHA4 configuration (b) is shown with colors indicating horizontal grid spacing (km) and the black box shows the spatial area covered in (a).

associated with less buoyancy loss, reducing the vertical depth of convection. While the

NAO index gives a useful measure of the sea-level pressure anomaly, it does not

guarantee conditions which promote significant air-sea heat loss (Moore et al., 2011)

and deep convection in the Labrador Sea.

Deep mixing can occur with weak surface buoyancy loss if the stratification has been eroded sufficiently due to multiple successive years with strong convection (Pickart et al., 2002; Schulze-Chretien et al., 2016). As it takes time for the stratification to rebuild, multiple years with strong buoyancy loss can produce a progressively thicker and denser Labrador Sea Water, leaving the basin weakly stratified for the following convection season (Lazier et al., 2002; Yashayaev and Loder, 2016). This occurred in the late 1980s to mid 1990s during a prolonged positive NAO phase with strong buoyancy loss, ultimately producing a thick layer of dense LSW (Yashayaev, 2007). If one uses NAO as a proxy for surface buoyancy loss, 1994 had the thickest LSW layer without the strongest forcing (Yashayaev, 2007). This implies that the buoyancy loss experienced during one convection period has lasting effects for the following year.

While the atmosphere removes buoyancy from the Labrador Sea, the boundary currents supply relatively buoyant water to restratify the region, steadily freshening the upper Labrador Sea while heating at depth (Straneo, 2006). This restratification process is strongly driven by the West Greenland Current (WGC) which carries fresh and cold water within the surface layer (0-200m) and warm and salty Irminger Water within the subsurface layer (200-700m: Cuny et al., 2002; Lazier et al., 2002; Chanut et al., 2008; Myers et al., 2009; Rykova et al., 2015; de Jong et al., 2016). The WGC and Labrador Current experience instabilities that produce buoyant eddies which make their way further offshore, bringing stratification into the interior Labrador Sea (Spall, 2004; Myers, 2005; Pickart and Spall, 2007; Schmidt and Send, 2007; Gelderloos et al., 2011; McGeehan and Maslowski, 2011). Wind-driven Ekman transport provides another route where freshwater within the boundary currents is able to travel towards the interior (Schulze-Chretien and Frajka-Williams, 2018).

The combination of overlying stratification and significant surface buoyancy loss produces deep convection in the Labrador Sea, forming Labrador Sea Water (LSW), a water mass with a potential density between 1027.68 and 1027.80 kg m^{-3} (Kieke et al., 2006; Yashayaev, 2007; Rhein et al., 2015). LSW is one part of the lower limb within the Atlantic Meridional Overturning Circulation (AMOC). As the AMOC is part of the global thermohaline circulation, any changes within the Labrador Sea that modify the production of LSW may ultimately influence this global circulation. Turbulent heat and freshwater fluxes that control the stratification within the Labrador Sea were found to impact the AMOC (Yeager and Danabasoglu, 2014). As atmospheric forcing strongly controls these fluxes, uncertainty in atmospheric forcing may force simulations to be very different, as Pillar et al. (2018) found to occur within the AMOC transport within 15 years, primarily due to zonal winds and surface heat flux. However, the role of the Labrador Sea in relationship to the overturning circulation is an active area of research (Lozier et al., 2019; Li et al., 2019).

Much research has been carried out on how atmospheric forcing can impact the Labrador Sea. Holdsworth and Myers (2015) performed numerical simulations without the presence of mid-latitude cyclones by filtering out high frequency variability present within their forcing data and found that the absence of cyclones reduced the sub-polar gyre and AMOC strength by about 25%. Garcia-Quintana et al. (2019) expanded upon this by performing a sensitivity study on the influence of LSW production by filtering storms as well as decreasing precipitation. They found that filtering storms reduced LSW volume production by 82%, primarily by producing a water mass with lighter density than LSW. Their simulation which reduced precipitation by 66% had the reverse response, producing a more voluminous water mass which was denser than LSW.

Bramson (1997) showed that alterations in wind stress and precipitation induced changes within the mixed layer of the Labrador Sea. Chadhuri et al. (2016) forced an ocean model with various atmospheric forcing datasets, noting significant differences in the meridional overturning streamfunction that they attributed to variability in the wind stress or heat flux within the North Atlantic. Others have found that the location of wind may be more important than the frequency or strength of winds; Schulze-Chretien et al. (2016) noted that the greatest heat loss was primarily due to the organization of the storm track. Moore et al. (2011) and Duvivier et al. (2016) note the importance of Greenland's strong tip jets on the surrounding seas, increasing the sensible and latent heat fluxes. Some suggest the maximum surface heat loss is due to the location of the sea-ice edge (Marshall and Schott, 1999), although Moore et al. (2014) suggest that upstream and downstream topography also influence the region of maximum turbulent heat loss.

While atmospheric forcing sets are useful for driving ocean simulations, they present other issues. Renfrew et al. (2002) found that these datasets may significantly deviate from observations within the Labrador Sea, suggesting simulations could be far from reality. The spatial and temporal resolution of atmospheric forcing datasets determines the scale of features that are included. Lower-resolution datasets may fail to properly resolve mesoscale features that strongly impact the surface heat flux (Condon and Renfrew, 2013; Jung et al., 2014) that is vital to controlling the stratification and deep convection within the Labrador Sea.

Long-term climate simulations (100+ years) often use low resolution (approximately 1/4° and coarser) to investigate future scenarios and situations (IPCC, 2014). These simulations help us understand and form policy on a changing climate

even though they misrepresent some aspects. Deep convection, within both the atmosphere and ocean, occurs at a much smaller scale (< 1 km) than these simulations can resolve. To fully resolve deep convection, ocean simulations require very high-resolution (Raasch and Etling (1997) had success with 25m) and non-hydrostatic physics. The computing requirements for such a coupled climate simulation that spans 100+ years is not feasible. However, numerical modelers have long since been able to work around these sub-grid scale features by adding parameterizations to their code that mimic the effects while not resolving the features. This allows for ocean simulations of any resolution to mimic the effects of deep convection while not physically resolving it.

Here we explore how the buoyancy fluxes associated with numerous atmospheric forcing products influence the formation rate and density of Labrador Sea Water. We investigate this by using five different atmospheric forcing products to drive a 1/4° eddy-permitting ocean simulation. We explore the differences between the different products as well as the ocean's response when driven by each product. While we do not explicitly resolve convection, our objective is to quantify how small differences in surface forcing influence an area where deepwater is formed. This is particularly relevant for a suite of simulations that differ in their atmospheric forcing; for example, the Representative Concentration Pathways simulations (Van Vuuren et al., 2011).

5.4. Methods

To investigate the differences in atmospheric forcing on LSW formation, we chose to use different atmospheric forcing datasets used by the ocean modelling community rather than carry out sensitivity simulations by perturbing a single forcing

set away from its original state. Such perturbations may identify the sensitivity of Labrador Sea Water formation on select aspects (e.g. Bramson, 1997; Garcia-Quintana et al., 2019) but perturbation simulations may no longer carry a realistic imprint of the surface forcing. To keep our simulations as realistic as possible, we examined five different atmospheric forcing datasets: ERA-Interim (Dee et al., 2011), Drakkar Forcing Set 5.2 (DFS5.2; Dussin et al. 2016), Canadian Meteorological Centre's Global Deterministic Prediction System Reforecasts (CGRF; Smith et al., 2014), ERA5 (Hersbach and Dee, 2016), and the Japanese Reanalysis product JRA55-do (Tsujino et al., 2018).

Each atmospheric dataset provides near-surface conditions to force ocean simulations. These datasets differ from one another (Table 5.1) in spatial/temporal resolution, reference height for data fields, as well as the type of product. We do not investigate how these differences influence the surface buoyancy flux provided by each dataset. However, others have noted that higher spatial resolution produces a larger variance in the wind speed and heat flux (Langlais et al., 2009; Brossier et al., 2012; Jung et al. 2014) while higher temporal resolution helps resolve the diurnal heating that stratifies the upper ocean and mesoscale features (Brossier et al., 2012). Differences in the reference height indicate a slightly different method to calculate the drag transfer coefficient (eq. 5.1 and 5.2 below; Large and Yeager, 2008), influencing the air-sea transport of momentum, freshwater, and heat. CGRF, the only reforecast product, stitches together daily forecasts to produce the final product. The authors of CGRF (Smith et al., 2014) even state that CGRF "… is not a reanalysis and thus is expected to be less well constrained by available observations", but highlight its high resolution and relatively small bias. As each dataset was produced using a different numerical

framework, readers should refer to the documentation listed above for further information regarding each dataset. It should be noted that each of these forcing sets have been used in ocean hindcast simulations (e.g. ERA-Interim: Lindsay et al., 2014; DFS5.2: Benetti et al., 2017; CGRF: Gillard et al., 2016; ERA5: Wilson et al., 2019; JRA55-do: Tsujino et al., 2018). Each atmospheric dataset was used to force a numerical simulation as detailed below.

Table 5. 1: Information regarding each atmospheric forcing dataset used to force the simulations. Spatial resolution is the average grid spacing over the red polygon in the Labrador Sea (Fig 5.1a).

Dataset	Spatial Resolution [km]	Temporal Resolution [hr] (wind/temperature/precip/radiation)	Temperature and Moisture Height	Wind Speed Reference Height	Years of Coverage	Product Type
ERA-Interim	45	3 / 3 / 24 / 24	2m	10m	1979+	Reanalysis
DFS 5.2	45	3 / 3 / 24 / 24	2m	10m	1958-2015	Reanalysis
CGRF	33	1 / 1 / 1 / 1	2m	10m	2002+	Reforecast
ERA5	30	1 / 1 / 1 / 1	2m	10m	1979[*]+	Reanalysis
JRA55-DO	31	3 / 3 / 3 / 3	10m	10m	1958+	Reanalysis

All simulations had the NEMO ocean model version 3.4 (Madec, 2008) coupled with the LIM2 sea-ice model (Fichefet and Maqueda, 1997). Each simulation used the regional 1/4° horizontal resolution Arctic and Northern Hemisphere Atlantic (ANHA4; Fig. 5.1b) configuration (Holdsworth and Myers, 2015; Müller et al., 2017; Courtois et al., 2017) with 50 vertical levels and open boundaries across Bering Strait and 20° S. Initial and open boundary conditions were obtained from the global 1/4° GLORYS2v3 simulation (Ferry et al., 2010). Interannual monthly runoff was a combination of Dai et al. (2009) as well as Greenland derived liquid runoff via a surface mass balance model (Bamber et al., 2012). While atmospheric products may include their own runoff data, we opted to keep this freshwater source constant between the simulations; see Gillard et al. (2016) or Garcia-Quintana et al. (2019) on how the Labrador Sea is impacted by

changes in runoff. Other than the prescribed atmospheric state, all simulations had identical settings and no restoring was performed on any simulation. We name each simulation by the atmospheric forcing product used, though we also shorten some of the names for brevity. Henceforth the simulation which used the DFS5.2 dataset is known as DFS, ERA-interim as ERA, CGRF as CGRF, ERA5 as ERA5, and JRA55-do as JRA. Each simulation was initialized at the start of the year 2002 and continued until the end of 2015. No spin-up was performed as the initial conditions from GLORYS2v3 (Ferry et al., 2010) already had about one decade of integration since initialization.

All simulations used the CORE bulk formulae for the heat, momentum, and freshwater flux between the atmosphere and the ocean (Large and Yeager, 2008). Sensible (eq. 5.1) and latent (eq. 5.2) turbulent heat fluxes are determined from the humidity, temperature, and velocity difference between the ocean's surface and the overlying atmosphere. Positive values indicate a heat flux from the atmosphere into the ocean. Equation variables are as follows: C is the specific heat of air at 1000.5 J kg^{-1} K^{-1}, ρ is the density of air at 1.22 kg m^{-3}, T_o is the ocean's surface temperature in degrees Kelvin, T_a is the potential air temperature in degrees Kelvin, L_v is the latent heat of vaporization (2.5 x 10^6 J kg^{-1}), q_o is the specific humidity (kg kg^{-1}) of 100% saturated air with a temperature equal ocean's surface, q_a is the specific humidity (kg kg^{-1}) of the air at 10m height, U_{ao} is the relative wind speed compared to the ocean's surface in m s^{-1}, while C_h and C_e are sensible and latent transfer drag coefficients (see Large and Yeager, 2008).

$$\text{Sensible Turbulent Heat Flux} = C * \rho * C_h * (T_a\text{-}T_o) * U_{ao} \tag{5.1}$$

$$\text{Latent Turbulent Heat flux} = \rho * C_e * L_v * (q_a - q_o) * U_{ao} \tag{5.2}$$

The various air-sea heat fluxes accumulate to produce a change in the temperature, and thus density, of the ocean's surface. However, each atmospheric forcing product also contains precipitation and snow which not only influences the sensible and latent heat fluxes but also contributes to the surface buoyancy flux via the addition of freshwater. To explore these effects, we examine both the air-sea heat fluxes as well as the net surface buoyancy flux (see Sathiyamoorthy and Moore, 2002).

To help illustrate the differences that atmospheric forcing products have on Labrador Sea Water production, we examine various diagnostics of the Labrador Sea. To calculate the stratification strength, convective energy is used (our eq. 5.3; Holdsworth and Myers, 2015). Convective energy is the amount of energy needed to be removed such that the water column is neutrally stratified to some reference depth. The convective energy to a reference depth, h, is calculated as:

$$Convective\ energy\ (h) = \frac{g}{Area} \int \int \left[h\, \rho_\theta(h) - \int_0^h \rho_\theta(z)\, dz \right] dA \qquad (5.3)$$

where g is the gravitational constant, $Area$ is the total surface area of our region of interest (Fig. 5.1a), $\rho_\theta\ (z)$ and $\rho_\theta\ (h)$ are the potential density at each grid cell and the potential density of the grid cell at the reference depth, and A is the surface area of each grid cell. Positive convective energy indicates stable stratification while negative values indicate unstable stratification. We selected a reference depth, h, of 2000m as convection can reach this depth (Yashayaev, 2007).

While convective energy indicates the degree of stratification, it does not provide any information on the depth of the mixed layer.. One calculation of the mixed layer depth is a 0.01 kg m^{-3} deviation between the potential density at the surface and that of the bottom of the mixed layer. For shallow regions this appears to work fine, but falters

for regions with deep convection (Courtois et al., 2017) as temperature and salinity can compensate to keep the density uniform while the water column properties are no longer well-mixed. To remedy this, we implemented a method (see Courtois et al., 2017) based on Holte and Talley (2009) which examines the water column to estimate the mixed layer depth based on the linear interception of the thermocline and the mixed layer as determined by a 0.01 kg m^{-3} change in potential density from the surface. The final mixed layer depth is the minimum of this intersection or the value found using the 0.01 kg m^{-3} difference in potential density method. This was carried out during all numerical simulations as well as on the observations from Argo floats.

The mixed layer alone doesn't provide enough information to determine the production volume of LSW as water can leave and enter the mixed layer in multiple ways. Production of LSW is determined via a kinematic subduction approach (our eq. 5.4; see Garcia-Quintana et al., 2019; Feucher et al., 2019). We use this approach to bin the total water mass which moves through the mixed layer by density class (1023.0 to 1028.4 kg m^{-3}) per year (τ), with density bins of 0.01 kg m^{-3} width. Water may enter and leave the mixed layer (Z_σ) via lateral advection ($v \cdot \nabla h$), vertical advection (W$_b$), as well as when the mixed layer changes depth ($\partial h/\partial t$).

$$Subduction = \frac{-1}{\tau} \int_0^\tau \int_{A_\sigma} \left[W_b + \frac{\partial h}{\partial t} + v \cdot \nabla h \right] dZ_\sigma \, dt \qquad (5.4)$$

Subduction identifies the total amount of LSW that was produced within a certain density class, though does not give information on the thickness of LSW. As mentioned above, LSW can be classified by density. Due to salinity-driven density drift of our model simulations, a common issue for numerical simulations in the Labrador Sea (Rattan et al, 2010; Marzocchi et al., 2015), we had to alter our definitions of LSW.

Instead of defining LSW using a density criteria between 1027.68 and 1027.80 kg m^{-3} (see Kieke et al., 2006; Yashayaev, 2007; Rhein et al., 2015), we allowed the classification to change in time based on the results from each simulation (see below, Fig. 5.10). Others have had success by classifying LSW that evolves in time to compensate for model drift; Feucher et al. (2019) investigated the link between LSW and Meridional Overturning Circulation. Our calculation of the density of LSW closely follows their approach which is based on observations of Labrador Sea Water that change in time. First, we calculated the yearly subduction (eq. 5.4) rate binned by density (bin width 0.01 kg m^{-3}); the densest bin with positive subduction was used to determine the density of LSW. Our LSW classification is defined from the greatest density within this 0.01 density bin to a minimum density 0.12 kg m^{-3} lighter; the 0.12 kg m^{-3} comes from the traditional density range of LSW (see above). We then divided LSW into 2 equal parts to produce a denser modified Classical Labrador Sea Water (CLSW) and less dense Upper Labrador Sea Water (ULSW); the midpoint between our LSW density range was where ULSW transitioned into CLSW. This was done for every simulation year and linearly smoothed between years to prevent any step jumping from occurring. Simulations will likely not have the same density drift due to changes in surface forcing and resulting lateral fluxes. This method forced the production of deepwater within the Labrador Sea to be classified as Labrador Sea Water despite any numerical drift which occurred. Other methods at classifying LSW were attempted, but the one described above best captured the interannual variability of ULSW and CLSW.

As heat and freshwater contribute to setting the stratification in the Labrador Sea, we calculate the westward heat and freshwater transport across a section which extends from Cape Farewell to the 2500m isobath (CF: Fig. 5.1a). This is done for both

water masses within the current system: cold and fresh (S<34.8, ρ_θ<1027.68 kg m^{-3}) East Greenland Current water, and warm salty Irminger Water (T>3.5°C, S>34.8, ρ_θ<1027.68 kg m^{-3}). Temperatures and salinities were chosen to be consistent with others who have investigated these water masses in the past (Kieke et al., 2006; Myers et al., 2007), although we also imposed a density criteria to prevent classification of water which might be Labrador Sea Water using a classical, non-drift density definition (see above).

To evaluate our simulations, we compare against data from Argo floats (http:www.argo.net). Argo float's temperature and salinity data are used to determine the mixed layer depth using the method outlined by Holte and Talley (2009) that works well for areas with deep convection (Courtois et al., 2017). Comparison against Argo data, as well as the above proxy calculations, took place over the red region of interest in Fig. 5.1a. This region is the area between the 2500m isobath and Atlantic Repeat Hydrography Line 7 West and was chosen as deep convection occurs over a large part of this region in our 1/4° simulations. While this region is larger than the observed convective region (see Yashayaev and Loder, 2016), the convective region remains too spacious in models even with 1/12° horizontal resolution (Courtois et al., 2017). Lengthy low-resolution climate simulations that investigate perturbations in forcing likely suffer as well. As our goal is to investigate how differences in surface forcing impact deepwater produced within the Labrador Sea, our findings should be pertinent for certain climate simulations.

5.5. Results

5.5.1. Atmospheric Variability over the Labrador Sea

Before we investigate the Labrador Sea's response to each of the five atmospheric forcing datasets, we first quantify the differences between the datasets. Figure 5.2 shows the 2002-2015 average daily precipitation and wind speed for the five atmospheric forcing datasets. DFS5.2 (Fig. 5.2a) and ERA-Interim (Fig. 5.2b) are very similar, primarily as DFS5.2 is built from ERA-Interim. JRA55-do (Fig. 5.2e) has less precipitation around Greenland than the others. CGRF (Fig. 5.2c) has less precipitation in and around the tropics and the Labrador Sea, with JRA55-do having slightly more, whereas ERA5 (Fig. 5.2d) has most precipitation. Wind speed appears very similar across the North Atlantic for these forcing sets. While these forcing sets have differences across the North Atlantic, we now focus within the Labrador Sea.

Figure 5.3 illustrates the (a) shortwave radiation, (b) longwave radiation, (c) near surface temperature, (d) near surface specific humidity, (e) precipitation, and (f) 10-meter wind speed for each of the five datasets as spatially averaged across the red polygon in Figure 5.1a, a region where the model simulations contain deep convection. Data were averaged across each month from 2002-2015 to construct these box and whisker plots. While this figure graphically illustrates that there are differences between each dataset, Table 5.2 quantifies the 2002-2015 mean and standard deviation. As each of these six atmospheric variables influence the surface buoyancy flux, we will describe the variability present in Figure 5.3 and Table 5.2 below.
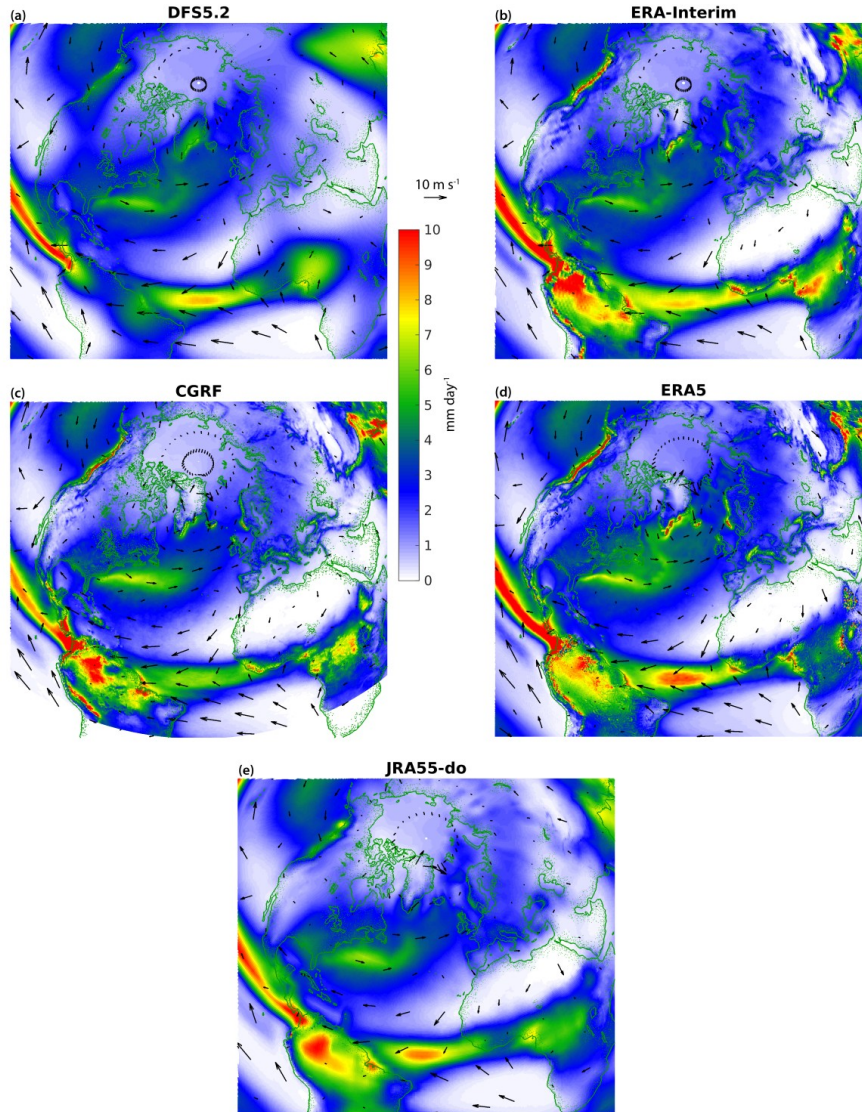
Figure 5. 2: Average daily precipitation (contours; mm day⁻¹) and wind velocity (barbs; m s⁻¹) from 2002 through the end of 2015 for each of our atmospheric forcing datasets. Wind barbs were selectively displayed to preserve visual quality and do not represent spatial resolution; see Table 5.1 for more details.

JRA55-do has the lowest average shortwave radiative heat flux (Fig. 5.3a; 89.9 W m⁻²) with CGRF slightly higher (93.7 W m⁻²). While both of these datasets have the least incoming shortwave radiation, they also tend to have higher longwave radiation values (Fig. 5.3b; JRA55-do: 289.2 W m⁻²; CGRF: 290.5 W m⁻²) compared to the remaining datasets. Combining radiative heat fluxes show that the DFS5.2 (390.3 W m⁻²) and ERA-
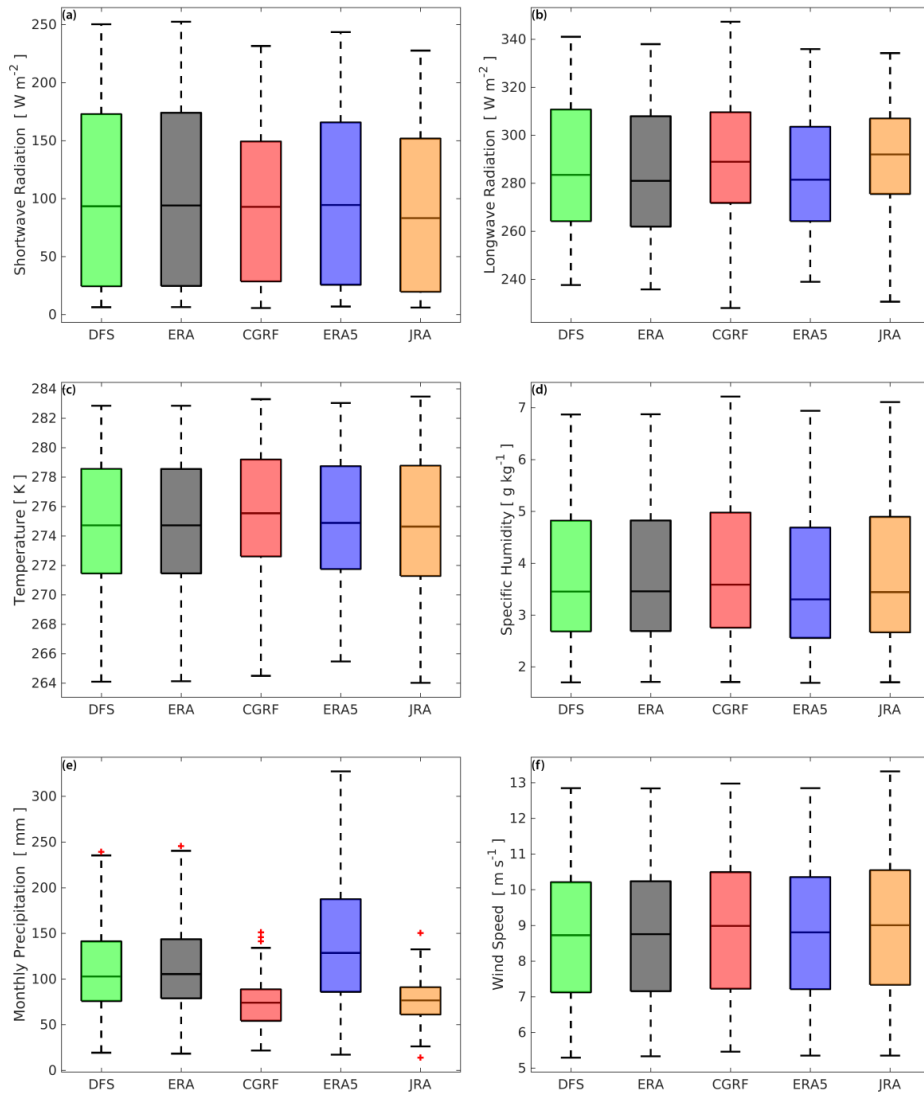
Figure 5. 3: (a) Downward shortwave radiation, (b) downward longwave radiation, (c) temperature, (d) specific humidity, (e) precipitation, and (f) wind speed as supplied by the five atmospheric datasets. Values were spatially and temporally averaged each month from 2002-2015 over the red polygon in Fig 5.1a. Colored boxes indicate the interquartile range. Whiskers lengths are, at most, 150% of the inter-quartile range while red crosses indicate outliers. The horizontal black line within the colored rectangles indicates the median.

Interim (388.5 W m^{-2}) sets are similar while CGRF (384.2 W m^{-2}), ERA5 (382.9 W m^{-2}),

JRA55-do (379.1 W m^{-2}) provide less heat via radiation.

Near-surface temperature (Fig. 5.3c) and specific humidity (Fig. 5.3d) show that

the CGRF simulation is the warmest (275.7 K) and most humid (3.9 g kg^{-1}). The

139

Table 5. 2: 2002-2015 average yearly atmospheric conditions as supplied by each atmospheric dataset to the red polygon in Fig. 5.1a. Numbers inside the square brackets indicate one standard deviation.

Atmospheric Forcing Dataset	Shortwave Radiation [W m^{-2}]	Longwave Radiation [W m^{-2}]	Temperature [K]	Specific Humidity [g kg^{-1}]	Precipitation [mm]	Wind Speed [m s^{-1}]
DFS5.2	103.6 [78.7]	286.7 [28.2]	274.7 [4.4]	3.8 [1.3]	110.4 [47.4]	8.7 [1.7]
ERA-Interim	104.4 [79.3]	284.1 [27.9]	274.7 [4.3]	3.8 [1.3]	112.6 [26.1]	8.7 [1.7]
CGRF	93.7 [65.8]	290.5 [25.2]	275.7 [4.1]	3.9 [1.4]	73.7 [26.2]	8.8 [1.7]
ERA5	99.5 [72.6]	283.4 [24.9]	274.9 [4.4]	3.7 [1.4]	141.2 [69.3]	8.8 [1.7]
JRA55-DO	89.9 [67.8]	289.2 [23.8]	274.9 [4.6]	3.8 [1.4]	77.3 [22.2]	9.0 [1.8]

remaining datasets have nearly the same mean temperature (274.7-274.9 K). ERA5 has the least humidity (3.7 g kg^{-1}) while ERA-Interim, DFS5.2 and JRA55-do have nearly the same (3.8 g kg^{-1}).

Monthly precipitation (Fig. 5.3e) is rather different between the datasets, with ERA5 having a mean of 141.2 mm while JRA55-do and CGRF have the least (77.3 and 73.7 mm). DFS5.2 and ERA-Interim had nearly the same monthly precipitation (110.4 and 112.6 mm). Whisker plots of the monthly average wind speeds (Fig. 5.3f) show that the JRA55-do forcing has the strongest wind (9.0 m s^{-1}) while the others are nearly the same (8.7 to 8.8 m s^{-1})

These small differences in surface forcing affect the Labrador Sea in multiple ways. Radiative fluxes increase the temperature of the ocean's surface, increasing stratification. The near-surface temperature and specific humidity not only influence the latent and sensible heat fluxes that deal with evaporation, but also the turbulent heat fluxes that wind speed influences. Precipitation supplies both a freshwater source that modifies the surface buoyancy flux and sensible/latent heat fluxes as well. The following

section examines NEMO simulations that are driven by these atmospheric forcing datasets and the resulting changes within the Labrador Sea.

5.5.2. Model Evaluation

The ANHA4 configuration has been evaluated within the North Atlantic in numerous studies (see Holdsworth and Myers, 2015; Gillard et al., 2016; Courtois et al., 2017; Müller et al., 2017; Garcia-Quintana et al., 2019), though we provide additional evaluation as it pertains to our research questions. Before investigating LSW production from the ANHA4 simulations, we first seek to determine if each simulation is representing reality to some acceptable level. To do this, we compare the volume, heat, and freshwater flux (Table 5.3) through Davis and Hudson Strait (see Fig. 5.1a) to determine the fluxes into the Labrador Sea. First, all simulations had nearly the same volume transport through Hudson Strait, with about 0.08 to 0.09 Sv of net transport towards the Labrador Sea in agreement with Drinkwater's (1988) and Straneo and Saucier's (2008a) estimates of between 0.08 Sv and 0.1 Sv. Davis Strait has much higher flow, around 1.6 +/- 0.5 Sv (Curry et al., 2014), vastly outweighing that of Hudson Strait. The ERA and DFS simulations (1.74 and 1.76 Sv) most closely matched the observed transport while JRA was higher (2.02 Sv). The CGRF simulation was the only one to have less volume transport (1.3 Sv) than observations suggest. All simulations were within a standard deviation of the observed volume transport across Davis Strait.

Table 5. 3: Observed and model calculated volume, freshwater (referenced to 34.8), and heat (referenced to 0°C) flux through Hudson and Davis Strait from 2004-2011, the same period as the observation moorings across Davis Strait. Positive values indicate equatorward flux. Citations list: (1) Drinkwater 1988, (2) Straneo and Saucier (2008a), (3) Curry et al. (2014), (4) Dickson et al. (2007), (5) Curry et al. (2011).

		Observations	DFS	ERA	CGRF	ERA5	JRA
Volume [Sv]	Hudson	0.1[1,2]	0.09	0.09	0.08	0.09	0.09
	Davis	1.6 +/- 0.5[3]	1.76	1.74	1.30	1.86	2.02
Freshwater [mSv]	Hudson	40[2,4]	28	35	31	32	34
	Davis	100[3]	108	116	78	124	116
Heat [TW]	Hudson		0.1	0.1	0.1	0.1	0.1
	Davis	-20[5]	-18	-22	-25	-21	-23

The net freshwater flux across Hudson Strait, using a salinity reference of 34.8, is 35 (ERA), 34 (JRA), 32 (ERA5), 31 (CGRF), and 28 mSv (DFS). As our simulations use the same runoff forcing, these freshwater transport differences arise from a combination of precipitation minus evaporation and circulation changes. Determining the relative strength of each factor was outside the scope of this manuscript. Ridenour et al. (2019) explored freshwater within the Hudson Bay Complex via numerical simulations that had varying runoff forcing. Both our study and Ridenour et al. (2019) had lower freshwater transport through Hudson Strait than observed (40 mSv: Dickson et al. 2007; Straneo and Saucier 2008a). Freshwater flux through Davis Strait, observed to have a southwards transport of about 100 mSv (Curry et al., 2014), is in agreement with our results which had between 78 (CGRF) and 124 mSv (ERA5). While the heat flux leaving Hudson Strait has been investigated (Straneo and Saucier, 2008a; Straneo and Saucier, 2008b), net heat flux estimates are lacking. However, our numerical simulations suggest the net heat flux is very small (0.1 TW) when compared against the neighboring Davis

Strait which compares well with observations (20 TW: Curry et al., 2011) as our simulations held between 18 TW (DFS) and 25 TW (CGRF) of poleward heat transport.

With reasonable fluxes through both Davis and Hudson Strait, the northern gateways into the Labrador Sea are adequately simulated. However, eddies known as Irminger Rings (Chanut et al., 2008) spawn along the west coast of Greenland and travel into the interior of the Labrador Sea, bringing relatively buoyant water. A comparison of the eddy kinetic energy (EKE: $0.5(\overline{U_g'^2} + \overline{V_g'^2})$), where U_g' and V_g' are the geostrophic velocities computed from the sea surface height anomaly, is carried out between our five simulations and AVISO observations (Fig. 5.4). While all simulations show similarities, they do not capture the high EKE southwest of Greenland or within the Northwest Corner near Newfoundland, Canada. Much of this can be attributed to the 1/4° horizontal resolution used by the model; these simulations are not eddy resolving in this region but rather eddy-permitting. EKE across the simulations are very similar except for perhaps CGRF which has higher EKE in the western Labrador Sea. Thus, eddy fluxes would be similar across these simulations unless there are changes within the boundary currents- we explore this later below. While the differences in simulated EKE and eddy fluxes into the interior of the Labrador Sea will be different than observed, the resolution used should suffice for understanding how differences in air-sea heat flux contribute to changes in the volume and density of Labrador Sea Water produced during convection. As modern long-term climate simulations have comparable horizontal resolution and likely also suffer from reduced eddy fluxes in this region, the results we present should be of interest to the climate modelling community.
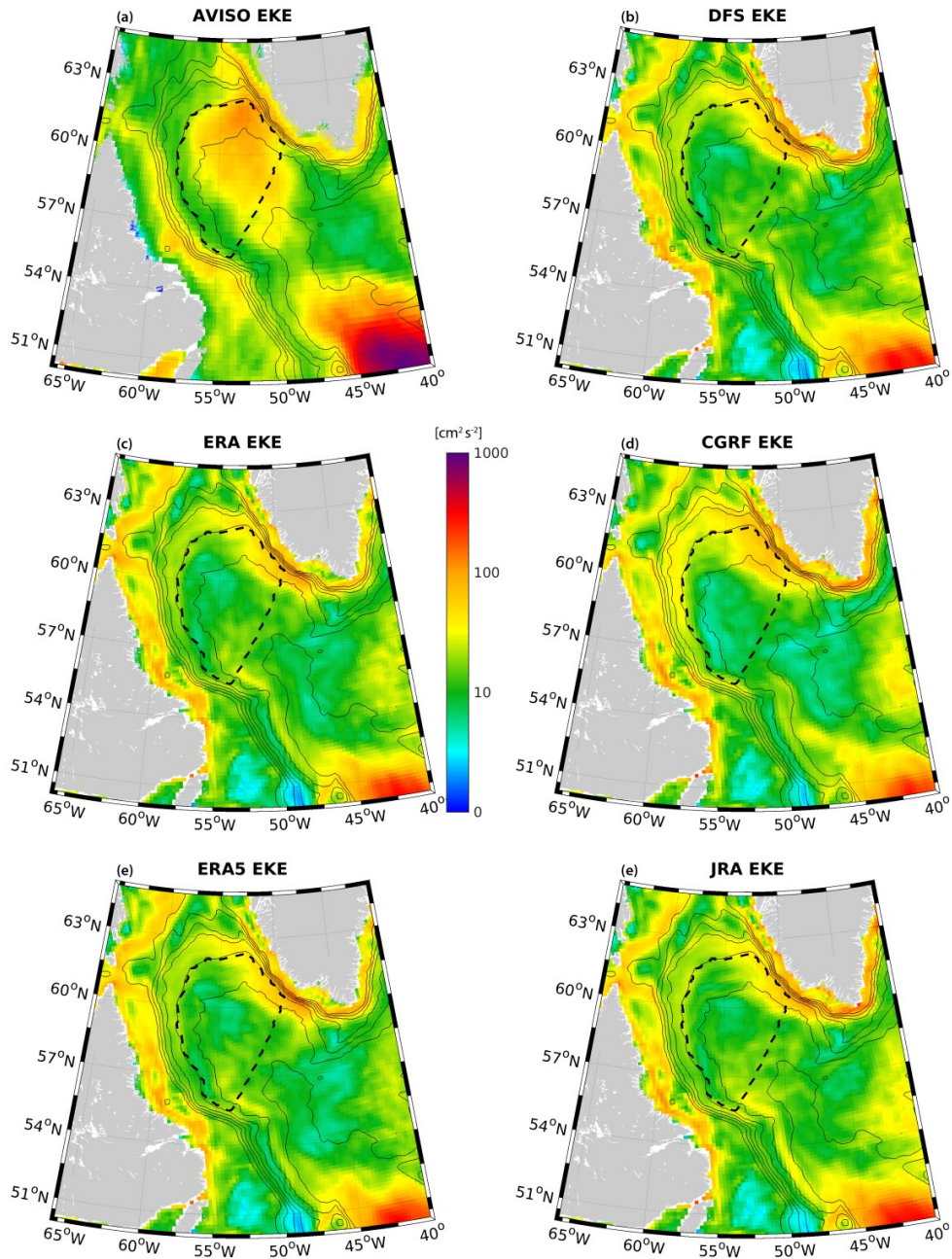
Figure 5. 4: Eddy Kinetic Energy (EKE, in cm² s⁻²) from 2004-2015 as derived from AVISO observations (a) as well as the five model simulations (b-f). The black dashed line indicated the region of interest (Fig. 5.1a).

5.5.3. Heat Fluxes

With acceptable representation through the gateways of the Labrador Sea, we can investigate how the Labrador Sea responds to different atmospheric forcing. First we

consider the monthly air-sea heat fluxes (Fig. 5.5). The top row indicates the sensible heat fluxes determined by turbulent process within our region of interest (Fig. 5.5a), sensible heat flux from rainfall (Fig. 5.5b), and sensible heat flux from snowfall (Fig. 5.5c). One can quickly identify that the sensible heat flux is dominated by turbulent processes with monthly values that range from an input of nearly 10 W m^{-2} to a release of about 90 W m^{-2}. Rainfall and snowfall provide and remove a sensible heat flux of order 1 W m^{-2}.
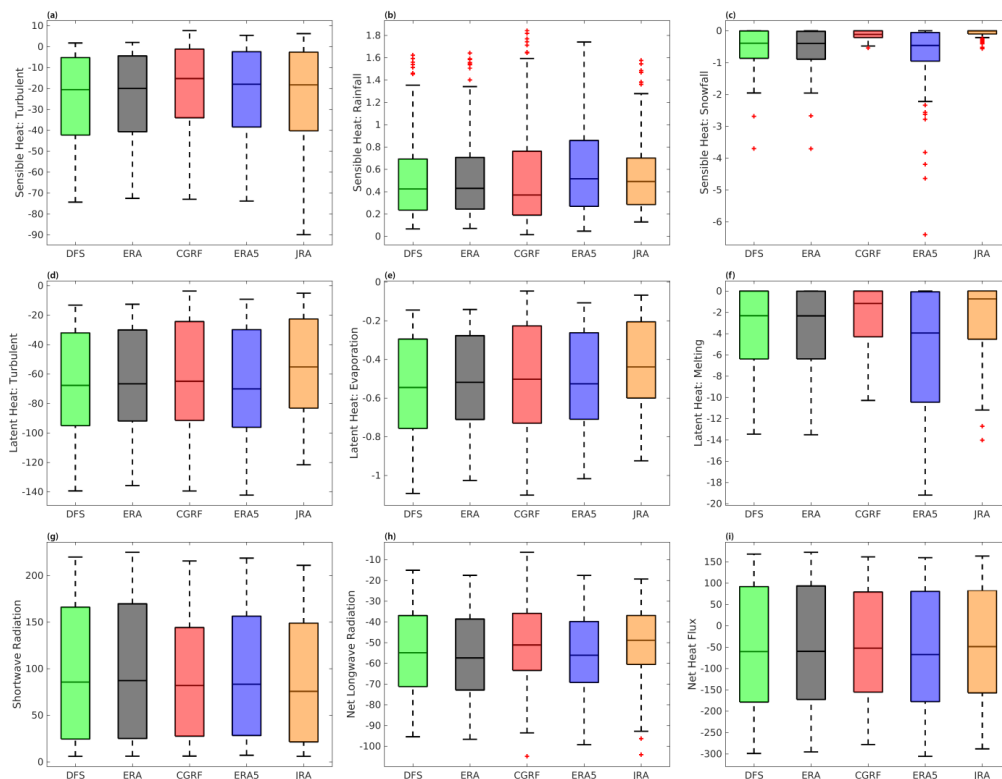
Figure 5. 5: Spatially-averaged (red polygon, Fig 1a) monthly air-sea heat fluxes (W m^{-2}) to the Labrador Sea from 2002-2015. Sensible heat from (a) turbulent motion, (b) rain, and (c) snow is shown in the top row. Latent heat from (d) turbulent motion, (e) evaporation, and (f) melt of snow is shown in the middle row. Radiative heating is shown for the net shortwave radiation (g) and net longwave radiation (h). All fluxes combine to produce the net air-sea heat flux (i). Whiskers lengths are, at most, 150% of the inter-quartile range while red crosses indicate monthly outliers.

The middle row of Figure 5.5 illustrates the latent heat flux via turbulent processes (Fig. 5.5d), evaporation (Fig. 5.5e), and melting of snowfall (Fig. 5.5f).

145

Evaporation occurs where there exists any difference in specific humidity between the air just above the ocean, calculated from the ocean's surface temperature with a relative humidity of 100%, and the air as supplied by the forcing products at 10m above sea level. Turbulent heat flux is greatly influenced by the speed difference between the ocean and atmosphere (eq. 5.2) but still requires a difference in specific humidity. The heat fluxes via latent processes remove more heat than sensible processes (Table 5.4) in this region. Turbulent latent heat fluxes, when averaged across each year (-5 to -140 W m^{-2}), remove much more heat than is associated with the evaporation of water (-0.1 to -1.1 W m^{-2}) and melting of snowfall (0 to -19 W m^{-2}).

The bottom row of Figure 5.5 illustrates the net radiative fluxes (shortwave, Fig. 5.5g; longwave, Fig. 5.5h) as well as the net air-sea heat flux (Fig. 5.5i). The shortwave radiative heat flux is slightly reduced compared to the input (Fig. 5.3a) due the albedo at the ocean's surface, a constant value set at 0.066 within NEMO. When all air-sea heat fluxes are accounted for (Fig. 5.5i), we see small differences between datasets. However, examination of the long-term air-sea fluxes (Table 5.4) shows that the CGRF simulation releases the least heat (46.6 W m^{-2}) compared to the others, with JRA close behind (47.9 W m^{-2}). ERA, DFS and ERA5 show heat losses of 51.0, 53.4, and 58.5, W m^{-2}, respectively. Both Table 5.4 and Figure 5.5 identify that the primary heat fluxes are via radiation and turbulent processes; the non-turbulent sensible and latent heat fluxes combine to remove a small amount of heat, between 3.4 and 7.7 W m^{-2}. The turbulent heat fluxes (eqns. 5.1 & 5.2) arise from the difference between the temperature, humidity, and speed of the ocean and the overlying atmosphere (S1).

The change in oceanic heat content is shown in Figure 5.6a. Winter periods are shown from the yearly minimums, driven by the air-sea heat losses described above,

while summer periods experience a heat gain. Summer maximums do not deviate much from one another (up to 100 W m^{-2}) although there is considerable spread across the winter minimums (up to about 350 W m^{-2}). This spread can be explained by the changes in air-sea heat loss as 2010 had very weak loss while 2008, 2012, and 2015 had much greater loss (our supplemental figure S5.2i; Yashayaev and Loder, 2017). As the long term average in the oceanic heat content change is positive, all simulations have a gradual warming of the Labrador Sea. With long-term cooling of the ocean via air-sea heat fluxes (Table 5.4), lateral advection, calculated from the change in oceanic heat content and air-sea heat flux, supplies this heat (Fig. 5.6b). We note that the variability in heat content is strongly linked to the air-sea heat fluxes (S5.2i) with correlation coefficients between 0.95 and 0.97. Lateral advection correlation coefficients are lower, between 0.78 (ERA) and 0.87 (JRA). The DFS simulation encountered the largest heat flux via lateral advection (83.9 W m^{-2}) while also having the second highest surface heat loss (-53.4 W m^{-2}). ERA, CGRF, JRA, and ERA5 supply less heat via lateral advection: 74.3, 73.1 70.0, and 69.1 W m^{-2}, respectively.

The likely candidates for this heating are the boundary currents around the Labrador Sea, specifically the warm Irminger Water layer within the West Greenland Current. As varying the atmospheric conditions do not only impact the Labrador Sea, we investigate this current system upstream to understand the differences in the above lateral heat fluxes. Figure 5.7a shows the westward heat transport within the Irminger Water layer (T>3.5°C, S>34.8, ρ_θ<1027.68 kg m^{-3}) extending south from Cape Farewell to the 2500m isobath (teal line, Fig 5.1a). While all simulations show similar interannual variability, the magnitudes are quite different; CGRF often transports the most heat within this water mass while the DFS and JRA simulations transports the
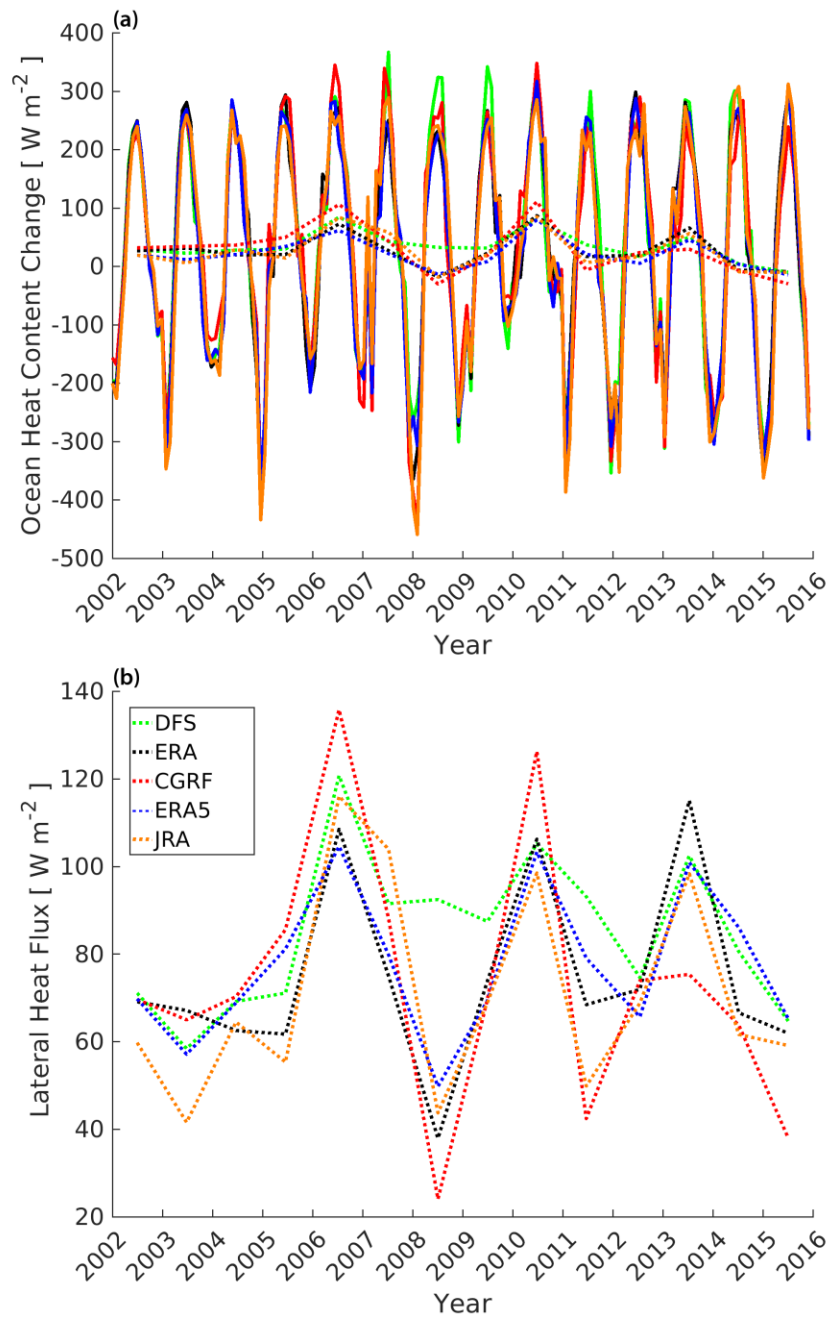
Figure 5. 6: Monthly averaged (a) change in oceanic heat content and (b) lateral heat flux for each of the five simulations. Dotted lines indicate the yearly mean. Monthly values (solid line) were omitted from (b) for clarity. Values were spatially averaged over the red polygon in Fig 5.1a.

Table 5. 4: Average heat flux (W m^{-2}) from 2002-2015 for the five simulations as calculated within the red polygon in Fig. 5.1a. Positive values indicate a supply of heat to the Labrador Sea. Numbers within the square brackets indicate one standard deviation.

Simulation	Net Downward		Sensible Heat Flux			Latent Heat Flux			Total
	Shortwave	Longwave	Snowfall	Rainfall	Turbulent	Melt	Evaporation	Turbulent	
DFS	97.3 [80.4]	-54.5 [29.4]	-0.5 [2.2]	0.5 [0.9]	-26.1 [31.5]	-3.6 [5.8]	-0.5[0.4]	-66.0 [52.8]	-53.4
ERA	99.1 [81.8]	-56.4 [29.0]	-0.5 [2.3]	0.5 [0.9]	-25.2 [31.0]	-3.6 [5.8]	-0.5 [0.4]	-64.4 [51.6]	-51.0
CGRF	88.9 [137.6]	-50.1 [32.8]	-0.1 [0.5]	0.5 [1.3]	-19.7 [28.3]	-2.3 [6.3]	-0.5 [0.4]	-63.3 [55.5]	-46.6
ERA5	95.4 [148.1]	-56.2 [29.2]	-0.7 [4.0]	0.6 [1.2]	-23.6 [32.2]	-5.8 [10.5]	-0.5 [0.4]	-67.7 [56.1]	-58.5
JRA	87.3 [132.3]	-50.9 [30.5]	-0.1 [0.2]	0.5 [1.0]	-24.9 [35.6]	-2.7 [5.2]	-0.4 [0.4]	-56.7 [51.2]	-47.9

least. However, as expressed above, the DFS simulation has the largest lateral heat flux while having low heat transport at the southern tip of Greenland for this water mass.

Differences in the amount of heat and freshwater transport (discussed below) across this section are likely due to a combination of many factors, including but not limited to: circulation changes in the Arctic and North Atlantic gyre, wind-stress curl and related Ekman pumping, Atmospheric oscillation modes, changes in sea ice, and differential heating/cooling. It is outside the scope of this manuscript to document how various atmospheric forcing datasets influence the oceanic conditions outside the Labrador Sea, although these factors produce slightly different conditions within the WGC. Heat transport along this coast does not explain the differences in lateral heat advection between simulations as heat must be advected from this current system into the interior of the Labrador Sea.

We suspect that the combination of heat transport within the water mass as well as eddy processes along the western coast of Greenland can address the differences in lateral heat flux. Figure 5.4 shows the 2004-2015 spatially averaged EKE as computed
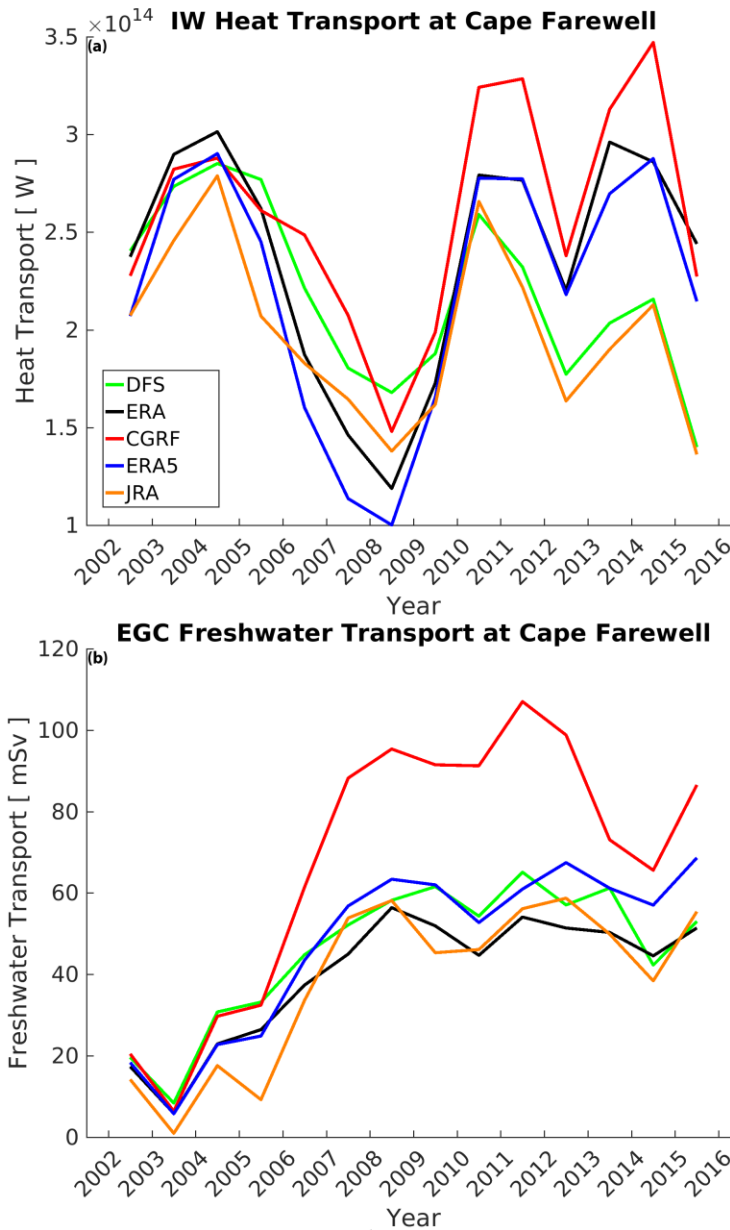
Figure 5. 7: Water mass properties between Cape Farewell and the 2500m isobath to the south (Teal line; Fig. 5.1a). The westward heat transport for Irminger Water (IW: $T>3.5°C$, $S>34.8$, $\rho_\theta<1027.68$ kg m⁻³) is shown in (a), while the westward freshwater transport (referenced to 34.8) associated with the East Greenland Current water mass (EGC: $S<34.8$, $\rho_\theta<1027.68$ kg m⁻³) is shown in (b).

from AVISO observations and our five simulations. All simulations experience

heightened EKE along the western coast of Greenland, suggesting the simulations do

produce some eddy fluxes in this region. Furthermore, the differences in the EKE field help explain the differences in lateral heat advection as described above. No single simulation appears to best represent the EKE along the western coast of Greenland. DFS, having a lower heat transport (Fig. 5.7a), has greater EKE than the other simulations, suggesting that DFS may have higher heat transport via eddy processes from the WGC to the Labrador Sea. The CGRF simulation, having the highest heat transport within the Irminger Water mass south of Cape Farewell, has a larger spatial extent but lower EKE values which also occurs slightly further northwest compared to the other simulations, as well as reduced EKE in the interior Labrador Sea. This suggests that the larger amount of heat simulated within the Irminger Water layer for the CGRF simulation could be less likely to enter the interior of the Labrador Sea, leading to reduced lateral heat flux as detailed above. This is supported by greater heat transported north through Davis Strait (Table 5.3).

However, heat alone does not set the stratification. Freshwater has a larger impact on density at these latitudes; any freshwater within the East and West Greenland Current can also enter the interior of the Labrador Sea, increasing stratification. Figure 5.7b illustrates the freshwater transport ($S<34.8$, $\rho_\theta<1027.68$ kg m^{-3}) that passes Cape Farewell and shows that the CGRF simulation has much more freshwater within this water mass than the remaining simulations. This freshwater resides above the Irminger Water mentioned above, and eddies that spawn from the WGC hold substantial surface freshwater which is carried towards the interior basin. CGRF, with sometimes nearly double the freshwater transport but less EKE compared to the remaining simulations, likely still transports more freshwater into the interior Labrador Sea, leading to a more stratified basin. While the lateral advection of heat and freshwater increases the

stratification of the Labrador Sea throughout most of the year, the removal of heat from the ocean occurs during the extended convective wintertime.

5.5.4. Labrador Sea Water

With variations in the air-sea heat flux, as well as lateral transport of heat and freshwater, each simulation produced a Labrador Sea with slightly different properties. A spatial plot of the average March mixed layer depth (MLD) is shown in Figure 5.8. With relatively few Argo floats in the Labrador Sea at any given time, the winter (January-March) maximum MLD at the corresponding ANHA4 grid-point are shown instead (Fig. 5.8f). Low resolution simulations often contain a mixed layer which is both too spacious as well as deep; a result of not resolving buoyant eddies produced within the WGC that enter the northern Labrador Sea (see model evaluation section). This promotes weaker stratification within the northern Labrador Sea, forcing deep mixing within this region that is not observed. This is clearly occurring for our five simulations (Fig. 5.8a-e) as the Argo observations are confined to a much smaller region with shallower depths (maximum 1800m). The CGRF simulation, with the weakest surface heat loss, has the thinnest and least widespread mixed layer depth (1600m; Fig. 5.8c). ERA5 has the strongest surface heat loss and the deepest mixed layer (2000m; Fig. 5.8d). DFS (Fig. 5.8a) has a larger spatial extent of its MLD, albeit slightly shallower than JRA (Fig. 5.8e) and ERA5.

The combination of air-sea heat flux and freshwater changes due to precipitation and evaporation sets the total surface buoyancy flux (Figure 5.9a). While solar radiation (dotted line) supplies buoyancy, the non-solar thermal fluxes including longwave radiation and other heat fluxes (dashed) removes far more. Processes that modify the
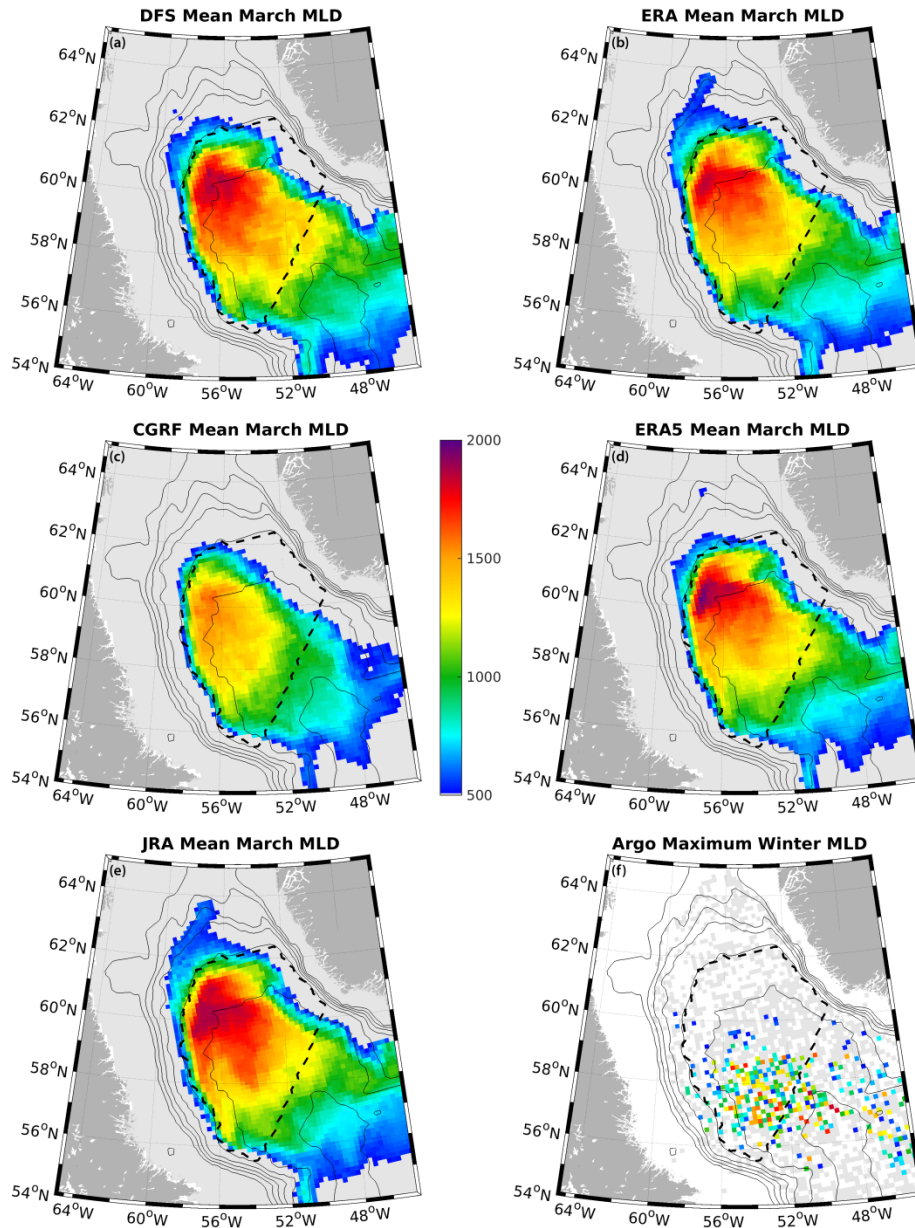
Figure 5. 8: Shaded colours indicate the 2002-2015 mean March mixed layer depth (MLD), in meters, for each simulation (a-e). Observed ARGO data showing the maximum grid-point winter (January-March) MLD from 2002-2015 are shown in (f) where whitespace indicates no data. Light grey indicates a MLD less than 500m. Bathymetric contours of 500m are indicated by the solid black lines while the dashed black line indicates the red polygon in Figure 5.1a.

sea surface salinity via precipitation or evaporation (dashed-dot) have similar values

across the five simulations for the entire evaluation period. As the non-solar thermal

fluxes drive most of the variability in the net buoyancy flux, the input and removal of

153

atmospheric freshwater between our simulations is relatively minor. The DFS and JRA simulations often have the greatest net buoyancy loss but it is clearer where this arises from; JRA has reduced solar input while DFS has stronger heat loss via the non-solar thermal term. A spatial comparison of the minimum grid-point surface buoyancy gain is shown in S3, highlighting regional differences.

Finally exploring how the various surface buoyancy and lateral fluxes translate into changes at depth within the Labrador Sea, Figure 5.9b illustrates the convective energy which must be removed such that the water column is neutrally stratified to 2000m. Simulations all present similar interannual variability with the weakest stratification simulated during the winters of 2008, 2012, 2014, and 2015. The JRA and DFS simulations, with the greatest buoyancy losses, are often the most weakly stratified simulations. Conversely, the CGRF simulation had the least buoyancy loss and tended to have the strongest stratification throughout the integration period. This is further exacerbated by the additional freshwater carried by the CGRF simulation within the EGC/WGC (Fig. 5.7b). We note that the ERA and ERA5 simulations start to deviate from the other simulations around 2010 when the WGC starts transporting more heat for these simulations (Fig. 5.7a). This heat, and CGRF's additional freshwater, will partially enter the interior Labrador Sea, increasing stratification.

The mixed layer depth (Fig. 5.9c) appears inverse to the convective energy, though the mixed layer gives understanding on how deep convection penetrates down to rather than how stratified the Labrador Sea is. The simulations over-estimated the
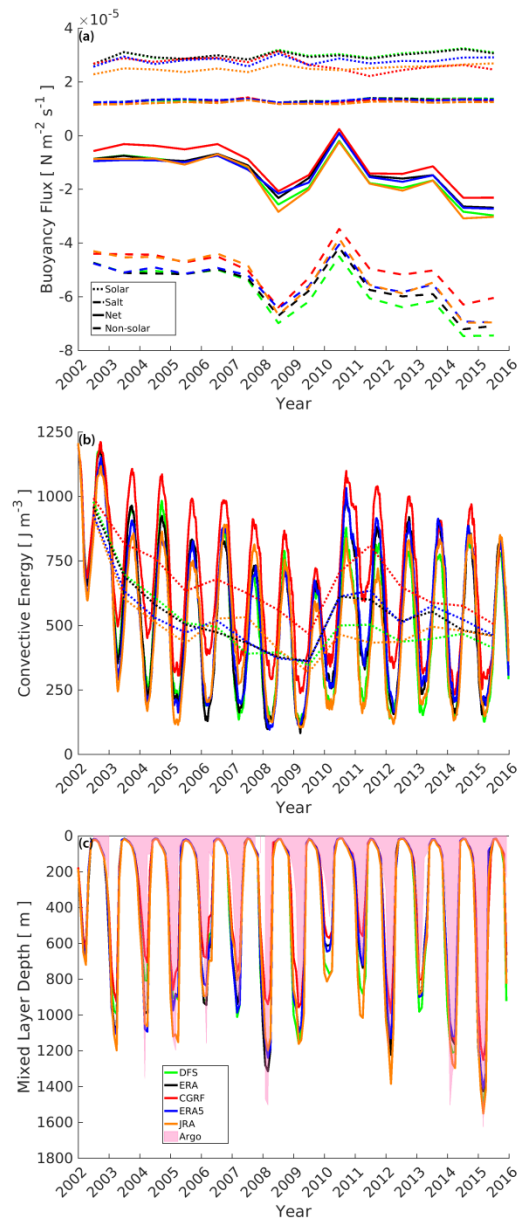
Figure 5. 9: Averaged (a) yearly solar, non-solar thermal, and precipitation minus evaporation surface buoyancy fluxes, (b) monthly convective energy values to a reference depth of 2000 meters, and (c) monthly mixed layer depths with ARGO observations for the five simulations. Dotted lines in (b) indicate the yearly mean. Values were spatially averaged over the red polygon in Fig 5.1a.

mixed layer depth when compared against Argo observations while matching the

observed interannual variability. This interannual variability is closely linked to the

NAO index (see Yashayaev and Loder, 2016; their Fig. 5). Years with a deep mixed layer

(2008, 2012, 2014-2015) have strongly positive NAO, while the opposite occurs for years with negative NAO (i.e. 2010). Both the DFS and JRA simulations tended to have the deepest mixed layer. Mixed layer depths provide some information on the depth of convection, though they do not convey any information on the volume or density class of Labrador Sea Water.

The two components of Labrador Sea Water, ULSW and CLSW, are produced during periods of deep convection (Fig. 5.10). Our calculated density range of LSW (Fig. 5.10a) shows the CGRF simulation has the lowest density while DFS and JRA have the densest, in line with the amount of buoyancy loss detailed above. This subfigure also shows that each simulation is slowly becoming more dense in our region of interest, highlighting numerical drift. LSW layer thicknesses deviate between simulations within one year of integration. Not only does the CGRF simulation have less dense LSW, it also forms thinner ULSW (Fig. 5.10b) and CLSW (Fig. 5.10c) layers, producing a thinner overall LSW layer (Fig. 5.10d). The DFS (JRA) simulation often held the thickest LSW layer, likely a product of enhanced (reduced) buoyancy loss (gain). While each simulation shows the ULSW/CLSW layer thickness changes up to 600 m between years, the total LSW layer thickness (Fig. 5.10d) only changes by up to 200 m if we ignore the first couple years that could be considered an adjustment phase from the initial conditions. Much of this layer thickness change is the conversion of ULSW into CLSW (or vice-versa), as Kieke et al. (2006) showed with a correlation of -0.85. However, our five simulations did not correlate that strongly, with the DFS simulation at -0.53, CGRF at -0.47, JRA at -0.47, ERA at -0.46, and ERA5 at -0.43. We suspect that our method of classifying LSW with a moving density as determined by subduction rate played a strong role here. Other methods to determine LSW density range were carried out, though we
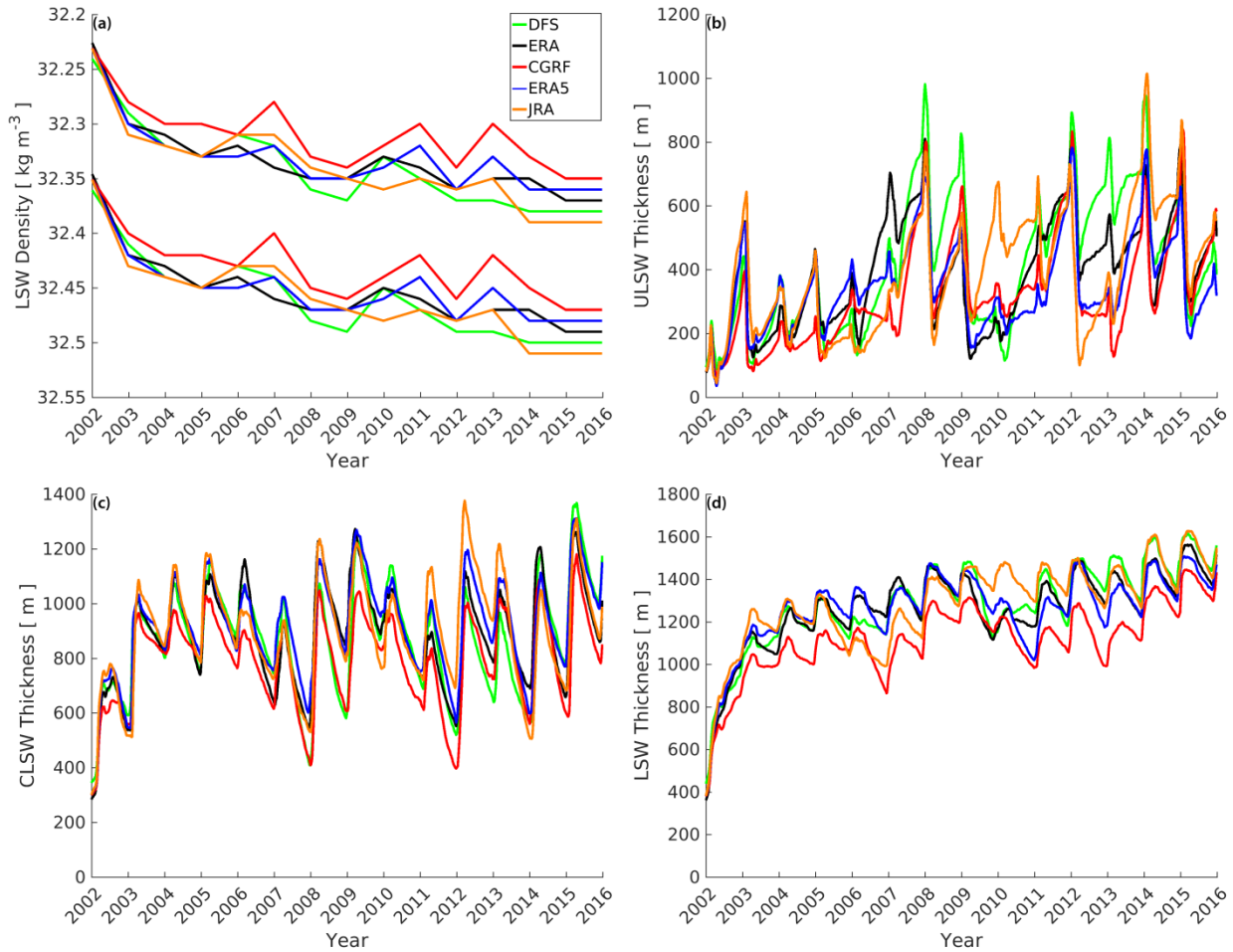
Figure 5. 10: Upper and lower yearly density (referenced to 1000 dbar) values of LSW are shown in (a). Monthly average layer thickness of Upper Labrador Sea Water (ULSW, (b)), Classical Labrador Sea Water (CLSW, (c)), and combined (d) are shown for each of the five simulations. Values were spatially averaged over the red polygon in Fig 5.1a.

settled on the above option as it factored in density drift and maintained an accurate representation of the layer thickness.

LSW thickness doesn't quite give enough information to determine the volume of LSW produced, which we calculate by a kinematic subduction approach (eqn. 4). The lateral advection term, opaque in Figure 5.11, shows primarily a positive contribution to the net subduction across the time series. The vertical motion of the mixed layer, translucent in this figure, always shows positive subduction. The vertical advection term

was between 1 and 2 orders of magnitude lower and is not displayed nor discussed further. While some simulations held greater subduction rates (e.g. ERA during 2014), they did not always have the densest value. This implies that strong subduction rate doesn't indicate denser LSW. No one simulation had the greatest subduction rate across the years, though the simulations with stronger buoyancy loss (DFS and JRA) more often had the densest LSW. Conversely, the simulation with the weakest buoyancy loss (CGRF) also had the least dense LSW. While numerical drift slowly caused LSW to increase in density, the CGRF simulation was closest to the observed value, often within the density range of observed LSW (1027.68-1027.80 kg m^{-3}) as discussed above.
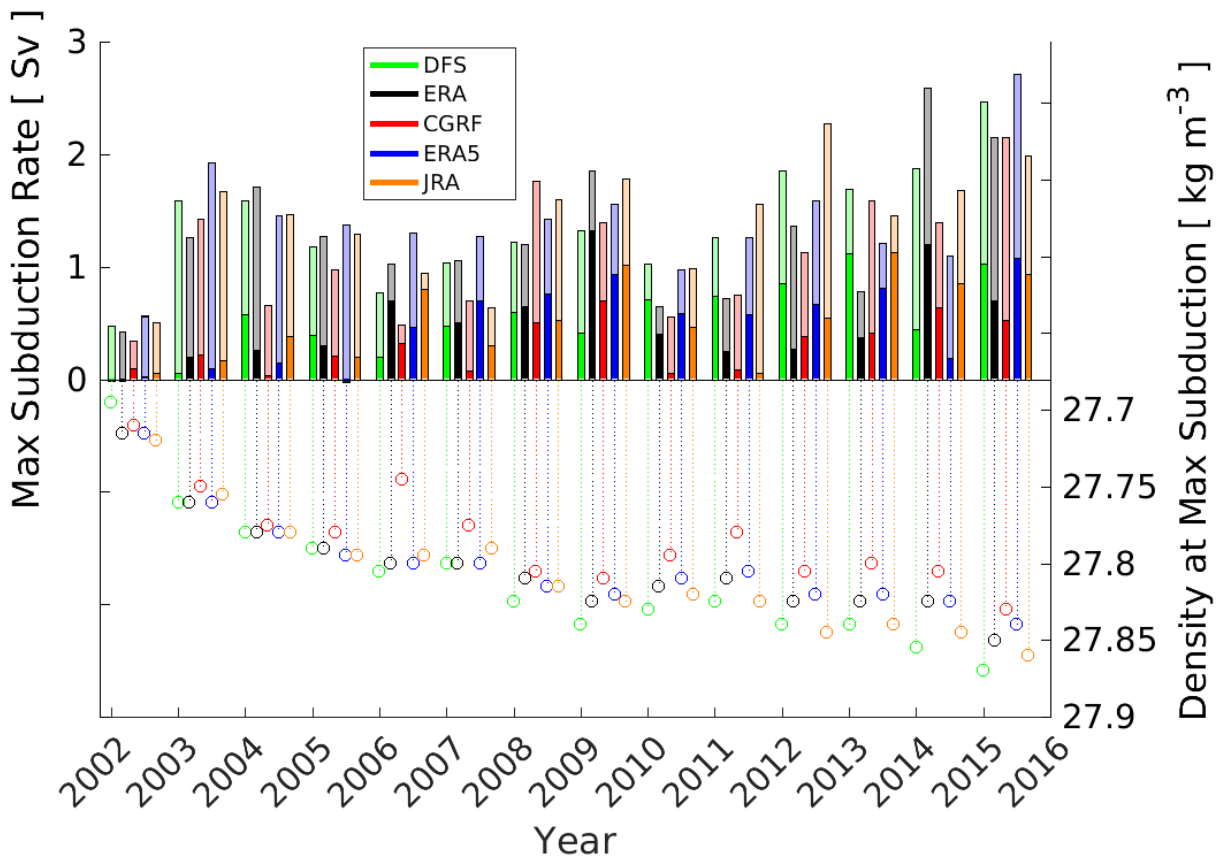
Figure 5. 11: Yearly maximum subduction rate (bars) along with the density for this maximum subduction rate (stems) for each of the five simulations within the red polygon in Fig. 5.1a. Subduction is categorized into 2 terms: lateral advection (opaque bars) and movement of the mixed layer (translucent bars). Vertical advection was negligible and is not shown. The horizontal axis illustrates discrete years and not monthly values of subduction.

5.6. Discussion and conclusion

This sensitivity study involved forcing an ocean model with five different atmospheric forcing datasets to evaluate the ocean's response over a portion the Labrador Sea primarily in regards to the production of LSW. The five datasets in question, ERA5, DFS5.2, ERA-Interim, JRA55-do, and CGRF, showed similar interannual variability across their forcing fields, though the small differences in each dataset resulted in varying levels of yearly-averaged air-sea heat loss, at 58.5, 53.4, 51.0,

47.9, and 46.6 W m^{-2}, respectively. ERA5 had the strongest heat loss but not the strongest surface buoyancy loss. Precipitation and evaporation, while significantly different among the forcing datasets, provided minimal difference in salinity-driven surface buoyancy flux. The DFS and JRA simulations extracted the most buoyancy from the Labrador Sea: DFS from stronger turbulent heat fluxes while JRA maintained strong buoyancy loss via a reduction in solar radiation. Our simulations were eddy-permitting and only small EKE differences are noted between the five simulations. We attribute these differences to wind speed frequency and strength within the atmospheric datasets, as well as baroclinic changes induced within the boundary currents. Eddies are very important in the Labrador Sea but numerical simulations require higher resolution to adequately resolve them (Rieck et al., 2019). We suspect that our conclusions will hold true for simulations with higher resolution, although future work is needed to confirm this.

We find that simulations with slightly stronger surface buoyancy loss experience greater mixed layer depths (up to 300 m). With greater mixed layer depths, the LSW layer thickness is also greater (up to 300 m). The maximum density of LSW which subducted the mixed layer is correlated to the surface buoyancy loss, leading to simulations with stronger forcing to produce denser LSW. However, the subduction volume associated with this density doesn't appear to be strongly influenced by small changes in the surface buoyancy flux. This apparent contrast to the above as the LSW layer thickness indicates there must be a larger volume of LSW produced with stronger surface buoyancy loss but not at the greatest density. We attribute this to a larger spatial extent of deep convection (Fig. 5.8) which would increase the overall LSW layer thickness.

Our results fit with those from Chaudhuri et al. (2016) who performed a similar sensitivity study. They forced an ocean model with four reanalysis products and found the largest changes occurred within the top 1000m, though areas with deep convection saw significant differences at great depths. They attributed this to either differences in wind speed or heat flux, both of which we show exist between forcing products over the Labrador Sea. Garcia-Quintana et al. (2019) took this further by dramatically reducing precipitation. Reducing precipitation to 1/3 of the original value resulted in a substantial densification of LSW, though the reduction in sensible heat flux was only about 1-2 W m^{-2}. While our above results have much larger heat loss changes, Garcia-Quintana et al. (2019) had a larger change in subduction density than what we found, indicating that the freshwater addition via precipitation impacts the stratification far stronger than the sensible and latent heat flux associated with precipitation. However, our CGRF and JRA simulations had much less precipitation than the other forcing sets (Fig. 5.3), but the surface buoyancy flux differences between these simulations and the others was minor compared to the other sources of buoyancy flux (Fig. 9a).Considering how strong the turbulent air-sea heat fluxes are, it is not surprising that both Garcia-Quintana et al. (2019) and Holdsworth and Myers (2015) had a reduction in the mixed layer depth, subduction rate and density of LSW when they filtered high frequency events from their atmospheric forcing. Bramson (1997) ran a series of sensitivity experiments varying heat flux components and identified changes in the air-sea fluxes clearly result in modifications to the mixed layer depth. From our five simulations, we also found that the mixed layer depth, subduction rate and density are all modified from variations in surface forcing.

The atmospheric datasets used in our study are relatively common products to force hindcast ocean simulations. The above sensitivity studies by Bramson (1997), Holdsworth and Myers (2015), and Garcia-Quintana et al. (2019) often used realistic forcing which was perturbed to such a state that was no longer realistic. While they all found LSW production was influenced by atmospheric forcing, we show that relatively small changes in forcing can impact LSW production rate and density. Such differences in forcing and resulting density of LSW identify that a traditional static density criteria for LSW classification may not be suitable. Simulations which use slightly stronger/weaker forcing may produce deepwater within the Labrador Sea which is too dense/light to be considered LSW by such a traditional method. The method used here, a moving density scale, showed success at the interannual variability of LSW formation rate for five simulations with different atmospheric forcing. This is further exacerbated by numerical drift.

Our simulations suffer from numerical drift, a seemingly unavoidable consequence of modelling within the Labrador Sea (Rattan et al, 2010; Marzocchi et al., 2015). Numerical drift does not appear sensitive to the model's configuration as Rattan et al. (2010) showed with similar drift between regional and global configurations. Our simulations' drift prevented us from using standard LSW density ranges (potential density 1027.68 to 1027.80) as later years were producing deep water denser than LSW. Using a technique to classify LSW using moving density definition allowed a far more useful analysis on these simulations. Our LSW density and thickness steadily increase over time while observations suggest that LSW density has been slowly decreasing (Kieke and Yashayaev, 2015). However, our simulations match well against Argo observations of the mixed layer, highlighting that simulations with numerical drift can

still have accurate aspects. Lower-resolution simulations that suffer from numerical drift have long been a useful tool to understand climate scenarios even with their shortcomings.

Our results show the relative impact of each of the air-sea heat flux terms within the Labrador Sea. The radiative and turbulent terms are the dominating source of air-sea heat flux, though the remaining terms should not be ignored. While our results suggest that an additional 1 to 12 W m^{-2} of surface heat loss produce a deeper mixed layer and denser LSW, our simulations had significant differences in the lateral freshwater and heat fluxes that govern the restratification rate. With lateral heat fluxes that differed between simulations of up to 15 W m^{-2}, the choice of atmospheric forcing strongly influenced the lateral restratification rate in the Labrador Sea as well as the surface buoyancy forcing. We speculate the additional lateral buoyancy flux was likely due to upstream changes within the Irminger Basin and Arctic, judging from the heat and freshwater transport in Fig. 5.7. Putting these heat flux values into perspective, the Representative Concentration Pathways simulations project the anthropogenic influence on the Earth's Climate range from 2.6 to 8.5 W m^{-2} (Van Vuuren et al. 2007; Riahi et al. 2007) while our planet is currently experiencing an additional 1 to 3 W m^{-2} of heating since before the industrial revolution (IPCC, 2014). However, these heat flux values are averaged over the entire planet, not just the Labrador Sea, and while each region will experience some variability in additional heating, we show that a large impact occurs when exposed to a similar magnitude change in heat flux.

As these atmospheric datasets are used to drive ocean simulations and we show that the small differences between realistic atmospheric datasets produce significant changes within the Labrador Sea, ocean modelers should take caution with the forcing

product they use. While we only investigated how the variability influenced production and density of LSW, many other regions are likely to be influenced by such variability between datasets. Long ocean simulations may be particularly sensitive to such differences, as a few additional watts supplied over the course of decades may produce very different, and perhaps unrealistic, results.

Bibliography

Bamber, J., van den Broeke, M., Ettema, J., Lenaerts, J., & Rignot, E. 2012. Recent large increases in freshwater fluxes from Greenland into the North Atlantic. *Geophysical Research Letters,* **39**(19), 4pp.

Benetti, M., Reverdin, G., Yashayaev, I., Holliday, N.P., Tynan, E., Torres-Valdes, S., Lherminier, P., Tréguer, P., &Sarthou, G. (2017). Composition of freshwater in the spring of 2014 on the southern Labrador shelf and slope. *Journal of Geophysical Research: Ocean*, **122**(2), 1102-1121.

Böning, C.W., Behrens, E., Biastoch, A., Getzlaff, K., & Bamber, J.L. (2016). Emerging impact of Greenland meltwater on deepwater formation in the North Atlantic Ocean. *Nature Geoscience*, **97**(7), 523-527.

Bramson, L.S. (1997): Air-sea interactions and deep convection in the Labrador Sea. M.S. thesis, Dept. of Oceanography. *Naval Postgraduate School*, 115 pp.

Brossier, C.L., Béranger, K., & Drobinski, P. (2012). Sensitivity of the northwestern Mediterranean Sea coastal and thermohaline circulations simulated by the 1/12°-resolution ocean model NEMO-MED12 to the spatial and temporal resolution of atmospheric forcing. *Ocean Modelling*, **43-44**, 94-107.

Chanut, J., Barnier, B., Large, W., Debreu, L., Penduff, T., Molines, J.M., & Mathiot, P. (2008). Mesoscale eddies in the Labrador Sea and their contribution to convection and restratification. *J. Phys. Oceanogr.*, **28**(8), 1617-1643.

Chaudhuri, A.H., Ponte, R.M., & Forget, G. (2016). Impact of uncertainties in atmospheric boundary conditions on ocean model solutions. *Ocean Modelling*, **100**, 96-108.

Condron, A., and Renfrew, I.A. (2013). The impact of polar mesoscale storms on northeast Atlantic Ocean circulation. *Nature Geoscience,* **6**(1), 34-37.

Courtois, P., Hu, X., Pennelly, C., Spence, P., & Myers, P.G. (2017) Mixed layer depth calculation in deep convection regions in ocean numerical models. *Ocean Modelling,* **120**, 60-78.

Cuny, J., Rhines, P.B., Niiler, P.P., & Bacon, S. (2002). Labrador Sea boundary currents and the fate of the Irminger Sea Water. *J. Phys. Oceanogr.,* **32**(2), 627-647.

Curry, B., Lee, C.M., & Petrie, B. (2011). Volume, freshwater, and heat fluxes through Davis Strait, 2004-05. *J. Phys. Oceanogr.,* **41**(3), 429-436.

Curry, B., Lee, C.M., Petrie, B., Moritz, R.E., & Kwok, R. (2014). Multiyear volume, liquid freshwater, and sea ice transports through Davis Strait, 2004-10. *J. Phys. Oceanogr.,* **44**(4), 1244-1266.

Curry, R.G., McCartney, M.S., & Joyce, T.M. (1998). Oceanic transport of subpolar climate signals to mid-depth subtropical waters. *Nature*, **391**(6667), 575-577.

Dai, A., Qian, T., Trenberth, K.E., & Milliman, J.D. (2009). Changes in continental freshwater discharge from 1948 to 2004. *J. Climate*, **22**(10), 2773-2792.

Dee, D.P., Uppala, S.M., Simmons, A.J., Berrisford, P., Poli, P., Kobayashi, S., et al. (2011). The ERA-Interim reanalysis: configuration and performance of the data assimilation system. *Quarterly Journal of the Royal Meteorological Society*, **137**, 553-597.

Dickson, R., Rudels, B., Dye, S., Karcher, M., Meincke, J., & Yashayaev, I. (2007). Current estimates of freshwater flux through Arctic and subarctic seas. *Progress in Oceanography,* **73**(3-4), 210-230.

Drinkwater, K.F. (1988). On the mean and tidal currents in Hudson Strait. *Atmosphere-Ocean*, **26**(2), 252-266.

Dussin, R., Barnier, B., & Brodeau, L. (2016). The making of Drakkar forcing set DFS5, *Grenoble, France: LGGE*.

Duvivier, A.K., Cassano, J.J., Craig, A., Hamman, J., Maslowski, W., Nijssen, B., Osinski, R., & Roberts, A. (2016). Winter atmospheric buoyancy forcing and oceanic response during String Wind Events around Southeastern Greenland in the Regional Arctic System Model (RASM) for 1990-2010. *J. Climate*, **29**(3), 975-994.

Ferry, N., Parent, L., Garric, G., Barnier, B., & Jourdain, N.C. (2010). Mercator global eddy permitting ocean reanalysis GLORYS1V1: Description and results. *Mercator-Ocean Quarterly Newsletter*, **36**, 15-27.

Feucher, C., Garcia-Quintana, Y., Yashayaev, I., Hu, X., Myers, P.G. (2019). Labrador Sea Water formation rate and its impact on the local Meridional Overturning Circulation. *Journal of Geophysical Research: Oceans*, **124**(8)*,* 5654-5670.

Fichefet, T., & Maqueda, M.A.M. (1997). Sensitivity of a global sea ice model to the treatment of ice thermodynamics and dynamics. *Journal of Geophysical Research: Oceans*, **102**(C6), 12609-12646.

Garcia-Quintana, Y., Courtois, P., Hu, X., Pennelly, C., Kieke, D., & Myers, P.G. (2019). Sensitivity of Labrador Sea Water formation to changes in model resolution, atmospheric forcing, and freshwater input. *Journal of Geophysical Research: Oceans*, **124**(3), 2126-2152.

Gelderloos, R., Katsman, C.A., & Drijfhout, S.S. (2011). Assessing the roles of three eddy types in restratifying the Labrador Sea after deep convection. *J. Phys. Oceanogr.*, **41**(11), 2102-2119.

Gelderloos, R., Straneo, F., & Katsman, C.A. (2012). Mechanisms behind the temporary shutdown of deep convection in the Labrador Sea: Lessons from the great salinity anomaly years 1968-71. *J. Climate*, **25**(19), 6743-6755.

Gillard, L., Hu, X., Myers, P.G., & Bamber, J.L. (2016). Meltwater pathways from marine terminating glaciers of the Greenland ice sheet. *Geophysical Research Letters*, **43**(20), 10873-10881.

Hersbach, H., & Dee, D.J.E.N. (2016). ERA5 reanalysis is in production. *ECMWF newsletter*, **147**(7), 5-6.

Holdsworth, A.M., & Myers, P.G. (2015). The influence of high-frequency atmospheric forcing on the circulation and deep convection of the Labrador Sea. *J. Climate*, **28**(12), 4980-4996.

Holte, J., & Talley, L. (2009). A new algorithm for finding mixed layer depths with applications to Argo data and Subantarctic Mode Water formation. *J. Atmos. Oceanic Technol.*, **26**(9), 1920-1939.

Hurrell, J.W. (1995). Decadal trends in the North Atantic Oscillation: regional temperatures and precipitation. *Science*, **269**(5224), 676-679.

Hurrell, J.W., & Deser, C. (2010). North Atlantic climate variability: The role of the North Atlantic Oscillation. *J. Marie Systems*, **78**, 28-41.

IPCC, (2014). Climate Change 2014: Synthesis Report. Contribution of Working groups I, II, and III to the Fifth Assessment Report of the Intergovemental Panel on Climate Change [Core Writing Team, R.K. Pachauri and L.A. Meyer (eds)]. IPCC, Geneva, Switzerland, 151 pp.

de Jong, M.F., Bower, A.S., & Furey, H.H. (2016). Seasonal and interannual variations of Irminger ring formation and boundary-interior heat exchange in FLAME. *J. Phys. Oceanogr.,* **46**(6), 1717-1734.

Jonsson, S., & Valdimarsson, H. (2004). A new path for the Denmark Strait overflow water from the Iceland Sea to Denmark Strait. *Geophysical Research Letters,* **31**(3), 4 pp.

Jung, T., Serrar, S., and Wang, Q. (2014). The oceanic response to mesoscale atmospheric forcing. *Geophysical Research Letters*, **41**, 1255-1260.

Kieke, D., Rhein, M. Stramma, L., Smethie, W.M., LeBel, D.A., & Zenk, W. (2006). Changes in the CFC inventories and formation rates of Upper Labrador Sea Water, 1997-2001. *J. Phys. Oceanogr.,* **36**(1), 64-86.

Lab Sea Group, (1998). The Labrador Sea deep convection experiment. *Bull. Amer. Meteor. Soc.*, **79**(10), 2033-2058.

Large, W.G., & Yeager, S.G. (2008). The global climatology of an interannually varying air-sea flux data set. *Climate Dynamics*, **33**(2-3), 341-364.

Lazier, J., Hendry, R., Clarke, A., Yashayaev, I., & Rhines, P. (2002). Convection and restratification in the Labrador Sea, 1990-2000. *Deep Sea Research Part I: Oceanographic Research Papers*, **49**(10), 1819-1835.

Li, F., Lozier, M.S., Danabasoglu, G., Holliday, N.P., Kwon, Y.-O., Romanou, A., et al. (2019). Local and downstream relationships between Labrador Sea Water volume and

North Atlantic meridional overturning circulation variability. *J. Climate,* **31**(13), 3883-3898.

Lindsay, R., Wensnahan, M., Schweiger, A., & Zhang, J. (2014). Evaluation of seven different atmospheric reanalysis products in the Arctic. *J. Climate*, **27**(3), 2588-2606.

Lozier, M.S., Li. F., Bacon, S., Bahr, F., Bower, A.S., Cunningham, S.A., et al. (2019). A sea change in our view of overturning in the subpolar North Atlantic, *Science*, **363**(6426), 516-521.

Madec, G. (2008). Note du Pôle de modélisation. Institut Pierre-Simon Laplace (IPSL), France, No **27**, ISSN No 1288-1619.

Marshall, J., & Schott, F. (1999). Open-ocean convection: Observations, theory, and models. *Reviews of Geophysics,* **37**(1), 1-64.

Marzocchi, A., Hurshi, J.J.M., Holiday, N.P., Cunningham, S.A., Blaker, A.T., & Coward, A.C. (2015). The North Atlantic subpolar circulation in an eddy-resolving global ocean model. *Journal of Marine Systems*, **142**, 126-143.

McGeehan, I., & Maslowski, W. (2011). Impact of shelf-basin freshwater transport on deep convection in the western Labrador Sea. *J. Phys. Oceanogr.,* **41**(11), 2187-2210.

Moore, G.W.K., Pickart, P.S., & Renfrew, I.A. (2011). Complexities in the climate of the subpolar North Atlantic: a case study from the winter of 2007. *Quarterly Journal of the Royal Metoeorological Society*, **137**(656), 757-767.

Moore, G.W.K., R.S. Pickart, I.A. Renfrew, and Våge, K. (2014). What causes the location of the air-sea heat flux maximum over the Labrador Sea? *Geophysical Research Letters,* **41**, 3628-3635.

Müller, V., Kieke, D., Myers, P.G., Pennelly, C., & Mertens, C. (2017). Temperature flux carried by individual eddies across 47° in the Atlantic Ocean. *Journal of Geophysical Research: Oceans*, **122**(3), 2441-2464.

Myers, P. (2005). Impact of freshwater from the Canadian Arctic Archipelago on Labrador Sea water formation. *Geophysical Research Letters*, **32**(6), 4 pp.

Myers, P.G., Kulan, N., & Ribergaard, M.H. (2007). Irminger Water variability in the West Greenland Current. *Geophysical Research Letters*, **34**, 6 pp.

Myers, P.G., Donnelly, C., & Ribergaard, M.H. (2009). Structure and variability of the West Greenland Current in Summer derived from 6 repeat standard sections. *Progress in Oceanography*, **80**(1-2), 93-112.

Pickart, R.S. & Spall, M.A. (2007). Impact of Labrador Sea convection on the North Atlantic meridional overturning circulation. *Journal of Physical Oceanography,* **37**(9), 2207-2227.

Pickart, R.S., Torres, D.J., & Clarke, R.A. (2002). Hydrography of the Labrador Sea during active convection. *J. Phys. Oceanogr.,* **32**(2), 428-457.

Pillar, H.R., Johnson, H.L., Marshall, D.P., Heimbach, P., & Takao, S. (2018). Impacts of Atmospheric Reanalysis Uncertainty on Atlantic Overturning Estimates at 25°N. *J. Climate*, **31**(21), 8719-8744.

Raasch, S., & Etling, D. (1997). Modeling Deep Ocean Convection: Large Eddy Simulation in Comparison with Laboratory Experiments. *Journal of Pjysical Oceanography*, **28**(9), 1786-1802.

Rattan, S., Myers, P.G., Trequier, A.M., Theetten, S., Biastoch, A., & Böning, C. (2010). Towards an understanding of Labrador Sea salinity drift in eddy-permitting simulations. *Ocean Modelling*, **35**(102), 77-88.

Renfrew, I.A., Moore, G.W.K., Guest, P.S., & Bumke, K. (2002). Comparison of Surface Layer and Surface Turbulent Flux Observations over the Labrador Sea with ECMWF Analysis and NCEP Reanalysis. *Journal of Physical Oceanography*, **32**, 383-400.

Rhein, M., Kieke, D., & Steinfeldt, R. (2015). Advection of North Atlantic Deep Water from the Labrador Sea to the southern hemisphere. *Journal of Geophysical Research: Oceans*, **120**(4), 2471-2487.

Riahi, K., Grübler, A., & Nakicenovic, N. (2007). Scenarios of long-term socio-economic and environmental development under climate stabilization. *Technical Forecasting and Social Change*, **74**, 887-935.

Ridenour, N., Hu, X., Jafarikhasragh, S., Landy, J.C., Lukovich, J.V., Stadnyk, T.A., et al., (2019). Sensitivity of freshwater dynamics to ocean model resolution and river discharge forcing in the Hudson Bay Complex. *Journal of Marine Systems*, **196**, 48-64.

Rieck, J.K., Böning, C.W., & Getzlaff, J. (2019). The nature of eddy kinetic energy in the Labrador Sea: Different types of mesoscale eddies, their temporal variability, and impact on deep convection. *Journal of Physical Oceanography*, **49**(8), 2075-2094.

Rykova, T., Straneo, F., & Bower, A.S., (2015). Seasonal and interannual variability of the West Greenland Current System in the Labrador Sea in 1993-2008. *Journal of Geophysical Research: Oceans*, **120**(2), 1318-1332.

Sathiyamoorthy, S., & Moore, G.W.K. (2002). Buoyancy flux at ocean weather station Bravo. *Journal of Physical Oceanography*, **32.2**, 458-474.

Schulze-Chretien, L.M., & Frajka-Williams, E. (2018). Wind-driven transport of fresh shelf water into the upper 30 m of the Labrador Sea. *Ocean Science,* **14**(5), 1247-1264.

Schulze-Chretien, L.M., Pickart, R.S., & Moore, G.W.K. (2016). Atmospheric forcing during active convection in the Labrador Sea and its impact on mixed-layer-depths. *Journal of Geophysical Research: Oceans*, **121**(9), 6978-6992.

Schmidt, S., & Send, U. (2007). Origin and Composition of Seasonal Labrador Sea Freshwater. *J. Phys. Oceanogr.,* **37**(6), 1445-1454.

Smith, G.C., Roy, F., Mann, P., Dupont, F., Brasnett, B., Lemieux, J.F., Laroche, S., & Bélair, S. (2014). A new atmospheric dataset for forcing ice-ocean models: Evaluation of reforecasts using the Canadian global deterministic prediction system. *Quarterly Journal of the Royal Meteorological Society*, **140**(680), 881-894.

Spall, M.A. (2004). Boundary currents and watermass transformation in marginal seas. *Journal of Physical Oceanography*, **34**(5), 1197-1213.

Straneo, F. (2006). Heat and freshwater transport through the central Labrador Sea. *Journal of Physical Oceanography*, **36**(4), 606-628.

Straneo, F., & Saucier, F. (2008a). The arctic-subarctic exchange through Hudson Strait. *Arctic-Subarctic Ocean Fluxes*, Springer, Dordrecht, 249-261.

Straneo, F., & Saucier, F. (2008b). The outflow from Hudson Strait and its contribution to the Labrador Current. *Deep Sea Research Part I: Oceanographic Research Papers*, **55.8**, 926-646.

Tsujino, H., Urakawa, S., Nakano, H., Small, R.J., Kim, W.M., Yeager, S.G., et al. (2018). JRA-55 based surface dataset for driving ocean-sea-ice models (JRA55-do), *Ocean Modelling*, **130**, 79-139.

Van Vuuren, D.P., den Elzen, M.G.L., Lucas, P.L., Eickhout, B., Strengers, B.J., van Ruijven, B., Wonink, S., & van Houdt, R. (2007). Stabilizing greenhouse gas concentrations at low levels: an assessment of reduction strategies and costs. *Climate Change*, **81**, 119-159.

Van Vuuren, D.P., Edmonds, J., Kainuma, M., Riahi, K., Thomson, A., Hibbard, K., Hurtt, G.C., Kram, T., Krey, V., Lamarque, J.F. and Masui, T. (2011). The representative concentration pathways: an overview. *Climate change*, **109**(1-2), 5pp.

Wilson, C., Harle, J., & Wakelin, S. (2019). Development of a regional ocean model for the Caribbean, including 3D dynamics, thermodynamics and full surface flu forcing. National Oceanography Centre Research and Consultancy Report, no. 65. National Oceanography Centre, Uk, 40pp.

Yashayaev, I. (2007). Hydrographic changes in the Labrador Sea, 1960-2005. *Progress in Oceanography*, **73**(3-4), 242-276.

Yashayaev, I., van Aken, H.M., Holliday, N.P., & Bersch, M. (2007). Transformation of the Labrador Sea water in the subpolar North Atlantic. *Geophysical Research Letters*, **34**(22), 8 pp.

Yashayaev, I., & Loder, J.W. (2016). Recurrent replenishment of Labrador Sea Water and associated decadal-scale variability. *Journal of Geophysical Research: Oceans*, **121**(11), 8095-8814.

Yashayaev, I., & Loder, J.W. (2017). Further intensification of deep convection in the Labrador Sea in 2016. *Geophysical Research Letters*, **44**(3), 1429-1438.

Yeager, S., & Danabasoglu, G. (2014). The origins of late-twentieth-century variations in the large-scale North Atlantic circulation. *J. Climate*, **27**(9), 3222-3247.

Supplemental Information:
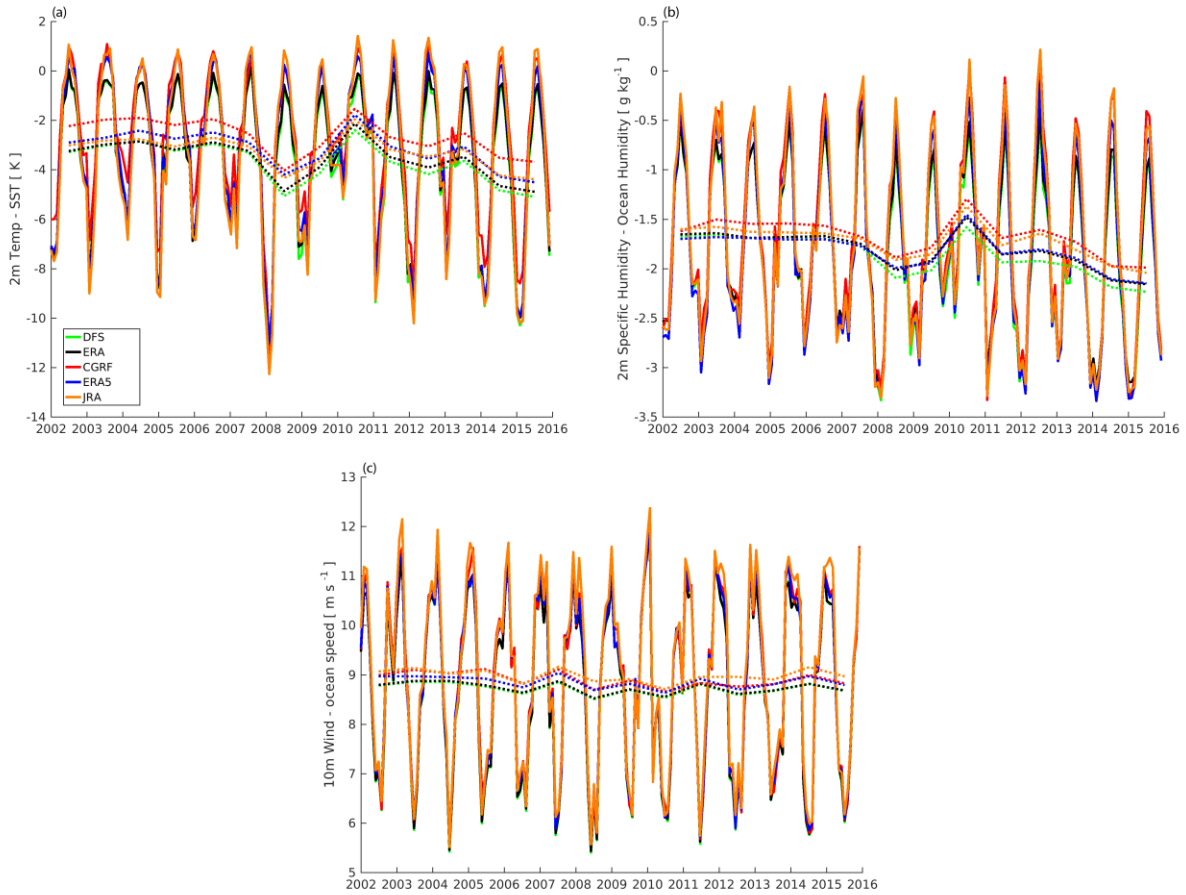
Supplemental Figure S5.1: Air-sea difference for (a) temperature, (b) specific humidity, and (c) wind speed for each of the five simulations. Dotted lines indicate the yearly mean. Values were spatially averaged over the red polygon in Fig. 5.1a.
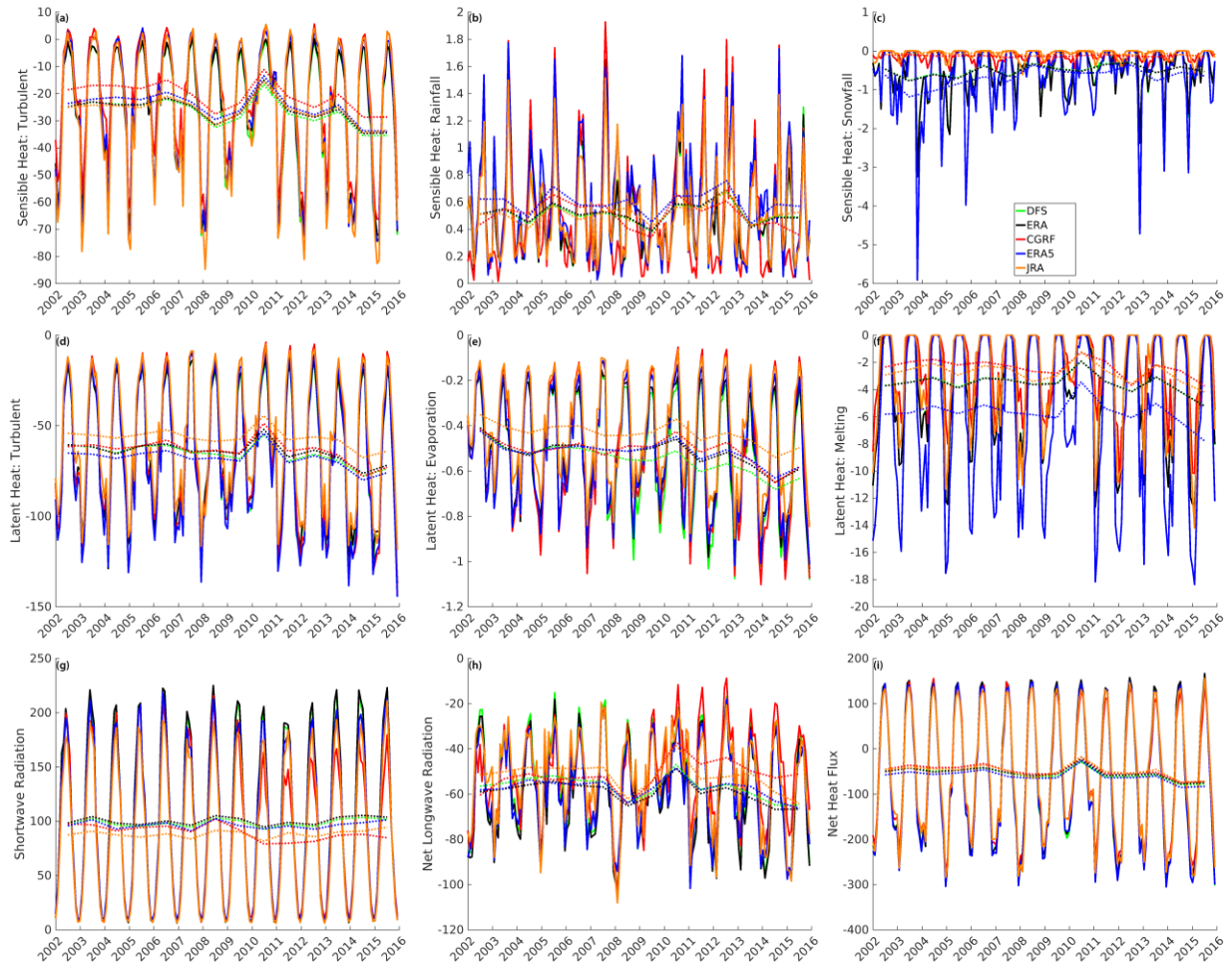
Supplemental Figure S5.2: Spatially-averaged (red polygon, Fig 1a) monthly air-sea heat fluxes (W m⁻²) to the Labrador Sea. Sensible heat as calculated from (a) turbulent motion, (b) rain, and (c) snow is shown in the upper panels. Latent heat as calculated from (d) turbulent motion, (e) evaporation, and (f) melt of snow is shown in the middle row. Radiative heating is shown by net shortwave radiation (g) and net longwave radiation (h). All fluxes combine to produce the net air-sea heat flux (i). Dotted lines indicate the yearly mean.
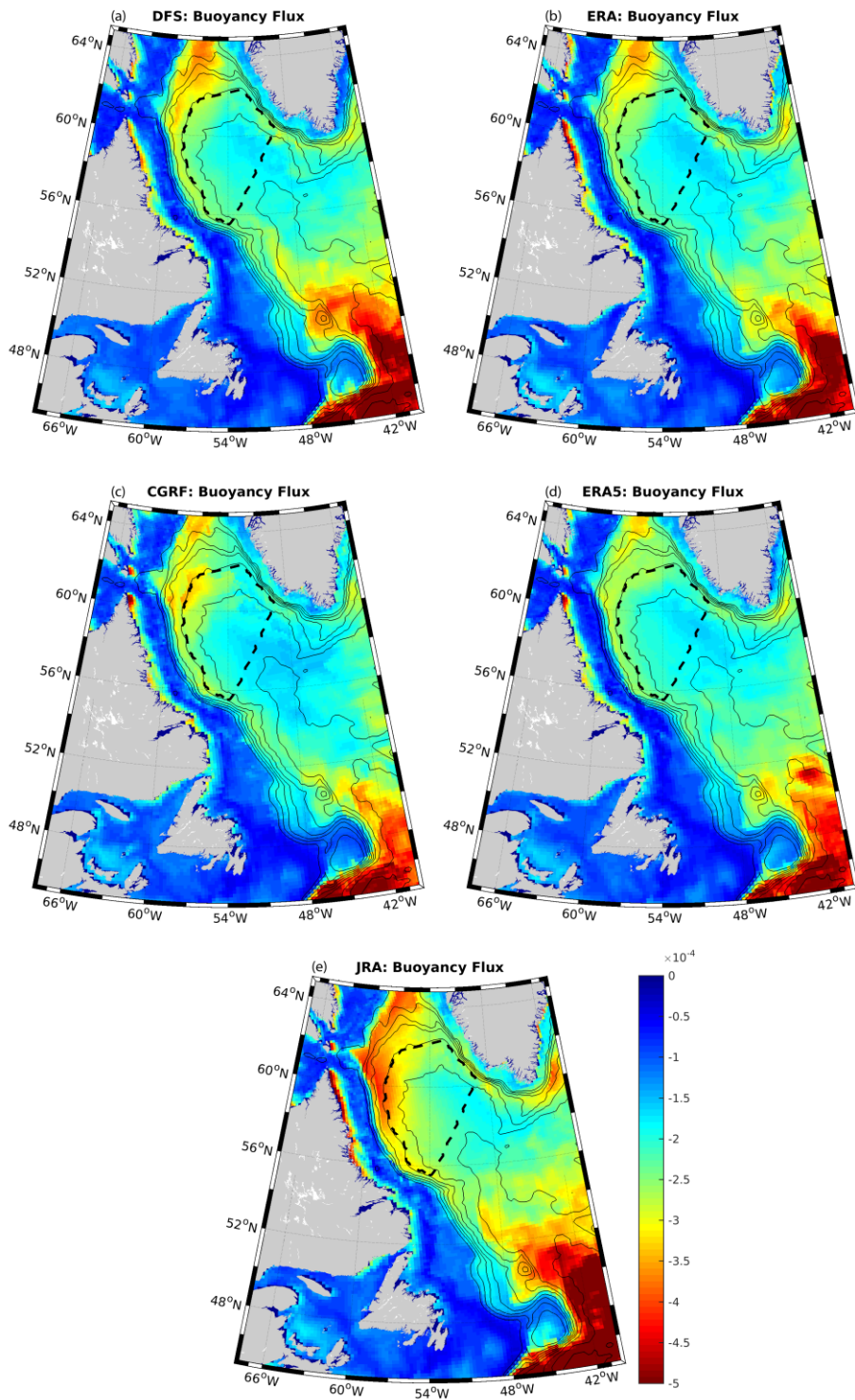
Supplemental Figure S5.3: Shaded colors indicate the grid point minimum buoyancy flux, in N m⁻² s⁻¹, for each simulation between 2002 and 2015. Bathymetric contours of 500m are indicated by the solid black lines while the dashed black line indicates our region of interest.

Chapter 6: Tracking Irminger Rings' properties using a sub-mesoscale ocean model

Clark Pennelly and Paul G. Myers

Department of Earth and Atmospheric Sciences, University of Alberta

Key words: Labrador Sea, submesoscale, numerical modelling, Irminger Rings, Eddies

6.1. Abstract

A 1/60° numerical simulation is carried out within the Labrador Sea to investigate eddies produced along the western coast of Greenland. These eddies, known as Irminger Rings, carry relatively buoyant water from the West Greenland Current system into the interior Labrador Sea. We detect and track 232 eddies produced within our 14 year simulation. Irminger Rings start with a significant layer of freshwater (median 4.4m) that erodes rather quickly during the convective winter. However, their heat reserve takes much longer to erode, indicating Irminger Ring's heat is the primary component to setting their stratification strength. Eddies generally travel southwestwards after formation, and eddies whose trajectory is close to the continental slope tend to have a reduced lifespan and quicker speed than those which drift into the interior deep basin. We find that eddies which spawn further north are more likely to end up influenced by the boundary currents, while those which form to the south are more likely to live longer and enter the deep interior basin. While the formation rate of eddies is generally uniform across our 2005-2018 simulation, Irminger Rings are far more likely to decay during the convective wintertime.

We find that most eddies quickly decay within a few months, although some survive long enough to endure two convective winters. All Irminger Rings increase the

local stratification in the Labrador Sea, limiting convection. However, the eddies which live for 2 winters experience a significant buoyancy loss over a long time span such that they may produce Labrador Sea Water within their core during their second winter. This constitutes a small volume of Labrador Sea Water (0.02 to 0.09 Sv) and updates our understanding of Irminger Ring's role on stratifying the Labrador Sea.

6.2. Plain Language Summary:

The Labrador Sea, between Canada and Greenland, experiences deep convection, a process where the surface water cools and becomes denser than the water at depth. This forces the surface water to sink and mix with the water below, homogenizing the water column and producing deepwater, an important component in the distribution of heat between the equatorial and polar regions. Deep convection is also important in ventilating the deep ocean with oxygen and carbon dioxide, sequestering these gasses for thousands of years. Deepwater is strongly influenced by the local weather as well as the current systems which surround the Labrador Sea. Oceanic eddies are produced from these current systems and bring their water mass properties into the region where deepwater is formed. These eddies are relatively buoyant, hindering deepwater formation, but also survive up to 2 years before decaying. We use a high-resolution ocean simulation to resolve these eddies so we can further understand how they evolve after being formed. Our simulation suggests that these eddies decay faster during the convective winter period, although eddies which survived to experience two winter's often experienced deep convection and the production of Labrador Sea Water. This paints the picture that these eddies not only significantly reduce deepwater formation, but can also act as local sources of deepwater formation.

6.3. Introduction

Deep convection within the Labrador Sea produces Labrador Sea Water (LSW), a potentially important water mass in the Atlantic Meridional Overturning Circulation

(AMOC) given recent work (Feucher et al., 2019; Lozier et al., 2019). The AMOC is the slow large-scale transport system which carries a significant amount of heat and dissolved gasses throughout the Atlantic, influencing the climate system (Buckley and Marshall, 2016). Gas uptake and ventilation is enhanced during convection, influencing the biological pump within the Labrador Sea (Rhein et al. 2017). Deep convection is strongly driven by cold winter storms which remove a sufficient amount of buoyancy such that the surface water becomes cooled to the point that it is denser than the water below (Lab Sea Group, 1998; Marshall and Schott, 1999). This static instability forces vertical mixing which can exceed 2000m (Yashayaev, 2007). However, this depth is dependent on both the surface buoyancy loss (Sathiyamoorthy and Moore, 2002) as well as the stratification of the Labrador Sea (Lazier et al., 2002). After convection ceases, a period of rapid restratification occurs due to large horizontal density gradients produced during the convective season (Frajka-Williams et al., 2014), forcing the mixed layer to shoal and leave behind a freshly ventilated and homogenous water mass: LSW. The newly produced LSW will slowly spread southwards with a large portion entering the Deep Western Boundary Current (Kieke et al., 2009), influencing the deep branch of the AMOC. Changes in deep convection and LSW production have been shown to impact AMOC strength (Böning et al., 2016), setting the Labrador Sea as a region of climate importance. As such, both the surface buoyancy loss and the supply of buoyant water from the boundary currents are important to understand, as changes in either will influence deep convection.

The surface buoyancy loss from the Labrador Sea is strongly controlled by the overriding atmospheric conditions. Winters with strong winds and very cold temperatures drive buoyancy out of the Labrador Sea, promoting deeper and denser LSW formation (Yashayaev, 2007). The inverse also hold true; less intense winters are correlated with a weaker LSW formation rate (Holdsworth et al., 2015; Garcia-Quintana et al., 2019). However, the oceanic stratification plays an important role, as it is possible for weak atmospheric conditions to promote deep convection if the ocean was weakly stratified to begin with, or vice-versa (Pickart et al., 2002; Schulze-Chretien et al., 2016). The boundary currents around the Labrador Sea (Fig. 6.1) are responsible for setting the stratification. Arctic water flows along the east coast of Greenland, containing cold and

fresh water. After rounding Cape Farewell, this current system is called the West Greenland Current (WGC) and has two layers: cold and fresh surface water within the top 200m and the warm and salty Irminger Water layer from roughly 200m to 700m (Cuny et al., 2002; Myers et al. 2009). The WGC flows cyclonically within the Labrador Sea, combining with fresh outflow from both Davis and Hudson Strait. The current system, called the Labrador Current after receiving Hudson Strait outflow, continues flowing southwards along the eastern North American coastline (Lazier and Wright, 1993). Seasonal and interannual variability in the water mass properties of these current systems modifies their stratification. This includes both layers, as melt from sea ice and Greenland's ice sheet (Myers et al., 2009; Luo et al., 2016) increases the surface freshness while the subsurface Irminger Water layer experiences seasonal changes in its volume and salinity (Rykova et al., 2015), further modifying the stratification carried within these current systems.

These boundary currents produce eddies and meanders which enter the interior Labrador Sea, modifying the stratification. This is particularly the case for Irminger Rings, eddies formed within the WGC near Cape Desolation (Eden and Böning, 2002). Irminger Rings are relatively small (roughly 15-30 km: Gelderloos et al., 2011; de Jong et al., 2014; de Jong et al., 2016), often anticyclonic eddies that are produced from barotropic instability from a narrowing of the continental shelf near Cape Desolation (Eden and Böning, 2002). Containing both water masses from the WGC (Hátún et al., 2007), Irminger Rings are very buoyant compared to the background Labrador Sea. After forming, Irminger Rings tend to flow roughly to the southwest (de Jong et al., 2016), bringing their strongly stratified waters across the Labrador Sea (Hátún et al., 2007; Gelderloos et al., 2011; de Jong et al., 2016). Their rotation and vorticity reduces lateral mixing and makes air-sea forcing the primary modifier of their water properties. Coupled with slow speeds (0.05 to 0.06 m s^{-1}; Lilly et al., 2003; Katsman et al., 2004), these eddies may survive for up to two years (Lilly et al., 2003; Chanut et al., 2008; de
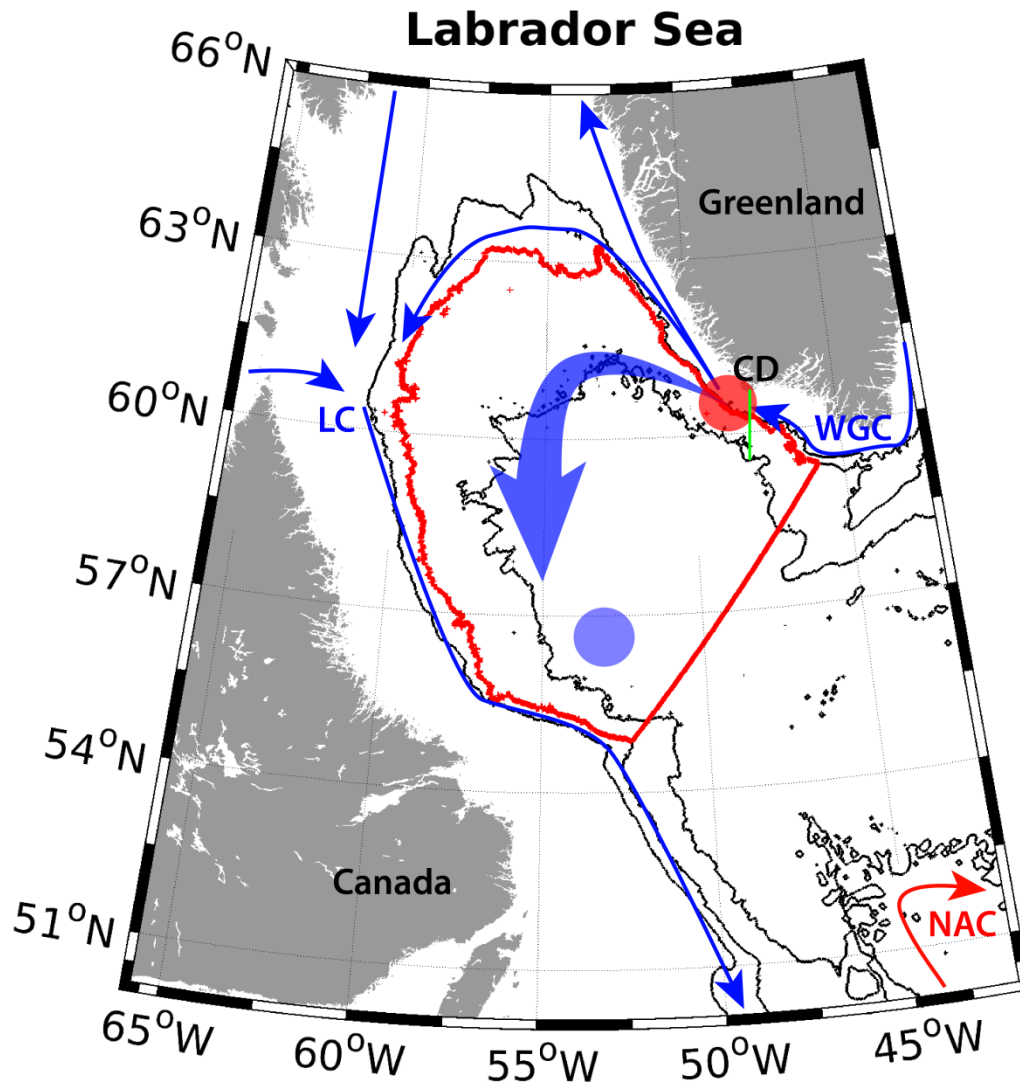
Figure 6. 1. The Labrador Sea (a) with currents identified in the colored thin arrows: West Greenland Current (WGC), Labrador Current (LC), and North Atlantic Current (NAC). The translucent red circle identifies the region where Irminger Rings spawn while their general trajectory is shown in the larger translucent blue arrow. The blue circle indentifies where the deepest convection often occurs. The red outline represents a Labrador Sea interior region where background calculations took place. CD identifies Cape Desolation.

Jong et al., 2016). Irminger Rings slowly decay and increase the local buoyancy along their path, causing the northern Labrador Sea to remain strongly stratified, resisting convection (Chanut et al., 2008) despite a large surface buoyancy loss (Hátún et al., 2007). Irminger Rings do not often flow into the southwestward portion of the inner Labrador Sea that experiences deep convection (de Jong et al., 2016), identifying that

Irminger Rings play a very strong role in controlling convection and Labrador Sea Water formation (Tagklis et al., 2020).

Irminger Rings have been explored from observations (Lilly et al., 2003; Hátún et al., 2007; de Jong et al., 2014) and modelling studies (Eden and Böning, 2002; Katsman et al., 2004; Chanut et al., 2008; Gelderloos et al., 2011; de Jong et al., 2016; Tagklis et al., 2020). Their small size makes a thorough investigation difficult. Satellite altimetry products may identify a useful 2-dimensional slice by locating individual eddies but they cannot provide sufficient information about their subsurface properties. Mooring arrays may capture the vertical profile as an eddy passes through the mooring, although these moorings cannot detect every eddy for their trajectories can vary significantly (Chanut et al., 2008; de Jong et al., 2016), let alone how these eddies evolve downstream. Hydrographic cruises are relatively limited in the Labrador Sea, often confined to the non-convective summer months. Numerical modelling may be a useful tool to explore these eddies, although modelling has its own issues. Bathymetry (Chanut et al., 2008) and lateral slip conditions (Rieck et al., 2019) have been shown to be particularly important as minor changes in either can completely prevent the formation of Irminger Rings. Numerical simulations with a resolution of 1/12° or higher appear sufficient to resolve these eddies (Chanut et al., 2008; de Jong et al., 2016; Rieck et al., 2019; Tagklis et al., 2020) while lower-resolution simulations fail to capture them and rely on eddy parameterization to mimic their effects. These lower-resolution simulations often experience a significantly broader and deeper mixed layer within the Labrador Sea than is observed (Courtois et al., 2017), often attributed to less eddy buoyancy fluxes than reality. This includes low-resolution climate simulations which may run for hundreds of years or longer. With a more weakly stratified basin, such low resolution simulations over-produce deepwater in the Labrador Sea (Garcia-Quintana et al., 2019; Tagklis et al., 2020). High-resolution simulations demand larger computing resources, often limiting the simulation's length, but are capable of resolving important eddy fluxes. We use a very-high resolution numerical ocean simulation capable of resolving small scale eddies within the Labrador Sea. We investigate these Irminger Rings, examine how their properties change as they flow through the Labrador Sea, shedding their strongly stratified water to an area that experiences deep convection.

Research has been carried out on how and where these rings form (Eden and Böning, 2002), how long they live for (Lilly et al, 2003; Chanut et al., 2008; de Jong et al., 2016), and the trajectory they often take (de Jong et al., 2016). We understand that they carry a significant amount of heat and low salinity water (Hátún et al., 2007; Gelderloos et al., 2011; de Jong et al., 2016) which drives the convective patch to not include the northern Labrador Sea (Chanut et al., 2008). Relatively little investigation has taken place on how Irminger Rings evolve after they are formed. Lilly et al. (2003) mention that these strongly stratified rings may experience a deep mixed layer exceeding 1000m if they experiencing two convective winters, but we have little information on how these eddies may end up reaching such a weakly stratified state. The primary goal of this manuscript is to investigate how these eddies evolve after being formed by detecting and tracking eddies in a high-resolution simulation to further understand their role in supplying stratification to the interior Labrador Sea.

6.4. Methods

6.4.1. Numerical setup

We use the Nucleus for European Modelling of the Ocean (NEMO v3.6; Madec, 2008) modelling framework, with a coupled sea-ice model (LIM2: Fichefet and Maqueda, 1997) to carry out our numerical simulation. We use the Labrador Sea 1/60° (LAB60) configuration as fully described by Pennelly and Myers (2020); we will briefly summarize this complex configuration below. This configuration has a regional 1/4° parent domain over the Arctic and Atlantic, with a 1/12° nest within the North Atlantic subpolar gyre, and a further 1/60° nest within the Labrador Sea (Fig. 6.2a). The Adaptive Grid Refinement in FORTRAN (AGRIF; Debreu et al., 2008) software is used to allow domain nesting. All nests feature two-way feedback where the parent domains supply boundary conditions to their nested domain while the nested domains supply interpolated grid-point values back to their parent domain. Vertical grid resolution is invariant of the domain; 75 vertical levels are used with a layer thickness that increases from 1.05m at the surface to 204m at the last level. Partial vertical steps are used (Barnier et al, 2006). As no-slip lateral boundary conditions aid in the formation of

Irminger Rings (Rieck et al., 2019), lateral slip conditions were set to be no-slip within the 1/60° nest and free-slip in the 1/12° and 1/4° domains.
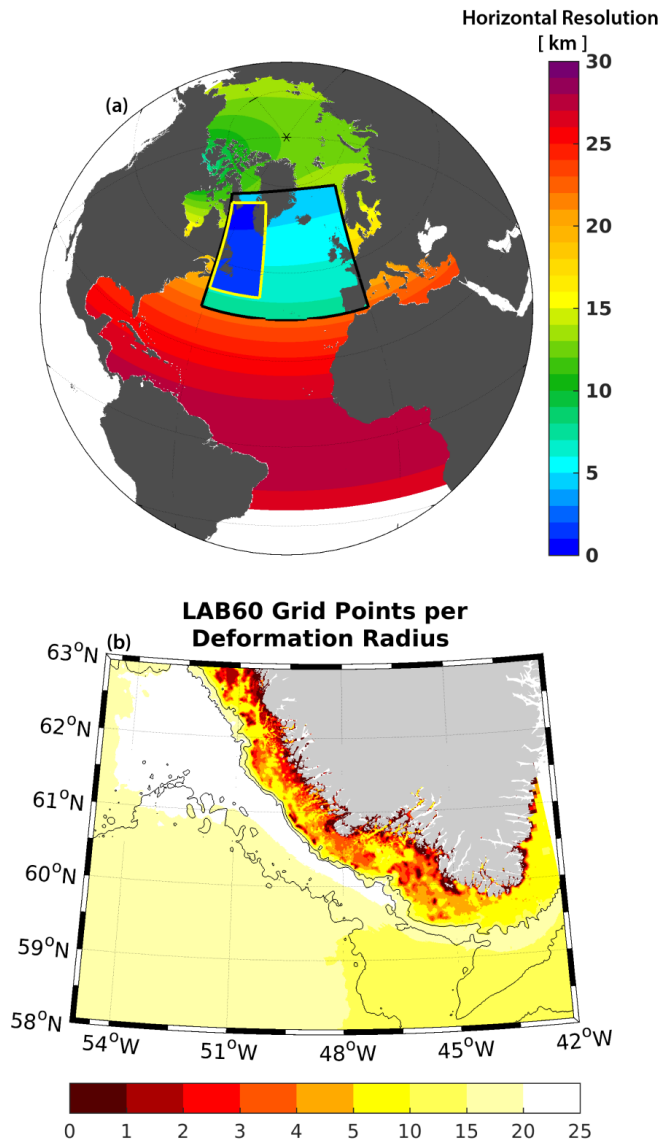
Figure 6. 2: Our double-nested model configuration is shown in (a) with horizontal resolution in colored contours. The number of grid points which fit inside the first Rossby deformation radius is shown in (b).

Initial conditions for this configuration are from GLORYS 1v1 (Ferry et al., 2010), interpolated to each domain's model mesh, starting 1 January 2002. Our regional parent domain has two open boundaries, at Bering Strait and 20°S across the Atlantic. Monthly GLORYS1v1 data was supplied as boundary conditions. Without an iceberg module

functioning with the AGRIF nests, we instead took our runoff data (Bamber et al., 2012) and converted all solid ice discharge to liquid. Atmospheric forcing was originally supplied by the Canadian Meteorological Centre's Global Deterministic Prediction System's Reforecast (CGRF; Smith et al., 2014) with hourly 2m temperature, 2m specific humidity, 10m zonal and meridional wind speed, downward shortwave and longwave radiation, and precipitation. We switched to the DRAKKAR Forcing Set version 5.2 (Dussin et al., 2016) in 2007 due to weak Labrador Sea convection in later years (2010+) when forced by CGRF. Another switch to ERA5 (Hersbach and Dee, 2016) occurred once we reached the end of the DRAKKAR forcing set in 2017.

6.4.2. Eddy detection and Tracking

In order to investigate the properties of Irminger Rings as they evolve across the Labrador Sea, automatic eddy detection and tracking was used. There are many different ways to detect eddies (e.g. Weiss, 1991; Doglioli et al., 2007; Nencioli et al., 2010), each with their own requirement criteria. We opted to use the approach as outlined by Nencioli et al. (2010; see their Figure 3 illustrating the below steps) as we had success with this technique in our 1/12° nested simulation (see Müller et al., 2017; Müller et al., 2019). We summarize this approach in two steps: detection and tracking.

Eddy detection starts by analyzing the surface velocity field. Four separate criteria must be met for the eddy to be detected.

(1) The meridional velocity must reverse direction along a zonal section. Furthermore, the magnitude must increase radially from the potential eddy centre over a distance 'a' number of grid points.

(2) For the points which follow (1) above, the same procedure is applied for zonal velocities across a meridional section.

(3) A possible eddy centre is determined to be at the velocity minimum within a box of length 'b' as centered wherever (1) and (2) above are met.

(4) A rotation check occurs within a box of 'a-1' grid points as centered about the possible eddy centre found in (3). This rotation check removes meanders that otherwise could be counted as an eddy.

The parameters a and b are adjustable values which the user must set and evaluate performance; we found that a=10 and b=8 grid points (approximately 9 and 7 km, respectively) appeared optimal. Any point which satisfies all four constraints is detected as an eddy centre. The eddy's boundary was determined from the largest closed contour of the streamfunction around the eddy centre. The eddy radius was set to be the minimum distance between the boundary and the eddy centre.

Eddy tracking took place once such an eddy was detected. The above procedure was carried out for the next output period, daily output for this simulation, in the vicinity of the previously located eddy centre. If the above criteria were met over a search radius of 0.5°, the eddy centre was updated and repeated until failure. Tracking failure occurred when 7 consecutive days came up with no updated eddy centre, the rotation changed direction, or when large differences were noted- common when eddies merge or split. Eddy tracks were visually inspected to remove splitting/merging and issues related to the search radius selecting a nearby eddy which was not the one being tracked.

Our first attempt to limit the spatial extent where eddies were detected was to produce a mask over a large portion of the WGC as Irminger Rings spawn over a limited area. However, many eddies were generated and detected that would not be classified as an Irminger Ring due to radius and/or formation location. Attempts to fully automate the process had limited success, primarily due to the computing costs of daily 1/60° output. To reduce computing time associated with analysis at 1/60°, we visually identified possible eddy centre's according to their surface velocity field, noting their formation date. We then ran the detection software on the identified centres to confirm or deny a true eddy and started the tracking procedure if confirmed. This removed a major time sink while still maintaining approximately the correct number of Irminger Rings, although their formation location and time might be slightly delayed (estimated <5 days) than if automatically detected. A few eddies may have escaped our detection

and tracking attempt; if any, they would likely have been relatively small eddies with weak surface velocity signatures and short lifetimes. As most of our analysis takes place on longer lived eddies (>30 days), the absence of these eddies should have little to no effect on our results.

Tracked eddies were investigated for their change in properties. As Irminger Rings hold low salinity water at their surface, we calculate the freshwater thickness (eq. 6.1) where salinity is less than 34.8, a common reference salinity value within the Labrador Sea (Aagaard and Carmack, 1989; Cuny et al., 2005; Curry et al., 2014). We also calculate the upper 2000m heat and salt content (eq. 6.2 and eq. 6.3) relative to 0°C. We normalize the heat and salt content by the eddy's surface area to keep eddies of different sizes comparable. To investigate how the eddies vertical stratification evolves, we calculate convective resistance (eq. 6.4) to a reference depth of 2000m. Convective resistance is how much energy must be removed such that the water column is neutrally stratified to the reference depth. Lastly, we estimate the depth of the mixed layer from the gradient in temperature and salinity (Holte and Talley, 2009) as opposed to a change in density as it may give a poor interpretation in areas with deep convection (Courtois et al., 2017).

$$Freshwater\ Thickness\ [m] = \frac{1}{Area} \int \int \frac{Sref - S}{Sref} dz\ dA \tag{6.1}$$

$$Heat\ Content\ [J\ m^{-2}] = \frac{1}{Area} \int \int c_p * \rho_\theta * T\ dz\ dA \tag{6.2}$$

$$Salt\ Content\ [g\ m^{-2}] = \frac{1}{Area} \int \int \rho * S\ dz\ dA \tag{6.3}$$

$$Convective\ Resistance\ [J\ m^{-3}] = \frac{g}{Area} \int \int \left[h\ \rho_\theta(h) - \int_0^h \rho_\theta(z)\ dz \right] dA \tag{6.4}$$

where $Sref$ = 34.8, S is the grid point salinity, c_p is the heat capacity of seawater at 4000 J kg^{-1} °C^{-1}, ρ is the ocean's density, T is the grid point temperature in °C, g is the acceleration due to gravity at 9.8 m s^{-2}, h is the reference depth of 2000m, ρ_θ is the potential grid point density, A is the grid cell's surface area, and $Area$ is the surface area of each Irminger Ring. These proxies are calculated for Irminger Rings as they travel

through the Labrador Sea as well as for the background Labrador Sea (red contour line in Fig. 6.1).

6.5. Results

6.5.1. Evaluation

Before identifying Irminger Ring's properties and how they evolve as they transit the Labrador Sea, we first evaluate the LAB60 simulation to assess its ability to carry out the research goals outlined above. The WGC system contains two layers: Arctic Water (AW) and Irminger Water (IW). We compare LAB60's volume, heat, and freshwater transport of these two layers against the observational study by Rykova et al. (2015) who investigated transports within the WGC. We use their water mass classifications where we calculate the upper 1000m transport between Cape Desolation and a nearby 3000m isobath while layers were separated by the 34.4 isohaline. LAB60's IW layer transports more volume (mean 10.2 Sv [1 Sv = 1×10^6 m^3 s^{-1}]; Fig. 6.3a) than Rykova et al. (2015) observed (8.1 Sv), although their analysis period was 1993-2008 and Yang et al. (2016) found elevated salt and heat transport associated with the IW layer within the WGC from 2005 through the end of their analysis in 2013. This also helps address why LAB60 has more heat transport (203 TW; Fig. 6.3b) than Rykova et al. (2015) found (153 TW).

Arctic Water volume transport initially is in good agreement with Rykova et al (1.8 Sv; 2015), although the long term mean of LAB60's AW volume transport (2.5 Sv) is a bit higher. However, de Steur et al. (2018) notes that southward AW volume transport through upstream Fram Strait has increased, and became fresher, from 2009 through 2014. As the upstream East Greenland Current turns into the West Greenland Current at the southern tip of Greenland, we use this observed transport to address discrepancies between LAB60 and that of Rykova et al. (2015) for years where data do not overlap (2008-2018). LAB60 presents both an increase in the volume transport as well as the freshwater transport during this period. This helps address why LAB60's AW volume transport is larger than Rykova et al. (2015) found. LAB60 AW freshwater transport (55.4 mSv) is greater than what Rykova et al. (2015) found (60.1 mSv), while
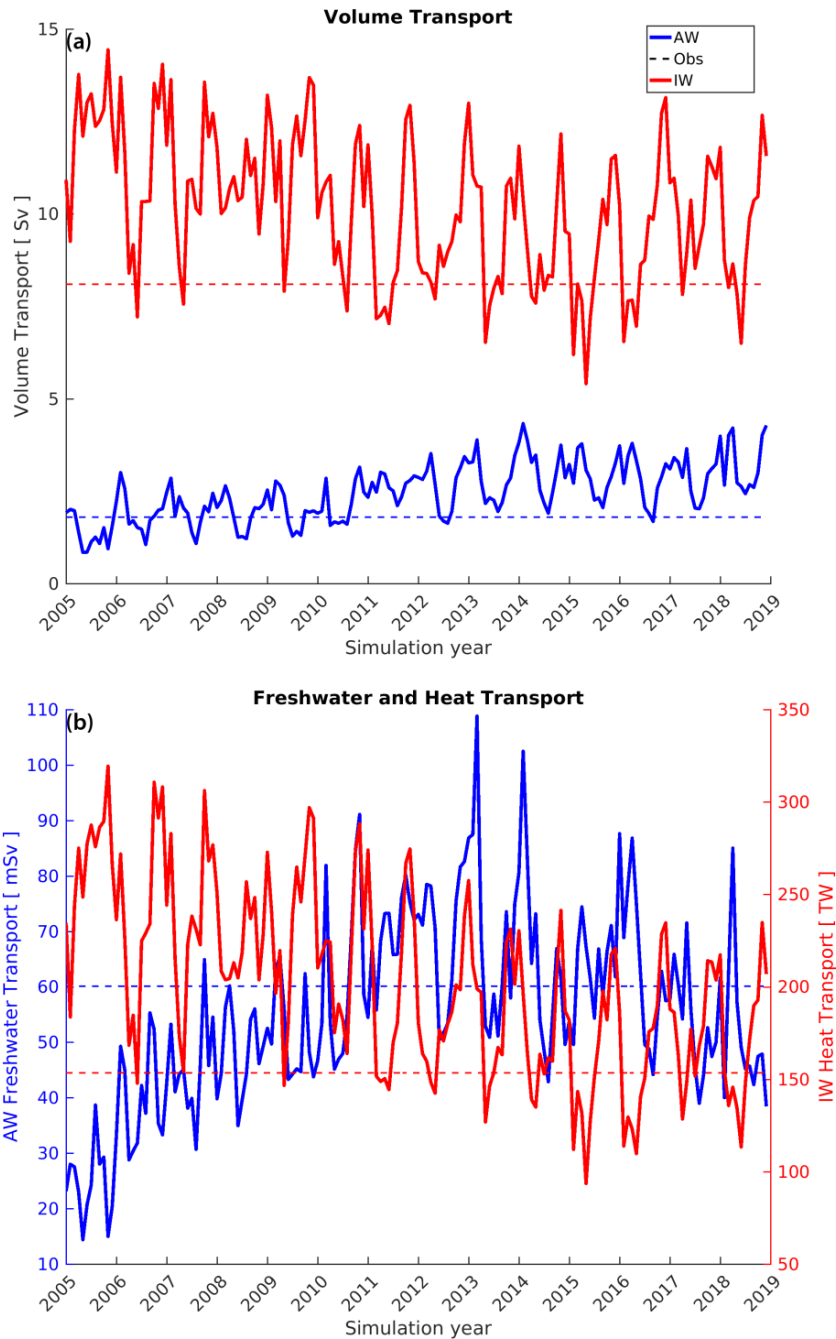
Figure 6. 3: Volume transport (a) for both water masses within the West Greenland Current: Arctic Water (AW: blue) and Irminger Water (IW: red). Freshwater transport (AW) and heat transport (IW) are shown in (b). Dotted lines indicate the observed 1993-2008 mean transports by Rykova et al, (2015).

still matching the increase in freshwater transport that de Steur et al. (2018) note.

LAB60's volume, heat, and freshwater fluxes thus appear fairly well comparable to the previous record of observations in close vicinity to the spawning region of Irminger

Rings, as well as matching more recent studies on both upstream AW and IW transports. We thus have confidence in LAB60's ability to adequately represent the WGC system in regards to properties it contains- strongly stratified water that will influence the Labrador Sea basin.

With LAB60 carrying similar volume, heat, and freshwater within its WGC system as observations suggest, we now address if this configuration is capable of resolving eddies in this region. The first baroclinic Rossby radius of deformation in this region is roughly 10-15 km, although quite lower along the shelf. Figure 6.2b illustrates the number of model grid points that fit into the first deformation radii. While not directly indicative of eddy resolving ability, most of LAB60's domain contains multiple grid cells per deformation radii; LAB60 should form eddies across its full domain. Furthermore, as detailed in their model configuration manuscript, Pennelly and Myers (2020) show that LAB60 has a similar amount of eddy kinetic energy along this coastline when compared against AVISO observations. Thus we have reason to believe our numerical eddies should be comparable to real eddies that form within LAB60's domain. Pennelly and Myers (2020) also find that LAB60 does not appear to suffer from numerical drift from either the total salt or heat content within the interior Labrador Sea- an issue that plagues many lower-resolution simulations in the North Atlantic (Rattan et al., 2010; Marzocchi et al., 2015). This implies that the boundary systems that feed the interior Labrador Sea are likely not drifting, further supporting the use of our simulation.

The LAB60 simulation produced and tracked 232 detectable eddies between 2005 and 2018. A snapshot from 21 October 2005 illustrates some features of Irminger Rings as produced by the LAB60 configuration. The relative vorticity normalized by the planetary vorticity (Fig. 6.4a) shows these eddies with a negative potential vorticity center surrounded by positive potential vorticity. As the WGC contains a significant freshwater layer thickness (Supplemental Video 6.1), Irminger Rings carry some portion of this freshwater (Fig. 6.4b) into the interior region. The WGC's Irminger Water layer provides a significant amount of heat (Fig. 6.4c) to each eddy which they carry along their path. The combination of additional freshwater and heat influences the stratification strength of the Labrador Sea, shown by the convective resistance (Fig.

6.4d). Irminger Rings are strongly stratified when they are created, and, depending on their trajectory and lifetime, may carry this stratification into the interior of the Labrador Sea.
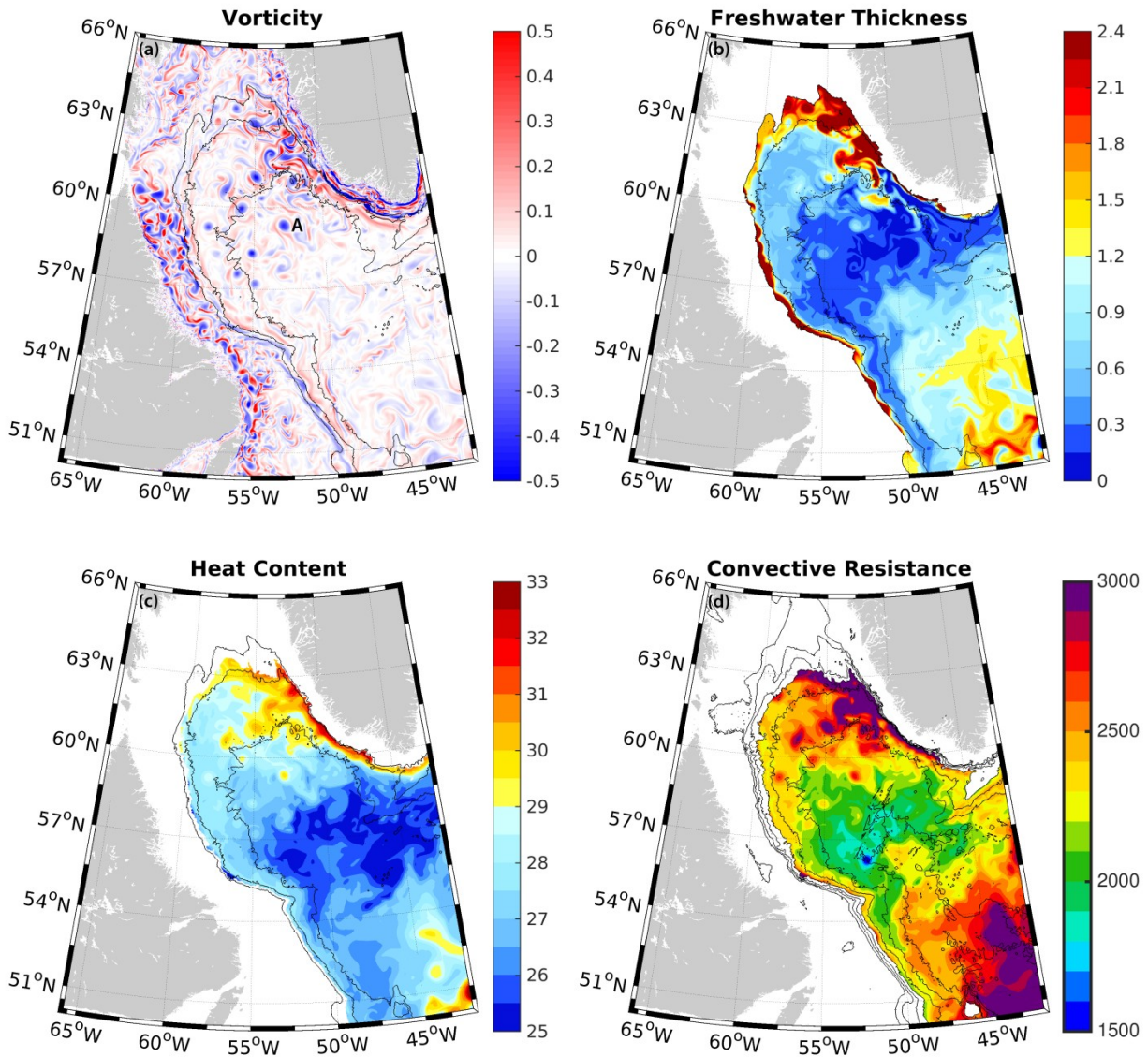
Figure 6. 4: Model snapshot from 21 October 2005 showing the relative vorticity normalized by the planetary vorticity (a), the freshwater layer thickness in meters (b), the heat content (GJ m^{-2}; c), and the convective resistance to 2000 m (J m^{-3}; d). The Irminger Ring identified by the black A in (a) has its vertical profile illustrated in Figure 6.5.

Figure 6.4 illustrates horizontal surface proxies, but Irminger Rings contain some significant differences in depth when compared to the background Labrador Sea. The

anticyclonic rotation of these eddies (Fig. 6.5) drives isopycnals downwards- opposite as the background Labrador Sea- increasing the layer thickness which must be eroded through to reach a certain isopycnal. Furthermore, both the temperature (Fig. 6.5a) and salinity (Fig. 6.5b) profiles are rather different than the background Labrador Sea. A fresh surface layer exists within each ring, roughly the same depth as the nearby background, but much fresher due to limited lateral mixing. The subsurface Irminger Water layer is both slightly more salty as well as much warmer than the waters surrounding each Irminger Ring. As this layer may exceed 700m in depth, Irminger Rings contain a significant amount of heat. This heat and freshwater will travel with the eddy along their path, although portions of it will be lost to the surrounding basin, increasing local stratification.
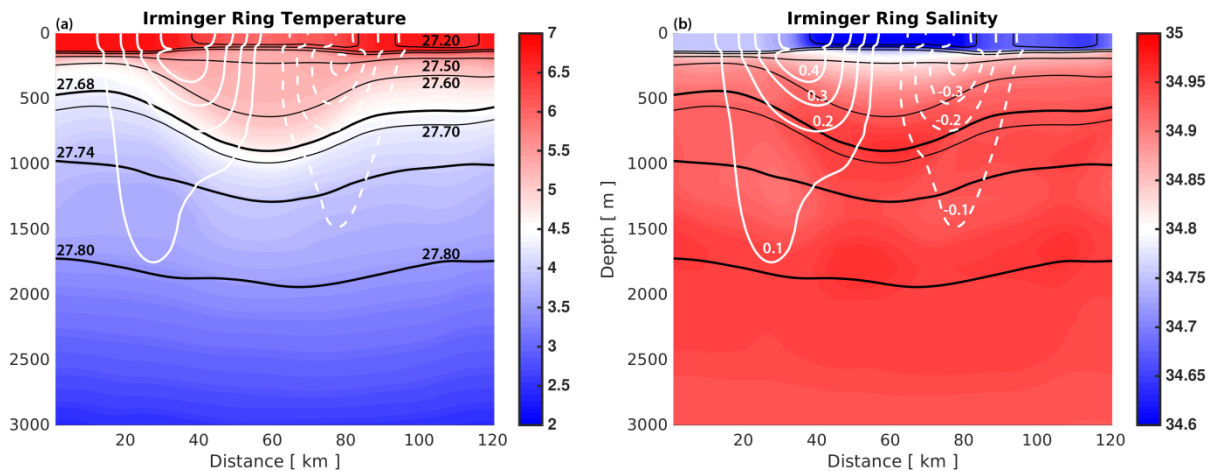
Figure 6. 5: East-west vertical cross section of the Irminger Ring shown by the black A in Figure 6.4a. The temperature in °C (a) and salinity (b) profiles are shown in colored contours while isopycnals are shown in black contours (interval 0.1 kg m⁻³). The upper and lower bounds of Upper and Classical Labrador Sea Water are identified via the thicker black contours. Solid (dashed) white contours show northward (southward) velocity normal to the cross-section, with a contour interval of 0.1 m s⁻¹.

Eddies which survived for longer than 30 days have their trajectory shown in Figure 6.6a. For the most part, Irminger Rings travel in a southwestward manner after being formed, loosely flowing between the 2000m and 3000m isobath. LAB60's Irminger Ring trajectories match well with modelling studies carried out by Chanut et al. (2008) and de Jong et al. (2016). Eddies tended to have higher transverse speed (Fig. 6.6b) immediately after being formed as well as when they drifted closer to the Labrador

Coast. As a whole, LAB60 had Irminger Rings with a median transverse speed of 0.04 m s^{-1} while other have found speeds of 0.05 m s^{-1} (Lilly et al., 2003) to 0.06 m s^{-1} (Katsman et al., 2004). At roughly 17 eddies spawned per year, this is slightly low compared to observational studies (15-45; Lilly et al., 2003) and other modelling studies (30,Chanut et al., 2008; 35, de Jong et al., 2016). This may be due to our detection and tracking method, which we discuss later. Others have determined Irminger Rings to have a radius that is somewhere around 15-30km (11-35km: de Jong et al., 2014; 20km: Hatún et al., 2007; 23km: Lilly et al., 2003; de Jong et al., 2013; Katsman et al., 2004). LAB60 produced Irminger Rings with a median radius of 23km, matching well with the above studies. LAB60 had some eddies live up to 2 years as both observations (Lilly et al., 2003) and modelling (Chanut et al., 2008) also find. As LAB60 may produce fewer Irminger Rings with a fairly correct trajectory, speed, and lifetime, we have confidence that this configuration can be used to explore how these eddies evolve and their individual contribution to stratifying the Labrador Sea.
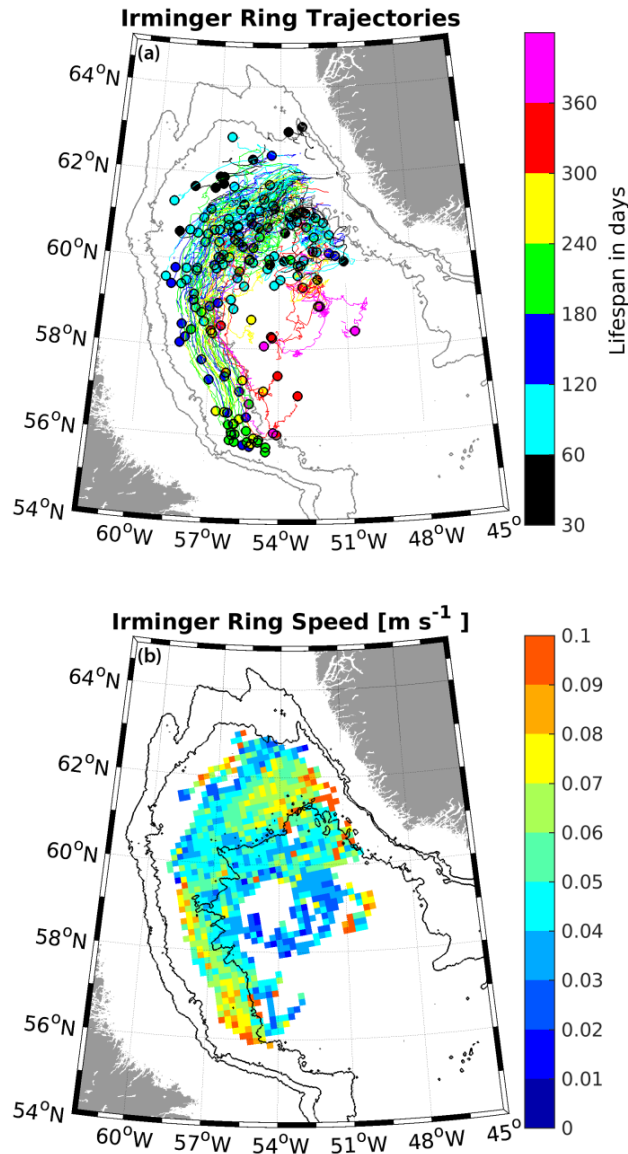
Figure 6. 6: Trajectories of Irminger Rings (a) which had a lifetime above 30 days. The location where each eddy was no longer detectable is shown with a solid circle with colour corresponding to its lifetime. The trajectory is determined from the daily center of each eddy; small gaps occur when the eddy was not detectable between segments. Average along-path Irminger Ring speed for eddies which lived longer than 30 days is shown in (b). Data were remapped to ¼ degree resolution for clarity.

6.5.2. Formation and Trajectory of Irminger Rings

Irminger Rings spawn slightly more frequently in the first half of the year than the second half (Fig. 6.7a). However, far more Irminger Rings decay during the winter

convection season than the other months of the year (Fig. 6.7b). We attribute this to the larger lateral and vertical mixing conditions that arise during convection as large air-sea buoyancy fluxes erode Irminger Rings. Some eddies had a lifespan which exceeded one year (Fig. 6.7c), although most eddies were detectable for far less. 158 eddies survived over 30 days; these will constitute the population for the remaining portion of this manuscript. We removed the shorter lived eddies (N= 74) as they did not fit our scope of investigating long-lived eddies. While remaining results and discussion will not include these short lived eddies, including 30 which were detectable for less than 5 days, they are still important to controlling the stratification and convection in the Labrador Sea.

The total number of detectable eddies at any month (Fig. 6.7d) was fairly similar across the first half of our simulation period, often between 5 and 7 eddies at any one time. This is less than the idealized simulation by Katsman et al. (2004) who found around 8-9 eddies occurring at any one time. We note a period from 2010 through 2014 with generally weaker LSW formation (Yashayaev and Loder, 2016) where fewer eddies were present during most months. However, there was little change in the number of eddies produced each year (around 17) so the reduced number of rings present during these years is due shorter eddy lifetimes. Others have investigated the density gradient between the inner Labrador Sea and the boundary current, identifying that a large density gradient, and thus circulation changes, do not appear to influence Irminger Ring formation frequency, but do promote larger and more energetic eddies (de Jong et al., 2016). However, LAB60 does not appear to have significant interannual variability in eddy energetics, radius, or spawning frequency- they remain fairly similar across all simulation years (not shown). We suspect greater buoyancy loss and/or weaker eddy stratification play a role as either would promote quicker eddy decay- we will examine this below.
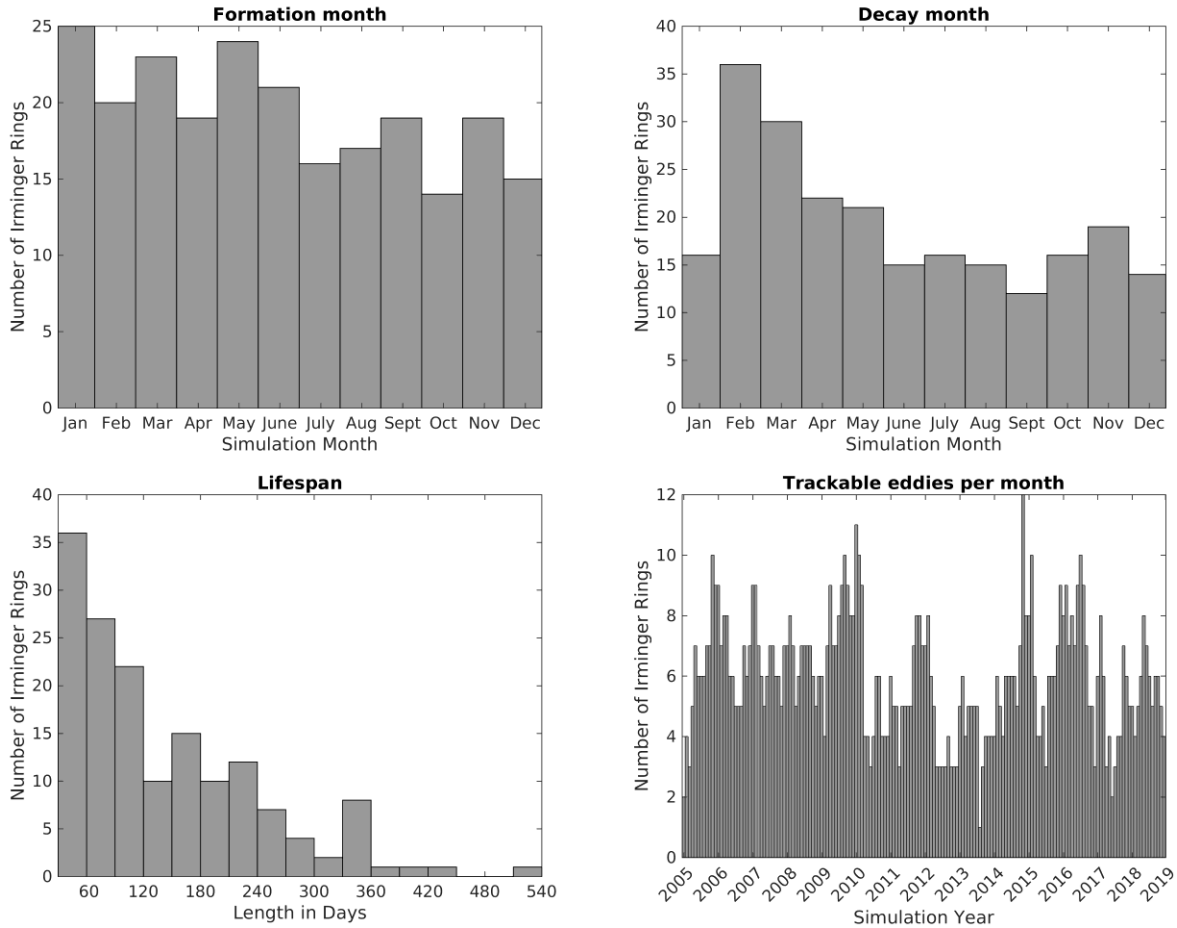
Figure 6. 7: Histogram of the total number of Irminger Rings formed every month (a) from our 2005-2018 simulation. (b) is the same as (a) but for the month when Irminger Rings decayed. The lifespan for eddies with a lifespan longer than 30 days is shown in (c). The total number of Irminger Rings which lived longer than 30 days and were detectable each month over our simulation is shown in (d).

Irminger Rings typically leave the WGC and loosely follow the 3000m isobath to the west and south (Fig. 6.6a). However, some eddies travel in a more southern direction and enter the interior Labrador Sea rather than flowing along the continental slope. These interior-seeking eddies were more likely to have longer lifetimes; we suspect this is due to limited interaction with other mesoscale features and boundary currents which can quickly erode eddies. We note two regions where a disproportionate number of eddies decayed (solid circles in Fig. 6.6a): west and north of their formation region, and around 56°N by 55.5°W where the continental shelf makes a sharp turn north of Hamilton Bank. Strong shear between mesoscale features, nearby currents, or lateral mixing induced via subduction can promote eddy decay (Schouten et al., 2000).

196

We attribute the decay occurring near the formation region from high eddy activity which produced numerous eddies and meanders which can collide and interact with Irminger Rings. Eddy decay along the Labrador Coast is attributed to interaction with the swift Labrador Current, effectively ripping apart Irminger Rings which travel too close. While we did not carry out a correlation, trajectory proximity to the boundary current visually appears correlated with a shorter eddy lifespan.

Eddies near the formation region and along the Labrador Coast have a greater transverse eddy speed (Fig. 6.6b) compared to those in the rest of the Labrador Sea. The greater speed just after formation is attributed to the swift WGC emitting Irminger Rings. Eddies which survive the formation region reduce in transverse speed. However, eddies which travel close to the Labrador Current, between the 2000m and 3000m isobath, accelerate before decaying north of Hamilton Bank. A few Irminger Rings along the Labrador Coast were able to re-circulate north into the interior basin- this appears to allow for a longer lifetime. For the most part, eddies which travel into the interior Labrador Sea have relatively low transverse speed and long lifetime.

6.5.3. Evolution of Irminger Rings

We investigate the water mass properties of Irminger Rings between their formation and decay, examining how these eddies evolve. Spawned from the WGC, Irminger Rings carry a significant amount of both freshwater and heat, as we have shown above (Fig. 6.4), although this will evolve in time. We show the cross-sectional evolution of a single eddy which had a lifespan of about 10 months (Fig. 6.8). We chose this eddy as it clearly showed the same features that many other eddies exhibit, but over a lengthy time period. This eddy spawned (Fig. 6.8a) with very similar features as the eddy shown in Figure 6.5: a thick freshwater layer, downward isopycnals, a warmer subsurface, and anticyclonic circulation. The black line at the top of each image quantifies the convective resistance, a measure of stratification. This resistance peaks at the eddy center and reduces radially outwards. The downward doming isopycnals inherently force these rings to be more strongly stratified than the surrounding water due to lighter water within the eddy at the same depth as denser water outside the eddy.
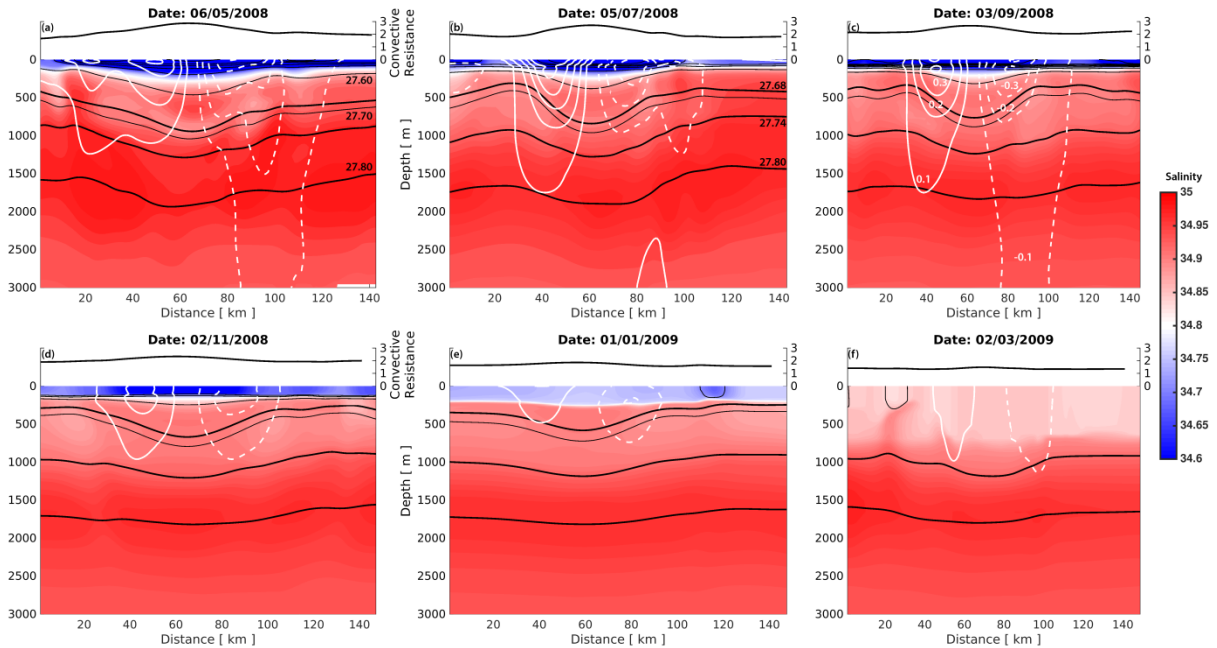
Figure 6. 8: The cross-section evolution of a single eddy over its lifespan (a-f). Colored contours indicate the salinity, black contours identify isopycnals (interval 0.1 kg m⁻³), and solid (dashed) white contours the northward (southward) velocity (interval 0.1 ms⁻¹). The thick black contours identify the bounds of Upper Labrador Sea Water (1027.68 to 1027.74 kg m⁻³) and Classical Labrador Sea Water (1027.74 to 1027.80 kg m⁻³). Convective Resistance, the black line on the top of each subpanel, has units of kJ m⁻³.

A few changes occur over the next few months (Fig. 6.8b): the eddy's rotation becomes more confined while the salinity in the subsurface layer (200-800m) freshens slightly. The surface freshwater layer also thins, and the combination of these changes reduces the overall stratification strength. Given a modification in the subsurface layer as well as a shallow mixed layer, this eddy loses some stratification laterally and not just to the atmosphere. Similar behavior occurs over the next 4 months (Fig. 6.8c and 6.8d). However, with the winter convection period approaching, we start to see larger changes occur at the surface in Figure 6.8d. The rotation speed has considerably weakened, weakening the isopycnal depression. The freshwater layer, both inside and outside the eddy, becomes more saline from vertical mixing induced via surface cooling. This mixing continues (Fig. 6.8e) where the surface freshwater layer inside is slightly more salty and thicker than the freshwater layer outside. However, the rotation and downward isopycnals are still present- the eddy has not decayed completely yet. This eddy survives another 2 months into March (Fig. 6.8f). Right before its decay, we note a

very interesting aspect of this eddy- convection within the eddy has produced water with a density that matches Upper Labrador Sea Water (1027.68 to 1027.74 kg m^{-3}). This eddy soon decays as its velocity signature was no longer automatically detectable.

Each Irminger Ring is different, particularly in terms of their lifetime, but we can compare their starting properties together. Analysis on the starting freshwater layer thickness (Fig. 6.9a) shows that the summer months hold a slightly thicker layer than during fall/winter. This is consistent but not as clear as Rykova et al. (2015) showed for the seasonality of the WGC's freshwater transport- they found a much larger change in freshwater transport throughout the year. Eddies typically held a median 3 to 5.5 meters of freshwater, although some held less than 1m or as much as 10m. Seasonality is much more noticeable for initial heat content (Fig. 6.9b) where Irminger Rings spawned during the spring months have less heat than eddies spawned in other months. This heat content was not selected per water mass although one can assume most of this heat resides within the thicker and warmer Irminger Water layer inside each Irminger Ring. Upstream heat transport within the Irminger Water (Fig. 6.3b) and Arctic Water (not shown) layer which passes Cape Desolation both show a reduction in heat transport from winter through late spring, explaining this seasonality.

Investigation into the rate which freshwater leaves these eddies (time to reach ½ of starting freshwater thickness) reveals strong seasonal variability (Fig. 6.9c). Eddies that spawn during the late convection and post-convection months (AMJ) hold onto their freshwater far longer (median between 125 and 150 d) than eddies spawned throughout the rest of the year. Furthermore, the freshwater decay time decreases as the convection season approaches, reaching a minimum for eddies spawned during January (median 39d). Shallow or deep convection mixes the surface layer with the salty layer beneath, removing this freshwater layer.
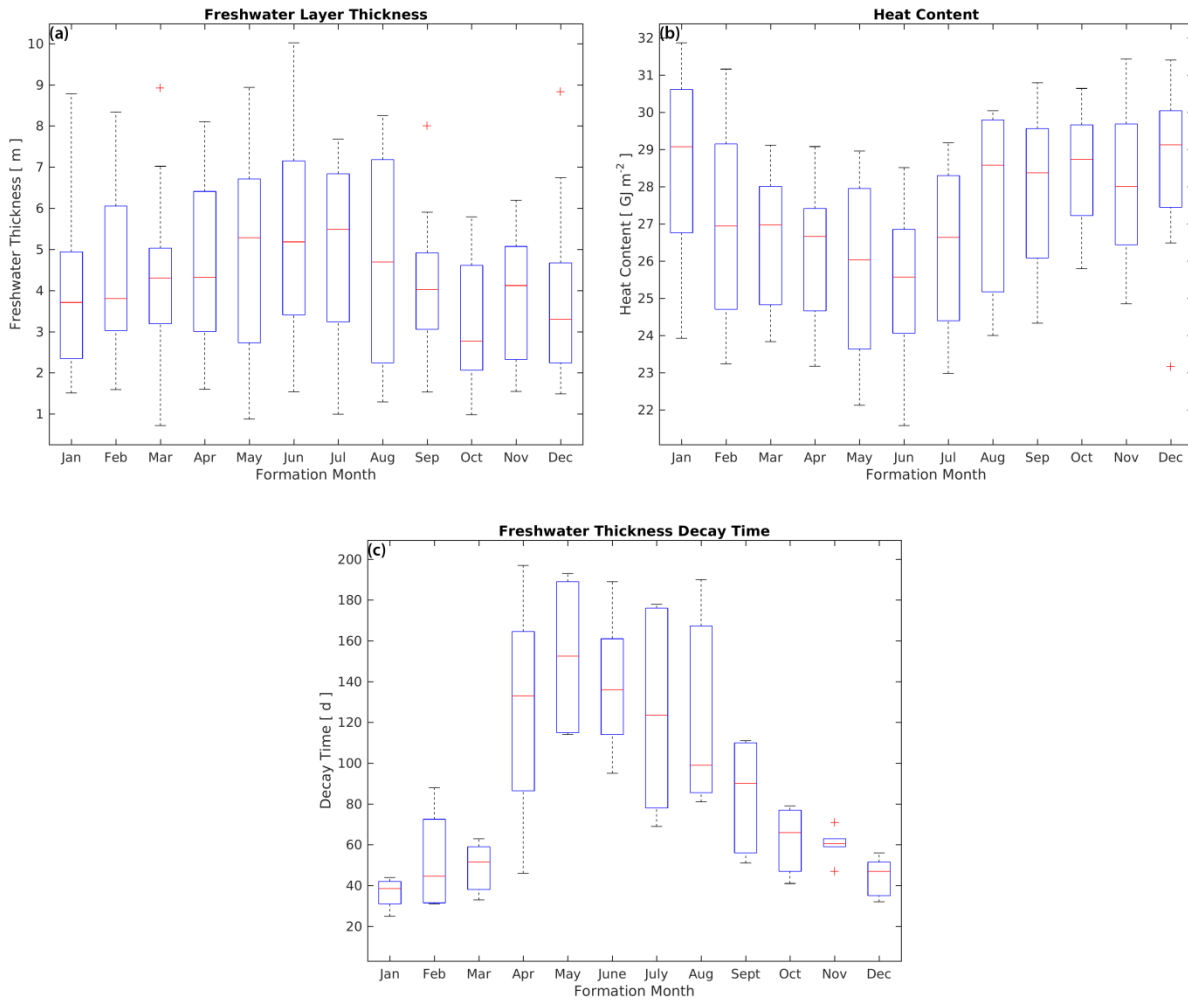
Figure 6. 9: Monthly variability of the freshwater layer thickness for Irminger Rings which lived longer than 30 days (a). (b) is the same as (a) but for heat content. The amount of time Irminger Rings took to lose ½ of their initial freshwater layer thickness is shown in (c). Red lines indicate the monthly median while outliers are shown as a red cross. The inter-quartile range (box) covers from the 25 to 75 percentile of the monthly data.

Eddies which lived longer than 30 days (N=158) have their evolution of our various proxies shown in Figure 6.10. The salt content within the top 2000m is plotted for these long lived eddies (Fig. 6.10a) as well as the background Labrador Sea. Eddies generally start with less salt than the background sea, likely due to their enhanced freshwater content at the surface. However, this salt content increases as eddies age, with most eddies having salt content approach the median value (black line) across the Labrador Sea, although a few eddies end up with more salt than median background

200

state. Both eddies and the background sea experience some freshening in the later simulation years, likely due to freshening that occurs within the WGC (Fig. 6.3b; Supplemental Video 6.1).
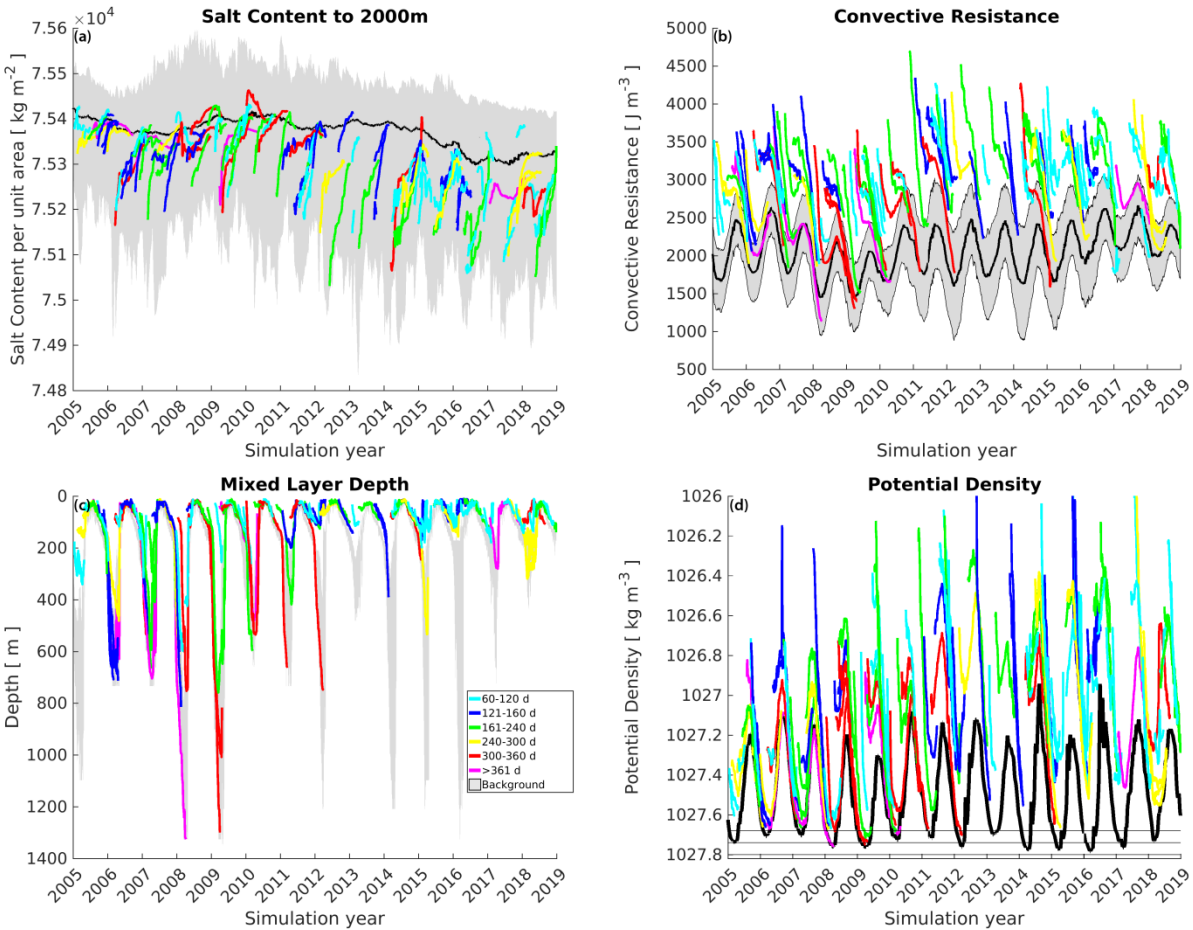
Figure 6. 10: Monthly variability of the salt content within Irminger Rings (colored lines) is shown in (a) where the background Labrador Sea values (red polygon in Fig. 6.1) indicate the minimum to maximum range with the median in black. Eddies are binned by lifespan in 60 day increments as indicated by line color. Convective resistance is shown in (b) where the background grey values indicate one standard deviation from the median (black line). Mixed layer depth is shown in (c) where grey indicates the 75-100% maximum which occurred within the background sea. The maximum potential density at the bottom of the mixed layer is shown in (d) where the thick black line indicates the maximum density within the mixed layer across the background region. The density range of Upper (Classical) Labrador Sea Water, 1027.68-1027.74 kg m⁻³ (1027.74-1027.80 kg m⁻³) is shown as horizontal black lines in (d).

The stratification strength for each eddy is shown in Figure 6.10b. While eddies generally start with strong stratification (3000-4500 J m^{-3}), this weakens quickly after being formed regardless of the time of the year. Eddies experience further weakening of their stratification strength during the convection season, causing their stratification to approach that of the background state of the Labrador Sea (median 1500-2500 J m^{-3}). Many eddies decay during the convective winter, as outlined above. Eddies that survive the convection season regain some stratification, likely from a combination of both atmospheric freshwater and net surface warming. However, eddies experience a weaker restratification than the background sea, likely due to their rotation reducing lateral buoyancy fluxes. A few of the long-lived eddies that experienced two winters show that their stratification was weaker during the second winter than the first. While only a handful of eddies survived long enough to experience some part of two convective winters, none experienced two complete convective seasons. Regardless of their starting stratification strength, longer-lived eddies were more likely to have weaker stratification upon their decay than shorter lived eddies. This is a product of enduring more time in a region with a net surface buoyancy loss, although it informs us that these long lived eddies will have different water mass properties than those which live for a shorter period of time.

This stratification strength gives a quantitative measure on how much energy must be removed such that the mixed layer will reach 2000m. However, it does not provide an actual depth of the mixed layer (Fig. 6.10c). Due to their initial strong stratification, Irminger Rings do not have a deep mixed layer when formed. However, fairly isolated from the surrounding Labrador Sea, these rings experience air-sea cooling, the erosion of their stratification, and subsequent deepening of their mixed layer. Eddies which experience a full convective winter have mixed layer depths that may reach 600-800m, although plenty of eddies did not experience much deepening of their mixed layer. Eddy trajectory appears important here; eddies which passed along the Labrador Coast tended to reach a mixed layer up to 800m while those that penetrated into the interior Labrador Sea reached up to 1400m (not shown). Three (of 158) eddies had a mixed layer which exceeded 1000m- these eddies lived longer than 300 days and experience some degree of two convective winters. Two of these eddies

nearly held the deepest mixed layer across the entire Labrador Sea between 2008 and 2009, years when the background Labrador Sea experienced significant deep convection. This suggests that long-lived Irminger Rings are capable of very deep convection- nearly the same depth as where deep convection generally occurs. Eddies which experienced only one convective winter were far less likely to have such a deep mixed layer, although some experienced mixing to a similar degree as the background Labrador Sea. Fewer Irminger Rings experienced a mixed layer depth surpassing 600m after the year 2013. We attribute some of this to some freshening which was taking place within the WGC (Fig. 6.3b; Supplemental Video 6.1) as well as fewer longer-lived Irminger Rings produced during this period.

Examination of the maximum potential density within each eddy's mixed layer (Fig. 6.10d) reiterates what has been stated above: Irminger Rings initially have relatively less dense water, although this density often increases after formation. The removal of buoyancy during the convection season increases the eddy's density, although eddies which survive or are formed right after the convection season have their maximum potential density decrease due to precipitation and surface heating. Long-lived eddies are more likely to have the highest density while the inverse is often true as well. Most eddies remain less dense than the background Labrador Sea (black line) which produces Labrador Sea Water each year. The horizontal black lines on this plot mark where the density is 1027.68, 1027.74, and 1027.8 kg m^{-3}- the density bounds of Upper and Classical Labrador Sea Water. Nine eddies lived long enough to lose enough stratification from surviving up to two convective winters, eventually producing a water mass with a density that could classify it as Labrador Sea Water. This occurred during 2008, 2009, 2010 and 2012, years with fairly strong convection across the Labrador Sea, although it did not occur during the 2014-2017 stretch which also contained strong convection (Fig. 6.10c). Eddies formed during these years held more freshwater which reduced the depth of mixing, producing lighter water within the eddy's core during winter.

Considering that eddies loosely follow the 3000m isobath (Fig. 6.6a), eddies that spawn further south may stay in deeper water than those which form further to the north. Figure 6.11 indicates the formation latitude of eddies which lived longer than 60

days as well as the depth of water where they decayed. While far more eddies were produced between 61°N and 62.5°N, these eddies not only were more likely to decay quicker but also at a shallower depth. These northern eddies were more likely to travel in shallower water and end up closer to the boundary current, increasing their transverse speed, effectively hastening their decay. This informs us that Irminger Rings' lifetime and trajectory are clearly influenced by the location at which they spawn. Eddies that spawn to the south are more likely to live longer and end up in deeper water- these are the potential Irminger Rings which may form LSW given two connective winters.
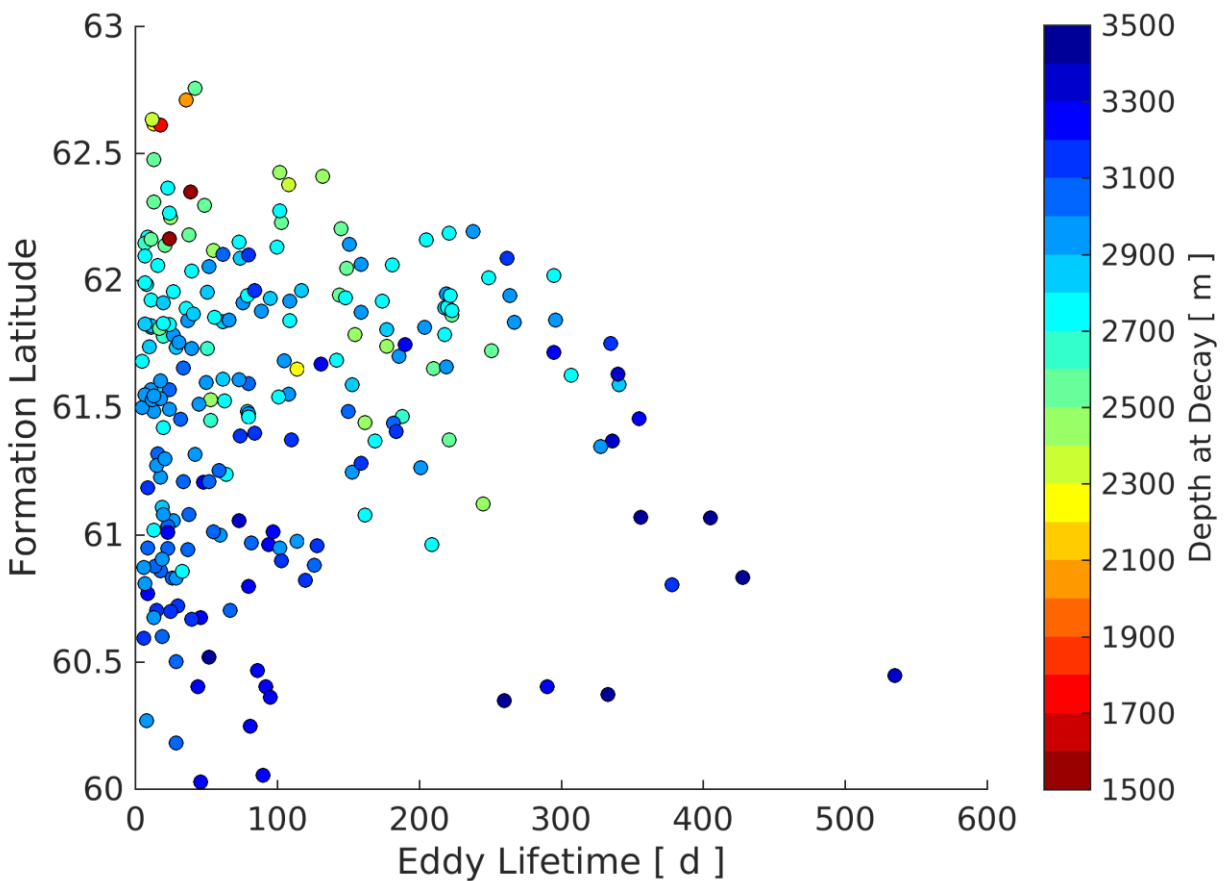
Figure 6. 11: Irminger Ring lifetime is compared against the formation latitude as well as the water column depth when the eddy decayed.

6.6. Discussion

A high-resolution numerical ocean configuration was carried out over the Labrador Sea. This 1/60° simulation was capable of resolving the fine scale processes which produce Irminger Rings from the West Greenland Current. We were able to detect and track 232 eddies over the 14 year integration period. These eddies were investigated on their initially strongly stratified properties and how these properties evolve as they transit within the Labrador Sea. Of the 232 tracked eddies, 158 survived longer than 30 days and 4 were detectable after 1 year. The longest lived eddy survived about 540 days- this is shorter than others who have identified that Irminger Rings may survive 2 full years (Lilly et al., 2003; Chanut et al., 2008). While this may imply that our Labrador Sea's circulation is faster than it should, or perhaps eddy tracking is not well suited for nearly-decayed eddies, we are still able to quantify how Irminger Rings evolve throughout their lifetime.

Irminger Rings typically travelled towards the southwest, flowing cyclonically around the Labrador Sea between the 2000m and 3000m isobath. Some eddies took a different route: a few went northwest and others travelled in a more southern route towards in the interior Labrador Sea. The trajectories, as well as distribution, match well with other who have modeled Irminger Rings at lower resolution (Chanut et al., 2008; de Jong et al., 2016). A disproportionate number of eddies decayed close in proximity to the formation region or north of Hamilton Bank along the Labrador Coast. We attribute the decay close to the formation region due to the large amount of eddy activity here- large meanders and turbulence often ripped eddies apart shortly after spawning. The decay occurring along the Labrador Coast is attributed to the sudden bend in topography, causing Irminger Rings to move into the Labrador Current, accelerating their decay. The area in-between these regions saw eddy decay as well, although we attribute this decay to a myriad of causes including eddy splitting, eddy merging, and deep convection. We further show that the latitude which these eddies spawn has a direct relationship on their trajectory and lifetime; eddies produced slightly further north are more likely to be influenced by the Labrador Current, increasing their translational speed and hastening their decay. Rings which form slightly further south,

while less common, experience a longer lifetime as they are more likely to stay within the interior Labrador Sea, well away from the boundary currents. These are the rings which are more likely to live to experience two convective winters.

Deep convection appears to be a major cause of eddy decay, judging strictly from the proportion of eddies which decay during the winter months. The intense vertical mixing during convection produces significant horizontal density gradients which may promote eddy decay. Furthermore, Irminger Rings, while initially strongly stratified, are still subject to air-sea buoyancy loss and experience convection as well. Irminger Rings thus require a greater amount of buoyancy loss to produce a vertically homogeneous layer to the same depth as the background Labrador Sea. A single convection winter will thus produce a mixed layer which extends to a shallower depth inside the eddy than outside. However, the homogenization of the water column may erode the eddy from the inside out, reducing rotation speed and promoting the depressed isopycnals to shoal.

Some eddies survive the winter convection season and may persist to endure a second one if conditions are right. While their rotation helps isolate these eddies from the surrounding water, they still experience an increase in their stratification strength via atmospheric freshwater and heating. This promotes these Irminger Rings to encounter a slower degree of restratification than the background sea. If such an eddy survives to endure a second convective winter, its relatively weak stratification may allow deep convection to surpass 1000m and even produce a water mass with density that matches Labrador Sea Water (1027.68 to 1027.80 kg m^{-3}). This suggests that Irminger Rings have a conflicting importance for the Labrador Sea: they clearly provide a substantial amount of buoyancy and limit convection, but a few of them can act as small sources for Labrador Sea Water production. Irminger Rings experiencing deep convection, particularly ones that endure two convective winters and associated surface cooling, was hinted at by Lilly et al. (2003), although they did not speculate on the formation of Labrador Sea Water within such an eddy. Our 14 year simulation had 9 of 232 eddies produce some volume of Labrador Sea Water. With a radius that is roughly 15 to 30 km (Lilly et al., 2003), one could roughly estimate the volume of Labrador Sea Water formed within LAB60's Irminger Rings to be 0.02 to .08 Sv, a small fraction compared to the full basin estimate from observations and models (2.0-9.0 Sv: see Table

1 from Courtois et al., 2020; 0.2 Sv: Pickart and Spall, 2007). Given recent OSNAP work suggests the formation rate is on the lower end of these estimates (Petit et al., 2020), and the fact that we had about ½ as many Irminger Rings produced as others have found (see above), this suggests that long-lived Irminger Rings may be responsible for up to 10% of the deepwater formed within the Labrador Sea; a non-negligible volume.

Considering that deep convection helps quickly decay Irminger Rings, we were surprised that rings which had a very thick freshwater layer, thus strong stratification, did not clearly survive longer then rings with weaker stratification. This was particularly the case after the year 2011, which had eddies with a thicker freshwater layer but shorter lifetime. Irminger Rings appear to have their freshwater layer quickly eroded from vertical mixing during the convective winter. Rings lose a considerable part of their stratification shortly after being formed- the additional stratification from a thicker freshwater layer may not be sufficient to reduce the degree of deep convection and allow the eddy to survive for a longer period of time. Instead, the vast heat reserve within Irminger Rings likely accounts for the majority of the stratification strength that must be overcome before deep convection can occur. As this takes considerable surface cooling, eddy lifetime appears far more related to the trajectory Irminger Rings transit through the Labrador Sea as we show proximity to boundary currents increases their decay rate. Rings which immediately drift southwards from the formation region appear the most likely to survive for a long period of time. These eddies are more likely to experience less interactions with other eddies and meanders, as well greater distance from the boundary currents and a resulting slower overall speed. This leaves them relatively free to drift and decay according to air-sea buoyancy fluxes and convective mixing rather than other influences.

Of our 232 tracked Irminger Rings, only 5 had cyclonic circulation (Supplemental Figure 6.1). And of these 5 rings, only one lived longer than 30 days, a far different ratio than what we found for anticyclonic eddies (157:227). While such few cyclonic eddies detected over 14 years did not yield enough data for thorough analysis, we briefly present some differences among Irminger Rings with different rotation. Cyclonic Irminger Rings tended to decay faster, have a smaller radius, hold about half the freshwater content and stratification strength, yet slightly more heat than anticyclonic

Irminger Rings (Supplemental Table 6.1). The literature shows that Irminger Rings can be either cyclonic or anticyclonic; with anticyclonic eddies spawning up to 15 times as frequent (Lilly et al., 2003). The reduced radius in our 5 cyclonic eddies might force the eddy detection and tracking software to incorrectly identify the decay of a cyclonic eddy more quickly than a larger anticyclonic eddy. However, this does not suggest why cyclonic Irminger Rings were relatively rare features within our LAB60 simulation. At first we suspected no-slip boundary conditions might limit the production of cyclonic eddies, but Rieck el al. (2019 and personal communication) confirms cyclonic eddies when using free-slip and no-slip lateral boundary conditions. Our 5 cyclonic Irminger Rings all happened within the last 5 years of our simulation, a period which the WGC and Labrador Sea were experiencing some freshening. We offer the suggestion that perhaps stronger baroclinic instability is needed for the formation of cyclonic Irminger Rings although the computational expense of our LAB60 simulation was too great to perform additional scenarios to investigate this. Furthermore, it may be a limitation of our selected eddy detection method as some upstream cyclonic eddies have potential vorticity signatures at depth and not always a velocity signature at the surface (Pacini et al., 2021).

We were able to estimate the integrated role of anticyclonic Irminger Ring (upper 2000m) from the WGC into the interior Labrador Sea. Approximately 17 eddies were produced each year, with a median radius around 23 km. Given this and the median freshwater thickness across all Irminger Rings was 4.4m, we find a yearly estimated Irminger Ring freshwater production rate of 4 mSv (relative to 34.8). This implies that Irminger Rings supply more freshwater to the inner Labrador Sea than ekman transport (1.5 mSv; Schulze-Chretien and Frajka-Williams, 2018), although Pennelly et al. (2017) find that about 20 mSv of freshwater leaves the western coast of Greenland. Irminger Rings appear to constitute about 20% of this flux. However, Irminger Rings deliver a substantial amount of heat: roughly 27 Gj m^{-2} each, translating to a heat production rate of 24 TW. This indicates that Irminger Ring's primary stratification role is thermally driven. Median eddy salt content was found to be 7500 kg m^{-2}, leading to a salt production rate of 7x10^6 kg s^{-1} by these rings. However, these results depend greatly on the eddy radius, which is sensitive to the eddy detection method used (Sun et al., 2017),

as well as the number of Irminger Rings which spawn per year. LAB60 underestimated this number by perhaps a factor of 2, so the observed freshwater, heat, and salt fluxes associate with Irminger Rings is likely greater. Cyclonic Irminger Rings were far less common, with a smaller radius, and would be expected to produce much less freshwater, salt, and heat to the interior Labrador Sea. However, we detected too few cyclonic Irminger Rings to run a proper analysis.

Our simulation differs from what others have found in regards to both the number of Irminger Rings and their travel speed. While we detected and tracked 232 eddies across 14 years of simulation output, others find more eddies produced per year (15-45, Lilly et al., 2003) than we do. Part of this would be the reduced number of cyclonic eddies we were able to detect and track (n=5). Others have found the ratio of anticyclonic to cyclonic eddy ratio to vary from 0.74:1 (de Jong et al., 2016) to 15:1 (Lilly et al., 2003), while we found approximately 55:1. Furthermore, our eddies had a median transverse speed of roughly 0.04 m s^{-1}, while other have found speeds of 0.05 m s^{-1} (Lilly et al., 2003) to 0.06 m s^{-1} (Katsman et al., 2004). Slower eddy speed implies that our eddies may live slightly longer, although we do not have any eddies which lived for 2 full years as Lilly et al. (2003) found. The eddy detection and tracking method may perform well for young energetic eddies but may falter for long-lived eddies with weak rotational speeds, underestimating the lifespan of Irminger Rings.

Our study adds much needed information regarding Irminger Rings and their stratification contribution to the Labrador Sea. We document how Irminger Rings evolve after their formation, a relatively untouched topic. Part of our research reveals that these eddies quickly lose their freshwater cap during the convective season, but their heat content keeps a mixed layer from exceeding 800m during their first convective season. Their freshwater content helps keep them stratified, but we find their heat reserve is more important for setting Irminger Ring's initial stratification. Thus upstream changes within the Irminger Current will affect the stratification of these eddies more than the East Greenland Current. Our work finds that the spawning frequency of Irminger Rings does not appear correlated to the freshwater and volume transport within the West Greenland Current, suggesting that the associated baroclinic/barotropic instability changes do not affect the production rate of Irminger

Rings. This suggests a changing climate may not experience a large change in the production rate of Irminger Rings. However, this was a bit of a surprise and we anticipate that large enough baroclinic/barotropic changes near the Irminger Ring spawning region would affect their formation frequency, rotation speed, radius, and water mass properties; we were just not able to confirm this with our 14 year simulation.

Perhaps our most interesting finding is that Irminger Rings can produce Labrador Sea Water given exposure to two convective winters. We find that both the relative formation region (slightly south) and spawning period (prior to winter) greatly help such eddies reach the interior Labrador Sea where they can slowly decay. This changes our previous notion of Irminger Rings in a substantial way; Irminger Rings were described as limiting deep convection within the Labrador Sea. We show that this is still the case, but the complete opposite also occurs under a rather limited set of conditions.

Having investigated 14 years of simulated Irminger Rings, from formation through their decay, certain questions still remain. While relatively isolated from surrounding water, there has been little effort to quantify the proportion of stratification loss/gain associated with air-sea fluxes against lateral fluxes. Most work, ours included, state that it is primarily via air-sea interactions, although we note subsurface changes deeper than the mixed layer indicating lateral fluxes clearly occur. These eddies have different surface/subsurface properties than the background Labrador Sea- they likely also experience different air-sea fluxes. A thicker fresh and cold layer should reduce heat loss during winter, but turbulent heat fluxes scale non-linearly according to the ocean-air differences, making eddy rotation and their water properties an interesting case of surface heat loss. Furthermore, the vast Irminger Water's heat reserve, if convected to the surface, will once again adjust the surface buoyancy flux. We didn't explicitly explore any variability in the instabilities inherent to the WGC that develop Irminger Rings; however we note that our 14 year simulation had little interannual variability in the number of Irminger Rings produced, their radius, or their energetics (not shown). Given the volume and freshwater transport within the WGC did experience interannual variability, Irminger Rings appear relatively unaffected, to some degree, by changes in WGC velocity and freshness. This appears counterintuitive as these changes should

modify the barotropic/baroclinic instability that exist in this region and promote Irminger Ring development; further research is warranted.

The mechanism which Irminger Rings decay also remains elusive. We show that they are far more likely to decay during the convective season, although we do not investigate the cause. Does deep convection outside the eddy produce significant baroclinicity that erodes the eddy from the outside, or does the eddy erode from within? Likely both may occur. Short lived eddies are more strongly stratified than the background sea, and outside convection should mix along the eddy front. Long-lived eddies that experience 2 winters may have a weaker stratification than the background Labrador Sea, and initiate their second deep convection before the water around them. These long-lived eddies are rather rare, but if they occur, may erode themselves from the inside.

The Labrador Sea is often studied due to its role of deep convection on the climate system. We understand that certain aspects of the Labrador Sea will occur in the future, such as the eventual gradual freshening that may prevent deep convection in the not-so-distant future (Böning et al., 2016). Will the freshening of the WGC produce stronger baroclinic instability, increasing the formation rate of Irminger Rings, altering their rotation speed and stratification? Small changes in the sub polar gyre and boundary current circulation would adjust barotropic instabilities, altering the eddy properties as well. The same can be asked for the Irminger Water layer which is heavily dependent on what occurs within the Irminger Basin and likely subject to large changes due to climate change (Lique and Thomas, 2018). In short, we are starting to have a good understanding regarding the influence Irminger Rings currently have on deep convection within the Labrador Sea, but there is limited understanding on what role they will have in the future.

6.7. Conclusions

A very-high resolution simulation (1/60°) was set up within the Labrador Sea to explore how Irminger Rings, eddies which spawn along the western coast of Greenland, evolve as they transit through the Labrador Sea. Our 14 year simulation produced 232

Irminger Rings, the vast majority which were anticyclonic. We show that small variations in the northward spawning position along the Greenland coast contribute to eddy lifetime and trajectory. More northern spawned Irminger Rings tended to encounter the Labrador Current and decay far quicker than those which formed slightly south. These southern eddies were slightly more likely to enter the interior Labrador Sea basin and have a longer lifetime. All Irminger Rings spawned with a thick freshwater layer that is quickly mixed away during the convective winter, but their substantial heat reserve within the Irminger Water layer was far more difficult to erode. This indicates that Irminger Ring's stratification is primarily thermally driven. While rare, eddies which survived to experience two convective winters had their heat reserve eroded and experienced deep convection such that they had produced water with a density that matches Labrador Sea Water.

Acknowledgements

Bibliography

Aagaard, K. and Carmack, E.C.: The role of sea ice and other fresh water in the Arctic Circulation. Journal of Geophysical Research: Oceans, 94(C10), 1989.

Barnier, B., Madec, G., Penduff, T., Molines, J-M., Treguier, A-M., Le Sommer, J., Beckmann, A., Biastoch, A., Böning, C., Dengg, J., Derval, C., Durand, E., Gulev, S., Remy, R., Talandier, C., Theetten, S., Maltrud, M., Mcclean, J., and De Cuevas, B.: Impact of partial steps and momentum advection schemes in a global ocean circulation model at eddy permitting resolution. Ocean Dynamics, 56 (5-6), 543-567, 2006.

Böning, C.W., Behrens, E., Biastoch, A., Getzlaff, K., and Bamber, J.L.: Emerging impact of Greenland meltwater on deepwater formation in the North Atlantic Ocean. Nature Geoscience, 97(7), 523, 2016.

Buckley, M.W., and Marshall, J.: Observations, inferences, and mechanisms of the Atlantic Meridional Overturning Circulation: A review. Reviews of Geophysics, 54(1), 5-63, 2016.

Chanut, J., Barnier, B., Large, W., Debreu, L., Penduff, T., Molines, J.M., and Mathiot, P.: Mesoscale eddies in the Labrador Sea and their contribution to convection and restratification. Journal of Physical Oceanography, 28(8), 1617-1643, 2008.

Courtois, P., Hu, X., Pennelly, C., Spence, P., and Myers, P.G.: Mixed layer depth calculation in deep convection regions in ocean numerical models. Ocean Modelling, 120, 60-78, 2017.

Cuny, J., Rhines, P.B., Niiler, P.P., Bacon, S.: Labrador Sea boundary currents and the face of the Irminger Sea Water, Journal of Physical Oceanography, 32(2), 2002

Cuny, J., Rhines, P.B., and Kwok, R.: Davis Strait volume, freshwater and heat fluxes. Deep Sea Research Part I: Oceanographic Research Papers, 52.3, 519-542, 2005.

Curry, B., Lee, C.M., Petrie, B., Moritz, R.E. and Kwok, R.: Multiyear volume, liquid freshwater, and sea ice transports through Davis Strait, 2004-10. Journal of Physical Oceanography, 44(4), 1244-1266, 2014.

de Jong, M.F., Bower, A.S., Furey, H.H. Two years of observations of warm-core anticyclones in the Labrador Sea and their seasonal cycle in heat and salt stratification. Journal of Physical Oceanography, 44(2), 427-444, 2014.

de Jong, M.F., Bower, A.S., Furey, H.H. Seasonal and interannual variations of Irminger Ring formation and boundary-interior heat exchange in FLAME. Journal of Physical Oceanography, 46(6), 1717-1734, 2016.

de Steur, L., Peralta-Ferriz, C. and Pavlova, O.: Freshwater export in the East Greenland Current freshens the North Atlantic. Geophysical Research Letters, 45, 13359-13366, 2018.

Debreu, L., Vouland, C., and Blayo, E.: AGRIF: Adaptive grid refinement in Fortran. Computers and Geosciences, 34(1), 8-13, 2008.

Doglioli, A.M., Blanke, B., Speich, S., Lapeyre, G. Tracking coherent structures in a regional ocean model with wavelet analysis: Application to Cape Basin eddies. Journal of Geophysical Research: Oceans, 112(C5), 2007.

Dussin, R., Barnier, B., and Brodeau, L.: The making of Drakkar forcing set DFS5, Grenoble, France: LGGE, 2016.

Eden, C. and Böning, C. Sources of eddy kinetic energy in the Labrador Sea. Journal of Physical Oceanography, 32(12), 3346-3363,2002

Ferry, N., Parent, L., Garric, G., Barnier, B., and Jourdain, N.C.: Mercator global eddy permitting ocean reanalysis GLORYS1V1: Description and results. Mercator-Ocean Quarterly Newsletter, 36, 15-27, 2010.

Feucher, C., Garcia-Quintana, Y., Yashayaev, I., Hu, X., Myers, P.G.: Labrador Sea Water formation rate and its impact on the local Meridional Overturning Circulation. Journal of Geophysical Research: Oceans, 124(8), 5654-5670, 2019.

Fichefet, T., and Maqueda, M.A.M.: Sensitivity of a global sea ice model to the treatment of ice thermodynamics and dynamics. Journal of Geophysical Research: Oceans, 102(C6), 12609-12646, 1997.

Frajka-Williams, E., Rhines, P.B., and Eriksen, C.C.: Horizontal stratification during deep convection in the Labrador Sea. Journal of Physical Oceanography, 44(1), 220-228, 2014.

Garcia-Quintana, Y., Courtois, P., Hu, X., Pennelly, C., Kieke, D., & Myers, P.G.: Sensitivity of Labrador Sea Water formation to changes in model resolution,

atmospheric forcing, and freshwater input. Journal of Geophysical Research: Oceans, 124(3), 2126-2152, 2019.

Gelderloos, R., Katsman, C.A. and Drijfhout, S.S.: Assessing the roles of three eddy types in restratifying the Labrador Sea after deep convection. Journal of Physical Oceanography, 41(11), 2102-2119, 2011.

Hátún, H., Eriksen, C.C., and Rhines, P.B.: Buoyant eddies entering the Labrador Sea observed with gliders and altimetry. Journal of Physical Oceanography, 37(12), 2838-2854, 2007.

Holdsworth, A.M. and Myers, P.G. The influence of high-frequency atmospheric forcing on the circulation and deep convection of the Labrador Sea. Journal of Climate, 28(12), 4980-4996, 2015.

Hersbach, H., and Dee, D.J.E.N.: ERA5 reanalysis is in production. ECMWF newsletter, 147(7), 5-6, 2016.

Holte, J., and Talley, L.: A new algorithm for finding mixed layer depths with applications to Argo data and Subantarctic Mode Water formation. Journal of Atmospheric and Oceanic Technology, 26(9), 1920-1939, 2009.

Katsman, C.A., Spall, M.A., Pickart, R.S. Boundary current eddies and their role in the restratification of the Labrador Sea. Journal of Physical Oceanography, 34(9), 1967-1983, 2004.

Lab Sea Group: The Labrador Sea deep convection experiment. Bulletin of the American Meteorological Society, 79(10), 2033-2058, 1998.

Lazier, J., Hendry, R., Clarke, A., Yashayaev, I., Rhines, P. Convection and restratification I the Labrador Sea, 1990-2000. Deep Sea Research Part I: Oceanographic Research Papers, 49(10), 1819-1835, 2002.

Lazier, J.R.N., and Wright, D.G.: Annual velocity variations in the Labrador Current, Journal of Physical Oceanography, 23(4), 659-678, 1993.

Lilly, J.M., Rhines, P.B., Schott, F., Lavender, K., Lazier, J., Send, U., and D'Asaro, E.: Observations of the Labrador Sea eddy field. Progress in Oceanography, 59(1), 75-176, 2003.

Lique, C. and Thomas, M.D. Latitudinal shift of the Atlantic Meridional Overturning Circulation source regions under a warming climate. Nature Climate Change, 8(11), 1013-1020, 2018.

Lozier, M.S., Li, F., Bacon, S., Bahr, F., Bower, A.S., Cunningham, S.A., de Jong, M.F., de Steur, L., DeYoung, B., Fischer, J. and Gary, S.F.: A sea change in our view of overturning in the subpolar North Atlantic. Science, 363(6426), 516-521, 2019.

Luo, H., Castelao, R.M., Rennermalm, A.K., Tedesco, M., Bracco, A., Yager, P.L., Mote, T.L. Oceanic transport of surface meltwater from the southern Greenland ice sheet. Nature Geoscience, 9(7), 528, 2016.

Kieke, D., Klein, B., Stramma, L., Rhein, M., and Koltermann, K.P.: Variability and propagation of Labrador Sea Water in the southern subpolar North Atlantic. Deep Sea Research Part I: Oceanographic Research Papers, 56(10), 1656-1674, 2009.

Madec, G.: Note du Pôle de modélisation. Institut Pierre-Simon Laplace (IPSL), France, No 27, ISSN No 1288-1619, 2008.

Marshall, J. and Schott, F.: Open-ocean convection: Observations, theory, and models. Reviews of Geophysics, 37(1), 1-64, 1999.

Marzocchi, A., Hirschi, J.J.M., Holliday, N.P., Cunningham, S.A., Blaker, A.T. and Coward, A.C.: The North Atlantic subpolar circulation in an eddy-resolving global ocean model. Journal of Marine Systems, 142, 126-143, 2015.

Müller, V., Kieke, D., Myers, P.G., Pennelly, C., and Mertens, C.: Temperature flux carried by individual eddies across 47° in the Atlantic Ocean. Journal of Geophysical Research: Oceans, 122(3), 2441-2464, 2017.

Müller, V., Kieke, D., Myers, P.G., Pennelly, C., Steinfeldt, R., and Stendardo, I.: Heat and freshwater transport by mesoscale eddies in the southern subpolar North Atlantic. Journal of Geophysical Research: Oceans, 124(8), 5565-5585, 2019.

Myers, P.G., Josey, S.A., Wheler, B., Kulan, N. Interdecadal variability in Labrador Sea precipitation minus evaporation and salinity. Progress in Oceanography, 73(3-4), 341-357, 2007.

Myers, P.G., Donnelly, C., Ribergaard, M.H. Structure and variability of the West Greenland Current in Summer derived from 6 repeat standard sections. Progress in Oceanography, 80(1-2), 93-112, 2009

Nencioli, F., Dong, C., Dickey, T., Washburn, L., McWilliams, J.C. A vector geometry-based eddy detection algorithm and its application to a high-resolution numerical model product and high-frequency radar surface velocities in the Southern California Bight. Journal of atmospheric and oceanic technology, 27(3), 564-579, 2010.

Pacini, A., Pickart, R.S., Le Bras, I.A., Straneo, F., Holliday, N.P., Spall, M.A.: Cyclonic eddies in the West Greenland boundary current system. Journal of Physical Oceanography, 2021.

Pennelly, C. and Myers, P.G.: Introducing LAB60: A 1/60° NEMO 3.6 numerical simulation of the Labrador Sea. Geoscientific Model Development, 13(10), 4959-4975, 2020

Pennelly, C., Hu, X. and Myers, P.G.: Cross-isobath freshwater exchange within the North Atlantic subpolar gyre. Journal of Geophysical Research: Oceans, 124, 6831-6853, 2019.

Petit, T., Lozier, M.S., Josey, S.A. and Cunningham, S.A.: Atlantic deep water formation occurs primarily in the Iceland Basin and Irminger Sea by local buoyancy forcing. Geophysical Research Letters, 47(22), 2020.

Pickart, R.S. and Spall, M.A.: Impact of Labrador Sea convection on the North Atlantic meridional overturning circulation. Journal of Physical Oceanography, 37(9), 2207-2227, 2007.

Pickart, R.S., Torres, D.J., & Clarke, R.A.: Hydrography of the Labrador Sea during active convection. Journal of Physical Oceanography., 32(2), 428-457, 2002.

Rattan, S., Myers, P.G., Treguier, A.M., Theetten, S., Biastoch, A. and Böning, C.: Towards an understanding of Labrador Sea salinity drift in eddy-permitting simulations. Ocean Modelling, 35(1-2), 77-88, 2010.

Rhein, M., Steinfeldt, R., Kieke, D., Stendardo, I., Yashayaev, I. Ventilation variability of Labrador Sea Water and its effects on oxygen and anthropogenic carbon: a review. Philosophical Transactions of the Royal Society A: Mathematical, Physical and Engineering Sciences, 374(2102), 20160321, 2017.

Rieck, J.K., Böning, C.W., and Getzlaff, K.: The nature of eddy kinetic energy in the Labrador Sea: Different types of mesoscale eddies, their temporal variability, and impact on deep convection. Journal of Physical Oceanography, 49(8), 2075-2094, 2019.

Rykova, T. Straneo, F., Bower, A.S. Seasonal and interannual variability of the West Greenland Current System in the Labrador Sea in 1993-2008. Journal of Geophysical Research: Oceans, 120(2), 1318-1332, 2015.

Sathiyamoorthy, S. and Moore G.K., Buoyancy flux at ocean weather station Bravo. Journal of Physical Oceanography, 31(2), 458-474, 2002.

Schouten, M.W., de Ruiter, W.P.M., van Leeuwn P.J.: Translation, decay and splitting of Agulhas rings in the southeastern Atlantic Ocean. Journal of Geophysical Research, 14(c9), 21913-21925, 2000.

Schulze-Chretien, L.M. and Frajka-Williams, E.: Wind-driven transport of fresh shelf water into the upper 30 m of the Labrador Sea. Ocean Science, 14(5), 1247-1264, 2018.

Schulze-Chretien, L.M., Pickart, R.S., & Moore, G.W.K.: Atmospheric forcing during active convection in the Labrador Sea and its impact on mixed-layer-depths. Journal of Geophysical Research: Oceans, 121(9), 6978-6992, 2016.

Smith, G.C., Roy, F., Mann, P., Dupont, F., Brasnett, B., Lemieux, J.F., Laroche, S., and Bélair, S.: A new atmospheric dataset for forcing ice-ocean models: Evaluation of

reforecasts using the Canadian global deterministic prediction system. Quarterly Journal of the Royal Meteorological Society, 140(680), 881-894, 2014.

Sun, M., Tian, F., Liu, Y., Chen, F. An improved automatic algorithm for global eddy tracking using satellite altimetry data. Remote Sensing, 9(3), 206, 2017.

Tagklis, F., Bracco, A., Ito, T. and Castelao, R.M. Submesoscale modulation of deep water formation in the Labrador Sea. Scientific Reports, 10(1), 1-13, 2020.

Weiss, J. The dynamics of enstrophy transfer in two-dimensional hydrodynamics. Physica D: Nonlinear Phenomena, 48(2-3), 273-294, 1991.

Yang, Q., Dixon, T.H., Myers, P.G., Bonin, H., Chambers, D., Van Den Broeke, M.R., Ribergaard, M.H. and Mortensen, J.: Recent increases in Arctic freshwater flux affects Labrador Sea convection and Atlantic overturning circulation. Nature Communications, 7(1), 1-8, 2016.

Yashayaev, I.: Hydrographic changes in the Labrador Sea, 1960-2005. Progress in Oceanography, 73(3-4), 242-276, 2007.

Yashayaev I., and Loder, J.W. Recurrent replenishment of Labrador Sea Water and associated decadal-scale variability. Journal of Geophysical Research: Oceans, 121, 8095-8114.

Supplemental Material
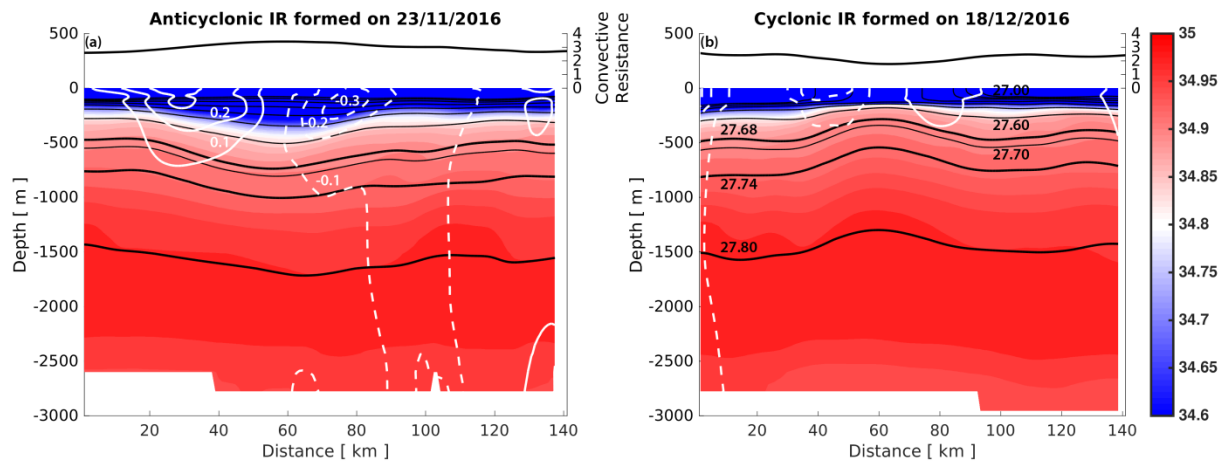
Supplemental Figure 6.1: East-west cross section through an anticyclonic (a) and cyclonic (b) Irminger Ring which were formed a few weeks apart in late 2016. Colored contours indicate the salinity, black contours identify isopycnals (interval 0.1 kg m^{-3}), and solid (dashed) white contours the northward (southward) velocity (interval 0.1 ms^{-1}). The thick black contours identify the bounds of Upper Labrador Sea Water (1027.68 to 1027.74 kg m^{-3}) and Classical Labrador Sea Water (1027.74 to 1027.80 kg m^{-3}). Convective Resistance, the black line on the top of each subpanel, has units of kJ m^{-3}.

Supplemental Table 6.1: Various differences between the formation properties of anticyclonic and cyclonic Irminger Rings are shown here. Other than the number of eddies, properties are given by the median value while the standard deviation is given in the square brackets. Salt and heat content is normalized by the surface area. Values are derived from the upper 2000m within each eddy.

	Anticyclonic	Cyclonic
Number of eddies	227	5
Lifetime [d]	73 [100]	32 [23]
Radius [km]	23 [5]	17 [4]
Freshwater Layer Thickness [m]	4.4 [2.0]	2.1 [0.9]
Salt Content [kg m^{-2}]	7500 [84]	7500 [30]
Heat Content [Gj m^{-2}]	27 [2]	31 [2]
Convective Resistance [kJ m^{-3}]	3.4 [0.4]	1.8 [0.2]

Supplemental Video 6.1: Freshwater layer thickness (relative to a salinity of 34.8) for the LAB60 simulation from 2005 through the end of 2018. https://doi.org/10.7939/r3-vcdp-sc81

Chapter 7: Conclusions and future work

The Labrador Sea is a region where stratification heavily influences the production of deepwater, a crucial component in the meridional overturning circulation of heat and dissolved gasses. This stratification can be modified via any source that changes the heat or salinity of the ocean: precipitation, evaporation, radiation, sea ice melt/formation, as well as heat and salt advection are a few sources that modify the ocean's stratification. This thesis uses a numerical model to investigate some of these sources in a region that is difficult to observe. The three main goals of this thesis are:

1. Understand the relative regional importance where freshwater within the boundary currents are exported towards the interior Labrador Sea basin.
2. Investigate how sensitive Labrador Sea Water formation is to various realistic atmospheric forcing products.
3. Explore the evolution of eddies which form along the west Greenland coast and travel into the interior basin, supplying heat and freshwater.

7.1 Primary findings

7.1.1. Regional shelf-basin freshwater exchange

This study showed that the eastern portion of the Labrador Sea is the primary supplier of freshwater which leaves the boundary currents and enters the interior basin. The western portion, including the Labrador coast, either has onshore exchange of freshwater, or relatively little offshore transport. After decomposing the transport into both mean and turbulent components, we learn that freshwater is exported across all regions of the Labrador Sea via turbulent transport (i.e. eddy fluxes), but often the mean transport acts in the opposite direction with a larger magnitude. This forces many regions to have a net freshwater flux towards the shore. The use of higher-resolution eddy-resolving configurations at 1/12° did not change the main findings above considerably. We also find a substantial volume of Irminger Water leaving the west

Greenland coast only to return along the other region's coastlines. This represents a significant amount of saltwater which leaves the interior Labrador Sea but does not provide insight on any shelf-basin exchange of heat. Lastly, we examine Labrador Sea Water which primarily leaves the interior deep basin and crosses the 2000m isobath along the northern Labrador coast. Given its close proximity to the convection region, this is the only region to experience seasonal variability in the shelf-basin exchange of LSW.

This study updates our knowledge regarding the shelf-basin transport of freshwater. Earlier studies have noted that the western Greenland coastline has a significant offshore transport of freshwater (Myers et al., 2009; Schmidt and Send, 2007) and perhaps the same along the Labrador coast (McGeehan and Maslowski, 2011; Myers, 2005; Schulze-Chretien and Frajka-Wlliams, 2018). I now document the remaining regions around the Labrador Sea and their relative offshore freshwater transport. My results corroborate with what others find along the western Greenland coast, but suggest that the net freshwater transport across all other regions either acts to freshen the boundary currents or have little overall effect. The use of various resolution simulations helps close this open topic regarding freshwater transport along the Labrador coastline. These results help identify what possible future warming and melting scenarios may indicate for the Labrador Sea: extra freshwater from upstream Davis or Hudson Strait will have relatively little impact on convection within the Labrador Sea. Any freshening within the East or West Greenland Current will add additional freshwater, strengthening the stratification, and making convection more difficult to begin. While this study quantifies the exchange, we only decomposed the transport into mean and turbulent components. Further research remains to investigate the source of our 'turbulent' transport, further quantifying the transport associated with eddies, mesoscale features, Ekman transport, etc.

7.1.2. Impact of different atmospheric forcing sets on modelling Labrador Sea Water production

This study examined the response of the Labrador Sea to various atmospheric forcing datasets when driving NEMO simulations. I show that forcing data not limited to precipitation, near-surface temperature, and wind speed influenced the net surface buoyancy loss. The resulting yearly net surface heat flux differed between simulations by up to 12 W m^{-2} when averaged over the interior Labrador Sea. Simulations with larger heat loss endured a deeper mixed layer, weaker stratification, and denser Labrador Sea Water. However, we found that the production volume of LSW was not as clearly affected by these datasets- larger heat losses didn't indicate more/less LSW was being formed. This study builds on others who have examined the Labrador Sea's response to atmospheric forcing. Bramson (1997), Garcia-Quintana et al. (2019), and Holdsworth and Myers (2015) significantly modified their forcing over the Labrador Sea and also found the above conclusions. We show that the innate variability between forcing sets is enough to drive large changes in LSW; modified forcing is not necessary albeit they indicate areas of sensitivity. As there are many different atmospheric datasets using data assimilation and bias correction to reduce errors, simulations forced with such data will still encounter differences in the density of LSW. This has implications on lengthy climate simulations as a few extra W m^{-2} is enough to drive changes in the density of LSW within a decade. These density changes indicate that a potential density classification of LSW may not be suitable, particularly so for climate simulations. Other methods of partitioning LSW may be required; I used a method from Feucher et al. (2019) that allows LSW to have a changing density criteria based on the subduction rate.

This study presents further research questions. We suspect that deepwater formed in regions other than the Labrador Sea would also be affected by such surface forcing, although further research would be required to confirm this. The role that spatial and temporal resolution of each forcing dataset contributes to the air-sea buoyancy flux in the Labrador Sea is an open question. Higher-resolution forcing datasets may inherently remove more heat from the Labrador Sea compared to their lower-resolution counterparts (Condron and Renfrew, 2013; Jung et al., 2014) due to

stronger wind speeds and better defined wind gusts and the resulting turbulent heat loss. This study's results may be quite different if coupled ocean-atmosphere simulations were carried out rather than ocean simulations forced by atmospheric data. The coupling feedback may reduce the net surface heat loss differences between realistically forced simulations; however, we still suspect our conclusions would hold valid.

7.1.3. Tracking Irminger Rings' properties using a sub-mesoscale ocean model

In this study I used a sub-mesoscale (1/60°) simulation to fully resolve coherent eddies which form from instabilities generated along the west Greenland coastline near Cape Desolation. These eddies are very buoyant and travel into the interior Labrador Sea, increasing the stratification strength of the Labrador Sea, impacting the location and strength of deep convection. I identify and track Irminger Rings from 15 years of simulation output, allowing for an investigation on how these eddies evolve. I show that their spawning latitude impacts their trajectory as well as lifetime. Boundary currents around the Labrador Sea appear to be one major cause which decays these eddies- the other is deep convection. Most eddies live for a few months, although a few live for longer than one year. I show that long lived eddies may experience 2 convective winter seasons, removing enough stratification that LSW is formed within their core. Eddies that spawn slightly to the south of the formation region are far more likely to survive long enough for this to occur. Irminger Rings producing LSW, while relatively rare, is rather different than the previous description of Irminger Rings: supplying heat and freshwater to the interior Labrador Sea, reducing the extent and depth of convection. I show that this is still the case for the vast majority of Irminger Rings, but a few Irminger Rings are also able to enhance the local production of LSW. Furthermore, I show that Irminger Rings' stratification strength lies primarily within its heat core, not their freshwater cap. Irminger Rings' freshwater cap is quickly eroded, but most Irminger Rings retain a significant portion of their starting heat capacity. It takes 2 convective winters to erode this layer, allowing for LSW production.

This study was the first to document the evolution of Irminger Rings from birth until decay. Others have investigated how they spawn at (Eden and Böning, 2002), their trajectory (Chanut et al., 2008), translational speed (Katsman et al., 2004), and freshwater/heat content (Hatún et al., 2007). Lilly et al. (2003) even hints at the production of LSW within their core but did not go far enough to explain how this occurred. However, much remains to be investigated. I find that Irminger Ring's experience modifications to their water mass properties below the mixed layer depth-they do not appear as isolated from lateral fluxes as many often assumed. Understanding their lateral fluxes more would help us further understand Irminger Ring's role in stratifying the Labrador Sea. These rings also did not appear to increase in strength or frequency throughout our 15 year simulation, but we suspect baroclinic/barotropic changes within the WGC should impact their formation strength and rate. Further research on this is warranted given a changing climate. Lastly, my simulation only produced a handful of cyclonic Irminger Rings when many more were expected to occur. We are not sure why the NEMO model produced a distinct lack of cyclonic Irminger Rings, but it is worth investigating as it might be of importance in other regions where sub-mesoscale modelling is required to resolve small scale features that exert a strong influence on some nearby phenomena.

7.2. Thesis summary

This thesis was designed to explore factors which impact the stratification strength within the Labrador Sea and influence deep convection. I used a variety of NEMO simulations with a horizontal resolution that varied from 1/4° to 1/60°. Low resolution simulations were adequate for exploring how atmospheric forcing datasets influence LSW production as they often had coarser resolution. Eddy effects and mesoscale features were less likely to be represented at 1/4° and I also used 1/12° simulations to explore regional cross-shelf freshwater transport. Finally, tracking individual eddies and their contribution to setting the stratification within the Labrador Sea requires an eddy-resolving model; so I built a complex 1/60° simulation to explore this topic. From these three topics I present the following contributions to our current understanding of stratification within the Labrador Sea:

- The western coast of Greenland is the primary supplier of freshwater from its shelf into deeper water.
- The remaining regions around the Labrador Sea either supply freshwater from the deep basin towards the shelf, or transport relatively little freshwater offshore.
- Variations in realistic atmospheric forcing datasets can produce changes in Labrador Sea Water density; although the production volume of LSW is less affected.
- Irminger Rings shed from the western coast of Greenland carry a substantial amount of buoyant water via their subsurface heat core
- Irminger Rings which experience two convective winters may have their heat core eroded sufficiently such that they produce Labrador Sea Water within their core before they decay.

Bibliography

References:

Aagaard, K. and Carmack, E.C. (1989): The role of sea ice and other fresh water in the Arctic Circulation, *Journal of Geophysical Research: Oceans*, 94(C10).

Amante, C. and Eakins, B.W. (2009): ETOPO1 1 Arc-minute global relief model: procedures data sources and analysis, *NOAA Technical Memorandum NESDIS*, NGDC-24 19.

Asselin, R. (1972): Frequency filter for time integrations, *Monthly Weather Review,* 100(6), 487-490.

Avisc, T., Karstensen, J., Send, U. and Fischer, J. (2006): Interannual variability of newly formed Labrador Sea Water from 1994 to 2005, *Geophysical Research Letters*, 33, 6p.

Bacon, S., Gould, W.J. and Jia, Y. (2003): Open-ocean convection in the Irminger Sea, *Geophysical Research Letters*, 30(5), 4p.

Bamber, J., van den Broeke, M., Ettema, J., Lenaerts, J. and Rignot, E. (2012): Recent large increases in freshwater fluxes from Greenland into the North Atlantic, *Geophysical Research Letters*, 39, 1-4p.

Barnier, B., Madec, G., Penduff, T., Molines, J-M., Treguier, A-M., Le Sommer, J., Beckmann, A., Biastoch, A., Böning, C., Dengg, J., Derval, C., Durand, E., Gulev, S., Remy, R., Talandier, C., Theetten, S., Maltrud, M., Mcclean, J. and De Cuevas, B. (2006): Impact of partial steps and momentum advection schemes in a global ocean circulation model at eddy permitting resolution, *Ocean Dynamics*, 56 (5-6), 543-567.

Belkin, I.M., Levitus, S., Antonov, J. and Malmberg, S.A. (1998): "Great salinity anomalies" in the North Atlantic, *Progress in Oceanography,* 41(1), 1-68.

Benetti, M., Reverdin, G., Yashayaev, I., Holliday, N.P., Tynan, E., Torres-Valdes, S., Lherminier, P., Tréguer, P. and Sarthou, G. (2017): Composition of freshwater in the

spring of 2014 on the southern Labrador shelf and slope, *Journal of Geophysical Research: Ocean*, 122(2), 1102-1121.

Böning, C.W., Behrens, E., Biastoch, A., Getzlaff, K. and Bamber, J.L. (2016): Emerging impact of Greenland meltwater on deepwater formation in the North Atlantic Ocean, *Nature Geoscience*, 97(7), 523.

Bouillon, S., Maqueda, M.A.M., Legat, V. and Fichefet, T. (2009): An elastic-viscous-plastic sea ice model formulated on Arakawa B and C grids, *Ocean Modelling*, 26(3-4), 174-184.

Bramson, L.S. (1997): Air-sea interactions and deep convection in the Labrador Sea, M.S. thesis, Dept. of Oceanography, Naval Postgraduate School, 115 pp.

Brossier, C.L., Léger, L., Giordani, H.,Beuvier, J., Bouin, M.N., Ducrocq, W. and Fourrié, N. (2017): Dense water formation in the north-western Mediterranean area during HyMeX-SOP2 in 1/36° ocean simulations: Ocean-atmosphere coupling impact, *Journal of Geophysical Research: Oceans*, 122(7), 5749-5773.

Bryden, H.L., Longworth, H.R. and Cunningham, S.A. (2005): Slowing of the Atlantic meridional overturning circulation at 25°N, *Nature*, 438(7068), 655.

Buckley, M.W., and Marshall, J. (2016): Observations, inferences, and mechanisms of the Atlantic Meridional Overturning Circulation: A review, *Reviews of Geophysics*, 54(1), 5-63.

Cael, B.B. and Jansen, M.F. (2020): On freshwater fluxes and the Atlantic meridional overturning circulation, *Limnology and Oceanography,* 5(2), 185-192.

Chaudhuri, A.H., Ponte, R.M. and Forget, G. (2016): Impact of uncertainties in atmospheric boundary conditions on ocean model solutions, *Ocean Modelling*, 100, 96-108.

Chanut, J., Barnier, B., Large, W., Debreu, L., Penduff, T., Molines, J.M. and Mathiot, P. (2008): Mesoscale eddies in the Labrador Sea and their contribution to convection and restratification, *Journal of Physical Oceanography*, 28(8), 1617-1643.

Chassignet, E.P. and Xu, X. (2017): Impact of horizontal resolution (1/12 to 1/50) on Gulf Stream separation, penetration, and variability, *Journal of Physical Oceanography*, 47(8), 1999-2021.

Chen, X. and Tung, K.K. (2018): Global surface warming enhanced by weak Atlantic overturning circulation, *Nature*, 559(7714), 387.

Condron, A. and Renfrew, I.A. (2013): The impact of polar mesoscale storms on northeast Atlantic Ocean circulation, *Nature Geoscience,* 6(1), 34-37.

Courant, R., Friedrichs, K. and Lewy, H. (1928): Über die partiellen Differenzengleichugen der mathematischen Physik, *Mathematische Annalen*, 100, 32-74.

Courtois, P., Hu, X., Pennelly, C., Spence, P. and Myers, P.G. (2017): Mixed layer depth calculation in deep convection regions in ocean numerical models, *Ocean Modelling*, 120, 60-78.

Cuny, J., Rhines, P.B., Niiler, P.P. and Bacon, S. (2002): Labrador Sea boundary currents and the fate of the Irminger Sea Water, *Journal of Physical Oceanography*, 32(2), 627-647.

Cuny, J., Rhines, P.B. and Kwok, R. (2005): Davis Strait volume, freshwater and heat fluxes, *Deep Sea Research Part I: Oceanographic Research Papers*, 52.3, 519-542.

Curry, B., Lee, C.M. and Petrie, B. (2011): Volume, freshwater, and heat fluxes through Davis Strait, 2004-05, *Journal of Physical Oceanography*, 41(3), 429-436.

Curry, B., Lee, C.M., Petrie, B., Moritz, R.E. and Kwok, R. (2014): Multiyear volume, liquid freshwater, and sea ice transports through Davis Strait, 2004-10, *Journal of Physical Oceanography*, 44(4), 1244-1266.

Curry, R.G., McCartney, M.S. and Joyce, T.M. (1998): Oceanic transport of subpolar climate signals mid-depth subtropical waters, *Nature*, 391(6667), 575.

Dai, A., Qian, T., Trenberth, K.E. and Milliman, J.D. (2009): Changes in continental freshwater discharge from 1948 to 2004, *Journal of Climate*, 22(10), 2773-2792.

de Jong, M.F., Bower, A.S. and Furey, H.H. (2014): Two years of observations of warm-core anticyclones in the Labrador Sea and their seasonal cycle in heat and salt stratification, *Journal of Physical Oceanography*, 44(2), 427-444.

de Jong, M.F., Bower, A.S. and Furey, H.H. (2016): Seasonal and interannual variations of Irminger Ring formation and boundary-interior heat exchange in FLAME, *Journal of Physical Oceanography*, 46(6), 1717-1734.

de Steur, L., Hansen, E., Gerdes, R., Karcher, M., Fahrbach, E. and Holfort, J. (2009): Freshwater fluxes in the East Greenland Current: A decade of observations, *Geophysical Research Letters*, 36(23).

de Steur, L., Peralta-Ferriz, C. and Pavlova, O. (2018): Freshwater export in the East Greenland Current freshens the North Atlantic, *Geophysical Research Letters*, 45, 13359-13366.

Debreu, L., Vouland, C. and Blayo, E. (2008): Agrif: Adaptive grid refinement in fortran, *Computers and Geosciences*, 34, 8-13.

Dee, D.P., Uppala, S.M., Simmons, A.J., Berrisford, P., Poli, P., Kobayashi, S., et al. (2011): The ERA-Interim reanalysis: configuration and performance of the data assimilation system, *Quarterly Journal of the Royal Meteorological Society*, **137**, 553-597.

Dengler, M., Fischer, J., Schott, F.A. and Zantopp, R. (2006): Deep Labrador Current and its variability in 1996-2005, *Geophysical Research Letters*, 13, 1-5p.

Dickson, R., Rudels, B., Dye, S., Karcher, M., Meincke, J. and Yashayaev, I. (2007): Current estimates of freshwater flux through Arctic and subarctic seas, *Progress in Oceanography*, 73(3-4), 210-230.

Doglioli, A.M., Blanke, B., Speich, S. and Lapeyre, G. (2007): Tracking coherent structures in a regional ocean model with wavelet analysis: Application to Cape Basin eddies, *Journal of Geophysical Research: Oceans*, 112(C5).

Drinkwater, K.F. (1988): On the mean and tidal currents in Hudson Strait, *Atmosphere-Ocean*, 26(2), 252-266.

Dussin, R., Barnier, B. and Brodeau, L. (2016): The making of Drakkar forcing set DFS5, Grenoble, France: LGGE, 2016.

Duvivier, A.K., Cassano, J.J., Craig, A., Hamman, J., Maslowski, W., Nijssen, B., Osinski, R. and Roberts, A. (2016): Winter atmospheric buoyancy forcing and oceanic response during String Wind Events around Southeastern Greenland in the Regional Arctic System Model (RASM) for 1990-2010, *Journal of Climate*, 29(3), 975-994.

Eden, C. and Böning, C. (2002): Sources of eddy kinetic energy in the Labrador Sea, *Journal of Physical Oceanography*, 32(12), 3346-3363.

Ferry, N., Parent, L., Garric, G., Barnier, B. and Jourdain, N.C. (2010): Mercator global eddy permitting ocean reanalysis GLORYS1V1: Description and results, *Mercator-Ocean Quarterly Newsletter*, 36, 15-27.

Feucher, C., Garcia-Quintana, Y., Yashayaev, I., Hu, X. and Myers, P.G. (2019): Labrador Sea Water formation and its impact on the local Meridional Overturning Circulation, *Journal of Geophysical Research: Oceans,* 124(8), 5654-5670.

Fichefet, T. and Maqueda, M.A.M. (1997): Sensitivity of a global sea ice model to the treatment of ice thermodynamics and dynamics, *Journal of Geophysical Research: Oceans*, 102(C6), 12609-12646.

Fischer, J. and Schott F.A. (2002): Labrador Sea Water tracked by profiling floats- From the boundary current into the open North Atlantic, *Journal of Physical Oceanography,* 32(2), 573-584.

Fischer, J., Visbek, M., Zantopp, R. and Nunes, N. (2010): Interannual to decadal variability of outflow from the Labrador Sea, *Geophysical Research Letters*, 37(24), 5p.

Frajka-Williams, E., Rhines, P.B. and Eriksen, C.C. (2014): Horizontal stratification during deep convection in the Labrador Sea, *Journal of Physical Oceanography*, 44(1), 220-228.

Fratantoni, P.S. and McCartney M.S. (2010): Freshwater export from the Labrador Current to the North Atlantic Current and the Tail of the Grand Banks of Newfoundland, *Deep Sea Research Part I: Oceanographic Research Papers,* 57(2), 258-283.

Fratantoni, P.S. and Pickart, R.S. (2007): The Western North Atlantic Shelfbreak Current System in Summer, *Journal of Physical Oceanography,* 37(10), 2509-2533.

Fröb, F., Olsen, A., Våge, K., Moore, G.W.K., Yashayaev, I., Jeansson, E. and Rajasakaren, B. (2016): Irminger Sea deep convection injects oxygen and anthropogenic carbon to the ocean interior, *Nature communications*, 7, 13244.

Fresnay, S., Ponte, A.L., Le Gentil, S. and Le Sommer, J. (2018): Reconstruction of the 3-D dynamics from surface variable in a high-resolution simulation of the North Atlantic, *Journal of Geophysical Research: Oceans*, 123(3), 1612-1630.

Garcia-Quintana, Y., Courtois, P., Hu, X., Pennelly, C., Kieke, D. and Myers, P.G. (2019): Sensitivity of Labrador Sea Water formation to changes in model resolution, atmospheric forcing, and freshwater input, *Journal of Geophysical Research: Oceans*, 124(3), 2126-2152.

Gary, S.F., Lozier, M.S., Biastoch, A. and Böning, C.W. (2012): Reconciling tracer and gloat observations of the export pathways of Labrador Sea Water, *Geophysical Research Letters*, 39(24).

Gelderloos, R., Katsman, C.A. and Drijfhout, S.S. (2011): Assessing the roles of three eddy types in restratifying the Labrador Sea after deep convection, *Journal of Physical Oceanography*, 41(11), 2102-2119.

Gelderloos, R., Straneo, F. and Katsman, C.A. (2012): Mechanisms behind the temporary shutdown of deep convection in the Labrador Sea: Lessons from the great salinity anomaly years 1968-71, *Journal of Climate*, 25(19), 6743-6755.

Gillard, L., Hu, X., Myers, P.G. and Bamber, J.L. (2016): Meltwater pathways from marine terminating glaciers of the Greenland ice sheet, *Geophysical Research Letters*, 43(20).

Grivault, N., Hu, X. and Myers, P.G. (2017): Evolution of Baffin Bay water masses and transports in a numerical sensitivity experiment under enhanced Greenland Melt. *Atmosphere-Ocean*, 55(3), 169-194.

Grivault, N., Hu, X. and Myers, P.G. (2018): Impact of the surface stress on the volume and freshwater transport through the Canadian Arctic Archipelago from high resolution numerical modelling, *Journal of Geophysical Research: Oceans,* 123, 9038-9060.

Gordon, A.L., Visbeck, M. and Comiso, J.C. (2007): A possible link between the Weddell Polynya and the Southern Annular Mode, *Journal of Climate*, 20(11), 2558-2571.

Häkkinen, S. and Rhines, P.B. (2004): Decline of subpolar North Atlantic circulation during the 1990s, *Science*, 304(5670), 555-559.

Handmann, P., Fischer, J., Visbeck, M., Karstensen, J., Biastoch, A., Böning, C. and Patara, L. (2018): The Deep Western Boundary Current in the Labrador Sea From Observations and a High-Resolution Model. *Journal of Geophysical Research: Oceans*, 123, 2828-2850.

Hansen, B. and Østerhus, S. (2000): North Atlantic-Nordic Seas exchanges, *Progress in Oceanography*, 45(2), 109-208.

Hátún, H., Eriksen, C.C. and Rhines, P.B. (2007): Buoyant eddies entering the Labrador Sea observed with gliders and altimetry, *Journal of Physical Oceanography*, 37(12), 2838-2854.

Hersbach, H. and Dee, D.J.E.N. (2016): ERA5 reanalysis is in production, *ECMWF newsletter*, 147(7), 5-6.

Holdsworth, A.M. and Myers, P.G. (2015): The influence of high-frequency atmospheric forcing on the circulation and deep convection of the Labrador Sea. *Journal of Climate*, 28(12), 4980-4996.

Holliday, N.P., Meyer, A., Bacon, S., Alderson, S.G. and de Cuevas, B. (2007): Retroreflection of part of the east Greenland current at Cape Farewell, *Geophysical Research Letters*, 34(7).

Holliday, N.P., Bacon, S., Allen, J. and McDonagh, E.L. (2009): Circulation and transport in the western boundary currents are Cape Farewell, Greenland, *Journal of Physical Oceanography*, 39(8), 1854-1870.

Holte, J. and Talley, L. (2009): A new algorithm for finding mixed layer depths with applications to Argo data and Subantarctic Mode Water formation, *Journal of Atmospheric and Oceanic Technology*, 26(9), 1920-1939.

Howatt, T., Palter, J.B., Matthews, R., deYoung, B., Bachmayer, R. and Claus, R. (2018): Ekman and Eddy Exchange of Freshwater and Oxygen across the Labrador Shelf Break, *Journal of Physical Oceanography*, 48(5), 1015-1031.

Hu, X., Sun, J., Chan, T.O. and Myers, P.G. (2018): Thermodynamic and dynamic ice thickness contributions in the Canadian Arctic Archipelago in NEMO-LIM2 numerical simulations, *Cryosphere*, 12(4), 1233-1247.

Hughes, K.G., Klymak, J.M., Hu, X. and Myers, P.G. (2017): Water mass modification and mixing rates in a 1/12° simulation of the Canadian Arctic Archipelago, *Journal of Geophysical Research: Oceans*, 122(2), 803-820.

Hurrell, J.W. (1995): Decadal trends in the North Atlantic Oscillation: regional temperatures and precipitation, *Science*, 269(5224), 676-679.

IPCC, (2014): Climate Change 2014: Synthesis Report. Contribution of Working groups I, II, and III to the Fifth Assessment Report of the Intergovernmental Panel on Climate Change [Core Writing Team, R.K. Pachauri and L.A. Meyer (eds)], IPCC, Geneva, Switzerland, 151 pp.

Jackson, L.C. and Wood, R.A. (2018): Hysteresis and Resilience of the AMOC in an Eddy-Permitting GCM, *Geophysical Research Letters*, 45(16), 8547-8556.

de Jong, M.F., Bower, A.S. and Furey, H.H. (2016): Seasonal and interannual variations of Irminger ring formation and boundary-interior heat exchange in FLAME, *Journal of Physical Oceanography*, 46(6), 1717-1734.

Jonsson, S. and Valdimarsson, H. (2004): A new path for the Denmark Strait overflow water from the Iceland Sea to Denmark Strait, *Geophysical Research Letters*, 31(3).

Jung, T., Serrar, S. and Wang, Q. (2014): The oceanic response to mesoscale atmospheric forcing, *Geophysical Research Letters*, **41**, 1255-1260.

Katsman, C.A., Spall, M.A. and Pickart, R.S. (2004): Boundary current eddies and their role in the restratification of the Labrador Sea, *Journal of Physical Oceanography*, 34(9), 1967-1983.

Kawasaki, T. and Hasumi, H. (2014): Effect of freshwater from the West Greenland Current on the winter deep convection in the Labrador Sea, *Ocean Modelling,* 75, 51-64.

Khatiwala, S., Schlosser, P. and Visbeck, M. (2002): Rates and mechanisms of water mass transformation in the Labrador Sea as inferred from tracer observations, *Journal of Physical Oceanography*, 32(2), 666-686.

Kieke, D., Klein, B., Stramma, L., Rhein, M. and Koltermann, K.P. (2009): Variability and propagation of Labrador Sea Water in the southern subpolar North Atlantic, *Deep Sea Research Part I: Oceanographic Research Papers*, 56(10), 1656-1674.

Kieke, D., Rhein, M., Stramma, L., Smethie, W.M., LeBel, D.A. and Zenk, W. (2006): Changes in the CFC inventories and formation rates of Upper Labrador Sea Water, 1997-2001, *Journal of Physical Oceanography,* 36(1), 64-86.

Koenigk, T., Mikolajewicz, U., Haak, U. and Jungclaus, J. (2007): Arctic freshwater export in the 20th and 21st centuries. *Journal of Geophysical Research: Biogeosciences*, 112(G4).

Lab Sea Group (1998): The Labrador Sea deep convection experiment, *Bulletin of the American Meteorological Society*, 79(10), 2033-2058.

Large, W.G. and Yeager, S.G. (2008): The global climatology of an interannually varying air-sea flux data set, *Climate Dynamics*, 33(2-3), 341-364.

Latif, M., Roechner, E., Mikolajewicz, U. and Voss, R. (2000): Tropical stabilization of the thermohaline circulation in a greenhouse warming simulation, *Journal of Climate*, 13(11), 1809-1813.

Lazier, J.R. (1980): Oceanographic conditions at ocean weather ship Bravo, 1964-1974, *Atmosphere-Ocean*, 18(3), 227-238.

Lazier, J., Hendry, R., Clarke, A. Yashayaev, I. and Rhines, P. (2002): Convection and restratification in the Labrador Sea, 1990-2000, *Deep Sea Research Part I: Oceanographic Research Papers*, 49(10), 1819-1835.

Lazier, J.R.N., and Wright, D.G. (1993): Annual velocity variations in the Labrador Current, *Journal of Physical Oceanography*, 23(4), 659-678, 1993.

Li, F., Lozier, M.S. and Johns, W.E. (2017): Calculating the meridional volume, heat, and freshwater transports from an observing system in the subpolar North Atlantic: Observing system simulation experiment, *Journal of Atmospheric and Oceanic Technology*, 34(7), 1483-1500.

Li, F., Lozier, M.S., Danabasoglu, G., Holliday, N.P., Kwon, Y.O., Romanou, A., Yeager, S.G. and Zhang, R. (2019): Local and downstream relationships between Labrador Sea Water volume and North Atlantic Meridional Overturning Circulation variability, *Journal of Climate*, 32(13), 3883-3898.

Lilly, J.M., Rhines, P.B., Visbeck, M., Davis, R., Lazier, J.R.N., Schott, F. and Farmer, D. (1999): Observing deep convection in the Labrador Sea during winter 1994/95, *Journal of Physical Oceanography*, 29, 2065-2098.

Lilly, J.M., Rhines, P.B., Schott, F., Lavender, K., Lazier, J., Send, U. and D'Asaro, E. (2003): Observations of the Labrador Sea eddy field, *Progress in Oceanography*, 59(1), 75-176.

Lin, P., Pickart, R.S., Torres, D.J. and Pacini, A. (2018): Evolution of the freshwater coastal current at the southern tip of Greenland, *Journal of Physical Oceanography*, 48(9), 2127-2140.

Lindsay, R., Wensnahan, M., Schweiger, A. and Zhang, J. (2014): Evaluation of seven different atmospheric reanalysis products in the Arctic, *Journal of Climate*, 27(3), 2588-2606.

Lique, C. and Thomas, M.D. (2018): Latitudinal shift of the Atlantic Meridional Overturning Circulation source regions under a warming climate, *Nature Climate Change*, 8(11), 1013-1020.

Loder, J.W., Ross, C.K. and Smith, P.C. (1988): A space-and time-scale characterization of circulation and mixing over submarine banks, with application to the northwestern Atlantic continental shelf, *Canadian Journal of Fisheries and Aquatic Sciences,* 45(11), 1860-1885.

Lozier, M.S., Bacon, S., Bower, A.S., Cunningham, S.A., de Jong, M.F., de Steur, L., deYoung, B., and coauthors (2017): Overturning in the Subpolar North Atlantic Program: A new international ocean observing system, *Bulletin of the American Meteorological Society*, 98(4), 737-752.

Lozier, M.S., Li, F., Bacon, S., Bahr, F., Bower, A.S., Cunningham, S.A., et al. (2019): A sea change in our view of overturning in the subpolar North Atlantic, *Science*, 363(6426), 516-521.

Luo, H., Bracco, A. and Di Lorenzo, E. (2011): The interannual variability of the surface eddy kinetic energy in the Labrador Sea, *Progress in Oceanography*, 91(3), 295-311.

Luo, H., Castelao, R.M., Rennermalm, A.K., Tedesco, M., Bracco, A., Yager, P.L. and Mote, T.L. (2016): Oceanic transport of surface meltwater from the southern Greenland ice sheet, *Nature Geoscience*, 9(7), 528.

Madec, G. (2008): Note du Pôle de modélisation, Institut Pierre-Simon Laplace (IPSL), France, No 27, ISSN No 1288-1619.

Madec, G., Delecluse, P., Imbard, M. and Lévy, C. (1998): OPA 8.1 ocean general circulation model reference manual. Note du Pôle de modélisation, Institut Pierre-Simon Laplace (IPSL), France, No 1, 91p.

Marshal, J., Jognson, H. and Goodman, J. (2001): A study of the interaction of the North Atlantic Oscillation with ocean circulation, *Journal of Climate*, 14(7), 1399-1421.

Marshall, J. and Schott, F. (1999): Open-ocean convection: Observations, theory, and models, *Reviews of Geophysics*, 37(1), 1-64.

Marson, J.M., Myers, P.G., Hu, X., Petrie, B., Azetsu-Scott, K., & Lee, C.M. (2017): Cascading off the West Greenland Shelf: A numerical perspective, *Journal of Geophysical Research: Oceans*, 122(7), 5316-5328.

Marzocchi, A., Hurshi, J.J.M., Holiday, N.P., Cunningham, S.A., Blaker, A.T., and Coward, A.C.: The North Atlantic subpolar circulation in an eddy-resolving global ocean model. Journal of Marine Systems, 142, 126-143, 2015.

McGeehan, I. and Maslowski, W. (2011): Impact of shelf-basin freshwater transport on deep convection in the western Labrador Sea, *Journal of Physical Oceanography*, 41(11), 2187-2210.

Mesinger, F. and Arakawa, A. (1976): Numerical methods used in atmospheric models. *GARP Publ. Ser., 17(1), WMO, Geneva, 64.*

Moore, G.W.K., Pickart, P.S. and Renfrew, I.A. (2011): Complexities in the climate of the subpolar North Atlantic: a case study from the winter of 2007, *Quarterly Journal of the Royal Meteorological Society*, 137(656), 757-767.

Moore, G.W.K., Pickart, R.S., Renfrew, I.A. and Våge, K. (2014): What causes the location of the air-sea heat flux maximum over the Labrador Sea? *Geophysical Research Letters,* 41, 3628-3635.

Müller, V., Kieke, D., Myers, P.G., Pennelly, C. and Mertens, C. (2017): Temperature flux carried by individual eddies across 47° in the Atlantic Ocean, *Journal of Geophysical Research: Oceans*, 122(3), 2441-2464.

Müller, V., Kieke, D., Myers, P.G., Pennelly, C., Steinfeldt, R. and Stendardo, I. (2019): Heat and freshwater transport by mesoscale eddies in the southern subpolar North Atlantic, *Journal of Geophysical Research: Oceans*, 124(8), 5565-5585.

Myers, P. (2005): Impact of freshwater from the Canadian Arctic Archipelago on Labrador Sea water formation, *Geophysical Research Letters*, 32(6).

Myers, P.G., Donnelly, C. and Ribergaard, M.H. (2009): Structure and variability of the West Greenland Current in Summer derived from 6 repeat standard sections, *Progress in Oceanography*, 80(1-2), 93-112.

Myers, P.G., Josey, S.A., Wheler, B. and Kulan, N. (2007): Interdecadal variability in Labrador Sea precipitation minus evaporation and salinity, *Progress in Oceanography*, 73(3-4), 341-357.

Myers, P.G., Kulan, N. and Ribergaard, M.H. (2007). Irminger water variability in the West Greenland Current, *Geophysical Research Letters*, 34(17).

Nencioli, F., Dong, C., Dickey, T., Washburn, L. and McWilliams, J.C. (2010): A vector geometry-based eddy detection algorithm and its application to a high-resolution numerical model product and high-frequency radar surface velocities in the Southern California Bight, *Journal of atmospheric and oceanic technology*, 27(3), 564-579.

Pacini, A., Pickart, R.S., Le Bras, I.A., Straneo, F., Holliday, N.P., Spall, M.A.: Cyclonic eddies in the West Greenland boundary current system. Journal of Physical Oceanography, 2021.

Pennelly, C. (2020): A 1/60 degree NEMO configuration within the Labrador Sea: LAB60, Zenodo, http://doi.org/10.5281/zenodo.3762748.

Pennelly, C. and Myers, P.G. (2020): Introducing LAB60: A 1/60° NEMO 3.6 numerical simulation of the Labrador Sea, *Geoscientific Model Development*, 13(10), 4959-4975, 2020

Pennelly, C. Hu, X. and Myers, P.G. (2019): Cross-isobath freshwater exchange within the North Atlantic Subpolar Gyre, *Journal of Geophysical Research: Oceans*, 124(10), 6831-6853.

Petit, T., Lozier, M.S., Josey, S.A. and Cunningham, S.A. (2020): Atlantic deep water formation occurs primarily in the Iceland Basin and Irminger Sea by local buoyancy forcing, *Geophysical Research Letters*, 47(22).

Pickart, R.S. and Spall, M.A. (2007): Impact of Labrador Sea convection on the North Atlantic meridional overturning circulation, *Journal of Physical Oceanography*, 37(9), 2207-2227.

Pickart, R.S., Torres, D.J. and Clarke, R.A. (2002): Hydrography of the Labrador Sea during active convection, *Journal of Physical Oceanography*, 32(2), 428-457.

Pillar, H.R., Johnson, H.L., Marshall, D.P., Heimbach, P. and Takao, S. (2018): Impacts of Atmospheric Reanalysis Uncertainty on Atlantic Overturning Estimates at 25°N, *Journal of Climate*, 31(21), 8719-8744.

Proshutinsky, A., Krishfield, R., Timmermans, M-L., Toole, J., Carmack, E., McLaughlin, F., Williams, W.J., Zimmermann, S., Itoh, M. and Shimada, K. (2009): Beaufort Gyre freshwater reservoir: State and variability from observations, *Journal of Geophysical Research*, 114, 1-25pp.

Quartly, G.D., de Cuevas, B.A. and Coward, A.C. (2013): Mozambique Channel eddies in GCMs: A question of resolution and slippage, *Ocean Modelling*, 63, 56-67.

Raasch, S. and Etling, D. (1997): Modeling Deep Ocean Convection: Large Eddy Simulation in Comparison with Laboratory Experiments, *Journal of Physical Oceanography*, 28(9), 1786-1802.

Rattan, S., Myers, P.G., Treguier, A.M., Theetten, S., Biastoch, A., and Böning, C. (2010): Towards an understanding of Labrador Sea salinity drift in eddy-permitting simulations, *Ocean Modelling*, 35(102), 77-88.

Renfrew, I.A., Moore, G.W.K., Guest, P.S. and Bumke, K. (2002): Comparison of Surface Layer and Surface Turbulent Flux Observations over the Labrador Sea with ECMWF Analysis and NCEP Reanalysis, *Journal of Physical Oceanography*, 32, 383-400.

Rhein, M., Kieke, D. and Steinfeldt, R. (2015): Advection of North Atlantic Deep Water from the Labrador Sea to the southern hemisphere, *Journal of Geophysical Research: Oceans*, 120(4), 2471-2487.

Rhein, M., Steinfeldt, R., Kieke, D., Stendardo, I. and Yashayaev, I. (2017): Ventilation variability of Labrador Sea Water and its effects on oxygen and anthropogenic carbon: a review, *Philosophical Transactions of the Royal Society A: Mathematical, Physical and Engineering Sciences*, 374(2102), 20160321.

Riahi, K., Grübler, A. and Nakicenovic, N. (2007): Scenarios of long-term socio-economic and environmental development under climate stabilization, *Technical Forecasting and Social Change*, 74, 887-935.

Ridenour, N., Hu, X., Jafarikhasragh, S., Landy, J.C., Lukovich, J.V., Stadnyk, T.A., et al., (2019): Sensitivity of freshwater dynamics to ocean model resolution and river discharge forcing in the Hudson Bay Complex, *Journal of Marine Systems*, 196, 48-64.

Rieck, J.K., Böning, C.W. and Getzlaff, K. (2019): The nature of eddy kinetic energy in the Labrador Sea: Different types of mesoscale eddies, their temporal variability, and impact on deep convection, *Journal of Physical Oceanography,* 49(8), 2075-2094.

Rykova, T. Straneo, F. and Bower, A.S. (2015): Seasonal and interannual variability of the West Greenland Current System in the Labrador Sea in 1993-2008, *Journal of Geophysical Research: Oceans*, 120(2), 1318-1332.

Saenko, O.A., Dupont, F., Yang, D., Myers, P.G., Yashayaev, I. and Smith, G.C. (2014): Role of resolved and parameterized eddies in the Labrador Sea balance of heat and buoyancy, *Journal of Physical Oceanography*, 44(12), 3008-3032.

Sathiyamoorthy, S. and Moore G.K. (2002): Buoyancy flux at ocean weather station Bravo, *Journal of Physical Oceanography*, 31(2), 458-474.

Schmidt, S. and Send, U. (2007): Origin and composition of seasonal Labrador Sea freshwater, *Journal of Physical Oceanography*, 37(6), 1445-1454.

Schouten, M.W., de Ruiter, W.P.M., van Leeuwn P.J.: Translation, decay and splitting of Agulhas rings in the southeastern Atlantic Ocean. Journal of Geophysical Research, 14(c9), 21913-21925, 2000.

Schulze-Chretien, L.M. and Frajka-Williams, E. (2018): Wind-driven transport of fresh shelf water into the upper 30 m of the Labrador Sea, *Ocean Science*, 14(5), 1247-1264.

Schulze-Chretien, L.M., Pickart, R.S., & Moore, G.W.K. (2016): Atmospheric forcing during active convection in the Labrador Sea and its impact on mixed-layer-depths, *Journal of Geophysical Research: Oceans*, 121(9), 6978-6992.

Smith, G.C., Roy, F., Mann, P., Dupont, F., Brasnett, B., Lemieux, J.F., Laroche, S. and Bélair, S. (2014): A new atmospheric dataset for forcing ice-ocean models: Evaluation of reforecasts using the Canadian global deterministic prediction system, *Quarterly Journal of the Royal Meteorological Society*, 140(680), 881-894.

Smith, W.H.F. and Sandwell, D.T. (1997): Global seafloor topography from satellite altimetry and ship depth soundings, *Science*, 277, 1957-1962.

Spall, M.A. (2004): Boundary currents and watermass transformation in marginal seas, *Journal of Physical Oceanography*, 34(5), 1197-1213.

Straneo, F. (2006): Heat and freshwater transport through the central Labrador Sea, *Journal of Physical Oceanography*, 36(4), 606-628.

Straneo, F. and Saucier, F. (2008a): The arctic-subarctic exchange through Hudson Strait, *Arctic-Subarctic Ocean Fluxes*, Springer, Dordrecht, 249-261.

Straneo, F. and Saucier, F. (2008b): The outflow from Hudson Strait and its contribution to the Labrador Current, *Deep Sea Research Part I: Oceanographic Research Papers*, 55(8), 926-946.

Su, Z., Wang, J., Klein, P., Thompson, A.F. and Menemenlis, D. (2018): Ocean submesoscales as a key component of the global heat budget, Nature communications, 9(1), 1-8.

Sun, M., Tian, F., Liu, Y. and Chen, F. (2017): An improved automatic algorithm for global eddy tracking using satellite altimetry data, *Remote Sensing*, 9(3), 206.

Sutherland, D.A. and Pickart, R.S. (2008). The East Greenland coastal current: Structure, variability, and forcing, *Progress in Oceanography,* 78(1), 58-77.

Swift, J.H. (1984): The circulation of the Denmark Strait and Iceland-Scotland overflow waters in the North Atlantic, *Deep Sea Research Part A. Oceanographic Research Papers,* 31(11), 1339-1355.

Tagklis, F., Bracco, A., Ito, T. and Castelao, R.M. (2020): Submesoscale modulation of deep water formation in the Labrador Sea, *Scientific Reports*, 10(1), 1-13.

Tréquier, A.M., Theetten, S., Chassignet, E.P., Penduff, T., Smith, R., Talley, L., Beismann, J.O. and Böning, C. (2005): The North Atlantic subpolar gyre in four high-resolution models, *Journal of Physical Oceanography*, 35(5), 757-774.

Tsubouchi, T., Bacon, S. Naveira Garabato, A.C., Aksenov, Y., Laxon, S.W., Fahrbach, E., et al. (2012): The Arctic Ocean in summer: a quasi-synoptic inverse estimate of boundary fluxes and water mass transformation, *Journal of Geophysical Research: Oceans*, 117(C1).

Tsujino, H., Urakawa, S., Nakano, H., Small, R.J., Kim, W.M., Yeager, S.G., et al. (2018): JRA-55 based surface dataset for driving ocean-sea-ice models (JRA55-do), *Ocean Modelling*, 130, 79-139.

Valcke, S. (2006): OASIS3 user guide (prism_2-5), *PRISM support initiative report*, 3, 64.

Van Vuuren, D.P., den Elzen, M.G.L., Lucas, P.L., Eickhout, B., Strengers, B.J., van Ruijven, B., Wonink, S. and van Houdt, R. (2007): Stabilizing greenhouse gas concentrations at low levels: an assessment of reduction strategies and costs, *Climate Change*, 81, 119-159.

Van Vuuren, D.P., Edmonds, J., Kainuma, M., Riahi, K., Thomson, A., Hibbard, K., Hurtt, G.C., Kram, T., Krey, V., Lamarque, J.F. and Masui, T. (2011): The representative concentration pathways: an overview, *Climate change*, 109(1-2), 5pp.

Volkov, D.L., Larnicol, G. and Dorandeu, J. (2007): Improving the quality of satellite altimetry data over continental shelves, *Journal of Geophysical Research: Oceans*, 112(C6).

Weiss, J. (1991): The dynamics of enstrophy transfer in two-dimensional hydrodynamics, *Physica D: Nonlinear Phenomena*, 48(2-3), 273-294.

Whiteworth, T. and Orsi, A.H. (2006): Antarctic Bottom Water production and export by tides in the Ross Sea, *Geophysical Research Letters*, 33(12).

Wilson, C., Harle, J. and Wakelin, S. (2019): Development of a regional ocean model for the Caribbean, including 3D dynamics, thermodynamics and full surface flu forcing, *National Oceanography Centre Research and Consultancy Report*, no. 65. National Oceanography Centre, Uk, 40pp.

Yang, Q., Dixon, T.H., Myers, P.G., Bonin, J., Chambers, D., van den Broeke, M.R., Ribergaard, M.H. and Mortensen, J. (2016): Recent increases in Arctic freshwater flux affects Labrador Sea convection and Atlantic overturning circulation, *Nature Communications*, 7.1, 8p.

Yashayaev, I. (2007): Hydrographic changes in the Labrador Sea, 1960-2005, *Progress in Oceanography*, 73(3-4), 242-276.

Yashayaev, I. and Loder, J.W. (2009): Enhanced production of Labrador Sea water in 2008, *Geophysical Research Letters*, 36(1).

Yashayaev, I. and Loder, J.W. (2016): Recurrent replenishment of Labrador Sea Water and associated decadal-scale variability, *Journal of Geophysical Research: Oceans*, 121(11), 8095-8814.

Yashayaev, I. and Loder, J.W. (2017): Further intensification of deep convection in the Labrador Sea in 2016, *Geophysical Research Letters*, 44(3), 1429-1438.

Yashayaev, I., van Aken, H.M., Holliday, N.P. and Bersch, M. (2007): Transformation of the Labrador Sea water in the subpolar North Atlantic, *Geophysical Research Letters*, 34(22), 8 pp.

Yeager, S. and Danabasoglu, G. (2014): The origins of late-twentieth-century variations in the large-scale North Atlantic circulation, *Journal of Climate*, 27(9), 3222-3247.

Yu, J., Gao, Y. and Otterå, O.H. (2016): The sensitivity of the Atlantic Meridional Overturning Circulation to enhanced freshwater discharge along the entire, eastern and western coast of Greenland, *Climate Dynamics*, 46(5-6), 1351-1369.

Yu. Z. and Wei, W. (2018): Convection: a neglected pathway for downward transfer of wind energy in the oceanic mixed layer, *Journal of Oceanology and Limnology*. 36.4, 1189-1197.

Zalesak, S.T. (1979): Fully multidimensional flux-corrected transport algorithms for fluids, *Journal of computational physics*, 31(3), 335-362.

Zantopp, R, Fischer, J., Visbek, M. and Karstensen, J. (2017): From interannual to decadal: 17 years of boundary current transports at the exit of the Labrador Sea, *Journal of Geophysical Research: Oceans*, 122, 1724-1748.